

## The effect of stray current on hardening and hardened cement-based materials

Susanto, A.

**DOI**

[10.4233/uuid:25de1e90-f586-4973-8f04-f2c744609959](https://doi.org/10.4233/uuid:25de1e90-f586-4973-8f04-f2c744609959)

**Publication date**

2020

**Document Version**

Final published version

**Citation (APA)**

Susanto, A. (2020). *The effect of stray current on hardening and hardened cement-based materials*. [Dissertation (TU Delft), Delft University of Technology]. <https://doi.org/10.4233/uuid:25de1e90-f586-4973-8f04-f2c744609959>

**Important note**

To cite this publication, please use the final published version (if applicable). Please check the document version above.

**Copyright**

Other than for strictly personal use, it is not permitted to download, forward or distribute the text or part of it, without the consent of the author(s) and/or copyright holder(s), unless the work is under an open content license such as Creative Commons.

**Takedown policy**

Please contact us and provide details if you believe this document breaches copyrights. We will remove access to the work immediately and investigate your claim.

# **The effect of stray current on hardening and hardened cement-based materials**

## **Proefschrift**

ter verkrijging van de graad van doctor  
aan de Technische Universiteit Delft,  
op gezag van de Rector Magnificus prof. dr.ir. T.H.J.J. van der Hagen,  
voorzitter van het College voor Promoties,  
in het openbaar te verdedigen op  
maandag 7 september 2020 om 15.00 uur

door

**Agus SUSANTO**

Master of Engineering aan de Bandung Institute of Technology, Indonesia  
geboren te Demak, Indonesië

Dit proefschrift is goedgekeurd door de promotoren.

Samenstelling promotiecommissie bestaat uit:

|                              |   |
|------------------------------|---|
| Rector Magnificus,           | voorzitter                                |
| Prof.dr.ir. K. van Breugel   | Technische Universiteit Delft, promotor   |
| Dr. ir. D. A. (Dessi) Koleva | Technische Universiteit Delft, copromotor |

Onafhankelijke leden:

|                                |   |
|--------------------------------|---|
| Prof.dr. Han Ay Lie            | Diponegoro University, Indonesia  |
| Prof. dr. ir. E.A.B. Koenders  | Technical University Darmstadt, Institute for<br>Construction and Building Materials, Germany |
| Prof.dr.ir. R.P.B.J. Dollevoet | Technische Universiteit Delft   |
| Prof.dr.ir. H.E.J.G. Schlangen | Technische Universiteit Delft   |
| Dr. G. Ye                      | Technische Universiteit Delft   |

Keywords: Stray current, Joule heating, cement-based materials, temperature, hydration process, microstructure, diffusion coefficient, insulation, service life.

Printed by: PrintSupport4U, The Netherlands

Cover design: Agus Susanto

ISBN: 978-94-92597-47-2

An electronic version of this dissertation is available at  
<http://repository.tudelft.nl/>

Copyright © 2020 by Agus Susanto

All rights reserved. No part of the material protected by this copyright notice may be reproduced or utilized in any form or by any means, electronic or mechanical, including photocopying, recording or by any information storage and retrieval system, without written permission from the author.

# Table of Contents

|   |           |
|---|-----------|
| List of figures   | vi        |
| List of tables  | xi        |
| List of symbols   | xii       |
| List of abbreviations   | xiv       |
| <br>  |           |
| <b>Chapter 1: Introduction</b>  | <b>1</b>  |
| 1.1 General introduction  | 2         |
| 1.2 Scope and Objectives  | 4         |
| 1.3 Research strategy   | 5         |
| 1.4 Layout of the thesis  | 6         |
| <br>  |           |
| <b>Chapter 2: State-of-the-art and practice-related challenges of stray current</b>   | <b>9</b>  |
| 2.1 Stray current flow in cement-based systems  | 10        |
| 2.1.1 Stray current flow in hardening cement-based materials .....  | 11        |
| 2.1.2 Stray current flow in hardened cement-based materials .....   | 13        |
| 2.1.3 Electrical curing of concrete .....   | 13        |
| 2.2 Stray current effect on material's properties with respect to durability  | 14        |
| 2.2.1 Electrical properties of cement-based materials .....   | 14        |
| 2.2.2 Microstructural parameters with respect to transport properties   | 16        |
| 2.2.2.1 Transport mechanism in cement-based materials .....   | 16        |
| 2.2.2.2 Determination of microstructural parameters of cement-based materials .....   | 17        |
| 2.3 Conclusions and outlook   | 18        |
| <br>  |           |
| <b>Chapter 3: Mechanical, electrical and microstructural properties of hardening cement-based materials in conditions of stray current flow</b> | <b>21</b> |
| 3.1 Introduction  | 22        |
| 3.2 Technical background  | 23        |
| 3.3 Materials and methods for experimental studies  | 24        |
| 3.3.1 Materials .....   | 24        |
| 3.3.2 Current regime .....  | 25        |
| 3.3.3 Test Methods .....  | 25        |
| 3.3.3.1 Compressive strength .....  | 25        |
| 3.3.3.2 Mortar electrical resistivity and water conductivity.....   | 25        |
| 3.3.3.3 Microstructural analysis.....   | 26        |
| 3.3.3.4 Mercury intrusion porosimetry (MIP) .....   | 26        |
| 3.3.3.5 Chemical analysis .....   | 27        |
| 3.3.3.6 Numerical simulation .....  | 27        |
| 3.4 Results of experimental studies and discussion  | 28        |
| 3.4.1 Chemical analysis – hydrated (chemically bound) water.....  | 28        |
| 3.4.2 Compressive strength .....  | 29        |
| 3.4.3 Microstructural properties.....   | 30        |
| 3.4.4 Discussion .....  | 33        |

|   |    |
|---|----|
| 3.5 Numerical simulation and correlation of results | 36 |
| 3.6 Conclusions                                     | 40 |

#### **Chapter 4: Stray current-induced development of cement-based microstructure in water-submerged, Ca(OH)<sub>2</sub>-submerged and sealed conditions** 43

|   |    |
|---|----|
| 4.1 Introduction  | 44 |
| 4.2 Materials and methods for experimental studies  | 45 |
| 4.2.1 Materials   | 45 |
| 4.2.2 Sample designation and current regime   | 46 |
| 4.2.3 Test Methods  | 47 |
| 4.2.3.1 Compressive strength  | 47 |
| 4.2.3.2 Mortar electrical resistivity   | 47 |
| 4.2.3.3 Determination of pore structure parameters and image analysis                                     | 47 |
| 4.2.3.4 Chemical analysis   | 47 |
| 4.3 Results of experimental studies and discussion  | 48 |
| 4.3.1 Compressive strength  | 48 |
| 4.3.2 Chemical analysis of the external medium  | 51 |
| 4.3.3 Microstructural analysis – MIP results  | 53 |
| 4.3.3.1 The effect of external medium   | 54 |
| 4.3.3.2 The effect of stray current and varying medium  | 56 |
| 4.3.4 Microstructural properties as derived by ESEM image analysis  | 57 |
| 4.3.4.1 Partly submerged conditions, H <sub>2</sub> O and alkaline (Ca(OH) <sub>2</sub> ) external medium | 57 |
| 4.3.4.2 Fully submerged conditions, H <sub>2</sub> O and alkaline (Ca(OH) <sub>2</sub> ) external medium  | 61 |
| 4.3.4.3 Sealed conditions   | 64 |
| 4.3.5 Bulk matrix electrical resistivity  | 66 |
| 4.4 Conclusions   | 68 |

#### **Chapter 5: The effect of stray current flow on hydration process and temperature development in cement-based materials** 71

|   |    |
|---|----|
| 5.1 Introduction  | 72 |
| 5.2 Experiments   | 73 |
| 5.2.1 Isothermal calorimetry tests of hardening cement paste  | 73 |
| 5.2.2 Semi-adiabatic tests: temperature development in hardening cement paste prism   | 73 |
| 5.3 Materials and methods for experimental studies  | 74 |
| 5.3.1 Materials   | 74 |
| 5.3.2 Test methods  | 75 |
| 5.3.2.1 Isothermal calorimetry tests  | 75 |
| 5.3.2.2 Semi-adiabatic tests of temperature development in hardening cement paste   | 75 |
| 5.3.2.3 Mercury intrusion porosimetry (MIP)   | 75 |
| 5.4 Numerical simulation of temperature development and hydration process of hardening concrete subjected to stray current flow | 75 |
| 5.4.1 Effects of stray current on hardening concrete  | 75 |

|         |   |     |
|---------|---|-----|
| 5.4.2   | Numerical simulation of temperature effects in hardening concrete .....   | 76  |
| 5.4.2.1 | Numerical simulation of temperature effect due to cement hydration.....   | 76  |
| 5.4.2.2 | Numerical simulation of thermal effects caused by hydration and stray current flow .....  | 78  |
| 5.4.2.3 | Boundary condition of the numerical simulation .....  | 80  |
| 5.4.2.4 | Numerical simulation of temperature effects on the evolution of microstructure .....  | 80  |
| 5.4.3   | Capillary porosity and apparent diffusion coefficient.....  | 82  |
| 5.4.3.1 | Capillary porosity of cement paste .....  | 82  |
| 5.4.3.2 | Apparent diffusion coefficient .....  | 82  |
| 5.4.4   | Input parameters of numerical simulations .....   | 82  |
| 5.5     | Results of experimental studies and discussion .....  | 84  |
| 5.5.1   | Isothermal calorimetry tests .....  | 85  |
| 5.5.1.1 | Heat generated in hardening cement paste under stray current .....  | 85  |
| 5.5.1.2 | Temperature development in hardening cement paste during isothermal hydration .....   | 85  |
| 5.5.1.3 | Analysis of stray current effect on hydration in isothermal calorimeter test .....  | 86  |
| 5.5.2   | Semi-adiabatic tests .....  | 88  |
| 5.5.2.1 | Temperature development in small hardening cement paste prism under stray current .....   | 88  |
| 5.5.3   | Measured effect of electrical current on pore structure of isothermally cured cement paste, w/c = 0.35 .....  | 90  |
| 5.6     | Numerical simulation of the effect of stray current on the hydration process .....  | 91  |
| 5.6.1   | Effect of stray current on hydration and temperature distribution in hardening concrete cube, 40×40×40 cm <sup>3</sup> .....  | 91  |
| 5.6.1.1 | Hydration and temperature development in a concrete cube, 40×40×40 cm <sup>3</sup> , <i>without</i> effect of stray current .....                                     | 91  |
| 5.6.1.2 | Effect of stray current on maximum temperature in hardening concrete walls .....  | 92  |
| 5.6.1.3 | Effect of stray current on degree of hydration, porosity and strength of a 40 cm thick concrete wall, with and without insulation .....                               | 95  |
| 5.6.2   | Simulated effect of stray current on concrete outer zone .....  | 102 |
| 5.6.2.1 | Effect of stray current on capillary porosity in the outer zone of concrete walls with and without insulation after 28 days hydration (outside temperature 20°C)..... | 102 |
| 5.6.2.2 | The effect of stray current on apparent diffusion coefficients in outer zones of concrete walls with and without insulation, after saturation with water .....        | 103 |
| 5.7     | Conclusions .....   | 105 |

## **Chapter 6: The effect of stray current flow on material properties of different mixtures of hardened mortar specimens 107**

|       |  |     |
|-------|--|-----|
| 6.1   | Introduction .....                       | 108 |
| 6.2   | Materials and experimental methods ..... | 109 |
| 6.2.1 | Materials .....                          | 109 |

|   |  |            |
|---|--|------------|
| 6.2.2   | Sample designation, current regimes and conditioning .....   | 109        |
| 6.2.3   | Experimental methods .....   | 111        |
| 6.2.3.1   | Standard compressive strength .....  | 111        |
| 6.2.3.2   | Mercury intrusion porosimetry (MIP).....   | 111        |
| 6.2.3.3   | Electrical resistivity measurements .....  | 111        |
| 6.3   | Results and discussion .....   | 111        |
| 6.3.1   | Compressive strength of hardened (28 day-cured) mortar specimens .....   | 111        |
| 6.3.2   | The effect of curing and stray current on pore structure (identical w/c ratio<br>0.5, varying curing time i.e. 24h and 28 days) .....  | 114        |
| 6.3.2.1   | Mortar specimens partly and fully submerged in water.....  | 114        |
| 6.3.2.2   | Calcium hydroxide immersed conditions .....  | 117        |
| 6.3.3   | The effect of w/c ratio (0.5 and 0.35) in stray current conditions on pore<br>structure development of equally cured (hardened) bulk matrix (28 days-<br>cured mortar) ..... | 120        |
| 6.3.4   | Evaluation of the effect of stray current on porosity and compressive strength<br>of mortar specimens .....  | 124        |
| 6.3.5   | Electrical resistivity of 28-days cured mortar in condition of stray current<br>flow.....  | 125        |
| 6.3.5.1   | Electrical resistivity development of mortar specimens in sealed<br>condition .....  | 125        |
| 6.3.5.2   | Electrical resistivity development of mortar specimens partly and<br>fully submerged in water or calcium hydroxide solution .....  | 126        |
| 6.4   | Conclusions .....  | 128        |
| <br><b>Chapter 7: Retrospection, Conclusions and Recommendations for Future<br/>Research</b>  |  | <b>129</b> |
| 7.1   | Retrospection .....  | 130        |
| 7.2   | Conclusions .....  | 131        |
| 7.3   | Recommendations for future research .....  | 134        |
| <br><b>Appendix A</b>   |  | <b>135</b> |
| Determination of pore structure parameters and image analysis   |  |            |
| <br><b>Appendix B</b>   |  | <b>139</b> |
| Numerical simulations results for the evolution of temperature, degree of hydration,<br>capillary porosity and compressive strength in the centre and outer zone of concrete<br>elements without insulation subjected to stray current for different wall thickness |  |            |
| <br><b>Appendix C</b>   |  | <b>143</b> |
| Numerical simulations results for the evolution of temperature, degree of hydration,<br>capillary porosity and compressive strength in the centre and outer zone of concrete<br>elements with insulation subjected to stray current for different wall thickness    |  |            |
|   | References .....   | 147        |
|   | Summary .....  | 159        |
|   | Samenvatting .....   | 161        |
|   | Acknowledgments .....  | 163        |
|   | Curriculum vitae .....   | 165        |

## List of figures

|           |   |    |
|-----------|---|----|
| Fig. 1.1  | Examples of concrete structures in submerged condition and sealed bulk matrix. Location: in front of the Amsterdam central station, the Netherlands. (Photo: A. Susanto).....   | 4  |
| Fig. 1.2  | (a) The typical of stray current flow through cement-based materials from subway transport systems with fluctuate current flow electrical curing; (b). Constant input of stray current through cement-based materials, can be from electrical curing and HVDC transmission system .....   | 4  |
| Fig. 1.3  | Schematic representation of research strategy of this research .....  | 5  |
| Fig. 1.4  | Layout of the thesis.....   | 8  |
| Fig. 2.1  | Rate of heat evolution during hydration of Portland cement (Mindess 2003).....  | 12 |
| Fig. 2.2  | Electrical resistivity measurement by two probes method.....  | 16 |
| Fig. 2.3  | Mercury intrusion and extrusion hysteresis (a) and pore size distribution differential curve of mortar specimen with critical pore diameter ( $d_c$ ) (b).....  | 18 |
| Fig. 3.1  | (a) Experimental set-up for group S; (b) electrical circuit, where $R_1=120\text{ k}\Omega$ and $R_2=20\text{ k}\Omega$ are current adjusting resistances.....  | 24 |
| Fig. 3.2  | (a) Schematic presentation, including geometry of the container and current flow direction, where $h=4\text{ cm}$ , $h_1=2\text{ cm}$ , $A=27\times 2\text{ cm}$ ; (b) schematic of the electrical resistance measurement where 1 and 2 titanium plate (mesh) and mortar cubes, respectively .....  | 25 |
| Fig. 3.3  | Schematic boundary conditions for numerical simulation of stray current .....   | 28 |
| Fig. 3.4  | Hydrated water at 1 day - 84 days of age for R and S specimens.....   | 29 |
| Fig. 3.5  | Evolution of compressive strength (MPa) for control R and “stray current” S groups .....  | 30 |
| Fig. 3.6  | Porosity (left) and pore size distribution (right) for control group R and “stray current” group S at hydration ages of 24h, 7 days and 28 days, determined via image analysis .....  | 30 |
| Fig. 3.7  | Porosity and pore size distribution for groups S and R from MIP tests: 28 days (a,b) and 84 days (c, d) .....   | 31 |
| Fig. 3.8  | ESEM micrographs of the bulk mortar matrix for specimens R (left column) and S (right column) at the hydration ages of 7 days, 28 days and 84 days .....  | 32 |
| Fig. 3.9  | Comparison of electrical resistivity values (columns) in Ohm.m for mortar specimens S and R (both in immersed condition and identical water levels) at hydration ages of 24h (a), 3 days (b), 7 days (c) 28 days (d) 56 days (e) and 84 days (f) .....  | 34 |
| Fig. 3.10 | An example of potential distribution in the container (a) and current density distribution (b,c) within the experimental set-up for group S, presenting the magnitude of current density, distributed in the total bulk material (b) and current density distribution lines per sections of the cubes (c) .....   | 37 |
| Fig. 3.11 | Stray current model (current density distribution) for specimens group S at 1 day (a, b), 7 days (c, d), 28 days (e, f) and 84 days (g, h) – top and middle cross sections (left columns) and bottom sections (right column) .....  | 38 |
| Fig. 3.12 | An example for the graphical presentation of the generated current distribution lines in the directions of x, y and z axis, including a schematic view of current distribution lines in one cube .....  | 39 |
| Fig. 3.13 | Stray current model for 28 days for group R, presenting hypothetic distribution of current flow .....   | 40 |
| Fig. 4.1  | Experimental set-up, electrical devices, multiplexer to automatically record resistance of the mortar specimens, and schematic presentation of the electrical current application through the cross section (A) of mortar specimens for sealed condition (a, b, c); schematic experimental set up for submerged (partially or full) conditions (d), as also previously reported (Susanto et al. 2013) ..... | 45 |
| Fig. 4.2  | Compressive strength as a function of hydration age for mortar specimens in rest and “under current” conditions: (a) partly submerged in $\text{H}_2\text{O}$ and $\text{Ca}(\text{OH})_2$ solution; (b) fully submerged in $\text{H}_2\text{O}$ ; (c) fully submerged in $\text{Ca}(\text{OH})_2$ solution; (d) sealed condition .....   | 49 |
| Fig. 4.3  | Cumulative concentration of calcium (a), sodium (b) and potassium (c) in the external medium due to leaching-out of mortar specimens, fully submerged in water (comparison of control (no current) and “under current” regimes) .....   | 52 |
| Fig. 4.4  | Example overlay of porosity (a) and pore size distribution (b) obtained from replicates of MIP data for mortar specimens submerged in water solution at 28 days of conditioning time.....   | 53 |

|           |   |    |
|-----------|---|----|
| Fig. 4.5  | MIP-derived porosity and pore size distribution for mortar at 28 days, 84(112) days of age – control and “under current” conditions, $10 \text{ mA/m}^2$ : (a, b) partly submerged in water; (c, d) partly submerged in $\text{Ca(OH)}_2$ solution .....  | 54 |
| Fig. 4.6  | MIP-derived porosity and pore size distribution for mortar at 28 days and 112 days of age for control and “under current” conditions of $100 \text{ mA/m}^2$ and $1 \text{ A/m}^2$ : (a, b) fully submerged in water; (c, d) fully submerged in $\text{Ca(OH)}_2$ .....   | 55 |
| Fig. 4.7  | MIP-derived porosity and pore size distribution for <i>sealed</i> mortar at 3 and 28 days of age - control and “under current” of $100 \text{ mA/m}^2$ & $1 \text{ A/m}^2$ .....  | 56 |
| Fig. 4.8  | ESEM micrographs, $500\times$ of mortar bulk matrix at 28 days (top row) and 84 days of age (bottom row) in <i>partly submerged in water</i> conditions: control (a,c) and “under current” regime ( $10 \text{ mA/m}^2$ ) (b,d) .....   | 58 |
| Fig. 4.9  | Porosity and pore size distribution – mortar bulk matrix in <i>partly submerged in water</i> conditions in control and “under current” regime ( $10 \text{ mA/m}^2$ ) – a) overlay of results for 7 and 28 days of age; b) overlay of results for 56, 84 and 112 days of age .....  | 58 |
| Fig. 4.10 | (a) Weight percent of hydrated (chemically bound water) per dry cement weight for specimens partly-submerged in water and in $\text{Ca(OH)}_2$ at various hydration ages; (b) degree of hydration, calculated as specified in Section 2.3.5.....  | 59 |
| Fig. 4.11 | ESEM micrographs, $500\times$ of mortar bulk matrix at 28 days (top row) and 112 days of age (bottom row) - <i>partly submerged in <math>\text{Ca(OH)}_2</math></i> conditions for control (a,c) and “under current” regime ( $10 \text{ mA/m}^2$ ) (b,d).....  | 60 |
| Fig. 4.12 | Porosity and pore size distribution for mortar bulk matrix in control and “under current” regime ( $10 \text{ mA/m}^2$ ) - <i>partly submerged in <math>\text{Ca(OH)}_2</math></i> conditions – a) overlay of results for 28 days of age; b) overlay of results for 112 days of age .....   | 61 |
| Fig. 4.13 | ESEM micrographs $500\times$ of mortar bulk matrix at 28 days (top row) and 112 days of age (bottom row) - <i>fully- submerged in water</i> conditions for control (a,d), “under current” regime of $100 \text{ mA/m}^2$ (b,e) and “under current” regime of $1 \text{ A/m}^2$ (c,f) .....  | 62 |
| Fig. 4.14 | Porosity and pore size distribution – mortar bulk matrix for control and “under current” regimes of $100 \text{ mA/m}^2$ and $1 \text{ A/m}^2$ in <i>fully submerged in water</i> conditions – a) overlay of results for 28 days of age; b) overlay of results for 112 days of age .....  | 62 |
| Fig. 4.15 | ESEM micrographs $500\times$ of mortar bulk matrix in <i>fully- submerged in <math>\text{Ca(OH)}_2</math></i> : 28 days (top row) and 112 days of age (bottom row) for control (a,d), “under current” regime of $100 \text{ mA/m}^2$ (b,e) and “under current” regime of $1 \text{ A/m}^2$ (c,f) .....                              | 63 |
| Fig. 4.16 | Porosity and pore size distribution for mortar bulk matrix in control and “under current” regimes of $100 \text{ mA/m}^2$ and $1 \text{ A/m}^2$ in <i>fully submerged in <math>\text{Ca(OH)}_2</math></i> conditions – a) overlay of results for 28 days of age and b) 112 days of age .....  | 64 |
| Fig. 4.17 | ESEM micrographs $500\times$ of mortar bulk matrix in <i>sealed conditions</i> : 28 days (top row) and 112 days of age (bottom row) for control (a,d), “under current” regime of $100 \text{ mA/m}^2$ (b,e) and “under current” regime of $1 \text{ A/m}^2$ (c,f) .....   | 65 |
| Fig. 4.18 | Porosity (a) and pore size distribution (b) for the bulk matrix of mortar specimens in control and “under current” regimes of $100 \text{ mA/m}^2$ and $1 \text{ A/m}^2$ in <i>sealed conditions</i> as an overlay of results for 7 days, 28 days and 112 days .....  | 65 |
| Fig. 4.19 | ESEM micrographs, $500\times$ , of the “ <i>anodic</i> ” side (left), <i>middle (bulk matrix)</i> (mid) and “ <i>cathodic</i> ” side (right) (see Fig.1c) of mortar specimens in <i>sealed conditions</i> for “under current” regimes of $1 \text{ A/m}^2$ (top row) and $100 \text{ mA/m}^2$ (bottom row) at 112 days of age ..... | 66 |
| Fig. 5.1  | (a) Isothermal calorimeter (TAM-Air-314) used to measure heat release of cement paste; (b) Schematic pictures of the holders for “under current” regime .....   | 73 |
| Fig. 5.2  | Experimental set-up for measurements of temperature increase in hardening cement paste specimens due to electrical current flow.....  | 73 |
| Fig. 5.3  | Adiabatic (a), semi-adiabatic (b) and isothermal (c) hydration curves and temperature development of concrete (log scale). Initial mix temperature is $20^\circ\text{C}$ .....  | 77 |
| Fig. 5.4  | Typical evolution of electrical conductivity $\sigma(t)$ of hardening cement paste as a function of time with w/c ratio 0.35 and 0.5 calculated with eq. (5.15), where $\sigma_{eff}(t)$ (eq. 5.16) was calculated with input parameters $\sigma_t=2.32$ , $\sigma_f=0.07$ , $t_s = 4.5$ (h), $b=1.85$ .....                        | 79 |
| Fig. 5.5  | Schematic of boundary conditions for numerical simulation of temperature development in hardening cement-based materials subjected to stray current with dimension $40\times 40\times 40 \text{ cm}^3$ ..   | 80 |
| Fig. 5.6  | Typical examples simulated virtual microstructure obtained with HYMOSTRUC3D (Gao Peng, 2018) .....  | 81 |

|           |  |     |
|-----------|--|-----|
| Fig. 5.7  | Effect of reaction temperature on microstructure. Microstructures formed at moderate temperature (a) and high temperature (b). Fig. 5.7c gives the conversion factor $v(T)$ (van Breugel, 1991).....   | 81  |
| Fig. 5.8  | Fitting curve of the degree of hydration from HYMOSTRUC3D simulation to obtain hydration parameter ( $\beta$ ) for concrete with w/c 0.35 and 0.5 .....  | 83  |
| Fig. 5.9  | Measured rate of discharge of heat $dQ_d(t)/dt$ (a) and discharged heat $Q_d(t)$ (b) in hardening cement paste (control) and with stray current level of $10\text{mA/m}^2$ , $100\text{mA/m}^2$ and $1\text{A/m}^2$ for w/c 0.35 in isothermal condition .....   | 85  |
| Fig. 5.10 | Temperature development of hardening cement paste as a function of time. Samples with w/c ratio 0.35, measured in isothermal condition .....   | 86  |
| Fig. 5.11 | Discharged heat $Q_d(t)$ in hardening cement paste (control) and with stray current level $1\text{A/m}^2$ for w/c 0.35 in isothermal condition .....   | 86  |
| Fig. 5.12 | Cumulative heat input from stray current flow $Q_{el}$ (calculated with eq. (5.25)). a) Cumulative heat curves for three current levels. b) Cumulative heat input from stray current (from 0 to 14 hours). Cement paste with w/c ratio 0.35.....   | 88  |
| Fig. 5.13 | Evolution of electrical conductivity $\sigma(t)$ of hardening cement paste under stray current flow with current density 1, 10, 40, and $60\text{A/m}^2$ calculated with eq. (5.15), where $\sigma_{eff}(t)$ (eq. 5.16) was calculated with input parameters $\sigma_i=2.32$ , $\sigma_f=0.07$ , $t_s = 4.5$ (h), $b=1.85$ .....   | 88  |
| Fig. 5.14 | Development of current density $J(t)$ in hardening cement paste with applied current density 1, 10, 40, and $60\text{A/m}^2$ , calculated with eq. (5.12) .....  | 89  |
| Fig. 5.15 | (a) Simulated and measured temperature development in hardening cement paste subjected to stray current (b). Comparison between temperature development of hardening cement paste subjected to stray current and temperature development caused by stray current only $T_{el}$ . Water-to-cement ratio used was 0.35. The sample size is $5.5 \times 5.5 \times 29.5 \text{ cm}^3$ ..... | 89  |
| Fig. 5.16 | Capillary porosity (a) and pore size distribution (b) of isothermally cured cement pastes at 4 days with w/c ratio 0.35 and summary porosity (c) of cement paste obtained from MIP tests with current density levels of $10\text{mA/m}^2$ , $100\text{mA/m}^2$ and $1\text{A/m}^2$ .....   | 90  |
| Fig. 5.17 | Heat of hydration $Q(t)$ (a) and degree of hydration $\alpha(t)$ (b) of isothermally hardening cement paste subjected to stray current with different current density calculated with eq. (5.4), where $Q_{max}$ is $367 \text{ kJ/kg}$ (see Table 5.2) .....  | 91  |
| Fig. 5.18 | Simulated temperature field (a) and temperature profile in hardening concrete specimen in x direction, for $y=20 \text{ cm}$ and $z=20 \text{ cm}$ (b). Sample size: $40 \times 40 \times 40 \text{ cm}^3$ . Imposed outside temperature is $20^\circ\text{C}$ .....   | 92  |
| Fig. 5.19 | Simulated temperature development, heat of hydration and degree of hydration of hardening concrete at three different locations (i.e. point 1 ( $xyz = 20,20,20$ ), point 2 ( $xyz = 20,8,20$ ), point 3 ( $xyz = 3,20,20$ )) with specimen size $40 \times 40 \times 40 \text{ cm}^3$ for w/c ratio 0.35 .....  | 93  |
| Fig. 5.20 | Maximum temperature ( $T_{max,2}$ ) in the centre of hardening concrete walls subjected to current level as a function of wall thickness for w/c ratio 0.35 (a) and 0.5 (b) .....  | 94  |
| Fig. 5.21 | Maximum temperature ( $T_{max,2}$ ) in centre of hardening concrete walls with w/c ratio 0.35 (a) and 0.5 (b) as a function of current density .....   | 94  |
| Fig. 5.22 | Schematic of boundary conditions for numerical simulation of temperature development in hardening concrete walls with insulation subjected to stray current. The wall thickness is L (in cm) .....   | 96  |
| Fig. 5.23 | Schematic of boundary conditions for numerical simulation of temperature development in hardening concrete walls without insulation subjected to stray current. The wall thickness is L (in cm) .....  | 96  |
| Fig. 5.24 | Typical curves of compressive strength of concrete as a function of capillary porosity of cement paste calculated with eq. (5.27) with different n values (left) and schematic range values of compressive strength of concrete as a function of capillary porosity of cement paste with w/c ratio 0.35-0.5 (right) .....  | 97  |
| Fig. 5.25 | Example of temperature profiles after 18 hours of hydration in a 40 cm thick concrete wall with and without insulation and meanwhile subjected to stray current .....  | 98  |
| Fig. 5.26 | Temperature development (a), degree of hydration (b), capillary porosity (c) and compressive strength (d) in the <i>centre</i> of hardening concrete <i>with and without insulation</i> for wall thickness 40cm and w/c ratio 0.35 .....   | 100 |

|           |  |     |
|-----------|--|-----|
| Fig. 5.27 | Temperature development (a), degree of hydration (b), capillary porosity (c) and compressive strength (d) in the <i>outer</i> zone of hardening concrete <i>with and without insulation</i> for wall thickness 40cm and w/c ratio 0.35 .....   | 101 |
| Fig. 5.28 | Maximum temperature ( $T_{\max,1}$ ) in outer zone of hardening concrete walls with and without insulation as a function of wall thickness for different magnitude of the stray current .....  | 102 |
| Fig. 5.29 | Maximum temperature $T_{\max,1}$ (a) and calculated capillary porosity of cement paste (eq. (5.19)) in outer zone of concrete walls <i>with and without insulation</i> subjected to stray current for different wall thickness after 3 days (a) and 28 days (b) hydration.....   | 103 |
| Fig. 5.30 | Apparent diffusion coefficient in outer zone of a 40 cm thick hardening concrete wall with and without insulation for different values of the stray current as a function of time .....  | 104 |
| Fig. 5.31 | Apparent diffusion coefficients in outer zones of concrete walls <i>with and without insulation</i> for different wall thickness after 3 days (a) and 28 days (b) of hydration calculated with eq. (5.21) .....  | 104 |
| Fig. 6.1  | a) Experimental set-up for mortar specimens under electrical current flow with multiplexer and PC data recorder to record resistance; b) electrical circuit, where $R_s$ is resistor to adjust electrical current flow through the mortar specimen .....   | 110 |
| Fig. 6.2  | Compressive strength with conditioning from 0 to 84 days (hydration age of 28 to 112 days) for 28 days-cured mortar specimens of w/c ratio 0.5 and 0.35 in partly (a, c) and fully (b, d) submerged in $H_2O$ and $Ca(OH)_2$ conditions - comparison of control and “under current” regimes .....  | 112 |
| Fig. 6.3  | Evolution of compressive strength of mortar specimens with w/c ratio 0.5 and 0.35 in partly (a) and fully (b) submerged in $H_2O$ after 28 days. Strength reduction between specimens under current and the relevant control cases (i.e. $MPa = (MPa_{\text{control}} - MPa_{\text{under current}})$ ) in partly and fully submerged in $H_2O$ with w/c ratio 0.35 (c) and 0.5 (d) .....   | 113 |
| Fig. 6.4  | Compressive strength development in 28-days cured mortar specimens, comparison for fully submerged in water and sealed conditions, w/c ratio 0.5 (a) and w/c 0.35 (b) .....  | 114 |
| Fig. 6.5  | MIP-derived porosity and pore size distribution at 112 days of age for specimens of identical 0.5 w/c ratio but different curing time intervals i.e. 24h cured and 28 days cured specimens: (a, b) half-immersed in water control and 10 mA/m <sup>2</sup> regime (c, d) fully immersed in water, 100 mA/m <sup>2</sup> and 1A/m <sup>2</sup> regimes .....  | 115 |
| Fig. 6.6  | Porosity ( <i>column; solid column for 24h cured</i> ) and critical pore size ( <i>symbol, “cr.pore” in legend</i> ) at hydration ages of 28 days, 112 days and 140 days for 24h and 28 days cured mortar of identical w/c ratio 0.5, <i>half immersed in H<sub>2</sub>O</i> . The plot presents a comparison of control cases ( <i>designation R for both 24h and 28d cured</i> ) and those, subjected to 10 mA stray current ( <i>designation 10 mA for both 24h and 28d cured</i> ).....  | 116 |
| Fig. 6.7  | Porosity ( <i>column; solid column for 24h cured</i> ) and critical pore size ( <i>symbol, “cr.pore” in legend</i> ) at hydration ages of 28 days, 112 days and 140 days for 24h and 28 days cured mortar of identical w/c ratio 0.5, <i>fully immersed in H<sub>2</sub>O</i> . The plot presents a comparison of control cases ( <i>designation R for both 24h and 28d cured</i> ) and those, subjected to 100 mA/m <sup>2</sup> and 1 A/m <sup>2</sup> stray current ( <i>designation 100mA and 1A for both 24h and 28d cured</i> ) .....    | 116 |
| Fig. 6.8  | MIP-derived porosity and pore size distribution at 112 days of age for specimens of identical 0.5 w/c ratio but different curing time intervals i.e. 24h cured and 28 days cured specimens: (a, b) half-immersed in $Ca(OH)_2$ control (R1/2) and 10 mA/m <sup>2</sup> regime (10mA) (c, d) fully immersed in $Ca(OH)_2$ control (Rfull), 100 mA/m <sup>2</sup> (100 mA) and 1A/m <sup>2</sup> (1A) regimes ( <i>designation 24h and 28d refers to the respective curing time</i> ).....   | 118 |
| Fig. 6.9  | Porosity ( <i>column; solid column for 24h cured</i> ) and critical pore size ( <i>symbol, “cr.pore” in legend</i> ) at hydration ages of 28 days, 112 days and 140 days for 24h and 28 days cured mortar of identical w/c ratio 0.5, <i>half immersed in Ca(OH)<sub>2</sub></i> . The plot presents a comparison of control cases ( <i>designation R for both 24h and 28d cured</i> ) and those, subjected to 10 mA stray current ( <i>designation 10 mA for both 24h and 28d cured</i> ) .....   | 119 |
| Fig. 6.10 | Porosity ( <i>column; solid column for 24h cured</i> ) and critical pore size ( <i>symbol, “cr.pore” in legend</i> ) at hydration ages of 28 days, 112 days and 140 days for 24h and 28 days cured mortar of identical w/c ratio 0.5, <i>fully immersed in Ca(OH)<sub>2</sub></i> . The plot presents a comparison of control cases ( <i>designation R for both 24h and 28d cured</i> ) and those, subjected to 100 mA/m <sup>2</sup> and 1 A/m <sup>2</sup> stray current ( <i>designation 100mA and 1A for both 24h and 28d cured</i> )..... | 119 |
| Fig. 6.11 | MIP-derived porosity and pore size distribution at 112 days of age for 28 day-cured mortar specimens: (a, b) <i>half-immersed in water</i> specimens as a comparison of w/c ratio 0.5 and 0.35 in control (R1/2) and 10 mA/m <sup>2</sup> current regime (10mA); (c, d) <i>fully immersed in water</i> , 28-day  |     |

|           |  |     |
|-----------|--|-----|
|           | cured specimens of w/c ratio 0.35 and 0.5 in control (R full), 100 mA/m <sup>2</sup> (100 mA) and 1 A/m <sup>2</sup> (1A) current regime .....   | 120 |
| Fig. 6.12 | Porosity ( <i>column; solid column for w/c 0.5</i> ) and critical pore size ( <i>symbol, "cr.pore" in legend</i> ) at hydration ages of 112 days and 140 days for 28 days cured mortar of different w/c ratio (0.5 and 0.35), <i>half immersed in H<sub>2</sub>O (a) and fully immersed in water (b)</i> . The plot a) presents a comparison of control cases ( <i>designation R1/2</i> ) and those, subjected to 10 mA/m <sup>2</sup> ( <i>designation 10 mA</i> ); b) compares control cases ( <i>designation R full</i> ) with 100 mA/m <sup>2</sup> ( <i>designation 100 mA</i> ) and 1 A/m <sup>2</sup> ( <i>designation 1A</i> ) ..... | 121 |
| Fig. 6.13 | MIP-derived porosity and pore size distribution at 112 days of age for 28 day-cured mortar specimens: (a, b) <i>half-immersed in Ca(OH)<sub>2</sub></i> specimens as a comparison of w/c ratio 0.5 and 0.35 in control (R1/2) and 10 mA/m <sup>2</sup> current regime (10mA); (c, d) <i>fully immersed in Ca(OH)<sub>2</sub></i> , 28-day cured specimens of w/c ratio 0.35 and 0.5 in control (R full), 100 mA/m <sup>2</sup> (100 mA) and 1 A/m <sup>2</sup> (1A) regime.....  | 122 |
| Fig. 6.14 | Porosity ( <i>column; solid column for w/c 0.5</i> ) and critical pore size ( <i>symbol, "cr.pore" in legend</i> ) at hydration ages of 112 days and 140 days for 28 days cured mortar of different w/c ratio (0.5 and 0.35), <i>half immersed in Ca(OH)<sub>2</sub> (a) and fully immersed in Ca(OH)<sub>2</sub> (b)</i> .....  | 123 |
| Fig. 6.15 | Measured and calculated compressive strength as a function of porosity of mortar specimens fully immersed (a) and partly immersed in water (b) subjected to stray current .....  | 125 |
| Fig. 6.16 | Electrical resistivity development of mortar specimens in sealed condition for w/c ratio 0.35 (a) and w/c ratio 0.5 (b). Conditioning time of t=0 is equal to 28 days of hydration age.....  | 126 |
| Fig. 6.17 | Electrical resistivity of mortar specimens cured in fog room for 28 days, <i>partly immersed</i> in water and calcium hydroxide, conditioned from 28 to 112 days: a) specimens of w/c ratio 0.5; b) specimens of w/c ratio of 0.35. Ambient temperature is about 25°C .....  | 127 |
| Fig. 6.18 | Electrical resistivity of mortar specimens cured in fog room for 28 days, <i>fully immersed</i> in water and calcium hydroxide, conditioned from 28 to 112 days: a) specimens of w/c ratio 0.5; b) specimens of w/c ratio of 0.35. Ambient temperature is about 25°C .....   | 127 |
| Fig. B.1  | Temperature development (a), degree of hydration (b), capillary porosity (c) and compressive strength (d) in the <i>centre</i> of hardening concrete <i>without insulation</i> for different wall thickness (i.e. 20cm, 40 cm and 80 cm) and w/c ratio 0.35 .....  | 140 |
| Fig. B.2  | Temperature development (a), degree of hydration (b), capillary porosity (c) and compressive strength (d) in the <i>outer zone</i> of hardening concrete <i>without insulation</i> for different wall thickness (i.e. 20cm, 40 cm and 80 cm) and w/c ratio 0.35.....   | 141 |
| Fig. C.1  | Temperature development (a), degree of hydration (b), capillary porosity (c) and compressive strength (d) in the <i>centre</i> of hardening concrete <i>with insulation</i> for different wall thickness (i.e. 20cm, 40 cm and 80 cm) and w/c ratio 0.35 .....   | 144 |
| Fig. C.2  | Temperature development (a), degree of hydration (b), capillary porosity (c) and compressive strength (d) in the <i>outer zone</i> of hardening concrete <i>with insulation</i> for different wall thickness (i.e. 20cm, 40 cm and 80 cm) and w/c ratio 0.35 .....   | 145 |

## List of tables

|           |   |     |
|-----------|---|-----|
| Table 3.1 | pH, alkali ions concentration and conductivity of water environment .....   | 35  |
| Table 4.1 | Test matrix: □ - compressive strength; ○ - MIP/ESEM tests; Δ - el. resistivity (* Full details on this (marked) investigation are reported in (Susanto et al. 2013) ..... | 46  |
| Table 4.2 | Non-evaporable water content for major phases (individual constituents) of cement .....   | 48  |
| Table 5.1 | The properties of cement CEM I 42.5 N .....   | 74  |
| Table 5.2 | Input parameters for simulating temperature development in hardening concrete .....   | 84  |
| Table 6.1 | Sample designation and experimental conditions .....  | 110 |
| Table 7.1 | Summary of the experiments of the effect of stray current on material properties (i.e. microstructural, mechanical and electrical properties) of mortar specimens .....   | 131 |
| Table 7.2 | Summary of the experiments of the effect of stray current on heat of hydration and temperature development in cement paste .....  | 132 |

## List of symbols

|                       |   |
|-----------------------|---|
| $J$                   | the current density   |
| $\rho_v$              | the charge density  |
| $E$                   | the electric field  |
| $\sigma$              | the electrical conductivity   |
| $\rho$                | the electrical resistivity  |
| $V$                   | the electrical voltage  |
| $\bar{D}$             | the electric flux density   |
| $\epsilon_0$          | the vacuum permittivity   |
| $\epsilon_r$          | the relative permittivity   |
| $D_{cl}$              | the diffusivity for chloride ions   |
| $R$                   | the gas constant  |
| $T$                   | the temperature   |
| $Z$                   | the ionic valence   |
| $F$                   | the Faraday constant  |
| $t_i$                 | the transfer number of the chloride ions  |
| $\gamma_i$            | the activity coefficient for chloride ions  |
| $c_i$                 | the chloride ions concentration in the pore water   |
| $D_0$                 | the effective diffusion coefficient at the reference time $t_0$   |
| $\rho_0$              | the electrical resistivity at $t_0$   |
| $C_s$                 | the boundary condition at the exposed surface   |
| $C_i$                 | the initial chloride concentration  |
| $D_a(t)$              | the apparent chloride diffusion coefficient   |
| $\text{erf}$          | the standard error function   |
| $b, n$                | the Rosin-Rammler constants   |
| $T$                   | the temperature in the concrete   |
| $\rho_c$              | the specific mass of concrete   |
| $c_c$                 | the specific heat of concrete   |
| $\lambda_c$           | the heat conduction coefficient   |
| $q_c$                 | the heat source   |
| $x, y, z$             | the coordinates of a particular point in the concrete   |
| $Q_a(t)$              | the heat of hydration in hardening concrete under adiabatic condition   |
| $Q_{max}^*$           | the amount of heat produced by the hydration reaction in adiabatic condition of the mixture in view                                       |
| $\tau$                | the hydration time  |
| $\beta$               | the hydration shape factor  |
| $\alpha_r(t)$         | the rate of reaction  |
| $\alpha_h(t)$         | the degree of hydration   |
| $\Delta Q_p/\Delta t$ | the reaction rate of the actual hydration process   |
| $\Delta Q_a/\Delta t$ | the reaction rate of the adiabatic hydration process at the same degree of hydration  |
| $k$                   | the rate factor   |
| $E_a$                 | the activation energy   |
| $R$                   | the universal gas constant  |
| $T_p(t)$              | the actual temperature of concrete  |
| $T_a(t)$              | the adiabatic temperature   |
| $T_R$                 | the reference temperature of the mixture  |
| $Q_p(t)$              | the amount of liberated heat at time $t$ in the hydrating concrete  |
| $C$                   | the cement content in the mixture   |
| $Q_{ei}(J, E)$        | the heat power per cubic meter due to the electrical current flow as a function of the current density $J$ and the electrical field $E$ . |
| $\epsilon_r$          | the relative permittivity   |
| $\epsilon_0$          | the vacuum permittivity   |
| $\rho_v$              | the charge density  |

|                               |   |
|-------------------------------|---|
| $\sigma$                      | the electrical conductivity   |
| $\rho_o$                      | the initial electrical resistivity  |
| $\alpha_T$                    | the temperature coefficient of resistivity  |
| $T_{ref}$                     | the reference temperature   |
| $v(T)$                        | the temperature-dependent conversion factor   |
| $V_{por}^{cap}(\alpha_{28d})$ | the capillary porosity of cement paste at an arbitrary degree of hydration $\alpha$ at 28 days          |
| $\omega_0$                    | the water-to-cement ratio   |
| $\rho_w$                      | the specific weight of water  |
| $\rho_s$                      | the specific weight of cement   |
| $D_o(J)$                      | the chloride diffusion coefficient at the reference time $t_o$ (i.e. 28 days) subject to stray current. |
| $t_o$                         | the reference time  |
| $n$                           | the ageing factor   |
| $C(x,t)$                      | the chloride concentration, measured at a depth $x$ at exposure time $t$                                |
| $C_s$                         | the chloride content at the exposed surface   |
| $C_i$                         | the initial chloride concentration in the concrete at the exposed surface                               |
| $x$                           | the depth below the exposed surface (concrete cover)  |
| $D_a(t)$                      | the apparent diffusion coefficient  |
| $t$                           | the exposure time   |
| erf                           | the standard error function.  |

## List of abbreviations

|                     |  |
|---------------------|--|
| DC                  | Direct current                             |
| AC                  | Alternating current                        |
| CP                  | Cathodic protection                        |
| HVDC                | High voltage direct current                |
| OPC                 | Ordinary Portland Cement                   |
| C <sub>3</sub> A    | Tricalcium aluminate                       |
| C <sub>3</sub> S    | Tricalcium silicate (alite)                |
| C <sub>2</sub> S    | Dicalcium silicate (belite)                |
| C <sub>3</sub> A    | Tricalcium aluminate                       |
| BSE                 | Back scattered electron                    |
| ESEM                | Environmental Scanning Electron Microscope |
| MIP                 | Mercury intrusion porosimetry              |
| DEC                 | Direct electric curing                     |
| 3D                  | Three-dimensional                          |
| FEM                 | Finite element method                      |
| CH                  | Calcium hydroxide                          |
| C-S-H               | Calcium silicate hydrate                   |
| w/c                 | Water-to-cement ratio                      |
| w/b                 | Water-to-binder ratio                      |
| PC                  | Personal computer                          |
| ITZ                 | Interfacial transition zone                |
| RCM                 | Rapid chloride migration                   |
| Ca(OH) <sub>2</sub> | Calcium hydroxide                          |



# 1

## **Introduction**

---

This chapter presents a general introduction to the topic of stray current, its occurrence and relevance to practice. The positive and/or negative effects of stray current on cement-based materials are outlined with respect to stray current levels as encountered in practical situations. The research strategy, developed towards the scope and objectives of this research project, is presented. The chapter concludes with a layout of the thesis, including a brief outline per chapter.

## 1.1 General introduction

Stray current is a current flowing in soil, water, or any other at least semi-conductive medium, produced by nearby electrical installations and distributed through metal conductors in these media.. It can be the result of direct current (DC) or alternating current (AC), predominantly with a frequency of 50 Hz (public electricity supply) or 162/3 Hz (traction power supply). The flow of stray current has to be avoided or minimized not only because of safety concerns, but also because of the possible negative effects on buried materials and structures. In order to minimize these negative effects, standards and safety regulations, e.g. EN50122-1 1997, EN50122-2 1999, EN50122-3 2010, IEC61439, specify the maximum permissible electrical current related to DC electrified railways, traction systems, grounding and returning circuits, interfaces between AC and DC installations.

EN50122-2 stipulates maximum values of 60 V for DC currents and 25 V<sub>rms</sub>\* for AC currents for the accessible (step) voltages as function of time during electrical leakage from public transport equipment, ancillary equipment (fixed installations) and electronic applications for railways. EN50122-3 states lower maximum permissible voltages of 25 V. Except the above general possibilities for stray current flow, there is a number of undesirable stray current sources, including external cathodic protection (CP) installations, DC transit systems, subways, streetcars, welding operations and electrical power transmission systems.

Stray currents were reported to affect not only steel reinforcement embedded in concrete (Bertolini *et al.* 2007; Chen *et al.* 2012; Lingvay *et al.* 2011; Yang *et al.* 2008; Chen *et al.* 2011), but they can also cause degradation of the cement-based matrix (Susanto *et al.* 2013). Any electrical field, including stray current, will influence cement hydration by altering ion and water transport. This is because in such condition, ion and water migration will add-up to diffusion-controlled ion transport process.

The rate of water migration in hardening concrete is strongly dependent on ion concentration and the magnitude of applied electric field (McInerney *et al.* 2004). Consequently, stray currents will modify material properties and can affect the behaviour and integrity of reinforced concrete structures. Negative effects of electrical current, including stray current have been reported, e.g. altered bulk matrix properties, reduced mechanical properties, increased permeability (Koleva *et al.* 2008; Susanto *et al.* 2013). Also positive effects of electrical current are reported, but only at early cement hydration in terms of strength development in case of “electrical” curing (Bredenkamp *et al.* 1993).

In addition, due to the cement hydration process a capillary pore refinement at early ages occurs in mortar specimens (Heritage 2001). The hydration process is accelerated by the application of electrical current. These microstructural changes, together with subsequently affected diffusivity and permeability of the matrix, would determine

---

\*In practice, AC voltages (and currents) are always given as rms values. The term rms stands for root mean square, the algorithm used to obtain the DC equivalent value from points on a waveform graph (e.g. sine wave, square wave, triangle wave etc.). The procedure consists of squaring all the positive and negative points on a waveform graph, averaging those squared values, then taking the square root of that average. The relationship between root mean square voltage ( $V_{rms}$ ) and maximum/peak voltage ( $V_{max}$ ) is given by (Boylestad 2016):  $V_{rms} = V_{max}/\sqrt{2}$ . For example, a 25V AC supply means 25V<sub>rms</sub> with the peak voltage about 35.4V.

altered transport properties, as well as long-term performance of a cement-based material. To this end, the aim of this research was to achieve a step forward towards defining the effect of stray current, in view of positive or negative influences, on cementitious material properties.

Various environmental conditions, to which structures may be exposed, were considered. Fig. 1.1 illustrates a scenario where stray current effects can be expected in a real concrete structure. The figure illustrates several exposure condition i.e. sealed, partly and fully submerged condition for a reinforced concrete structure. The stray currents in real practice are hard to measure, while stray current effects on corrosion of steel reinforcement are reported extensively. These effects on concrete bulk properties are normally not considered because they are assumed not to effect the concrete properties significantly. The stray current levels have been reported in the range from less than one Ampere to several Amperes or even tens of Amperes (Chen 2017, Xu et al. 2017, Xu et al. 2016, Kolář 2014). The stray current density levels depend on the cross section/surface area where the currents flow through. For instance, in practical cases stray current levels have been measured between  $1\text{A/m}^2$  and  $1.5\text{ A/m}^2$  (Galsgaard and Nielsen 2006). Sandidzadeh and Shafipour (2012) reported stray current leaks from rails of 1.37 Amperes, of which 0.06 Amperes flow through the reinforced concrete structure and cause severe damage to the steel reinforcement. By considering three different cross-sectional areas of reinforced concrete structures i.e. 1963, 804, and  $314\text{ mm}^2$  (i.e. values from BS EN 10080 (2005)), the stray current density through reinforced concrete structures would be 31, 75 and  $191\text{ A/m}^2$ , respectively.

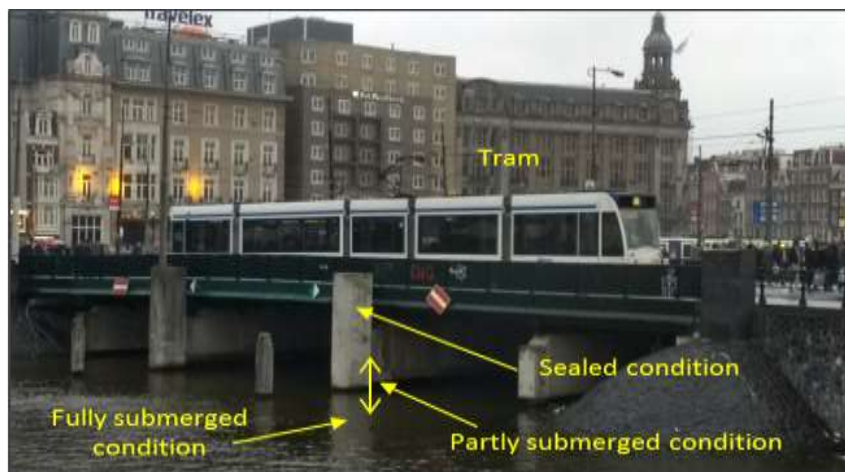


Fig. 1.1 Examples of concrete structures in submerged condition and sealed bulk matrix. Location: in front of the Amsterdam central station, the Netherlands. (Photo: A. Susanto)

High levels of stray current were reported by Sun et al. (2017) from high voltage direct current (HVDC) transmission systems. They pointed out that the current leaking from HVDC transmission system into the earth is 1200A. From the current of 1200A, the stray current flow through buried structures (e.g. water/gas pipeline, reinforced concrete structures) is still 238.8A. By considering the diameter of water pipelines between 30 and 48 inches, the stray current flow through the steel water pipeline will be

in the range of 98 and 527 A/m<sup>2</sup>. A schematic picture of stray current spectrum is given in Fig. 1.2.

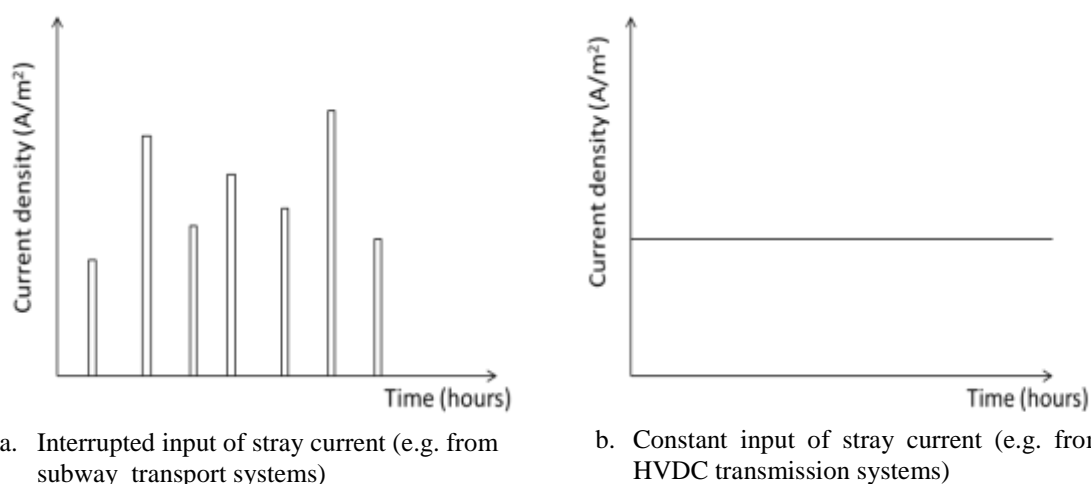


Fig. 1.2 Schematic picture of stray current spectrum: a) Interrupted input of stray current; b). Constant input of stray current.

Estimation of resulting corrosion damage over a certain period of time can be made using Faraday's law, supposed that the magnitude of stray current is known and that there is a uniform mass loss. Since stray current induced steel corrosion is non-uniform (i.e. anodic and cathodic areas result from the stray current outflow and inflow, respectively) such calculations cannot easily be made and are not reported for damage quantification with regard to (reinforced) cement-based materials. More importantly, the cumulative effect of stray current on a bulk concrete matrix is perhaps more significant, considering the fundamental principles and behaviour of a cement-based matrix with age and with respect to environmental conditions. This includes the effect of electrical currents (incl. stray current) on cement hydration, potential leaching-out effects, microstructural and micromechanical properties.

## 1.2 Scope and Objectives

The main objective of this research project was to investigate the effects of stray current on long-term performance of cement-based materials. The results from this work will contribute to a better understanding on the influence of, and consequences from, stray current flow. For instance, a differentiation between beneficial (positive) and detrimental (negative) effects of stray current on cement-based materials was aimed at in this research, which is a point of significant importance for the real practice. The exposure conditions of real structures (as in Fig. 1.1) were simulated, focusing on the following aspects:

- a) Evaluation of the effect of low stray current levels on the properties of cement-based materials (i.e. microstructural, mechanical and electrical properties).

- b) Investigation of the potentially beneficial and/or detrimental effects of stray current on the properties of cement-based materials in different environmental conditions.
- c) Numerical simulations of the effect of stray current flow on the hydration process and temperature development in cement-based materials, and evolution of materials properties.
- d) Assessment of the effect of stray current on materials' properties of different mixtures of hardened, 28-days old, cement-based materials.

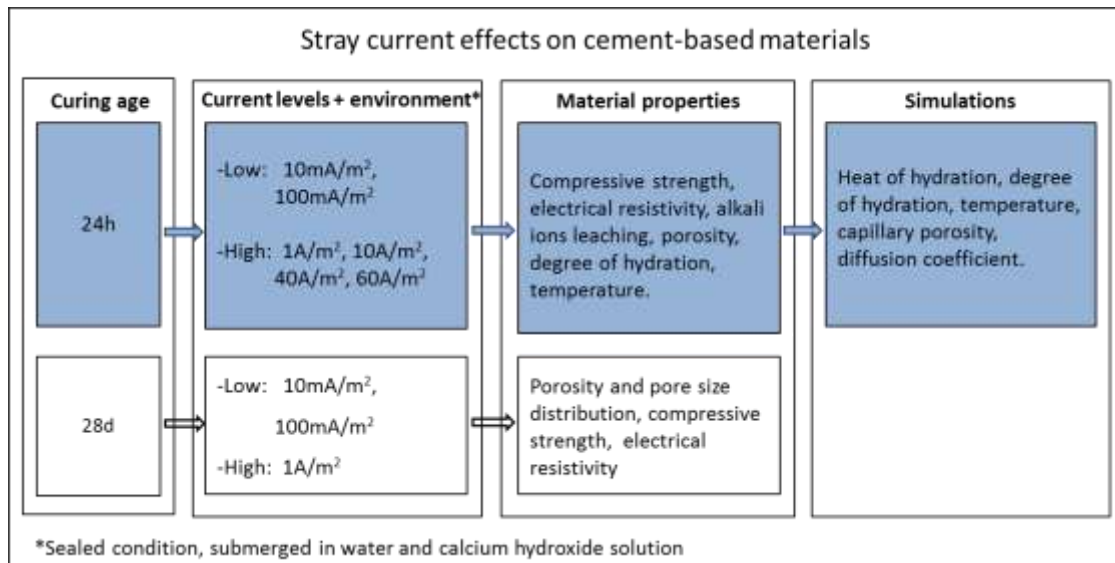


Fig. 1.3 Schematic representation of research strategy of this research

### 1.3 Research strategy

In view of the main objective of this work and to address the aspects of research interest and of practical significance listed in Section 1.2, a research strategy was developed, schematically presented in Fig. 1.3. The research strategy comprised an experimental sequence as outlined below.

- a) Preliminary study to investigate the effect of low level stray current ( $10\text{mA/m}^2$ ) on material properties of hardening mortar specimens in different external environmental conditions. Compressive strength and electrical resistivity development of hardening mortar specimens were measured. Pore structure changes in mortar specimens subjected to stray current flow were evaluated by Mercury Intrusion Porosimetry (MIP) and through Environmental scanning electron microscopy (ESEM) and compared to control (no stray current) conditions. Chemical analysis of the conditioning water (external medium) was also carried out, using Inductive Coupled Plasma spectrometer (ICP-AES). These results were of interest for evaluating possible leaching out of alkali ions in conditions of stray current (or without stray current) for specimens partly submerged in water. Numerical simulation of stray current distribution in the external medium and through the solid (mortar) matrix in partly-submerged conditions was also performed. The results

indicated the potential (voltage) and current density distribution in mortar specimens and were linked to the mechanical and microstructural properties of these specimens in conditions of 10 mA/m<sup>2</sup> stray current.

- b) To quantify the potentially positive and/or negative effects of stray current, a range of stray current was considered (i.e. 100mA/m<sup>2</sup> and 1A/m<sup>2</sup>). Different environmental conditions i.e. sealed condition, partly submerged and fully submerged in water and alkaline medium were considered. The development of compressive strength and electrical resistivity of the mortar specimens were measured. Porosity and pore size distribution of the bulk mortar matrix under stray current flow were determined using MIP and ESEM image analysis and compared to control specimens. Chemical analysis of the conditioning water was performed using ICP-AES to determine changes in alkali ions concentration (Na<sup>+</sup>, K<sup>+</sup> and Ca<sup>++</sup>) due to leaching of ions from the mortar cubes. Chemically bound water in all conditions was measured for calculating the degree of cement hydration.
- c) To quantify the temperature development in cement paste due to stray current, low current density levels (i.e. 10mA/m<sup>2</sup> and 100mA/m<sup>2</sup>) and high current density levels (i.e. 1A/m<sup>2</sup> 10A/m<sup>2</sup> 40A/m<sup>2</sup> and 60A/m<sup>2</sup>) were applied. The heat release in cement paste under low levels of stray current flow was measured using isothermal calorimetry. The heat release data was used to calculate the degree of hydration. Porosity and pore size distribution in the bulk matrix, affected by stray current flow, were characterized using MIP. Numerical simulation and experimental validation were performed to quantify the influence of stray current flow on the hydration process and temperature development in hardening cement-based materials and evolution of materials properties.
- d) To address the influence of stray current flow on the properties of hardened mortar specimens (i.e. initially cured in a fog-room with 98% RH for 28 days), compressive strength, electrical resistivity and pore structure were measured. The results were compared to those of young mortar specimens, after curing in a fog-room with 98% RH for 24h only, to elucidate the effect of curing age. The effect of stray current on the pore size distribution of hardened bulk matrix with different w/c ratio (i.e. 0.35 and 0.5) was also studied. The effect of stray current on porosity and compressive strength of mortar specimens were evaluated and compared with calculated effects.

1

## 1.4 Layout of the thesis

This thesis consists of seven chapters. The layout of the thesis is given in Figure 1.4.

Chapter 1 presents a brief introduction, including an outline of the levels of stray current as encountered in the field, practical implications in real practice and stray current effects on cement-based materials, scope and objectives, and research strategy.

Chapter 2 comprises a literature survey on the state of the art and practice-related challenges for cement-based materials, subject to stray current flow, including stray current through porous materials (e.g. concrete), stray current flow in hardening and hardened cement-based materials, electrical curing of concrete, ion and water transport

due to stray current flow. In addition, the effects of stray current on material properties (i.e. electrical, microstructural and transport properties) are discussed.

Chapter 3 deals with the effects of low level stray current (i.e.  $10\text{mA/m}^2$ ) on microstructural, mechanical and electrical properties of hardening mortar in arbitrary environmental condition (i.e. the hardening mortar specimens were partly submerged in water).

Chapter 4 deals with the effect of stray current flow on the development of material properties of mortar at early ages in water-submerged,  $\text{Ca(OH)}_2$ -submerged and sealed conditions. The tests in various surrounding media aimed at a clear differentiation of a diffusion-controlled process (alkali ions leaching due to concentration gradient between pore solution in mortar specimen and surrounding medium) and a migration-controlled process (ions and water transport in stray current conditions). The effect of stray current on the evolution of material properties of cement-based materials by considering various environmental conditions was examined.

Chapter 5 deals with the effect of stray current flow on the hydration process and temperature development and evolution of materials properties in cement-based materials. Experiments were performed in isothermal condition at  $20^\circ\text{C}$  to investigate heat release and microstructural changes in hardening cement paste due to the effect of stray current on the rate of hydration. In order to quantify effects of stray current on microstructural properties of cement-based materials, the evolution of the capillary porosity of cement paste as a function of the degree of hydration was calculated. The evolution of the capillary porosity of cement paste as a function of the degree of hydration was calculated. Apparent diffusion coefficients were calculated from microstructure parameters (i.e. capillary porosity).

Chapter 6 deals with the effect of stray current on material properties of hardened mortar specimens, cured for 28-days in a fog-room with 98% RH. The effect of w/c ratio, curing conditions and various external environments on the microstructural, electrical and mechanical properties of hardened mortar specimens subjected to stray current were investigated.

Chapter 7 summarizes the results of the research and presents the conclusions. Recommendations for future research topics are also presented.

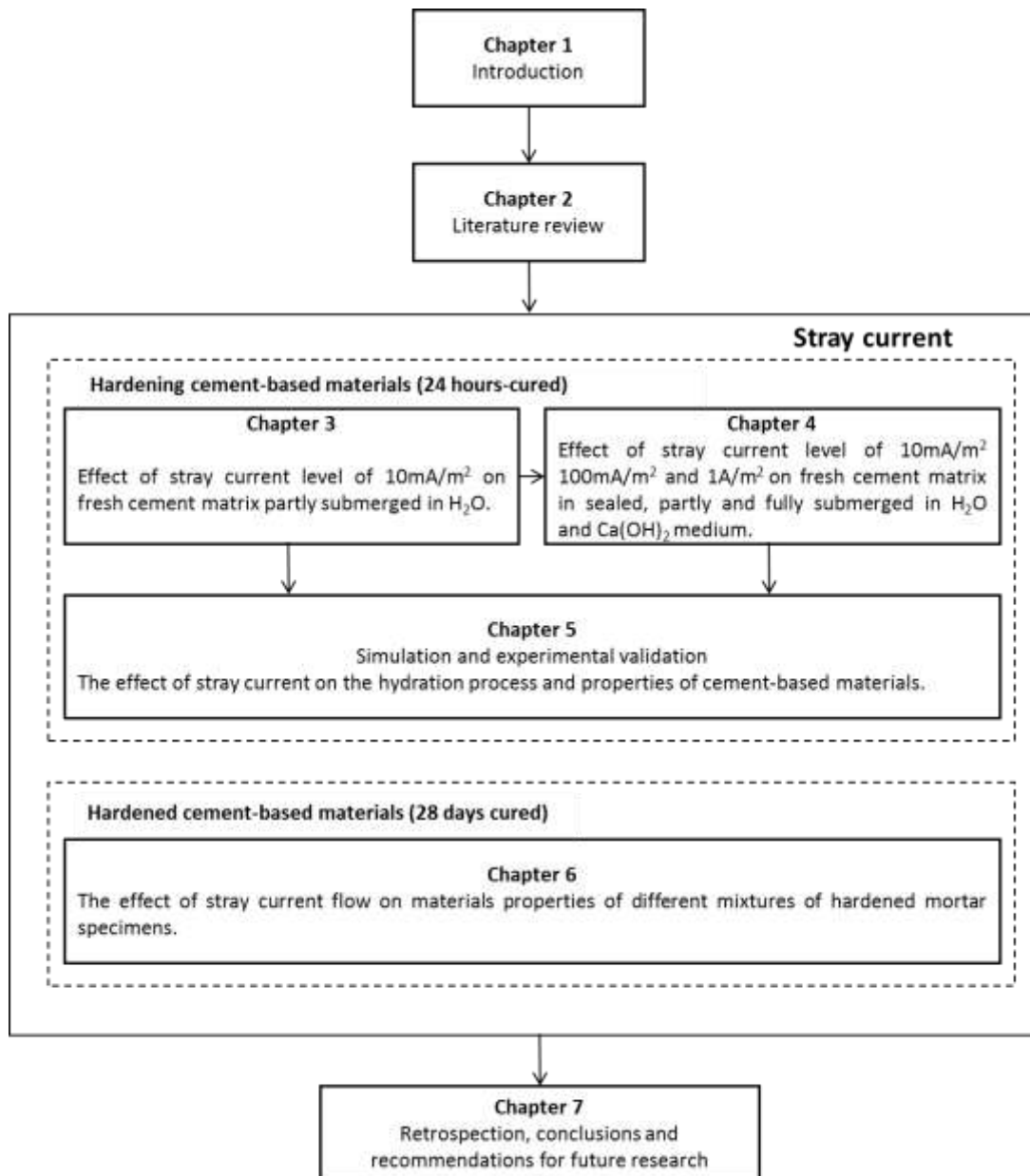


Fig. 1.4 Layout of the thesis

# 2

## **State-of-the-art and practice-related challenges of stray current**

---

This chapter outlines main aspects and considerations with regard to stray current flow through porous materials. First, a literature survey of stray current flow in cement-based systems is presented. This is done by presenting stray current flow in hardening and hardened cement-based materials and electrical curing of concrete. Moreover, the effects of stray current on (the evolution of) material properties (i.e. electrical, microstructural, transport properties) with respect to durability are highlighted.

## 2.1 Stray current flow in cement-based materials

Porous solids, as concrete, contain a continuous solid phase that forms the basis of the porous framework. This porous framework, or pore structure, comprises pores of different number, shape, size, different level of pore interconnectivity, etc. The pore structure can contain fluid, gas, or a mixture of these (Liu and Chen, 2014). The liquid phase, contained by the pore structure, or the pore water, may vary in chemical composition. For an ordinary (e.g. Portland cement-based) concrete, the pore water is predominantly alkali ions and water based. Ions and pore water can be transported within the pore structure under concentration gradients from one to another portion of the pore network i.e. ion and water transport are in this case diffusion controlled. When an external electrical field is applied to a cement-based system, an additional water ion transport mechanism will be initiated i.e. ion and water migration, that can either add-up equally to diffusion controlled transport, or can be a predominant transport mechanism. In the former case, as with diffusion-controlled transport only, chemical alterations in the bulk matrix are possible, e.g. enhanced cement hydration for a material in fresh state (Heritage 2001, Bredenkamp 1993). In the latter case, when migration would be a predominant mechanism, microstructural changes, as for instance variation in the portion of connected and disconnected pore space, would be possibly predominant (Babaahmadi et al. 2015, Susanto et al. 2017). This is because not only enhanced hydration would take place (for a fresh hydration stage), but it is likely that enhanced formation of hydration products in one area of the network, would not be the same as in other locations, considering properties of the pore network as interconnectivity and tortuosity (Layssi et al. 2015, Sengul et al. 2008, Backe et al. 1998). This will result in a non-uniform distribution of connected and disconnected pore space, the consequence of which will be non-uniform electrical properties as conductivity/resistivity of the bulk vs concrete cover for instance (Liu and Shi 2012, Zhang et al. 2018).

In all occasions when a cement-based system is affected by an electrical field, as for instance stray current, conductivity of the material, which is inversely proportional to resistivity, would be affected by ion and water transport as a result of migration. This is because in an electrical field, ions can be forced to drift as a response to that field. The drift velocity is proportional to the magnitude of an electric field (Griffiths 1999). Hence, the magnitude of the electrical field will determine the level of change (if any) in material properties of the cement-based system, e.g. microstructure, electrical properties, micromechanical properties, strength, etc. In other words, since all these properties are determined by cement hydration, any alteration of the hydration process, e.g. due to ion and water migration, would be reflected in altered material properties. In conclusion, if concrete as a porous material in conditions of electrical current flow (stray current respectively) is considered, the main phenomena with regard to ion/water transport are diffusion and migration-related. More details with regard to diffusion and migration are discussed in Section 2.2.2.1.

Electrical conduction in composite porous materials (e.g. in concrete) is related to the mobility of ions in the pore solution. For concrete, the aqueous phase is initially saturated with hydroxyl, sodium and potassium ions, accompanied later on by a smaller concentration of calcium ions. These ions determine and/or affect the electrical conduction. Other soluble ions, such as aluminium, silicates and others are present, but only at a low concentration, and thus don't significantly affect electrical conduction

(Neville 1995). The electrical conductivity, as well as electrical resistivity, of porous materials (e.g. concrete) is significantly affected by the pore network and pore connectivity, conductance of the pore fluid, temperature and degree of saturation.

### 2.1.1 Stray current flow in hardening cement-based materials

A detailed knowledge of the cement hydration process is a prerequisite for understanding the microstructure development in hardening concrete with and without the influence of stray current flow, including pore network characteristics of the cement matrix. Specific conditions, which could exert negative effects, can be, for example, low relative humidity, elevated reaction temperature, electrical (stray) current flow, etc.

Stray current flow through hardening concrete causes an increase in temperature of the hydrating material due to resistive heating, or Joule heating. Basically, Joule heating is a transformation of electrical energy into thermal energy, following the energy conservation principle. The heat generated when stray current flows through the material (e.g. concrete) for a specific time is given by the square of the current multiplied by the product of the resistance of concrete and the time (Halliday et al. 2013). The heat generated, which is reflected in an increase of temperature of the concrete, increases with increasing level of stray current flow. It was reported that temperature increases in cement paste in the range of 2-10°C under applied current density of 10-60A/m<sup>2</sup> (Susanto et al. 2015). The temperature increase due to Joule heating may influence the hydration process and properties of cement-based materials.

Cement hydration is a process involving a series of chemical and physico-chemical reactions. These reactions are accompanied by liberation of heat of hydration, the result of the exothermic chemical reaction between cement and water. The heat generated by cement hydration raises the temperature of concrete. The hydration process depends on the chemical composition of cement, cement fineness, water-cement ratio, and temperature as main factors (Hewlet 2004). The chemical composition of cement is the most important influencing factor. It has been reported that the cement fineness determines the ultimate degree of hydration as well as the hydration rate (Hu et al. 2014; Bentz et al. 2010). As cement fineness is increased, the peak temperature increases (Bentz et al. 2010). Water-to-cement ratio also influences the kinetics of cement hydration. At early stage, cement pastes with higher w/c generally exhibit a higher rate of hydration than the lower w/c pastes. This is due to more water available for the dissolution of reactants and the nucleation/precipitation of hydration products (Bentz 2006).

During the cement hydration process, heat evolution as a result of cement hydration can be measured using an isothermal calorimeter. The rate of heat evolution during cement hydration can be classified in five stages, i.e. dissolution stage, dormant period, acceleration stage, deceleration stage and steady stage (Fig. 2.1) (Mindess et al. 2003). Stage 1 represents the dissolution stage, which starts immediately after the contact of cement with water, where dissolved ions and water react with Tricalcium aluminate (C<sub>3</sub>A) and gypsum. The rapid early reaction rate in Stage 1 is followed by a period of low reactivity in Stage 2, known as the dormant stage. The length of the dormant period depends on the fineness of the cement, the temperature, the presence of retarders or accelerators and the chemical composition of the cement (including the gypsum content and admixtures (Odler et al. 1979; Livingston et al. 2001). This stage will generally not exceed 5 hours. In Stage 3, the alite (C<sub>3</sub>S) and belite (C<sub>2</sub>S) phases start to hydrate and

release heat. Cement setting begins and heat generation is remarkably accelerated. In stage 4 (i.e. deceleration stage), the rate of heat release slows down gradually as the amount of available, un-hydrated, cement declines. A shoulder/second peak can be observed in this stage (Fig. 2.1), which can be attributed to a renewed formation of ettringite as a result of secondary  $C_3A$  hydration. In the stage 5 (the steady stage), the rate of hydration is very low and proceeds until reaching a steady state.

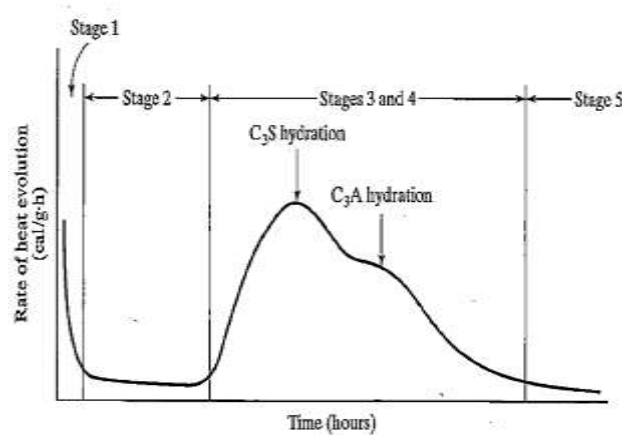


Figure 2.1 Rate of heat evolution during hydration of Portland cement (Mindess 2003).

Temperature has two effects on hydration kinetics. The first effect is an increase of reaction rate. Secondly, an increase of the amount of hydration products at higher temperature, which slows down the permeation of free water through the hydration products (Pimenta Teixeira et al. 2016, Lothenbach et al. 2007, Escalante-Garcia 2005). The maximum temperature in hardening concrete structures should not exceed  $60^{\circ}\text{C}$ , which is related to the risk of internal damage, e.g. crack formation (DANISH Ministry of Transport 1985). In line with this result Odler et al. (1986) found that curing temperatures above  $50^{\circ}\text{C}$  result in a lower ultimate strength of concrete. The effect of temperature on properties of cement-based materials has been investigated by many researchers. Elkhadiri et al. (2009) reported that curing temperatures from  $22$  to  $55^{\circ}\text{C}$  increase the hydration rate and strength development at early age. However, higher temperatures, up to  $85^{\circ}\text{C}$ , have an adverse effect on long-term strength. Experimental results showed that after 28 days the porosity was more than 20 % higher due to increasing meso- and macro-porosity, which would explain the decline in strength of the pastes cured at  $85^{\circ}\text{C}$ . Brue stated that high curing temperatures result in coarsening of the pore structure due to ettringite dissolution and C-S-H alteration (Brue et al. 2012). In agreement with Brue, Van Breugel (1991) pointed out that reaction temperatures beyond  $20^{\circ}\text{C}$  result in less outward growth of the reaction product and hence a higher capillary porosity.

Beside temperature effects, electrical current flow in cement-based materials may also effect ion and water transport. In hardening cement-based materials, migration involves transport of charged ions and complex ions (Thaker 2012). Aghajani et al. (2015) and Saito et al. (2000) reported that electrical current accelerates alkali ions leaching in cement-based materials submerged in water, in which concentration gradient between pore solution in cement-based materials and external medium are present

(Aghajani et al. 2015, Saito et al. 2000). With regard to alkali ions leaching, Babaahmadi et al. (2015) pointed out that  $\text{Na}^+$  and  $\text{K}^+$  ions have higher solubility and mobility in the pore solution than that of  $\text{Ca}^{2+}$  ions. Consequently,  $\text{Na}^+$  and  $\text{K}^+$  ions will dominate the diffusion and/or migration process more significantly in the early hydration stages, and will not vary substantially on later stages. Alkali ions leaching promotes coarsening of the pore structure, leads to increase transport properties (e.g. permeability, diffusivity) and decrease in mechanical properties (Roessler et al. 1985, Young et al. 1988). Under electrical current flow, the concrete bulk material undergoes changes in materials properties (i.e. mechanical, electrical and microstructural properties), thus influencing the overall performance of the concrete.

### 2.1.2 Stray current flow in hardened cement-based materials

Dry/hardened concrete has a relatively high electrical resistivity (i.e. in the order of  $10^5$  Ohm.m) compared to that of wet concrete (with electrical resistivity in the order of  $10^1$  Ohm.m) (Gjorv et al. 1977, Tuuti 1982). Therefore, hardened concrete acts as an insulator. In an insulator, internal electric (ionic) charges do not flow freely. Consequently, only little electric current will flow through it under the influence of an electric field. Accordingly, the stray current is more difficult to “pass through” hardened bulk matrix than in fresh or young concrete. This can be attributed to higher electrical resistivity of hardened concrete due to a denser matrix that could resist the stray current flow.

In saturated (water submerged) condition, stray current may have a more significant effect on material properties of hardened concrete due to decreasing electrical resistivity of the hardened concrete. Saito et al. (2000) found that an electrical field accelerated leaching of  $\text{Ca}^{2+}$  ions from the mature/hardened mortars (after 28 and 56 days cured in a moist condition) in contact with water, leading to increased water permeability and reduced compressive strength of specimens. In agreement with Saito, Huang et al. (2016) point out that an electrical field promotes dissolution of portlandite and decomposition of C–S–H gel due to leaching. As a consequence, it will increase the porosity of concrete, resulting in a decrease in the electrical resistivity and an increase in the permeability of hardened concrete (Aghajani et al. 2015). These effects would be more pronounced in hardened concrete with a high porosity, i.e. with a high w/c ratio. Huang et al. (2016) also reported that an electrical field can accelerate other degradation mechanisms, for instance sulphate attack induced deterioration of hardened mortar. Furthermore, the sulphate attack in combination with an electrical field accelerated the damage process of hardened mortars compared with only sulphate attack.

### 2.1.3 Electrical curing of concrete

Curing is a process of controlling the adequate moisture content and temperature in concrete at early ages during concrete hydration. Proper curing plays an important role to obtain the desired properties (e.g. strength) for its intended use (James et al. 2002). In addition, it can reduce life-cycle cost. Heritage (2001) reported that concrete specimens with different w/c ratios under direct electric curing (DEC), reach higher compressive strength than that of normally (non DEC) cured samples. He found that concrete under direct electric curing (DEC) has a compressive strength about 26 MPa after 1 day which is about 71% of its 28 days compressive strength. Furthermore, the samples showed to

be denser, but tend to have a less uniform structure with coarser pores distributed more prevalent/widespread. Conversely, improper curing results in undesired effects, such as lower strength, cracking, low resistance to weathering, high permeability, dusting (Neville 1995), ACI 1981, ACI 1982). Basheer et al. (2001) stated that improper curing is one of the factors that have reduced the service life of many structures.

The required period of curing of concrete depends on several factors, such as mixture proportions, specified strength, size and shape of the concrete member, environmental and exposure conditions (IS 2000). In general, 28 days of moist curing is required, or recommended, for cement-based materials, resulting in properties (both mechanical and microstructural) sufficiently developed for the required performance.

In order to achieve high early age strength of concrete, accelerated curing of concrete is commonly used especially in the prefabrication industry to reduce the cycle time resulting in cost-saving benefits (Erdem 2003). Various methods of accelerated curing of concrete have been used, including steam curing, autoclaving (high pressure steam curing), microwave heating, hot water, hot air heating, infrared heating, and electrical curing (Bredenkamp et al. 1993, Heritage 2001, John and Narendra 2004, Wilson and Gupta 1996). Electrical curing can be performed by using several techniques (ACI 1992, Kosmatka et. al 2002), such as: (1) use of the concrete itself as the electrical conductor, (2) use of reinforcing steel as the heating element, (3) use of a special wire as the heating element, (4) electric blankets, and (5) the use of electrically heated steel forms (presently the most popular method).

In DEC curing, an electrical current is passed directly through the cement-based systems to produce a Joule heating effect, thus increasing the rate of cement hydration. Bredenkamp (1993) stated that DEC is one of the most energy efficient methods for accelerated curing of concrete and after the initial investment for equipment, the running costs of direct electric curing are substantially lower than that of externally applied heat curing (steam, autoclave, etc.). The energy cost of DEC with field strength between 300 and 500 V/m and rate of energy input 76kWh/m<sup>3</sup> is about 5% of the total cost for one m<sup>3</sup> of concrete. Kafry (1980) stated that energy consumed per cubic meter of concrete is 30-40 (kWh/m<sup>3</sup>), while other investigators mentioned about 50-60 (kWh/m<sup>3</sup>) (Wadhwa et al. 1987). Electrical curing has been used in several applications, for instance to accurately control the reaction temperature, and is a reliable system requiring minimal labour. Electrical curing methods are used primarily in the precast concrete industry.

## **2.2 Stray current effect on material properties with respect to durability**

### **2.2.1 Electrical properties of cement-based materials**

Electrical resistivity measurements are a rapid and non-destructive testing method to assess durability of concrete structures. Electrical resistivity is affected by several factors, e.g. concrete mixture (e.g. binder/cement type, water to cement ratio, aggregates, pozzolanic admixtures) and environmental conditions (e.g. temperature, humidity) (Sengul 2013). The electrical resistivity of concrete strongly depends on the microstructure of the cement matrix (i.e. pore structure, porosity, and pore size distribution) and the concentration of ions and their mobility in the pore solution (Hunkeler, 1996; Bürchler, et al., 1996). The electrical current is carried by the

dissolved charged ions in the pore solution in the concrete. Therefore, all factors affecting the pore structure of the concrete (i.e. cement type, water/cement ratio, pozzolanic admixtures) also affect the electrical resistivity of concrete.

According to Elkey (1995), the cement type has an impact both on pore structure characteristics and the pore water chemistry. Consequently, concrete cast with two different cement types may have different electrical resistivity. Hammond (1955) showed that a high alumina cement paste had 10 times higher electrical resistivity than OPC pastes with the same water-to-cement ratio and moist curing condition. Ahmed and Ragai (2013) also showed that ordinary Portland cement pastes tend to have lower electrical resistivity than blended cement pastes. This can be explained by the hydration products of the supplementary cementitious materials, e.g. fly ash or blast furnace slag, lead to a more refined pore structure.

The water-to-cement ratio (w/c) is another important factor that influences the electrical resistivity of concrete. This is because the w/c ratio plays an important role in the microstructure of the cement paste. An increase in w/c ratio causes a higher porosity and a lower electrical resistivity (Monfore et al. 1968). Monfore and Hughes also investigated the influence of aggregate on electrical resistivity of concrete. They found that the electrical resistivity increased with increasing aggregate content. This can be explained by the much higher electrical resistivity of aggregate than that of cement paste (Monfore 1968; Hughes et al. 1985). The resistance of normal aggregates is approximately 100 times higher compared to that of cement paste (Monfore 1968).

The last factor that influences the electrical resistivity is the environment (i.e. temperature and moisture conditions). According to Layssi et al. (2015), at high temperatures the viscosity of the electrolyte in the pores or pore solution in the concrete is lower, leading to accelerated ionic mobility. As a consequence the electrical resistivity will decrease. Regarding to moisture content, Whiting et al. (2003) stated that the electrical resistivity of concrete increases with decreasing moisture content in the concrete. Conversely, a higher moisture content results in a lower electrical resistivity. Electrical resistivity of cement-based materials can be measured using various setups, e.g. two probes measurements, four probes measurements (Wenner configuration), involving the rebar network as one electrode, etc., are generally used. A review of these setups can be found in detail in (Susanto et al. 2013, Polder et al. 2000, Singh 2013). The general approach to record resistance values of concrete is by applying an alternating DC current of 1mA at a frequency of 100 Hz to 1 kHz through a cross section of the specimens, and then the electrical potential between two points/electrodes is measured (or vice versa). Basically the resistance  $R$  of a specimen is determined by Ohm's law,  $R = V/I$ , where  $V$  is the electrical potential (in volts) and  $I$  is the applied current (in Ampere).

The two-probe measurement is the simplest method of measuring electrical resistivity – a schematic illustration is presented in Fig. 2.2. In this method a DC current is applied to the specimens via metal plates with surface area  $A$ , equal to the sides (cross-sections) of the specimen. The electrical potential across the specimens is measured and the electrical resistivity is calculated using the equation:

$$\rho = \frac{RA}{l} \quad (2.1)$$

where  $\rho$  is the electrical resistivity of the sample (in Ohm.m),  $R$  is the resistance (in Ohm),  $A$  is the cross-section of the sample (in  $\text{m}^2$ ), and  $l$  is the length of the sample (in m).

The two-probe method is often used to measure electrical resistivity of concrete in lab tests. It is a relatively simple test and can be used to precisely define geometrical constants and minimize other contributing factors in measurements. For example, the two probe method can be executed at constant relative humidity or in sealed conditions, can overcome gradients of humidity and can be employed on specimens that can be further used for other tests (e.g. compressive strength).

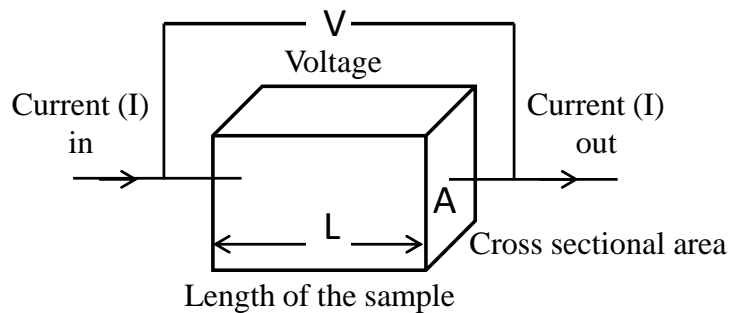


Fig. 2.2 Electrical resistivity measurement by two probes method

## 2.2.2 Microstructural parameters with respect to transport properties

Durability of cement-based materials can be defined as its ability to resist weathering action, chemical attack, abrasion, or any other process of deterioration. Durability of cementitious materials strongly depends on transport properties, such as permeability and diffusivity. The pore structure of hydrated cement paste is a decisive physical parameter that controls those two properties (Larbi 1993; Neville 1995). The transport properties of cement-based materials are further discussed in the following section.

### 2.2.2.1 Transport properties and mechanisms in cement-based materials

#### a. Permeability

Permeability of concrete determines how fast a fluid will flow through concrete when a pressure is applied (Claisse 2014). Water permeability of cement paste is governed by its microstructure (i.e. porosity, pore size distribution, connectivity and shape of pores) (Hughes 1985). Permeability naturally decreases with increasing cement hydration. Several methods are used to measure permeability. From a macroscopic point of view, permeability of cement paste can be determined by using Darcy's law (Mehta and Manmohan 1980, Hughes 1985). It can also be calculated from microstructural parameters obtained from mercury intrusion porosimetry (MIP) measurements i.e. the threshold pore diameter, the total porosity, and the effective porosity (Garboczi 1990). In addition, permeability of cement paste can also be determined quantitatively from image analysis of 2D sections of BSE images (Ye 2003, Zhang 2013).

## b. Diffusion

Diffusivity of concrete refers to the movement of ions in the pore solution due to a concentration gradient or chemical potential (Tang 1996). It is commonly determined by the diffusion of chloride ions. Chloride ion transport in concrete is mainly linked to corrosion of steel reinforcement. The apparent diffusion coefficient of concrete  $D_{ap}(t)$  can be calculated using the following equation (Maage et al. 1996):

$$D_a(t) = D_o \left( \frac{t_o}{t} \right)^n \quad (2.2)$$

where  $D_o$  is the chloride diffusion coefficient at the reference time  $t_o$  (usually 28 days age),  $n$  is the ageing factor ( $0 \leq n \leq 1$ ) that refer to densification of the pore structure with time, including the effect of ongoing hydration, and  $t$  is the age of concrete. The apparent diffusion coefficient of concrete subject to stray current flow will be further elaborated and calculated in Chapter 5, section 5.6.3.2.

## c. Migration

Since natural diffusion is a very slow process, accelerated diffusion test methods are also used, e.g. the rapid chloride migration (RCM) test, where chloride ions migration, as a predominant transport mechanism due to the applied voltage in the RCM cell, is in parallel with diffusion of chloride ions (details of the RCM tests are as described in (Audenaert et al. 2010; Mangat et al. 1994).

In condition of stray current flow, permeability and diffusivity of cement-based materials may change. Aghajani et al. (2016) reported that concrete samples submerged in distilled water for 30 days subjected to a DC voltage of 50 V cause an accelerated leaching of portlandite due to the concentration gradient between the pore solution in the concrete and the external medium (distilled water). Consequently, it increases capillary porosity of concrete resulting in an increase in permeability of the concrete. This phenomenon can be explained by migration of calcium and hydroxyl ions out of the pore solution and the dissolution of  $\text{Ca}(\text{OH})_2$  from the hydrated cement.

### 2.2.2.2 Determination of microstructural parameters of cement-based materials

There are several methods to determine microstructural parameters of cement-based materials including Mercury Intrusion Porosimetry (MIP), Nitrogen Sorption, Scanning Electron Microscopy (SEM) image analysis (Ye 2003). In this study, only MIP and SEM images analysis will be discussed briefly in the following.

#### a) Mercury intrusion porosimetry (MIP)

Mercury intrusion porosimetry (MIP) is a technique commonly used for characterizing the pore structure (i.e. the porosity and the pore size distribution) of cement paste (see Fig. 2.3) (Diamond 1971, Aligizaki 2006). The total porosity is defined as the ratio between the total volume of intruded mercury at the maximum pressure during the test and the bulk volume of the specimen. The effective porosity can be defined from the volume of mercury removed during extrusion or the total porosity minus the inkbottle porosity (see Fig. 2.3a) (Ye 2003). Effective porosity is the most important parameter for the transport properties of concrete. The pore size distribution is defined as the pore

volume per unit interval of pore diameter (Ritter and Drake 1945). For cement paste and mortar specimens, several peaks can be found in the pore size distribution curve (see Fig. 2.3b). These peaks are the so-called critical pore diameters (Cook *et al.* 1999). According to Katz and Thompson (1986), the critical pore diameter can also be identified experimentally from the inflection point in the cumulative intrusion curve. The MIP technique has certain limitations in view of both MIP tests as such but also within interpretation of the experimental results. These limitations have been reported by Diamond (1971) and Cook (1993).

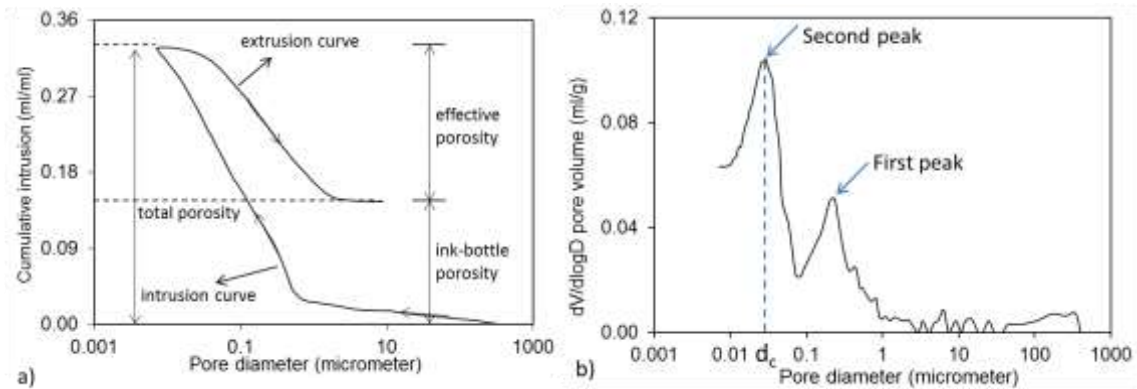


Figure 2.3 Mercury intrusion and extrusion hysteresis (a) and pore size distribution differential curve of mortar specimen with critical pore diameter ( $d_c$ ) (b) (After Ye 2003).

### b) Scanning Electron Microscopy (SEM) image analysis

Because of the various limitations of the MIP technique (Diamond 1971, Cook 1993), other techniques for characterising the pore structure have been proposed. Among these is the application of scanning Electron Microscopy (SEM) to derive pore structure parameters, providing a reliable alternative to observe the microstructural parameters of cement-based materials. Back scattered electron (BSE) images have been used to study the microstructure of cement paste (Lange *et al.* 1994; Scrivener 1989; Ye 2003). Porosity and pore size distribution of specimens can be quantified from BSE image analysis. Scrivener (1989) stated that macroscopic properties, such as permeability, can be determined from 2D sections. A general methodology used for BSE image analysis of pore structure of cement based materials was reported by Ye (2003), Hu (2004) and Koleva (2007). Pore size distributions are obtained based on mathematical morphology transformations by using a sequence of similarly shaped structuring elements of increasing size (Serra 1982).

## 2.3 Conclusions and outlook

In this chapter, a brief literature survey on the topic of stray current flow through porous materials, i.e. hardening and hardened cement-based materials, has been presented. Electrical curing of concrete was briefly described. Stray current effects on material properties with respect to durability were discussed. It was reported in literature that the levels of stray current flow through reinforced concrete range from low to high levels, i.e. between  $10\text{mA/m}^2$  and  $70\text{ A/m}^2$ . The effect of stray current on cement-based

materials can be positive (e.g. accelerate hydration process) and/or negative (e.g. increase porosity, decrease strength and durability, etc.).

Those effects can be attributed to acceleration of cement hydration due to Joule heating and enhanced ionic migration under stray current. Joule heating may increase the rate of cement hydration, resulting in an increase of the rate of strength development, which is a positive effect. However, at higher reaction temperatures, eventually due to Joule heating, coarsening of the capillary pore structure may occur, resulting in a lower compressive strength and an increase in permeability of cement-based materials, which jeopardizes the concrete's durability.

Electrical current may accelerate ionic migration from the pore solution of a concrete specimen towards the external medium, which will affect the material properties. This effect depends on the intensity/level of the applied electric field and the maturity of the cement matrix. Negative effects of stray current due to alkali ion leaching may occur due to concentration gradients between concrete and external environment (e.g. underground concrete structures in contact with water/soil). As a consequence, mechanical properties of concrete may decrease due to coarsening of the capillary pore structure. Conversely, if the concentration gradient between concrete and the external environment is not present, a positive effect of stray current may be expected at early ages, i.e. accelerated cement hydration and faster strength development.

More detailed research needs to be done, including:

- Experimental tests to investigate the effect of low level of current density (i.e. 10 mA/m<sup>2</sup>) on the properties of hardening cement-based materials in (partly) saturated and sealed conditions.
- Experimental approaches to quantify the potentially beneficial and/or detrimental effects of stray current on cement-based materials in different surrounding mediums (i.e. sealed conditions, partly and fully submerged conditions).
- Numerical simulations and experimental validations to quantify the effect of stray current on the hydration process and temperature development in hardening cement-based materials and evolution of materials properties (i.e. porosity, strength and diffusivity).
- Numerical simulations to estimate the effects of stray current levels on generated temperature field and associated probability of thermal cracking in real-size hardening structural elements.
- Study on the effect of stray current on materials properties of different mixtures, i.e. with w/c ratios 0.35 and 0.5, of hardened cement-based materials in different surrounding medium.

All these aspects will be addressed in the following chapters.



## Hardening cement-based materials properties in conditions of stray current\*

---

**Abstract:** This chapter presents a comparative study on mechanical properties, electrical resistivity and microstructure of hardening mortar specimens under DC stray current, compared to hardening mortar in rest (no current) conditions. The hardening mortar specimens were half immersed in tap water. Monitoring was performed from 24h after casting until 84 days of cement hydration. A low level of stray current density (i.e. 10 mA/m<sup>2</sup>) was chosen as a simulation regime. This current density level was 10 times higher compared to the lowest reported level of stray current in practice (i.e. between 1 and 1.5 mA/m<sup>2</sup>). Additionally, numerical simulation of the stray current distribution was performed, meant to serve as a basis for further elaborated modelling of the level of current density that could exert significant microstructural alterations in a bulk cement-based matrix.

---

\*This chapter is based on:

1. Susanto, A., Koleva, D. A., Copuroglu, O., van Beek, K., and van Breugel, K. (2013). Mechanical, electrical and microstructural properties of cement-based materials in conditions of stray current flow. *Journal of Advanced Concrete Technology*, 11(3), 119-134.

### 3.1 Introduction

Stray current is a current flowing in an electrolyte (soil and water respectively) that arises from metal conductors in these media and is produced by electrical installations. It can be the result of direct current (DC) or alternating current (AC), predominantly with a frequency of 50 Hz (public electricity supply) or 162/3 Hz (traction power supply). The flow of stray current has to be avoided or minimized not only because of safety concerns, but also because of the possible negative effects on buried materials and structures. In order to minimize these effects and risks of physical and assets damages, standards and safety regulations, e.g. EN50122-1 1997, EN50122-2 1999, EN50122-3 2010, IEC61439, specify the maximum permissible electrical current related to DC electrified railways, traction systems, earthing and returning circuits, interfaces between AC and DC installations. EN50122-2 stipulates maximum values of 60 V for DC currents and 25 Vrms for AC currents for the accessible (step) voltages as function of time during an electrical failure of public transport equipment, ancillary equipment (fixed installations) and electronic applications for railways. EN50122-3 states lower maximum permissible voltages of 25 V. Except the above general possibilities for stray current flow, there are a number of undesirable stray current sources, including foreign cathodic protection (CP) installations, DC transit systems, subway, streetcars, welding operations, electrical power transmission systems. Whereas safety regulations are strictly monitored, the materials' properties on microstructural levels are not as widely studied and reported.

Regarding steel and reinforced concrete structures, apart from environmental conditions and other factors that can significantly compromise corrosion resistance, stray DC and/or AC currents can be corrosion-initiating or corrosion-contributing factors (Bertolini et al. 2007, Wu et al. 2011, Zhiguang et al. 2011, Yang et al. 2008, Tang et al. 2010). Stray currents tend to enter a buried steel or reinforced concrete structure in a certain location, which becomes a cathodic site and hydrogen gas is produced at this entering point (Kish 1981). The current leaves the structure on another location, which becomes anodic and corrosion initiation or severe corrosion propagation occurs (Bertolini et al. 2007, Wu et al. 2011, Zhiguang et al. 2011, Yang et al. 2008, Tang et al. 2010, Kish 1981, Merrick 1994).

With respect to corrosion initiation and propagation, including negative effects of stray currents but also as a controlling factor for stray current distribution, electrical resistivity is a parameter with high significance. In fact, the principle to deal with stray current distribution in the engineering practice is related to adjusting electrical resistivity levels (Whiting et al. 2003). For reinforced concrete structures the ionic conduction path is essentially the pore network of the concrete bulk matrix. Resistivity values of less than 50 Ohm.m can support a rapid steel corrosion process; resistivity for Ordinary Portland cement (OPC) concrete for air-dry condition and w/c ratio of 0.5 is reported to be 23 Ohm.m (Whiting et al. 2003, Brown 1980). High resistance to the passage of current, or dry condition, are unable to support ionic flow, hence corrosion is minimal if occurring at all (Brown 1980). Corrosion can be limited by increasing concrete resistivity to above 200 Ohm.m (Tremper et al. 1958, Vassie 1980, Alonso et al. 1988). For aggressive environments and/or actively corroding steel, concrete resistivity needs to be higher than 500 Ohm.m - 1000 Ohm.m (Broomfield et al. 1993, Broomfield 1997) in order to account for reduced or minimum corrosion rates.

Clearly, electrical resistivity is a parameter, influencing both corrosion phenomena and stray current distribution and as such needs constant attention. Logically, if any

external influence affects the electrical or microstructural properties (and vice versa) of a concrete/reinforced concrete structure, not only corrosion-related issues but also susceptibility to detrimental effects of current flow can be increased or decreased. It is therefore important to define thresholds for the negative or possibly positive influence of electrical current flow on concrete/reinforced concrete microstructure.

### 3.2 Technical background

So far, the effect of stray currents has mainly been investigated in terms of steel corrosion: the mechanisms of corrosion initiation on initially passive reinforcement and the effects on already corroding reinforcement have been both reported (Kai et al. 2011, Chen et al. 2012). In a few extreme cases, severe structural damage was observed and recorded as a result of stray current leakage (Chen et al. 2012, Ding et al. 2008, Lingvay et al. 2011, Bertolini et al. 2004, Shreir et al. 1994, Jones 1978, Hamlin 1986). The influence of several accompanying factors such as: cement type, AC or DC current, current density, interruptions in the current circulation, as well as coexisting chlorides were also reported (Chen et al. 2012, Ding et al. 2008, Lingvay et al. 2011, Geng et al. 2008). AC currents are far less detrimental than DC currents, even at high current densities of  $50 \text{ A/m}^2$ . In contrast, DC would dramatically decrease bond strength within a few months at current density levels between 1 and  $10 \text{ A/m}^2$  (Bertolini et al. 2007, Duranceau et al. 2011, Velivasakis et al. 1998, Chang 2003, Marcotte et al. 1999). The presence of even small amounts of chlorides e.g. 0.2 to 2 wt.%, leads to a remarkable decrease in the charge required for corrosion initiation (Bertolini et al. 2007). Numerical simulation for the influence of stray current and modelling the performance of reinforced concrete structures with this regard are reported (Yu-qiao et al. 2010, Peelen, Smulders, Steyn et al., Liu et al. 2011, Kerimov et al. 2006, Kim et al. 1999, Brichau et al. 1996, Weyers et al. 1998, Liang et al. 1999, Liang et al. 2002, Andrade 2010). Clearly, the degradation of cement-based systems due to stray current and chloride penetration followed by corrosion has been largely recognized as a serious problem in civil engineering for many years (Bertolini et al. 2007, Kish 1981, Whiting 2003, Brown 1980 and references therein). Even, the hydrolytic degradation of cement-based materials via the application of voltage/current regimes in the range of 25 V and current densities not exceeding  $1 \text{ A/m}^2$  has long been recognized (Wittmann 1997, Saito et al. 1992). However, the majority (if not all) of related works are not reporting any in-depth investigation on the microstructural properties of the bulk cementitious matrix i.e. most of the reported studies are with respect to corrosion issues only.

Since microstructural properties determine mechanical properties, as well as chloride diffusivity and therefore corrosion initiation, the alterations of the cement-based bulk matrix cannot be neglected and deeper investigation is needed in order to properly predict the behaviour of reinforced concrete in the above discussed environments. Within previous studies, related to impressed current CP for reinforced concrete, as well as DC current regimes as simulation of CP only (Koleva et al. 2008 (1-3)), it was found that current densities in the range of  $5\text{-}30 \text{ mA/m}^2$  result in microstructural alterations of the bulk mortar and concrete matrix. The outcomes depend on the hydration stage and environmental conditions. These studies were mainly related to corrosion and CP. Therefore a systematic investigation on the influence of

current flow on cement-based microstructure and definition of current limits, exposure conditions and time scales was not previously performed and is still lacking in the reported literature.

The emphasis in this chapter is on the mechanical and electrical properties and microstructural characteristics of plain mortar, subjected to DC stray current flow. The DC current regime of  $10 \text{ mA/m}^2$  was chosen as a start-point investigation (current ranges of  $100 \text{ mA/m}^2$ ,  $1 \text{ A/m}^2$  and more than  $10 \text{ A/m}^2$  are on-going). Numerical simulation of the stray current distribution was performed and coupled to the bulk matrix properties. These outcomes will further serve as a basis for predicting stray current density distribution and resulting electrical and microstructural properties of cement-based systems.

### 3.3 Materials and methods for experimental studies

#### 3.3.1 Materials

Mortar cubes of  $40 \times 40 \times 40 \text{ mm}^3$  (Fig. 3.1) were cast from OPC CEM I42.5N, water-to-cement ratio of 0.5 and cement-to-sand ratio of 1:3. The chemical composition (in wt. %) of CEM I 42.5N (ENCI, NL) is as follows: 63.9% CaO; 20.6% SiO<sub>2</sub>; 5.01% Al<sub>2</sub>O<sub>3</sub>; 3.25% Fe<sub>2</sub>O<sub>3</sub>; 2.68% SO<sub>3</sub>; 0.65% K<sub>2</sub>O; 0.3% Na<sub>2</sub>O.

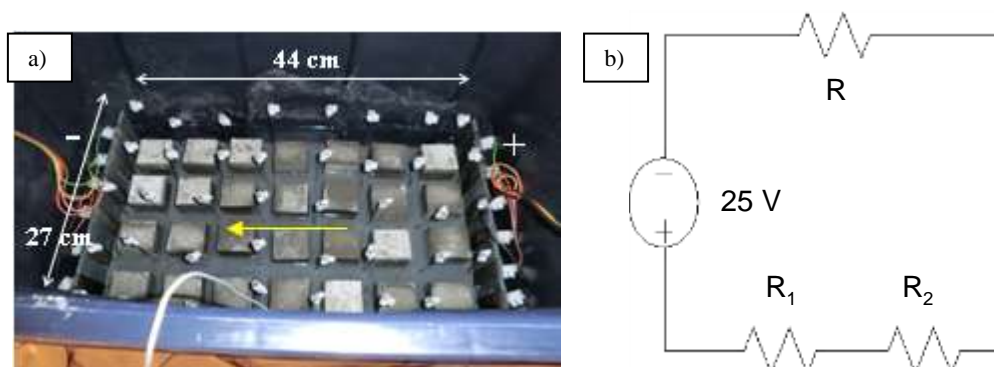


Fig. 3.1 (a) Experimental set-up for group S; (b) electrical circuit, where  $R_1=120 \text{ k}\Omega$  and  $R_2=20 \text{ k}\Omega$  are current adjusting resistances.

Two groups of specimens were monitored: group R – reference/control group (no current flow involved) and group S – “stray current” group (mortar cubes subjected to stray current flow). Both groups were tested from 1 day until 84 days in two replicate series of tests. The mortar cubes from groups R and S were half immersed in tap water - aqueous environment was necessary to ensure electrical conductivity for the S group, whereas an accurate comparison requires equal environmental condition for R group. After casting and prior to conditioning, the specimens were cured in a fog-room with 98% RH, 20°C for 24 hours; after de-moulding they were positioned in the relevant containers, Fig. 3.1, without – group R and with – group S current flowing in the medium.

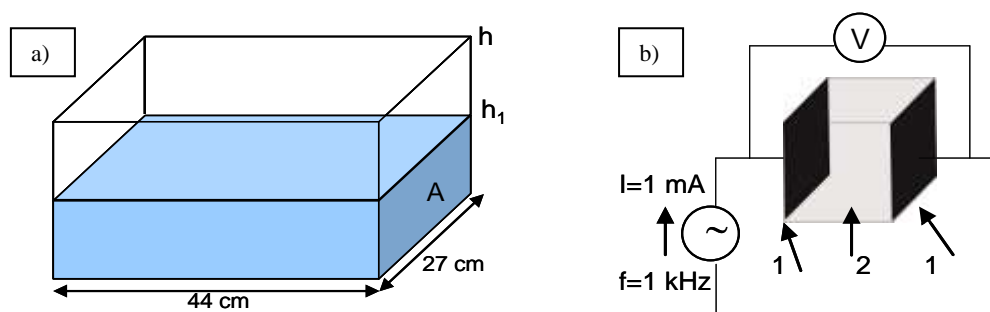


Fig. 3.2 (a) Schematic presentation, including geometry of the container and current flow direction, where  $h=4$  cm,  $h_1=2$  cm,  $A=27 \times 2$  cm; (b) schematic of the electrical resistance measurement where 1 and 2 titanium plate (mesh) and mortar cubes, respectively.

### 3.3.2 Current regime

A simulation of stray current was achieved by “injecting” a DC current at the level of  $10 \text{ mA/m}^2$ , Fig. 3.1. The relevant surface area was calculated based on the geometry of the set-up, essentially the cross section A, Fig. 3.2a), of the environmental medium. This allows further estimation of cumulative current, flown through the mortar cubes, as stray current in the medium. A negative and a positive terminal were connected to a 25V source, the current level was adjusted via resistors in the circuit, Figs. 3.1b) and 3.2a) i.e. the cubes in the container are positioned in aqueous environment, where controlled stray DC flows throughout the experiment for 84 days.

### 3.3.3 Test Methods

#### 3.3.3.1 Compressive strength

Standard compressive strength tests were performed at the hydration ages of 24h, 3, 7, 14, 28, 56 and 84 days. The compressive strength tests (using CE04 MATEST Srl machine, Italy) were performed on air-dry specimens i.e. at each relevant hydration stage three replicates of each group were taken out from the conditioning set-up, cloth-dried and tested within a 30 min time interval. Before the test, a loading speed of 1,5 MPa/s and maximum load of 300 kN were set. The maximum applied load on the specimen was recorded and the compressive strength was calculated by dividing the maximum load at failure by cross-sectional area, in this case  $1600 \text{ mm}^2$ .

#### 3.3.3.2 Mortar electrical resistivity and water conductivity

The development of electrical properties of the mortar cubes in both control and “under current” conditions was measured by recording electrical resistivity as output from PC-controlled multiplexer devices. A “2-pin method” (Fig. 3.2b) was used, where the “pins” were initially cast-in brass plates with dimensions equal to the sides of the mortar cubes. In order to minimise polarisation effects, the resistance was measured by applying an alternating DC current of 1mA at a frequency of 1 kHz. A PC-controlled R-meter was used, the output being the resistance value, calculated based on measured

voltage at the time of current interruption. For the “under current” regime (groups 10 mA/m<sup>2</sup>, 100 mA/m<sup>2</sup> and 1A/m<sup>2</sup>), the resistance measurement was performed after current supply interruption of approx. 30 min and surface drying of the cubes. The electrical resistivity was calculated using Ohm’s Law:  $\rho=R.A/l$ , where  $\rho$  is the resistivity in Ohm.m,  $R$  is the resistance in Ohm,  $A$  is the cross-section of the mortar cube in m<sup>2</sup>, and  $l$  is the length in m. Electrical conductivity measurements for the testing environment were performed using a conductivity meter by immersing a probe into the water solution. The SI unit of electrical conductivity is S/m and refers to 25 °C (standard temperature).

### 3.3.3.3 Microstructural analysis

Microstructural analysis was performed at the hydration ages of 24h, 7days and 28 days. The sample preparation followed well defined and accepted procedures of sample cutting, vacuum impregnation, grinding, polishing etc. which were after ceasing cement hydration in liquid nitrogen and freeze-drying of the samples to constant weight before impregnation (Ye et al. 2002, Ye 2003). Scanning electron microscopy (using environmental SEM (ESEM Philips XL30)) and image analysis (OPTIMAS software) were used to determine the pore structure parameters of the specimens. The physical size of the reference region of each image is 226  $\mu\text{m}$  in length and 154  $\mu\text{m}$  in width, with a resolution of 0.317  $\mu\text{m}/\text{pixel}$  (corresponding to a magnification of 500 $\times$ ); the pore size considered for image analysis is larger than 0.317  $\mu\text{m}$ . In order to quantify the pore structure, the analysis was performed on an average of 25 locations per sample. The image analysis in this study complies with the generally used methodology for pore structure and phase distribution analysis of cement based materials, implementing mathematical morphology and stereology approaches (Ye et al. 2002, Ye 2003, Hu et al. 2003, Hu 2004, Hu et al. 2005, Hu 2006 et al., Sumanasooriya et al. 2009, Serra 1982).

### 3.3.3.4 Mercury intrusion porosimetry (MIP)

Sample preparation for MIP analysis followed the aforementioned generally accepted procedure (Ye et al. 2002, Ye 2003, Hu et al. 2003, Sumanasooriya et al. 2009). The MIP tests for porosity and pore size distribution of the specimens were conducted in duplicate, using Micromeritics Poresizer 9320 (with a max. pressure of 207 MPa). The Washburn equation (Washburn 1921) was used to calculate the pore diameter, intruded at each pressure step, which is shown as:  $D=-4\gamma\cos\theta/P$ , where  $D$  is the pore diameter,  $\gamma$  is the surface tension of mercury,  $\theta$  is the contact angle between mercury and the pore wall and  $P$  is the applied pressure. The surface tension of mercury was  $484 \times 10^{-3}$  N/m and the contact angle was 130°. The measurement was conducted in two stages: the first stage was at low pressure: from 0 to 0.0036 MPa and the second stage was at high pressure running from 0.0036 to 210 MPa. According to Washburn equation (Washburn 1921), the pore size range detected is from 350  $\mu\text{m}$  to 7 nm.

### 3.3.3.5 Chemical analysis

Chemical analysis for hydrated water and ion concentrations in the conditioning water: alkali ions concentrations in the tap water in the containers at the beginning of the test and after 28-56 days were determined by plasma spectrometry using Inductive Coupled Plasma spectrometer (ICP-AES). The hydrated (chemically bound) water at certain hydrations age was determined according NEN 5931 (which is a standard loss of ignition test).

### 3.3.3.6 Numerical simulation

Numerical simulation of stray current was performed to obtain potential and current density distribution in the mortar cubes. The current density depends on the electrical resistivity/conductivity of the mortar and the external aqueous medium. The model used as input parameters electrical potential, electrical conductivity and relative permittivity for both mortar and water. The electrical potential difference between the positive and negative terminals is a direct measurement, using multi-meter. The water and mortar conductivity are also experimentally derived (section 3.3.2 above). The input for mortar and water relative permittivity of 4.5 and 80 F/m respectively were taken as literature data [Udaya et al. 1988, Taoufik et al. 2008, Taoufik et al. 2012].

The governing equations for the stray current model are as follows:

$$\nabla \cdot \bar{J} = -\partial \rho_v / \partial t \quad (3.1)$$

$$\bar{J} = \sigma \bar{E} \quad (3.2)$$

$$\bar{E} = -\nabla V \quad (3.3)$$

$$\bar{D} = \epsilon_0 \epsilon_r \bar{E} \quad (3.4)$$

where equation (3.1) gives the relationship between current density  $\bar{J}$  (A/m<sup>2</sup>) and charge density  $\rho_v$  (C/m<sup>3</sup>) (continuity equation). For steady current (DC) as used in this experiment, the charge density does not change with time so that the divergence of the current density is always zero ( $\nabla \cdot \bar{J} = 0$ ); equation (3.2) known as Ohm's Law for conduction current that gives relationship between current density  $\bar{J}$  (A/m<sup>2</sup>) and electric field  $\bar{E}$  (V/m) where the constant  $\sigma$  is proportionality called electrical conductivity (S/m); equation (3.3) gives relationship between electric field  $\bar{E}$  (V/m) and gradient of a scalar potential  $V$  (Volt); equation (3.4) gives relationship between electric flux density  $\bar{D}$  (C/m<sup>2</sup>) and electric field  $\bar{E}$  (V/m) that describe the interaction between charged material with relative permittivity  $\epsilon_r$  and vacuum permittivity  $\epsilon_0$ .  $\bar{D}$  is related to the charge densities associated with this interaction, while  $\bar{E}$  is related to the forces and potential differences.

To solve the equations (3.1-3.4), initial and boundary condition need to be specified (see Fig. 3.3), as follows:

$$\nabla \cdot \bar{J} = 0, \quad (x,y,z) \in A_n$$

$$V(x,y,z)=0, \quad (x,y,z) \in A_-$$

$$V(x,y,z)=V, \quad (x,y,z) \in A_+$$

$$-\mathbf{n} \cdot \mathbf{J}=0, \quad (x,y,z) \in A_1, A_2, A_3$$

where,  $A_n$  indicates the representative 3D volume model system i.e.  $A_+$  and  $A_-$  are the surface areas at the positive and negative terminals;  $A_1$  (front surface part),  $A_2$  (back surface part), and  $A_3$  (bottom surface part) represent the surfaces without current flow due to electric insulation condition in the set-up (a wooden bottom plate). By surface area, the relevant cross sections of the aqueous environment are meant. These equations were implemented in the finite element method (FEM) of COMSOL Multiphysics V 4.2 software in the AC/DC module (Pryor et al. 2011). The number (degree) of freedom, the maximum step-size and the number of iterations used in this model are 114011, 12, and 25, respectively.

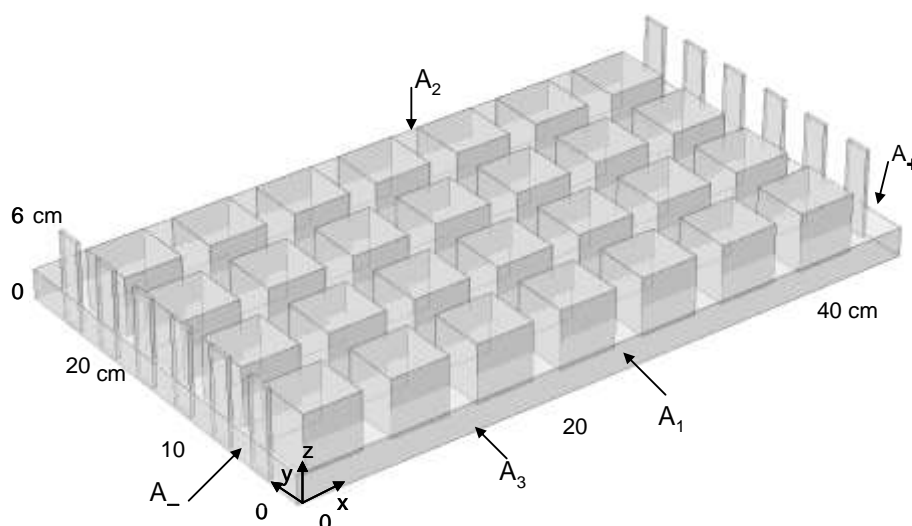


Fig. 3.3 Schematic boundary conditions for numerical simulation of stray current

### 3.4 Results of experimental studies and discussion

#### 3.4.1 Chemical analysis – hydrated (chemically bound) water.

The hydration mechanisms in cementitious materials are of generally high complexity, where water plays a decisive role. Being the main source for mass transport in the cement-based porous structure, water can be classified into different forms (chemically bound, interlayer, absorbed, free (capillary) water) (Basheer 2001). Chemically bound (hydrated) water is part of the hydration products, and could be released only with decomposition of hydrates. The bound water is further related to the hydration rate of the cement-based material i.e. can approximate the degree of cement hydration, hence is related to electrical resistivity and ease of ion transport.

Relevant to the present study, the amount of hydrated water at certain time intervals was obtained wet chemically and the recorded values served as an indication of possibly different hydration mechanisms when stray current flow was involved (as in group S) compared to control conditions (group R). Figure 3.4 presents the amount of hydrated

water (in percent per dry cement weight) for both groups R and S in the time interval of 1d – 84 days. The derived values can be considered as almost equal for both groups (just 1 to 2 wt.% difference). Apparently, within the time scale of this experiment pronounced alterations in hydrated water content due to current flow cannot be claimed. However, the observed differences are well in line with the recorded electrical resistivity for both R and S specimens (presented further below in Section 3.4.4) as well as the recorded compressive strength and microstructural characteristics (Sections 3.4.2 and 3.4.3).

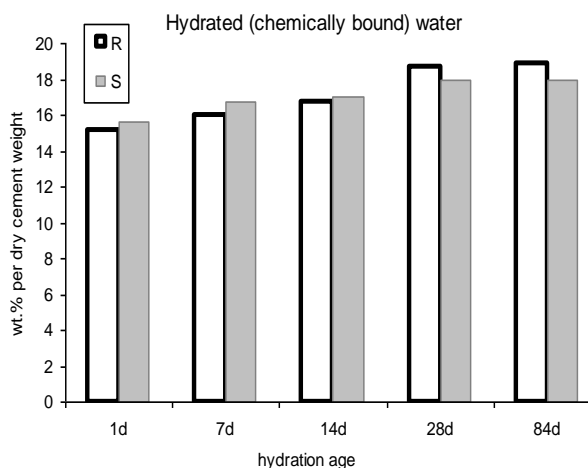


Fig. 3.4 Hydrated water at 1 day - 84 days of age for R and S specimens.

### 3.4.2 Compressive strength

Compressive strength, as an engineering property of cement-based materials reflecting mechanical performance, is generally expected to increase with cement hydration (i.e. with time and if no other external factors are present). Figure 3.5 presents the development of compressive strength for both control (R) and “stray current” (S) groups from initial conditioning (24h) until the end of the test (84 days). Three replicates per condition were tested. Considering the high level of structural heterogeneity of cement-based materials (and therefore the well-known outcome of similar but never the same strength values even within a single batch of specimens), it can be stated that the average difference in strength is minimal (or practically none) between groups R and S. However, it can also be observed that after the initially stable increase of strength for specimens group S, similar to specimens group R, the former group shows an evident trend to maintain lower strength values (from 28 days and onwards). The recorded values are in line with the percentage of bound water (Fig. 3.4) and are supported by microstructural observation of the bulk matrix.

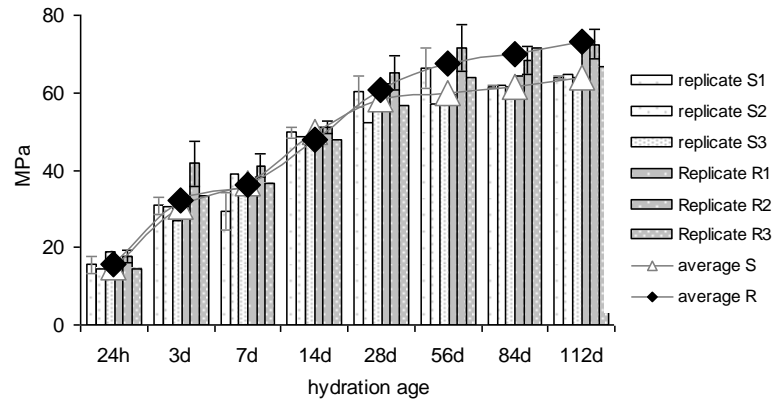


Fig. 3.5 Evolution of compressive strength (MPa) for control R and “stray current” S groups.

### 3.4.3 Microstructural properties

The development of the pore structure in hardening cementitious materials is fundamental to their mechanical behaviour. It influences ion and water transport and their interaction as well as the diffusion characteristics of the bulk matrix. Previous studies on the influence of electrical current within CP applications revealed that a current flow in the range of 5 to 20 mA/m<sup>2</sup> brings about initial densification of the concrete bulk matrix, but leads later-on (more than 120 days of age) to enlargement of the interfacial transition zones and coarsening of the pore structure (Koleva et al. 2008 (1-3)). Although the electrical current flow involved within this investigation is a simulation of stray current i.e. the relevant positive and negative terminals were not embedded in the mortar cubes but external, and therefore a direct comparison to previous results cannot be made, influence on the material structure (including pore structure) of the hereby studied mortar specimens was expected. Figure 3.6 depicts the calculated porosity and pore size distribution for the control specimens R and the “stray current” specimens S at the stages of 24h, 7d and 28 days. It should be noted that Fig. 3.6 presents porosity and pore size distribution values, which are calculated via image analysis (as previously introduced). The employed method can distinguish pore sizes larger than 0.317  $\mu\text{m}$ .

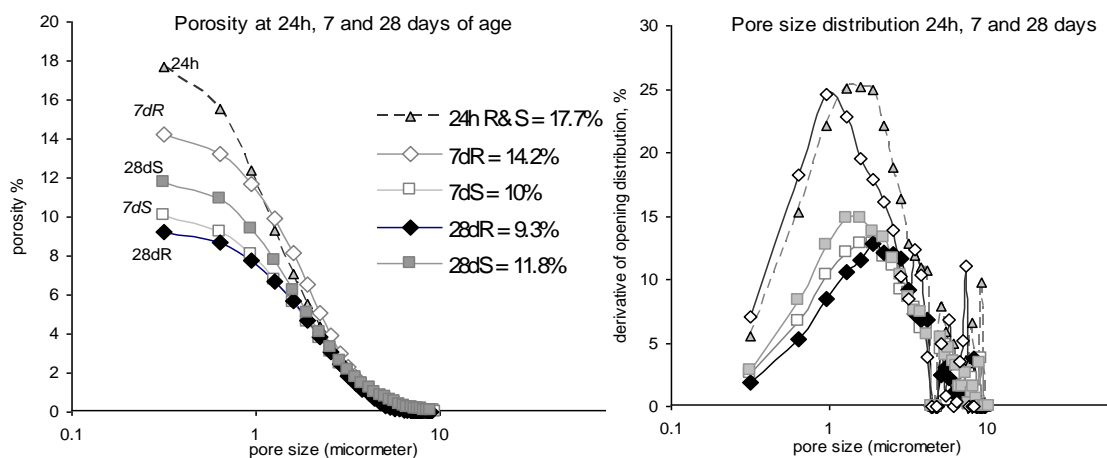


Fig. 3.6 Porosity (left) and pore size distribution (right) for control group R and “stray current” group S at hydration ages of 24h, 7 days and 28 days, determined via image analysis.

The derived values are not claimed to be absolute, but rather serve as a comparison of bulk matrix characteristics of equally handled samples from both groups R and S (via equal sample preparation respectively). Both S and R specimens present equal characteristics for the first time interval (24h). Development of the pore structure follows with cement hydration, resulting in densification of the matrix for both R and S groups. Porosity decreases from  $\sim 18\%$  at 24h to  $\sim 14\%$  for specimens R and  $\sim 10\%$  for specimens S at 7 days age. The microstructure of specimens S is affected by enhanced ion and water transport in the matrix, resulting from parallel diffusion and migration controlled mechanisms in the presence of electrical current flow, whereas diffusion controlled mechanisms only are relevant for group R. The lower porosity values for group S at this stage are in line with the slightly higher amounts of hydrated water (Fig. 3.4) and would generally result in higher compressive strength (Fig. 3.5, strength development from 7 to 14 days). At the stage of 28 days, a reversed trend was observed for specimens S – porosity increases from  $\sim 10\%$  to  $\sim 12\%$ , whereas decreases only for specimens R (from  $14.2\%$  to  $9.3\%$ ). The result supports the lower compressive strength values for specimens S, compared to specimens R at this stage (Fig. 3.5, 28 days and later stages).

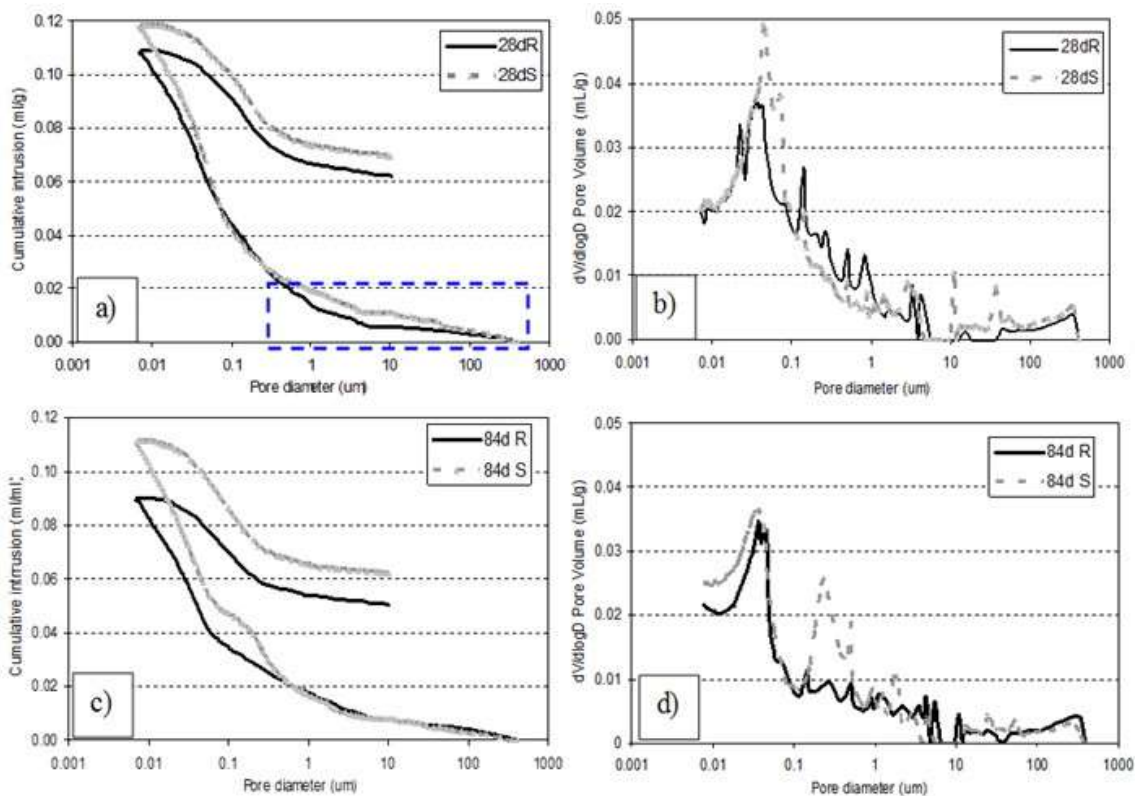


Fig. 3.7 Porosity and pore size distribution for groups S and R from MIP tests: 28 days (a,b) and 84 days (c, d).

Porosity and pore size distribution were also derived via conventional MIP tests, Fig. 3.7. Here again, absolute values are not claimed, neither a direct absolute comparison with pore structure parameters derived from image analysis can be made.

For the hydration age of 28 days, the MIP results present analogical trend of material behaviour as previously defined within image analysis for this time interval (Fig. 3.7a,b); the rectangular area in Fig. 3.7a defines the region, where image analysis can determine porosity and pore size). Coarser pore structure for specimens S was derived at 28 days, relevant to pores larger than 10  $\mu\text{m}$  and the gel pore family (below 0.1  $\mu\text{m}$ ) – Fig. 3.7b); total and effective porosity for specimens S are also slightly higher, compared to specimens R (Fig. 3.7a).

At 84 days of age, the total and effective porosity for both S and R groups decrease (Fig. 3.7c), compared to 28 days of age (Fig. 3.7a). For specimens S, the trend of higher than specimens R (total and effective porosity) was maintained (Fig. 3.7c) and a more pronounced difference in pore distribution density was observed i.e. capillary porosity increased as evident from the well pronounced peak between 1  $\mu\text{m}$  and 0.1  $\mu\text{m}$  in the differential curve for specimen S – Fig. 3.7d.

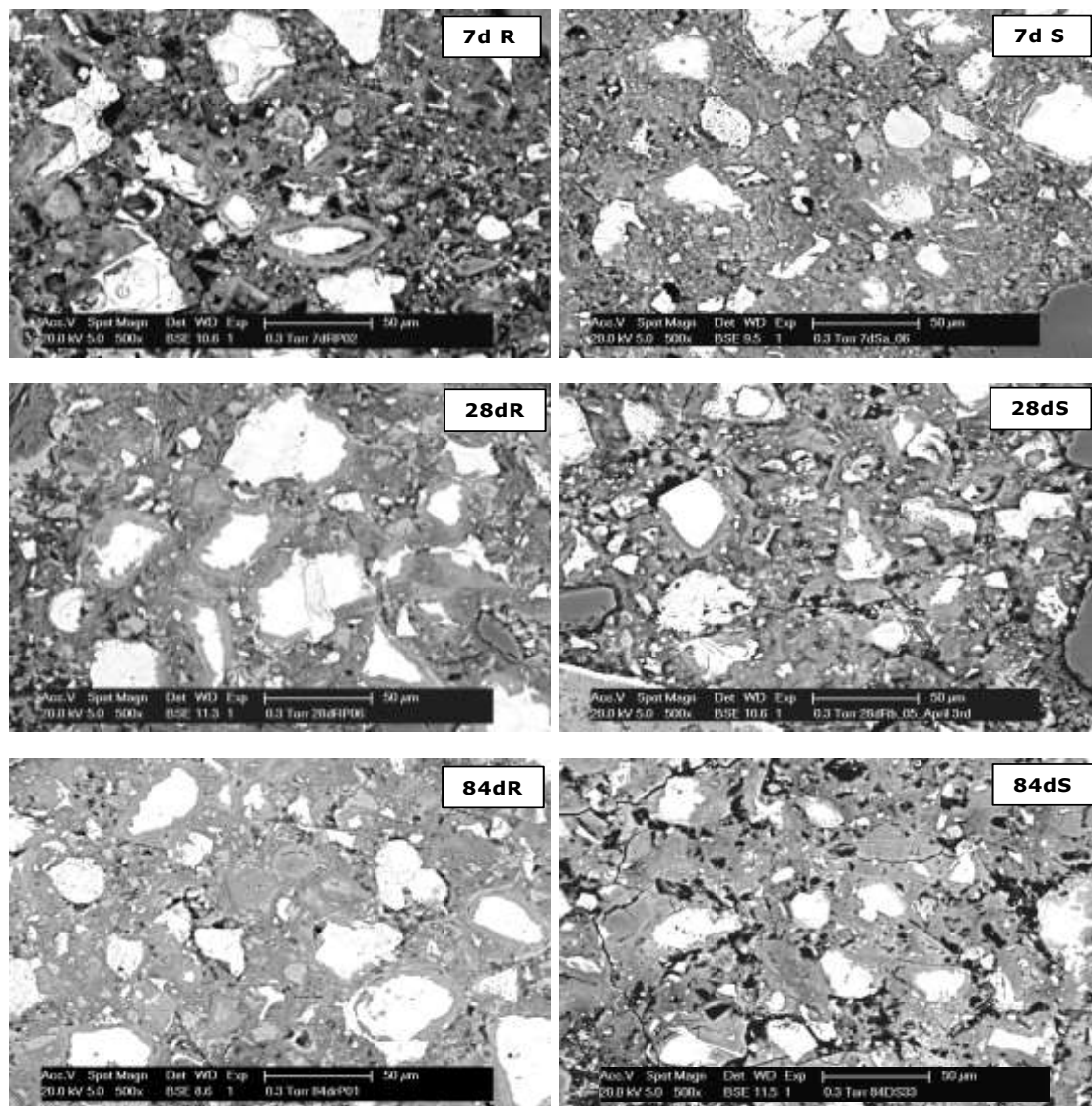


Fig. 3.8 ESEM micrographs of the bulk mortar matrix for specimens R (left column) and S (right column) at the hydration ages of 7 days, 28 days and 84 days.

The results from microstructural analysis (both image analysis, Fig. 3.6 and MIP analysis, Fig. 3.7 are “visualized” by Fig. 3.8, presenting ESEM micrographs of the bulk mortar matrix (at equal magnification of 500x) for the control specimens R (left column) and the “stray current” specimens S (right column). Well visible is the denser matrix in specimens S at 7 days of age (Fig. 3.8 top); followed by coarsening (compared to R) at 28 days of age (Fig. 3.8 middle) and an even coarser pore structure for specimens S at 84 days of age (Fig. 3.8 bottom). The global performance of the here investigated mortar specimens is determined by the above discussed microstructural characteristics. The derived pore structure parameters support the findings for development of compressive strength and are also in line with the electrical properties (electrical resistivity in this case) of the investigated specimens. Discussion on the experimental results and additional supporting evidence for the different material development in conditions of current flow (as within specimens group S) will be presented in what follows.

### 3.4.4 Discussion

The electrical resistivity, conductivity respectively, is a property of a cement-based material, related to the ability of the matrix to resist the passage of electrical current. Electrical resistivity is fundamentally related to the permeability of fluids and diffusivity of ions through porous materials such as mortar/concrete. Resistivity monitoring for the S and R specimens was continuously performed throughout the total duration of the test. Figure 3.9 depicts derived electrical resistivity values for both groups S and R: from initial values (24h) until 84 days. The plots in Fig. 3.9 additionally depict information for the stray current density that flows through each cube (for the S specimens), and the hypothetic current density for the control group R, calculated with numerical simulation (Section 3.5 further below). As can be observed, electrical resistivity increases with time for both S and R specimens, which is more pronounced for the R specimens; the electrical resistivity for specimens S is on average higher than that for specimens R at earlier hydration stages (e.g. 3 days, Fig. 3.9b). At the latest time interval (84 days, Fig. 3.9f) the electrical resistivity for the S cubes is lower (in the range of 8-9 Ohm.m) compared to the R cubes (in the range of 10-16 Ohm.m). Previously discussed were the lower compressive strength values for specimens S, compared to specimens R with time of conditioning, which actually corresponds well to the lower resistivity values for group S. However, no straightforward relation can be made, since microstructural alterations play an important role as well; the average stray current density, flowing per cube decreases with time which is with increasing the electrical resistivity of the matrix, and maintains higher values for the S specimens. This corresponds to the lower electrical resistivity, lower compressive strength and the coarser pore structure in specimens S.

After correlating the results from chemical analysis (hydrated (bound) water content), compressive strength tests, microstructural analysis of the bulk mortar matrix and electrical properties, it can be stated that the stray DC current, flowing through the specimens group S, exerts changes in material behaviour. Compared to group R, initially similar or higher values of hydrated water content were recorded for group S at earlier stages, whereas still increasing, but slightly lower values compared to the control group R were recorded later on (Fig. 3.4).

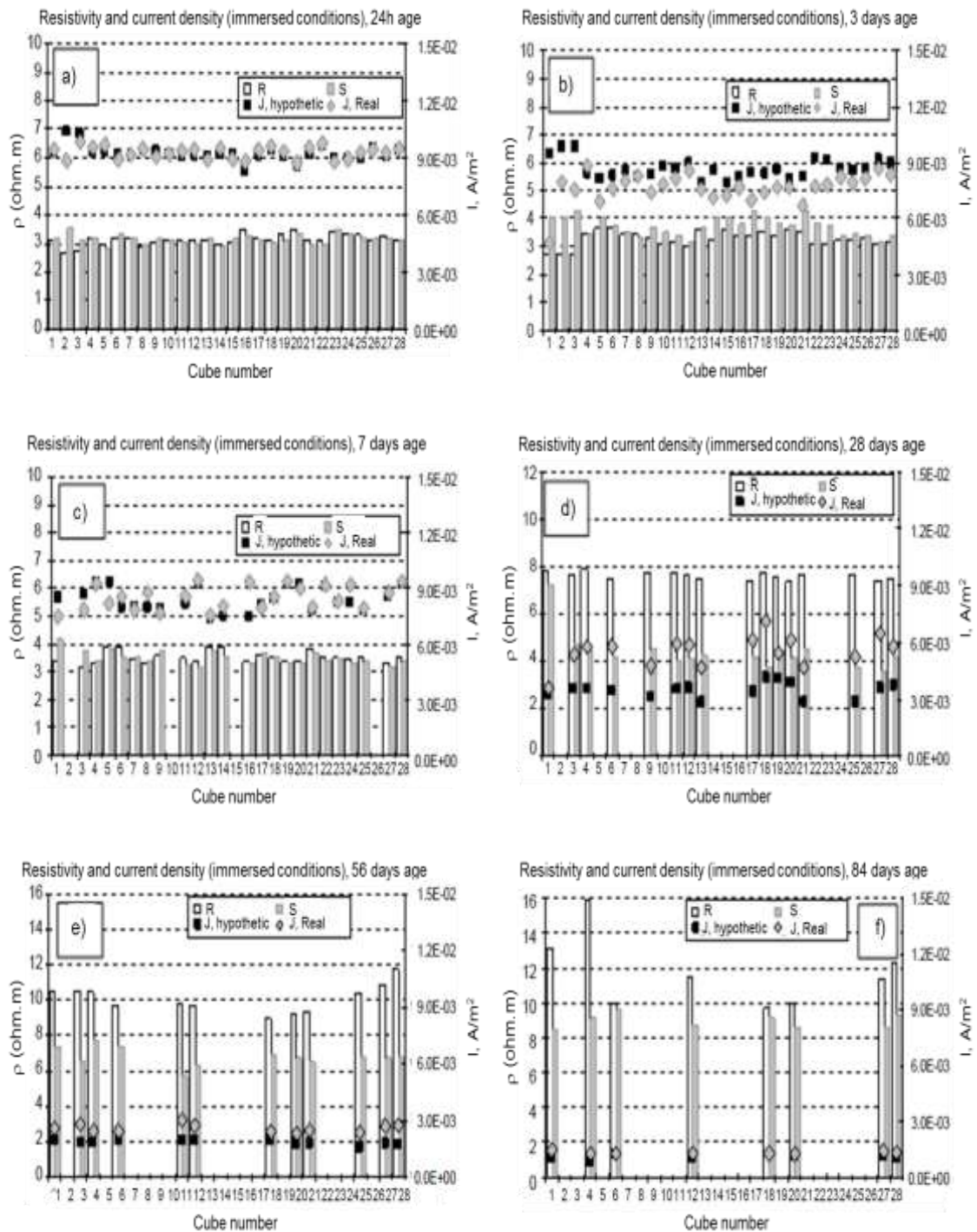


Fig. 3.9 Comparison of electrical resistivity values (columns) in Ohm.m for mortar specimens S and R (both in immersed condition and identical water levels) at hydration ages of 24h (a), 3 days (b), 7 days (c) 28 days (d) 56 days (e) and 84 days (f). The number of cubes (depicted values respectively) reduces with time, relevant to removing of 4 replicates per stage for the relevant tests (the plots contain current density values as cumulative stray current flow per cube as calculated by numerical simulation, discussed further below in Section 3.5).

In an advanced stage of the hydration process, diffusion processes are the limitation ones and these are solely relevant for specimens group R. As for specimens group S, the hydration process is determined by diffusion but also migration due to an accelerated ion and water transport under current flow. Therefore, the current flow initially accelerates cement hydration for group S. This is confirmed by increasing compressive strength values for group S (Fig. 3.5), initially denser pore structure e.g. 7 days age, Figs. 3.6 - 8) and higher electrical resistivity of the mortar specimens S, compared to specimens R – Fig. 3.9b). The effect shows a reversed trend on later stages (after 28 days of age), which is denoted to the simultaneous contribution of stray current flow and concentration gradients on cement hydration, as well as possible calcium and alkali ions leaching. These latter phenomena, denoted to the influence of current/voltage flow in water environment have already long been recognized and reported to result in hydrolytic degradation of hardened cement-based materials within less than 50 days of conditioning in similar to the hereby discussed environment (Saito et al. 1992, Wittmann 1997). Consequently, alterations in microstructural and electrical properties, further resulting in lower electrical resistivity (Fig. 3.9d-f), lower compressive strength (Fig. 3.5) and coarser pore structure (Figs. 3.6-8) were expected and are actually as recorded starting 28 days of age for specimens S, compared to the control cases (specimens R). These trends and dependencies, although relatively less pronounced within the hereby relevant period of 84 days, are expected to be significantly more evident for longer conditioning, which is subject to an on-going investigation.

The development of the internal microstructural characteristics, resulting from chemical and physico-chemical phenomena related to cement hydration, determine the mechanical performance of cement-based materials. A general perception for a cement-based material is that porosity will decrease with time and with prolonged cement hydration respectively. This, however, is not always the case. Microstructural alterations and Ca-leaching for example would affect the matrix. For the case of this experiment, leaching cannot be claimed in the generally accepted sense of these types of experiments, since the mortar cubes were immersed in stagnant water that was not exchanged during the tests, but only maintained at the same level by adding fresh water. However, the recorded calcium, sodium and potassium concentrations at the beginning of the test and after 28 to 56 days show five to ten or more times increased ion concentrations within conditioning (Table 3.1).

Table 3.1 pH, alkali ions concentration and conductivity of water environment

| Conditioning<br>water, group: | pH  |      | Na <sup>+</sup> , g/l |         | K <sup>+</sup> , g/l |         | Ca <sup>2+</sup> , g/l |         | σ, S/m |         |
|-------------------------------|-----|------|-----------------------|---------|----------------------|---------|------------------------|---------|--------|---------|
|                               | 24h | 28 d | 24h                   | 28-56 d | 24h                  | 28-56 d | 24h                    | 28-56 d | 24h    | 28-56 d |
| R                             | 8.5 | 13.3 | 0.041                 | 0.232   | 0.009                | 0.563   | 0.048                  | 0.307   | 0.92   | 2.9     |
| S                             | 8.5 | 13.1 | 0.041                 | 0.206   | 0.009                | 0.480   | 0.048                  | 0.391   | 0.92   | 1.8     |

For this experiment, leaching will result from concentration and pH gradients between the cement-matrix and the external (tap water) environment (the pH values were measured to be approx. 8 at the beginning of the test and approx. 13 after 28 days). Leaching is expected to be accelerated in the presence of current flow. Although conductivity values of the environment for S and R groups and ion concentration are not far different, conductivity, as well as K<sup>+</sup> and Na<sup>+</sup> concentrations) for the S groups were

lower, whereas  $\text{Ca}^{2+}$  concentration was slightly higher, compared to the conditioning water for group R (no absolute values are claimed, but a comparison of initial and cumulative 28 to 56 days values are given). Since alkali ion concentrations also increase in the conditioning water for group R, the most plausible reason for the coarsening of the pore structure in specimens S is the electrical current contribution towards enhanced ion and water migration. It can therefore be concluded that the electrical current flow initially affects the bulk matrix properties in terms of matrix densification; whereas a coarser pore structure was observed towards the end of the test as a result of simultaneous stray current and leaching effects.

### 3.5 Numerical simulation and correlation of results

Considering all experimental data and the above discussed outcomes of this investigation, a further objective of this study was to initiate and present first trials on numerical simulation of the dependence of stray current density, flown per cube and the relevant development of mechanical and microstructural properties. Figure 3.10 presents an example for the numerical simulation of potential (Fig. 3.10a) and current (Fig. 3.10b,c) distribution in the specimens S. The simulation can provide data for the distribution of current density flow per cube i.e. current distribution lines within the matrix of each cube (Fig. 3.10b) or per defined cross section of each cube (Fig. 3.10c, top and bottom sections are depicted). This is of particular interest when aiming to correlate bulk matrix properties as strength or resistivity – in this case the total cumulative stray current, flown per cube (Fig. 3.10b) can be coupled to the obtained results; or similarly – for the case of porosity and pore size analysis via image analysis – the current flow through a relevant (in our case middle section) of each cube (Fig. 3.10c) can be correlated to derived pore structure parameters in this same section. These correlations, however, need to consider also if the cubes were near the negative or near the positive terminals of the conditioning set-up, since the relevant opposite ion flow determines structural characteristics (Wittmann 1997, Koleva et al. 2008). For this experiment the above correlations were not performed.

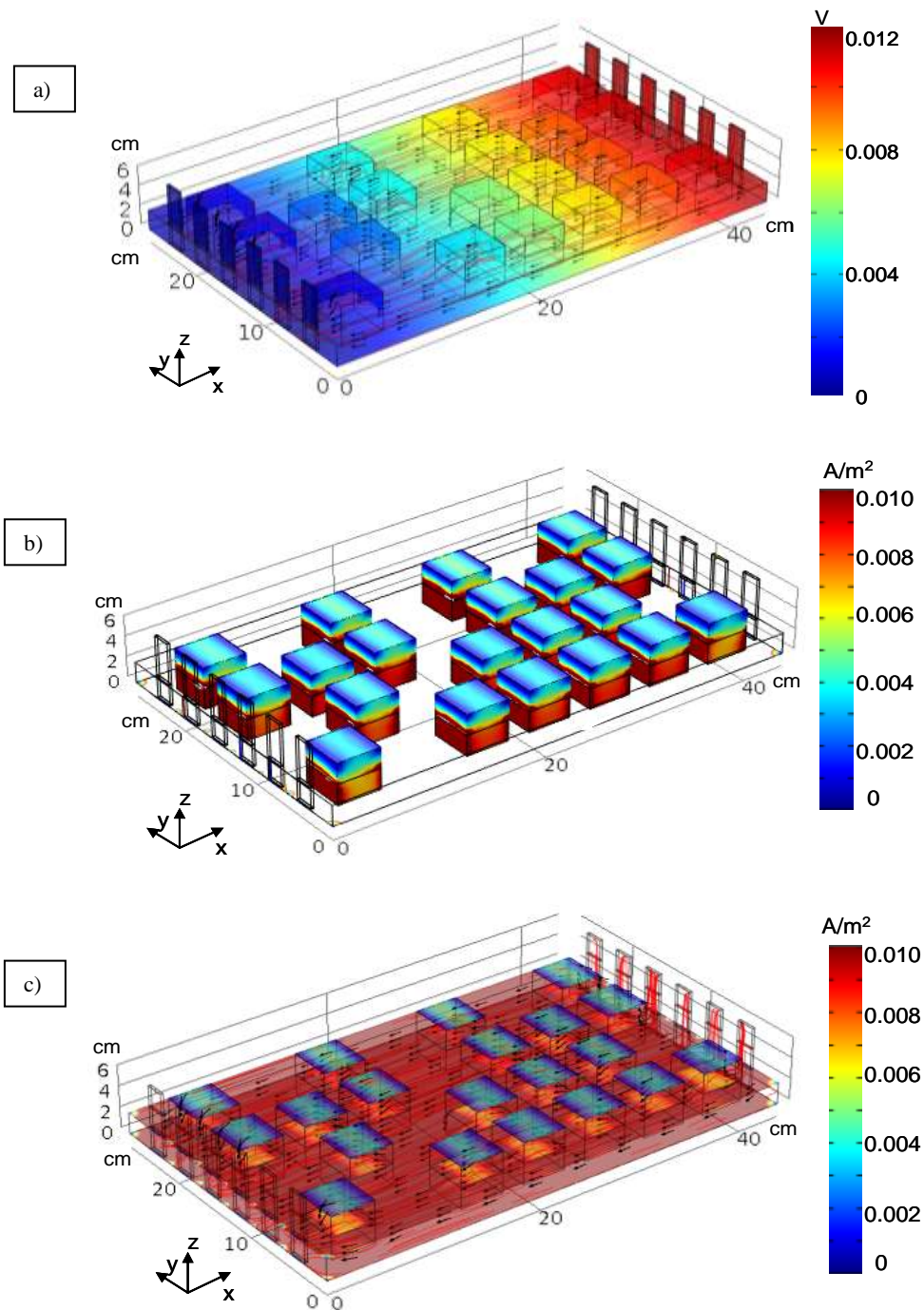


Fig. 3.10 An example of potential distribution in the container (a) and current density distribution (b,c) within the experimental set-up for group S, presenting the magnitude of current density, distributed in the total bulk material (b) and current density distribution lines per sections of the cubes (c).

Figure 3.11 presents the output of the model for series S at 1 day (a,b), 7 days (c,d), 28 days (e,f) and 84 days (g, h) of cement hydration. For clarity of the discussion and the data depicted in Fig. 3.11, Fig. 3.12 gives an example for the graphical presentation of one cube in terms of current lines, Fig. 3.12a)b) and the distribution of the generated current density lines in the x direction, Fig. 3.12c).

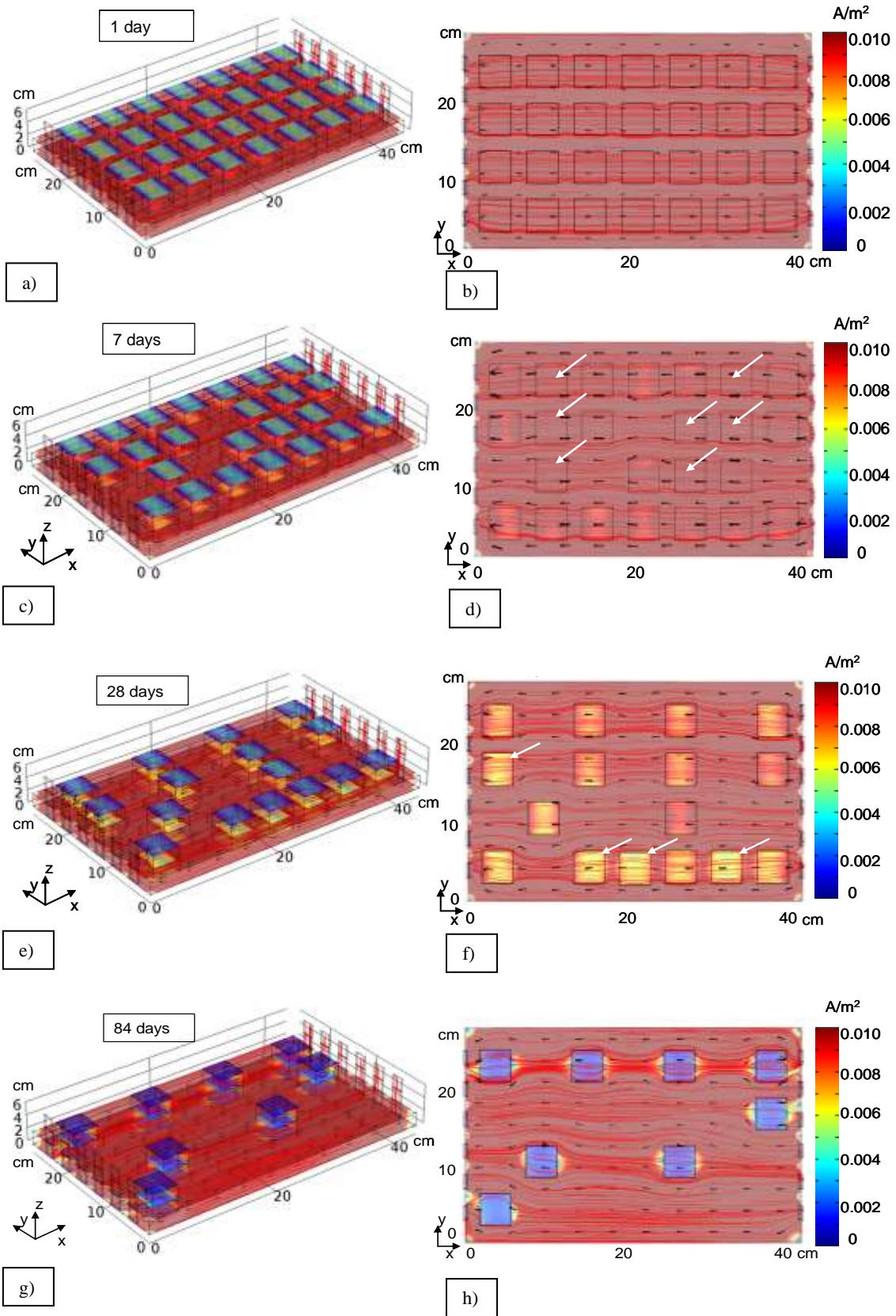


Fig. 3.11 Stray current model (current density distribution) for specimens group S at 1 day (a, b), 7 days (c, d), 28 days (e, f) and 84 days (g, h) – top and middle cross sections (left columns) and bottom sections (right column).

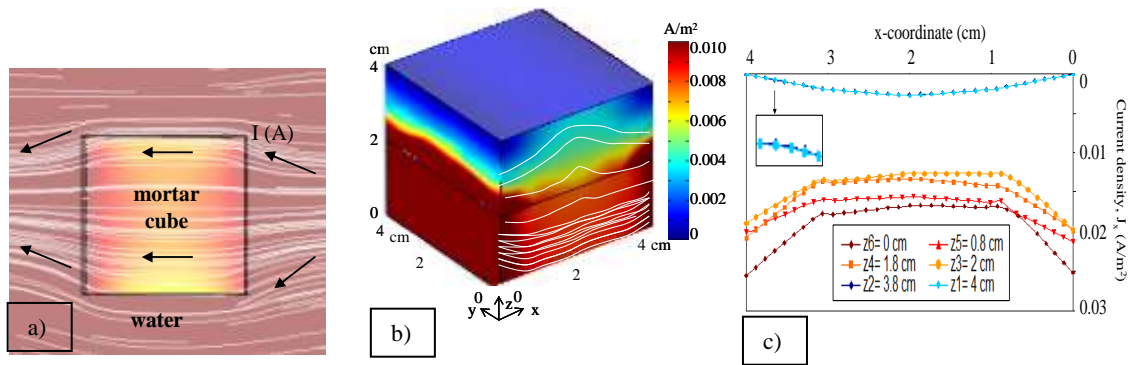


Fig. 3.12 An example for the graphical presentation of the generated current distribution lines in the directions of x, y and z axis, including a schematic view of current distribution lines in one cube.

At the beginning of the test (1 day, Fig. 3.11a,b), the level of current density, flowing in the immersed (bottom) sections of the cubes (Fig. 3.11b) almost equals the current distribution flow in the external aqueous environment, whereas lower currents are relevant for the top (higher resistant) sections of the cubes (Fig. 3.11a). After 7 days of conditioning (and with time of cement hydration) densification of the matrix and developing of mechanical strength lead to lower current, flowing through the highly resistive top sections of the cubes (Fig. 3.11c). The bottom sections also become more resistive (Fig. 3.11d). At later stages (28 and 84 days, Fig. 3.11e-h), the current flow decreases through both top and bottom sections of the cubes, maintaining lower values for the bottom sections. The source of electrical current throughout the experiment is current controlled (not voltage controlled), meaning that the level at which the 10 mA/m<sup>2</sup> DC stray current is supplied, is constant. The difference in the actual current density, flowing through each cube, is therefore determined from the difference in electrical and microstructural properties of the cement matrix with time of conditioning. In other words, although all cubes theoretically “receive” the same amount of current, the accumulated current that flows through each cube is different and this is well visible from Fig. 3.11. For example at 7 days of age (Fig. 3.11d) the bottom sections of the cubes in the upper and middle part of the experimental set-up (indicated with arrows in Fig. 3.11d) “receive” higher current, compared to those in the bottom part (i.e. their electrical resistivity is lower). At 28 days some cubes are more resistant to current flow (arrows in Fig. 3.11f), compared to others. Gradually (e.g. 84 days, Fig. 3.11g,f), the cubes becomes more and more resistive to current flow (also reflected by gradual increase in electrical resistivity values, Fig. 3.9, which however maintain lower, compared to the control R group). A simulation for the “hypothetic current flow” can be performed for the cubes group R (control case) - the resulting current flow distribution for 28 days for example is as presented in Fig. 3.13. Well seen is that for equal environmental conditions, as well as equal current levels applied, the current density, flowing through specimens R will be significantly lower compared to that in specimens S (compare Fig. 3.11e)f) with Fig. 3.13) in both top (Fig. 3.13 left) and bottom (Fig.3.13 right) sections of the cubes.

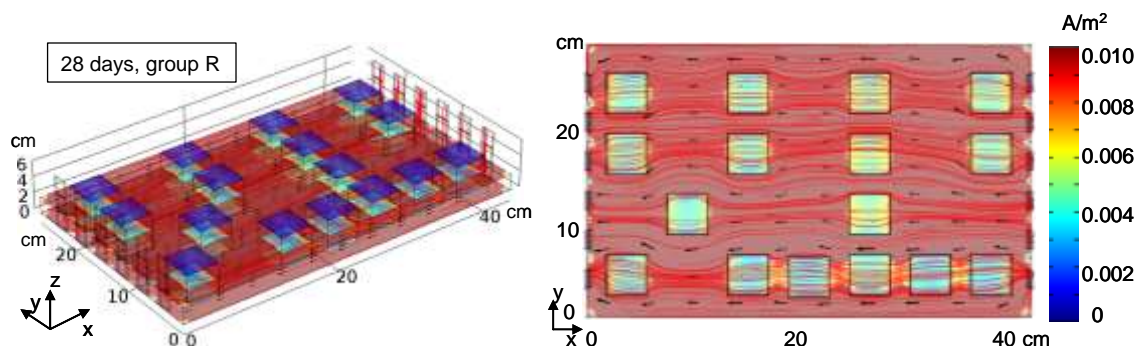


Fig. 3.13 Stray current model for 28 days for group R, presenting hypothetical distribution of current flow.

The model can thus provide the distribution of current flow per cube and the current distribution flow with time of conditioning. With additional input parameters (as matrix permeability for example) and mathematical transformations (which are subject to ongoing study) the level of current flow can be correlated to microstructural and mechanical properties for each cube. The end result would be a correlation of stray current flow and bulk matrix properties i.e. the influence of current flow on cement-based matrix can be evaluated and further extrapolated to predict performance within longer time intervals and for various current regimes.

3

### 3.6 Conclusions

The chapter discussed microstructural, mechanical and electrical properties of mortar specimens in conditions simulating stray current flow, compared to control, “no-current” conditions. Numerical simulation for the distribution of the stray current flow in aqueous medium and the presence of mortar cubes was performed and validated with experimentally derived results. The following conclusions can be summarized:

- At the level of  $10 \text{ mA/m}^2$  (surface area of the cross section of the conditioning environment in direction of current flow) the stray current flow results in slightly higher percentages of hydrated water content and denser bulk matrix of the mortar bulk matrix, which is due to reduced porosity and critical pore size;
- Compressive strength and electrical resistivity for the mortar, maintained in conditions of stray current flow (group S) increased with time, but maintained lower values, compared to these for the control group R;
- At later conditioning intervals (28 to 84 days of age), the stray current flow brings about microstructural alterations in terms of coarsening of the mortar bulk matrix, with a possible contribution of calcium leaching in the testing environment. The difference in porosity and pore size distribution between specimens S and specimens R at the latest time interval of 84 days, higher for the former and lower for the latter cases, are attributed to accelerated ion and water migration in the presence of current flow.
- Apart from diffusion, ion and water migration have a positive effect on cement-based properties; however, the enhanced water and ion transport on later stages induce

negative alterations, which correspond to reduced mechanical and electrical properties, that in turn would ease aggressive ions transport (if any) and reduce corrosion resistance, if reinforcement was present.

- Further tests need to be performed in suitable external environment e.g. sat.  $\text{Ca}(\text{OH})_2$ , fully immersed or sealed conditions, in order to separately evaluate leaching and/or stray current-induced effects. Such tests and related considerations are subject to the next chapters.



# 4

## **Stray current-induced development of hardening cement-based microstructure in different environmental conditions\***

---

Abstract: This chapter presents the development of microstructural and mechanical properties of mortar cubes under the synergetic action of stray current and various environmental/curing conditions. The mortar specimens were cured for 24h only, followed by a 112 days period of partial or full submersion in water or alkaline medium. Additionally, equally prepared mortar specimens were tested in sealed conditions. The outcomes for submerged and saturated conditions were compared to sealed conditions. Three current density regimes were employed i.e.  $1 \text{ A/m}^2$ ,  $100 \text{ mA/m}^2$ , and  $10 \text{ mA/m}^2$ , simulating different levels of stray (DC) current environment. The highest level of  $1 \text{ A/m}^2$  was also comparable to stray current densities, as measured in field conditions. The tests were designed in a way, so that the effects of diffusion-controlled transport (ions leaching due to concentration gradients), were distinguished from migration-controlled ones (ion/water transport in stray current conditions). Mechanical, microstructural and electrical properties were monitored throughout the test.

---

\*This chapter is based on:

1. Susanto, A., Koleva, D. A., van Breugel, K., and van Beek, K. (2017). Stray current-induced development of cement-based microstructure in water-submerged,  $\text{Ca(OH)}_2$ -submerged and sealed conditions. *Journal of Advanced Concrete Technology*, 15(6), 244-268.

## 4.1 Introduction

During their service life, cement-based materials are exposed to various external environments that can have either beneficial or negative effect on the cement-based matrix. Generally, concrete degrades with age in aggressive environment (e.g. acidic, sodium chloride-containing environments, stray current flow, etc.). For instance, main constituents (as Ca-bearing compounds) of the hydrated cement paste in concrete, when exposed to aqueous solutions, may leach out due to concentration gradient or chemical potential. Leaching occurs from regions with higher concentration to regions with lower concentration of the diffusing substance (a process occurring for example in underground storage tanks, dams, water tanks and radioactive waste disposal containers). Since calcium leaching coarsens the pore structure, the result is a porous bulk matrix (Jain et al. 2009; Puertas et al. 2010; Marinoni et al. 2008; Gaitero et al. 2008; Cheng et al. 2012), increased permeability, reduced mechanical strength (Dariusz et al. 2009; Kamali et al. 2003; Marchand et al. 2000; Carde et al. 1996). Generally, the leaching process starts with a total dissolution of portlandite (calcium hydroxide, CH), ettringite, followed by a progressive decalcification of the calcium-silicate-hydrate (C-S-H) phase. Long term leaching follows a square root of the leaching duration (Ulm et al. 1999; Detlef et al. 2004). Other degradation processes may occur when aggressive chemical species from the external environment as chlorides, carbon dioxide, sulphates penetrate into the cement-based material, e.g. concrete sulphate attack, corrosion of the steel reinforcement, etc.

When the above chemical and physico-chemical degradation mechanisms are enhanced due to faster ion and water transport, i.e. due to ion migration as for example in conditions of stray current flow, an increased level of structural degradation would be expected. Any electrical field, including stray current, will influence cement hydration by altering ion and water transport. Consequently, stray currents will modify material properties and can affect the behaviour and integrity of a reinforced concrete structure.

Several works reported on quantifying the influence of stray current on cement-based materials via modelling approaches only (Yu-qiao et al. 2010; Xia et al. 2013; Peelen et al. 2011). In contrast, Chapter 3 combined both experimental and numerical approach, resulting in more insight into the related phenomena. Previously reported was the positive effect of stray current on partially submerged in water mortar specimens at early stages only (<14 days of cement hydration). The positive effect of stray current was due to accelerated cement hydration, accompanied by increasing compressive strength, denser pore structure and higher electrical resistivity for the “under current regime”, compared to control specimens. However, a reversed trend was observed at later stages (>28 days), where the stray current induced negative effects, leading to coarsening of the mortar bulk matrix, reduced mechanical and electrical properties. The effect of stray current on cement-based microstructure was *hypothesized* to depend and vary with respect to the environmental conditions and the current density level.

Therefore, the extensive investigation subject to this chapter, including varying external medium, different curing regimes and higher current densities, was performed in order to elucidate the effect of stray current on cement-based materials. In particular, this work aims to clarify some of the previously posed research questions on different environmental conditions and leaching phenomena. The aim is to clearly distinguish the effects of ions leaching due to concentration gradient from those, resulting from enhanced ion and water migration, i.e. when stray current is involved. Hence, hereby presented and discussed is the effect of stray current flow on mortar specimens

submerged in water, compared to stray current effects on mortar in sealed conditions and in conditions of partial or full submersion in alkaline medium ( $\text{Ca}(\text{OH})_2$ ) solution). Except the effect of concentration gradient, an important aspect is the level of stray current density.

In this Chapter, three levels of stray current densities were applied, considering main points as follows: the lowest current density level of  $10 \text{ mA/m}^2$  was employed as a simulation of current flow due to electrochemical protection techniques (e.g. impressed current cathodic protection). Although much lower levels of stray current densities e.g. in the range of 1 to  $1.5 \text{ mA/m}^2$  were reported (Charalambous et al. 2014; Aylott et al. 2013), considering previous studies (Susanto 2013) an increase with a factor of 10 was chosen for obtaining better distinguishable results. The highest level of employed current density of  $1 \text{ A/m}^2$  was chosen as comparable to levels also measured in real field situations, i.e. between 1 and  $1.5 \text{ A/m}^2$  (Galsgaard and Nielsen 2006). The step in-between i.e.  $100 \text{ mA/m}^2$  adds to the series of tested steps by a factor of 10 and for completeness of the tests.

## 4.2 Materials and methods for experimental studies

### 4.2.1 Materials

For partly submerged and fully submerged conditions: the specimens were treated in water or  $0.02\text{M}$   $\text{Ca}(\text{OH})_2$  solution (Seidell et al. 1953). For sealed conditions: a specifically designed mould was used, where the specimens were sealed with a rubber gel sealant 24h after casting and remained insulated from each other in the mould (Fig. 4.1).

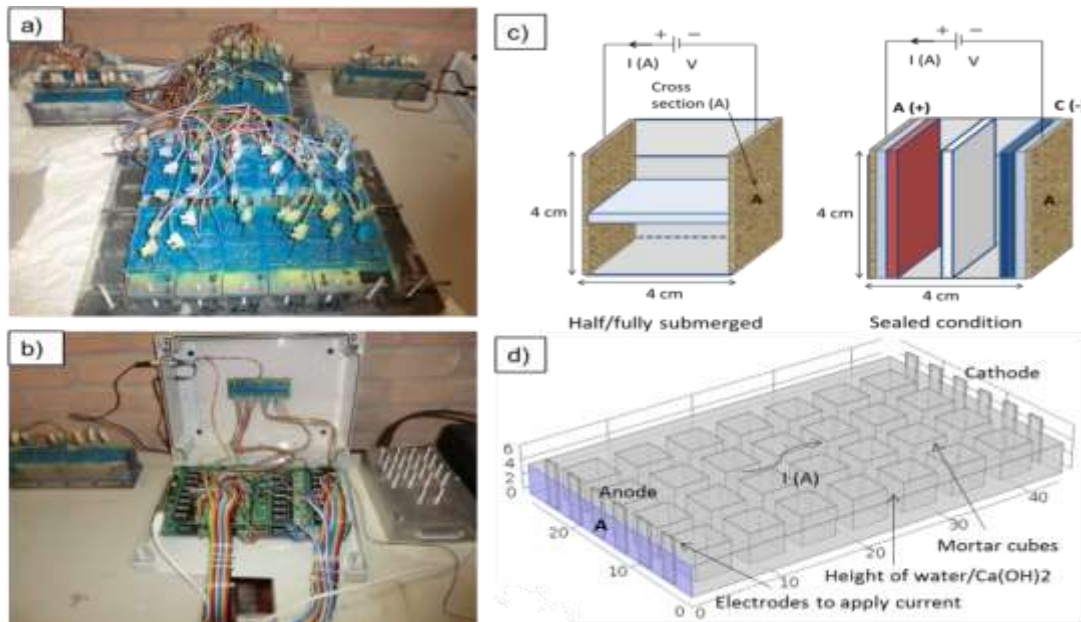


Fig. 4.1 Experimental set-up, electrical devices, multiplexer to automatically record resistance of the mortar specimens, and schematic presentation of the electrical current application through the cross section (A) of mortar specimens for sealed condition (a, b, c); schematic experimental set up for submerged (partially or full) conditions (d), as also previously reported (Susanto et al. 2013).

## 4.2.2 Sample designation and current regime

Table 4.1 summarizes the experimental conditions and studied specimen-groups. Four groups of experiments were conducted in different conditions (submerged, partly submerged, sealed condition), varying environment (water, 0.02M Ca(OH)<sub>2</sub>) and three levels of DC current density (10 mA/m<sup>2</sup>, 100 mA/m<sup>2</sup>, 1A/m<sup>2</sup>). The current regimes were adjusted through external current sources, following previously reported set-up for partly submerged conditions (Susanto et al. 2013), Fig. 4.1d) and a specifically designed one for sealed conditions, Fig. 4.1a,c). The electrical current flow was “injected” via surface area A, in m<sup>2</sup>, Fig. 4.1c,d), calculated based on the geometrical orientation of the specimens and set-up - 0.27 m x 0.04 m for submerged conditions (Fig. 4.1d) and 0.04 m x 0.04 m for sealed condition (Fig. 4.1c). Figure 4.1 (a, b, c) presents the experimental set up for sealed conditions, where the electrical current was applied per cube, via cast-in conductive plates (brass mesh), completely covering the cross-sections A of the cubes (Fig. 4.1c). Fig. 4.1c) also depicts the sampling strategy for MIP and ESEM analysis and the geometrical location for microstructural analysis: middle section for fully or partly submerged conditions and middle section and sides for sealed conditions. More details with regard to Fig. 4.1c) are discussed in the relevant results section for sealed conditions. To be noted is that for both MIP and ESEM microstructural analysis, the comparison of results refers to identically handled specimens and identical geometrical location within one test series.

Table 4.1 Test matrix: □ - compressive strength; ○ - MIP/ESEM tests; Δ - el. resistivity (\* Full details on this (marked) investigation are reported in (Susanto et al. 2013)

| Current density<br>Groups | Hydration age | Condition and environment |                     |                  |                     |        |
|---------------------------|---------------|---------------------------|---------------------|------------------|---------------------|--------|
|                           |               | Partly submerged          |                     | Fully submerged  |                     | Sealed |
|                           |               | H <sub>2</sub> O          | Ca(OH) <sub>2</sub> | H <sub>2</sub> O | Ca(OH) <sub>2</sub> |        |
| Control                   | 3             | Δ *                       | -                   | Δ                | -                   | □ ○ Δ  |
|                           | 7             | Δ *                       | -                   | -                | -                   | □ Δ    |
|                           | 14            | □ Δ *                     | □ Δ                 | □ Δ              | □ Δ                 | -      |
|                           | 28            | □ ○ Δ *                   | □ ○ Δ               | □ ○ Δ            | □ ○ Δ               | □ ○ Δ  |
|                           | 84            | □ Δ *                     | □ Δ                 | □                | □ Δ                 | -      |
|                           | 112           | □ ○ Δ *                   | □ ○ Δ               | □ ○ Δ            | □ ○ Δ               | □ Δ    |
| 10mA/m <sup>2</sup>       | 3             | Δ *                       | -                   | -                | -                   | -      |
|                           | 7             | Δ *                       | -                   | -                | -                   | -      |
|                           | 14            | □ Δ *                     | □ Δ                 | -                | -                   | -      |
|                           | 28            | □ ○ Δ *                   | □ ○ Δ               | -                | -                   | -      |
|                           | 84            | □ Δ *                     | □ Δ                 | -                | -                   | -      |
|                           | 112           | □ ○ Δ *                   | □ ○ Δ               | -                | -                   | -      |
| 100mA/m <sup>2</sup>      | 3             | -                         | -                   | Δ                | -                   | □ ○ Δ  |
|                           | 7             | -                         | -                   | -                | -                   | □ Δ    |
|                           | 14            | -                         | -                   | □ Δ              | □ Δ                 | -      |
|                           | 28            | -                         | -                   | □ ○ Δ            | □ ○ Δ               | □ ○ Δ  |
|                           | 84            | -                         | -                   | □                | □ Δ                 | -      |
|                           | 112           | -                         | -                   | □ ○ Δ            | □ ○ Δ               | □ Δ    |
| 1A/m <sup>2</sup>         | 3             | -                         | -                   | □ Δ              | -                   | □ ○ Δ  |
|                           | 7             | -                         | -                   | -                | -                   | □ Δ    |
|                           | 14            | -                         | -                   | □ Δ              | □ Δ                 | -      |
|                           | 28            | -                         | -                   | □ ○ Δ            | □ ○ Δ               | □ ○ Δ  |
|                           | 84            | -                         | -                   | □                | □ Δ                 | -      |
|                           | 112           | -                         | -                   | □ ○ Δ            | □ ○ Δ               | □ Δ    |

Multiplexer devices (PC connected) were used to automatically output the electrical resistance of the mortar specimens in real time (the current supply was interrupted in the time of the measurement, details in section 4.2.3.2 below). The electrical current was applied from 24h of hydration age onwards i.e. immediately after de-moulding of the specimens for submerged conditions and after sealing the moulds for the sealed conditions. The tests duration was 112 days.

### 4.2.3 Test Methods

#### 4.2.3.1 Compressive strength

Standard compressive strength tests were performed on 40×40×40 mm<sup>3</sup> mortar cubes at the hydration ages of 3(7), 14, 28(84) and 112 days. Three replicate mortar specimens were taken out from the conditioning set-up, cloth-dried and tested within a 30 min time interval.

#### 4.2.3.2 Mortar electrical resistivity

The measurement of electrical resistivity of mortar specimens is done in the same manner as previously reported in Section 3.3.3.2, Chapter 3.

#### 4.2.3.3 Determination of pore structure parameters and image analysis

The pore structure parameters (MIP and ESEM) were determined via well-known and reported procedures, main details for which are given in Appendix A.

#### 4.2.3.4 Chemical analysis

Chemical analysis of the conditioning water (external medium) was performed to determine changes in alkali ions concentration (Na<sup>+</sup>, K<sup>+</sup> and Ca<sup>++</sup>) due to ions leaching-out from the mortar cubes. The tests were performed using Inductive Coupled Plasma Spectrometry (ICP-AES) after 1, 3, 14, 28, 44, 56 and until 112 days of conditioning of the mortar specimens. Additionally, chemical analysis for hydrated (chemically bound) water at certain hydration ages (1, 7, 14, 28, 84 and 112 days of conditioning) and for some of the tested specimens was determined according NEN 5931 (which is a standard loss of ignition test). According to NEN 5931 standard, the mass loss per gram of original cement was measured between 105°C and 775°C. The specimens were stored in the oven with temperature 105 °C to constant weight (at least 12 hours) and transferred to a desiccator to cool down to room temperature. Afterwards, the specimens were conditioned at 775 °C for at least 3 hours (but no more than 6 hours). After cooling of the specimens, the mass loss was determined. Based on the bound water content, the degree of hydration was calculated, using the following equation (Copeland et al. 1953):

$$\alpha = \left( \frac{w_n}{c} \right) / \left( \frac{w_n}{c} \right)_{max} \quad (4.1)$$

where  $(w_n/c)$  is the non-evaporable water content per gram of original cement in the mixture and  $(w_n/c)_{max}$  is  $(w_n/c)$  for complete hydration. The non-evaporable water

content per gram of original cement in the mixture  $W_n/c$  is calculated as follow (Copeland et al. 1953):

$$\frac{W_n}{c} = \frac{W_1}{W_2} (1 - L) - 1 \quad (4.2)$$

where  $W_1$  is the mass of paste prior to ignition (g),  $W_2$  is the mass of paste after ignition (g), and  $L$  is the loss of ignition for the sample of the original dry cement powder (g/g of original cement).

The  $(w_n/c)$  for complete hydration  $((w_n/c)_{max})$  mainly depends on the clinker composition of the cements and the amount of reacted cement and can be calculated using the following equation (Copeland et al. 1960):

$$\left(\frac{W_n}{c}\right)_{max} = w_1 * (C_3S) + w_2 * (C_2S) + w_3 * (C_3A) + w_4 * (C_4AF) \quad (4.3)$$

where  $w_{1..4}$  is non evaporable water content for individual constituents (g/g) and the designations in bracket (..) is the content of major constituents of the cement considered (g).

Table 4.2 Non-evaporable water content for major phases (individual constituents) of cement

| Cement Phase | Coefficient ( $w_{1..w4}$ )<br>(g water/g cement phase) (Neville 1981;<br>Taylor 1990) | Mineral composition of cement CEM I 42.5<br>(% by weight) |
|--------------|--|---|
| $C_3S$       | 0.23   | 0.62  |
| $C_2S$       | 0.21   | 0.105   |
| $C_3A$       | 0.40   | 0.073   |
| $C_4AF$      | 0.37   | 0.102   |

By using Eq. (4.3) and the data in Table 4.2, the value of 0.238 can be obtained for the term  $(w_n/c)_{max}$ . This value is close to the previously reported results, e.g. 0.23 (Taylor 1990) or in a range between 0.23 and 0.25 (Sun et al. 2005).

## 4.3 Results of experimental studies and discussion

### 4.3.1 Compressive strength

The compressive strength development of cement-based materials is determined by several factors, including water-to-cement ratio, cement type, admixtures and curing conditions including humidity, temperature and age (Hu 2004; Mehta et al. 2001). Generally, compressive strength increases with the progress of cement hydration and is directly related to microstructural development of the cement-based matrix with time (with maturity development). Figure 4.2 presents the recorded compressive strength as a

function of hydration age for mortar specimens as follows: *partly submerged in water and  $\text{Ca}(\text{OH})_2$*  (Fig. 4.2a), as a comparison for control specimens and “under current” condition at the lowest current density level of  $10 \text{ mA/m}^2$ ; *fully submerged in water* (Fig. 4.2b) and in  $\text{Ca}(\text{OH})_2$  (Fig. 4.2c) - control and “under current” conditions at current density levels of  $100 \text{ mA/m}^2$  and  $1 \text{ A/m}^2$  - Fig. 4.2b); *sealed conditions* (Fig. 4.2d) - control and “under current” at current density levels of  $100 \text{ mA/m}^2$  and  $1 \text{ A/m}^2$ .

The varying environment i.e. water or  $\text{Ca}(\text{OH})_2$ , as well as the different levels of stray current ( $10 \text{ mA/m}^2$ ,  $100 \text{ mA/m}^2$  and  $1 \text{ A/m}^2$ ) were designed to elucidate the effects of ion and water diffusion and ion and water migration, separately or as a synergy. It was expected that leaching-out would occur in water environment, will be minimum in alkaline medium and will not be relevant for sealed conditions. Ion and water migration were a factor when current flow was involved. The resulting mechanical properties were expected to vary with respect to the external medium, the level of stray current density and the above transport mechanisms.

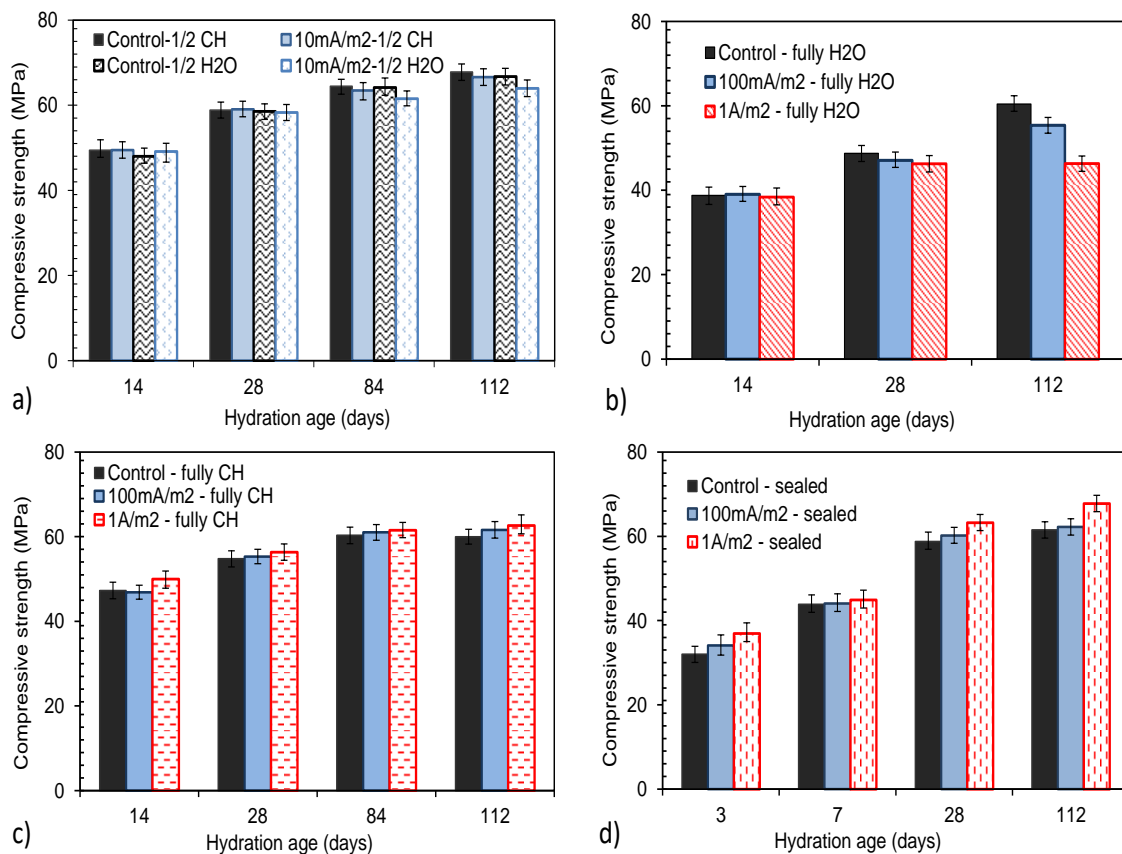


Fig. 4.2 Compressive strength as a function of hydration age for mortar specimens in rest and “under current” conditions: (a) partly submerged in  $\text{H}_2\text{O}$  and  $\text{Ca}(\text{OH})_2$  solution; (b) fully submerged in  $\text{H}_2\text{O}$ ; (c) fully submerged in  $\text{Ca}(\text{OH})_2$  solution; (d) sealed condition

As shown in the Fig. 4.2, the compressive strength for all mortar specimens tends to increase with time of conditioning and with on-going cement hydration. This was as expected, and as observed, for all conditions and irrespective of external medium or current density levels. At 28 days of age all specimen groups present compressive

strength in the range of 60-65MPa, with the exception of water-submerged conditions, where approx. 45MPa was recorded. Despite this difference, the recorded compressive strength fulfils the expected from OPC CEM I 42.5N minimum mechanical properties at 28 days of age. The importance of the tests was also in view of recording performance with prolonged treatment, with relevance to environment and current density levels, which are discussed in what follows.

For *partly submerged conditions* in control and “under current” regimes at the lowest current density levels ( $10 \text{ mA/m}^2$ ) - Fig. 4.2a, there was no substantial effect of the treatment and/or the current flow on compressive strength development. For mortar specimens partly submerged in  $\text{Ca(OH)}_2$  solution, similar compressive strength development was observed for both control and “ $10 \text{ mA/m}^2$ ” groups. However, a general trend to lower compressive strength values towards the end of the test was recorded for the “under current” regime - group  $10 \text{ mA/m}^2$ , partly submerged in water.

For *fully submerged conditions* (Figs. 4.2b and 4.2c), a more pronounced effect of both external medium and current flow was already observed, bearing in mind that in these conditions the current density level was also higher than that in partly submerged conditions i.e.  $100 \text{ mA/m}^2$  and  $1 \text{ A/m}^2$ . For water submerged specimens (Fig. 4.2b) the effect of current flow was especially pronounced for the specimens subjected to the highest current density level of  $1 \text{ A/m}^2$ , where 45 MPa was recorded after 112 days, while 60 MPa was recorded for the control group at the same age and equal environmental conditions (Fig. 4.2b). A reduction of compressive strength between 28 days of age and the end of the test (112 days) was recorded for the  $1 \text{ A/m}^2$  group only. The specimens in group “ $100 \text{ mA/m}^2$ ” maintained higher values at the end of the test (approx. 50MPa), but in a lower range, if compared to control conditions (60MPa). In contrast, the fully submerged in  $\text{Ca(OH)}_2$  specimens, Fig. 4.2c, exhibit an increasing trend only of compressive strength development over time, irrespective of the current regime. As seen from Fig. 4.2c, a slight increase even of compressive strength was recorded for mortar in the “under current” regimes. This effect was again more pronounced for the “ $1 \text{ A/m}^2$ ” group if compared to the lower current density level of  $100 \text{ mA/m}^2$  and control specimens.

For *sealed conditions* – Fig. 4.2d), an increase only of compressive strength was relevant for all tested specimens. A more significant effect was again relevant to the highest current density regime ( $1 \text{ A/m}^2$ ), in which the mortar specimens exhibited the highest compressive strength at the end of the test ( $\sim 65 \text{ MPa}$ ), (Fig. 4.2d).

What can be concluded from the results in this section is as follows: the development of compressive strength is related to cement hydration with time (with age). This follows the increase in maturity of the cement-based bulk matrix. Consequently, in control (rest) conditions, when other factors were not relevant, the compressive strength would present an increasing trend, followed by stabilisation. The evolution of mechanical properties, following microstructural development, however, is directly linked to the chemical reactions within the cement hydration process. Cement hydration on the other hand is a process, involving (among other factors) ion and water transport due to diffusion and/or migration (capillary suction and permeation were not of significance in the conditions of this work, and are therefore not discussed). In conditions of current flow, diffusion and migration are taking place in parallel. Therefore, enhanced ion and water transport, as in “under current” conditions, would result in altered (mostly enhanced at early stage) cement hydration. Enhanced ion and water transport will also lead to elevated alkali ions leaching-out in conditions, where

concentration gradients between the mortar matrix and the external medium are present. Consequently, competing or parallel mechanisms would be relevant for the “under current” regimes: on one hand, enhanced cement hydration, microstructure densification and mechanical strength development *at early stage* will be relevant for all tested specimens. These will dominate throughout the test, i.e. including also the later stages of the test for sealed and  $\text{Ca}(\text{OH})_2$ -conditioned specimens.

Enhanced alkali ions leaching and potentially reversed effects on microstructural development, and mechanical performance respectively, *at later stages* will be relevant for water-conditioned specimens. These mechanisms will be affected by the absence or presence of current flow and were expected to be more pronounced for higher current density levels (i.e. enhanced ions and water migration), as actually observed and recorded. In other words, the effect of stray current on mechanical properties is negative, when a concentration gradient between the cement-based material and external environment is present. In contrast, the effect of stray current would be positive at earlier ages of the cement-based system when concentration gradients are minimum or none i.e. when leaching is avoided.

Chemical analysis of the external medium (for water-treated specimens), together with overall microstructural characterisation of the bulk mortar matrix for all tested conditions, elucidate and support the observed mechanical performance in control and “under current” conditions. The results and discussion on these aspects are presented in the following sections.

#### 4.3.2 Chemical analysis of the external medium

When a cement-based material is in a prolonged contact with water, dissolution of cement hydrates will occur (due to alkali ions ( $\text{Ca}^{2+}$ ,  $\text{Na}^+$ ,  $\text{K}^+$ ) leaching). The transport of sodium and potassium is faster than that for calcium ions (Saito et al. 1992), and more pronounced at early stages (less mature cement matrix, hence more open pore structure), whereas stable and/or negligible with longer treatment. Leaching of calcium ions promotes coarsening of the pore structure, leads to increased transport properties (permeability, diffusivity) and decrease in mechanical properties (Roessler et al. 1985, Young et al. 1988). Several studies report on calcium ions leaching from cement-based materials submerged in water (Alonso et al. 2006; Faucon et al. 1996; Faucon et al. 1998; Haga et al. 2005; Maltais et al. 2004). Calcium leaching was also tested and reported when accelerated methods were applied, involving electrical or chemical gradients (Ryu et al. 2002; Saito et al. 1992; Wittmann 1997). The results showed that the application of a potential gradient to mortar specimens can be successfully used to assess deterioration mechanisms due to calcium ions leaching.

In this work, the dissolution process, in terms of alkali ions leaching, was only relevant to the partly submerged and fully submerged in water mortar specimens, with applied current density of  $10\text{mA/m}^2$ ,  $100\text{mA/m}^2$  and  $1\text{A/m}^2$ , respectively. Obviously, leaching was not expected for sealed conditions and in  $\text{Ca}(\text{OH})_2$  environment. In the former case, there was no aqueous external environment. In the latter case, calcium leaching was expected to be minimum or none, since there was no concentration gradient or chemical potential between the mortar specimens and the external  $\text{Ca}(\text{OH})_2$  solution. Therefore, chemical analysis of the external aqueous medium was performed only for the groups of water-treated specimens.

The concentration of leached-out calcium, sodium and potassium (in mg/l) in the external medium was recorded after 1, 3, 14, 28, 44, 56 and 112 days (Fig. 4.3). The concentration of relevant ions in the external solution was analysed at each of the above stages, after which the medium was exchanged with a fresh one until a subsequent exchange at the next stage. As expected, the leaching process was faster at early ages (early hydration age, higher porosity) and gradually stabilised at later ages, along with increasing the maturity level of the mortar specimens.

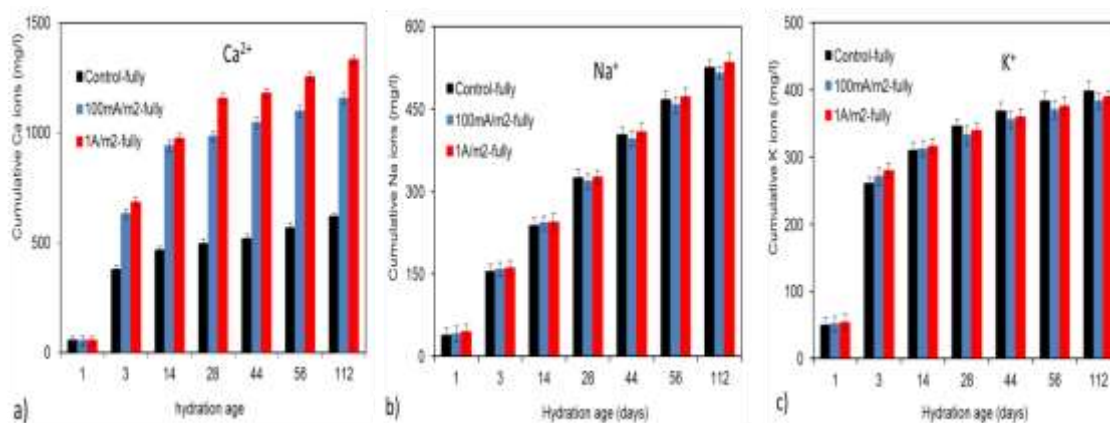


Fig. 4.3 Cumulative concentration of calcium (a), sodium (b) and potassium (c) in the external medium due to leaching-out of mortar specimens, fully submerged in water (comparison of control (no current) and “under current” regimes).

4

As previously reported in Chapter 3, current density of 10mA/m<sup>2</sup> in partly submerged in water conditions accelerated the calcium leaching process approx. 1.27 times, if compared to control conditions. Fig. 4.3a) presents the result for fully submerged in water specimens, subjected to the higher current density level regimes i.e. 100 mA/m<sup>2</sup> and 1A/m<sup>2</sup> in comparison to control specimens in these series. The calcium ions concentration in the external medium after 56 days was 567.3 mg/l, 1099.18 mg/l and 1254 mg/l for control cases, 100 mA/m<sup>2</sup>, and 1A/m<sup>2</sup>, respectively. Calcium leaching increased with 1.93 times for the lower current density regime and 2.04 times for the 1A/m<sup>2</sup> regime, if compared to the control specimens. There was no further substantial change in the calcium ions concentration between 56 and 112 days.

As above mentioned, absolute values are not claimed, but only trends of material behaviour are discussed, in relation to the effects of stray current for all test series. It can be concluded that irrespective of the current density level (100 mA/m<sup>2</sup> or 1A/m<sup>2</sup>), calcium leaching was enhanced for the “under current” regimes, if compared to the control cases (Fig. 4.3a). Leaching of sodium (Na<sup>+</sup>) and potassium (K<sup>+</sup>) ions was also recorded (Figs. 4.3b)c). Na<sup>+</sup> and K<sup>+</sup> ions have higher solubility and mobility in the pore solution than that of Ca<sup>2+</sup> ions. As a consequence, Na<sup>+</sup> and K<sup>+</sup> ions will dominate the diffusion and/or migration process more significantly in the beginning of the tests, and will not vary substantially on later stages, as also reported by Babaahmadi et al. (Babaahmadi et al. 2015). As can be observed in Fig. 4.3b)c), leaching out of sodium and potassium was relevant and gradually increased over time for all specimens and conditions. The concentration of leached out Na<sup>+</sup> and K<sup>+</sup> ions for the “under current”

specimens was not significantly different from that for the control specimens on later ages. This is in accordance with the abovementioned mechanisms and outcomes from other studies and related to the increasing portion of disconnected pore network with age of the mortar matrix, which is independent from the dissolution of calcium bearing phases and re-distribution of the pore network e.g. enlargement of initially smaller pores.

Overall, for the “under current” conditions the current flowing through both submerged mortar matrix will logically accelerate ion and water transport and consequently promote the leaching process. This effect has to be judged also from the view point of microstructure development with time of conditioning. The consequence of calcium ions leaching in particular is an increase of porosity and a global decrease in mechanical performance (compressive strength) of cement-based materials (Carde et al. 1996; Nehdi et al. 2011; Saito et al. 1992; Saito et al. 1999). Therefore, the leaching process will be determined not only by the ion and water migration within the connected pore network, but would be largely dependent on microstructural alteration over time. Hence, the leaching-out effects, or limitations thereof, could be counterbalanced as well, resulting in similar amounts of leached out alkali ions for otherwise different conditions. For the hereby tested series of specimens, and as can be observed in Fig. 4.3, higher current density promoted higher leaching-out effects.

### 4.3.3 Microstructural analysis – MIP results

Figure 4.4 to Figure 4.7 depict MIP-derived porosity and pore size distribution for the bulk matrix of all tested specimens. The plots present an overlay of results for 28 days of age and the latest tested age of 112 days (3 days and 84 days of age for some groups are also presented). The discussion is in view of trends for pore network development in time and in varying experimental conditions, rather than comparing absolute values. Figure 4.4 shows the MIP results as an overlay of two replicates for mortar specimens submerged in water solution at 28 days. It can be seen from Fig. 4.4 that MIP data have a good reproducibility.

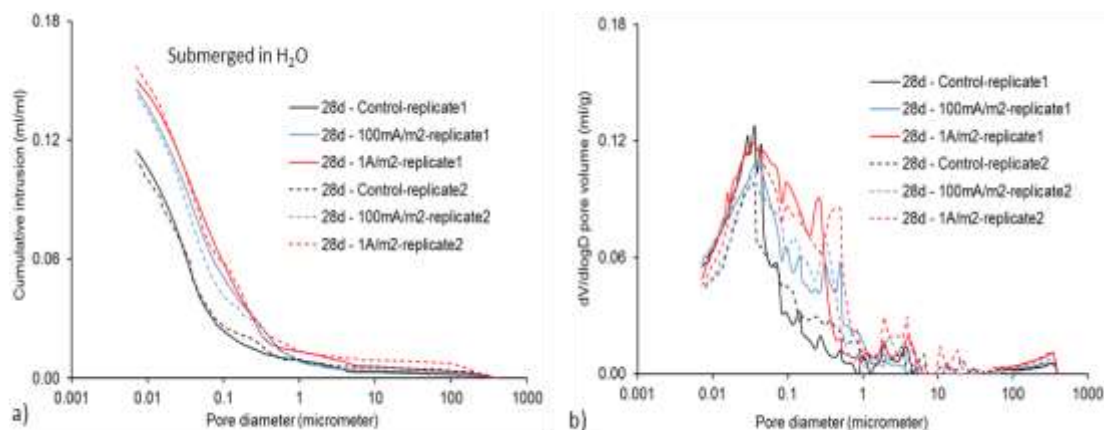


Fig. 4.4 Example overlay of porosity (a) and pore size distribution (b) obtained from replicates of MIP data for mortar specimens submerged in water solution at 28 days of conditioning time.

#### 4.3.3.1 The effect of external medium

*Partly submerged conditions, H<sub>2</sub>O and alkaline (Ca(OH)<sub>2</sub>) external medium:* Fig. 4.5 presents the MIP results for control specimens and those subjected to 10 mA/m<sup>2</sup> current flow in partly submerged conditions. The MIP results show that for water-conditioned control specimens, a reduction in porosity was observed between 28 days and 84 days but increase towards 112 days of age, Fig. 4.5a)b). Similarly, first reduction and later-on increase in porosity holds for the “under current”, water-conditioned specimens (Fig. 4.5a), however, in these conditions a more pronounced re-distribution of pore size was observed in the course of the experiment between 28 and 112 days of age (Fig. 4.5b).

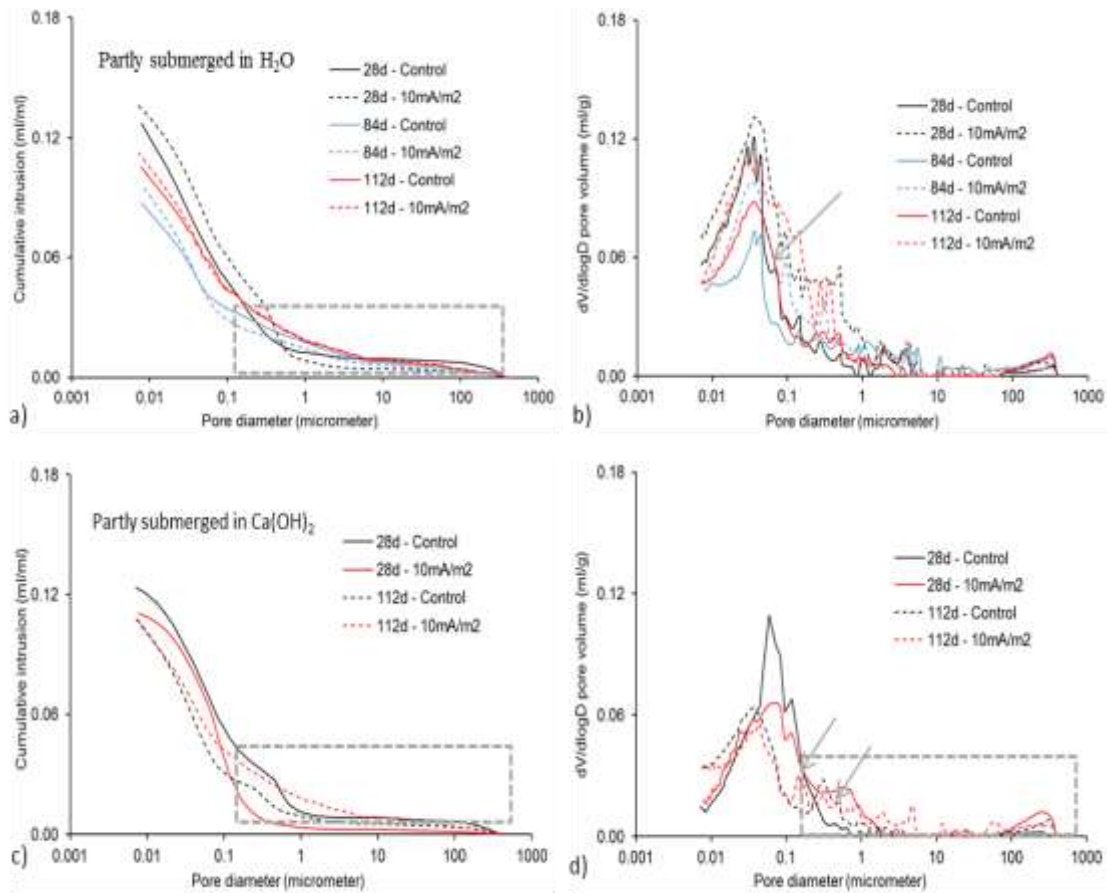


Fig. 4.5 MIP-derived porosity and pore size distribution for mortar at 28 days, 84(112) days of age - control and “under current” conditions, **10 mA/m<sup>2</sup>**: (a, b) partly submerged in water; (c, d) partly submerged in Ca(OH)<sub>2</sub> solution.

Both porosity and pore size maintained higher values for the “under current” (10 mA/m<sup>2</sup>) regime, compared to control conditions i.e. 9.6% higher at 28 days of age, 10.3 % at 84 days of age and 6.9% at 112 days of age. In contrast, for Ca(OH)<sub>2</sub>-conditioned mortar, stray current at the same level of 10 mA/m<sup>2</sup> induced densification at 28 days of age and no substantial changes at 112 days, Fig. 4.5c)d). The control specimens in this series also presented reduction in porosity and pore size between 28 days and 112 days.

Concentration gradients were not relevant for the Ca(OH)<sub>2</sub>-conditioned specimens, hence densification only (reduced porosity) was observed due to ongoing cement

hydration. For “under current”, water-conditioned specimens, diffusion controlled transport was in parallel (or counter-acting) with migration-controlled transport (along with cement hydration). Therefore, a more pronounced coarsening of the matrix and changes in pore size distribution was observed. In other words, migration enhanced the leaching-out process, resulting in pore size re-distribution i.e. enlarging pores of initially smaller size. For the  $\text{Ca}(\text{OH})_2$ -conditioned specimens, migration did not have a significant effect, although a slight re-distribution of the pore network (in the range of pore size larger than  $0.317 \mu\text{m}$ ) was observed in the MIP results (marked regions in Fig. 4.5c,d) and confirmed by ESEM image analysis (discussed further below in Section 4.3.4).

*Fully submerged conditions ( $\text{H}_2\text{O}$  and alkaline ( $\text{Ca}(\text{OH})_2$ ) external medium) and Sealed conditions:* Figures 4.6 and 4.7 present the MIP results for specimens in fully submerged and sealed conditions, respectively. For *water-conditioned specimens*, the mechanisms controlling pore structure development were: a) cement hydration and b) diffusion-controlled water and ion transport under concentration gradient – for control cases, together with c) migration-controlled ion and water transport – for “under current” cases.

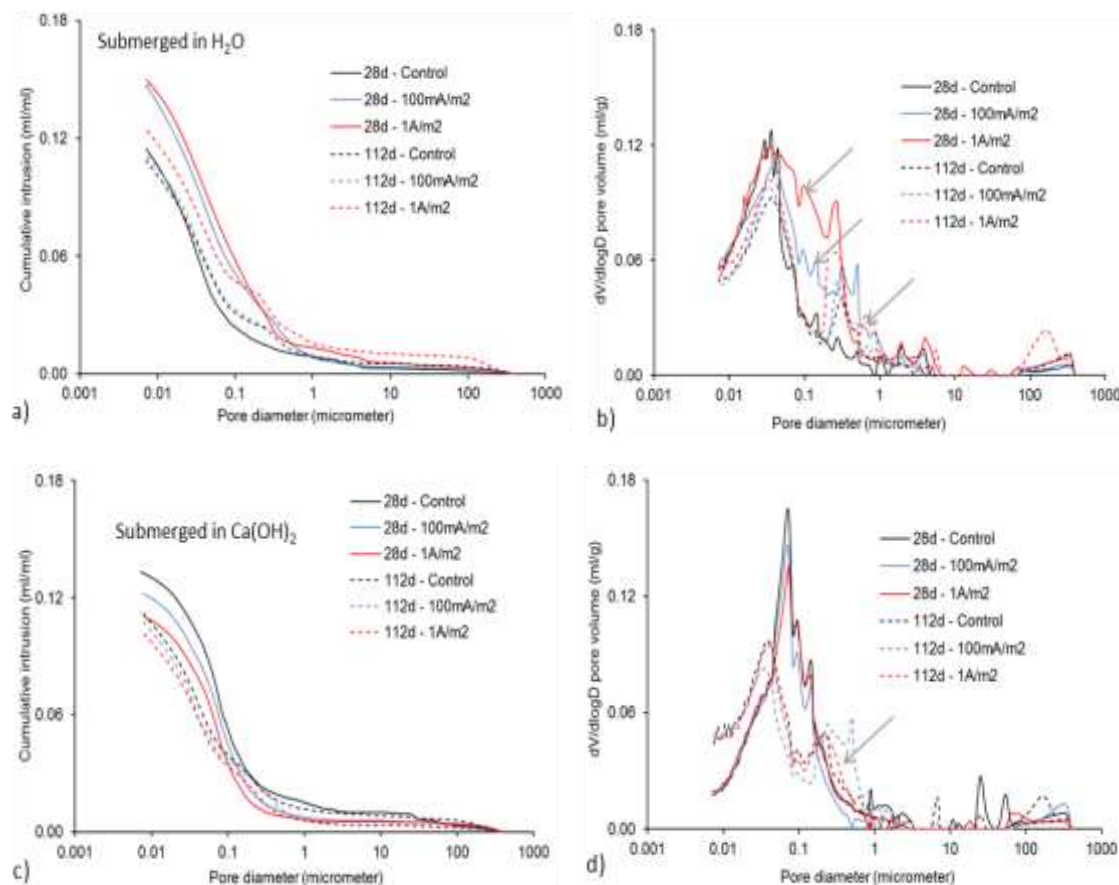


Fig. 4.6 MIP-derived porosity and pore size distribution for mortar at 28 days and 112 days of age for control and “under current” conditions of  $100 \text{ mA/m}^2$  and  $1 \text{ A/m}^2$ : (a, b) fully submerged in water; (c, d) fully submerged in  $\text{Ca}(\text{OH})_2$

For *Ca(OH)<sub>2</sub>-conditioned and sealed specimens*, two mechanisms were predominant: a) cement hydration and c) migration-controlled transport. The effect of cement hydration for all groups would be seen in densification of the bulk matrix with time in both control and “under current” regimes. The changes under a synergetic effect of stray current and varying external medium are discussed in what follows.

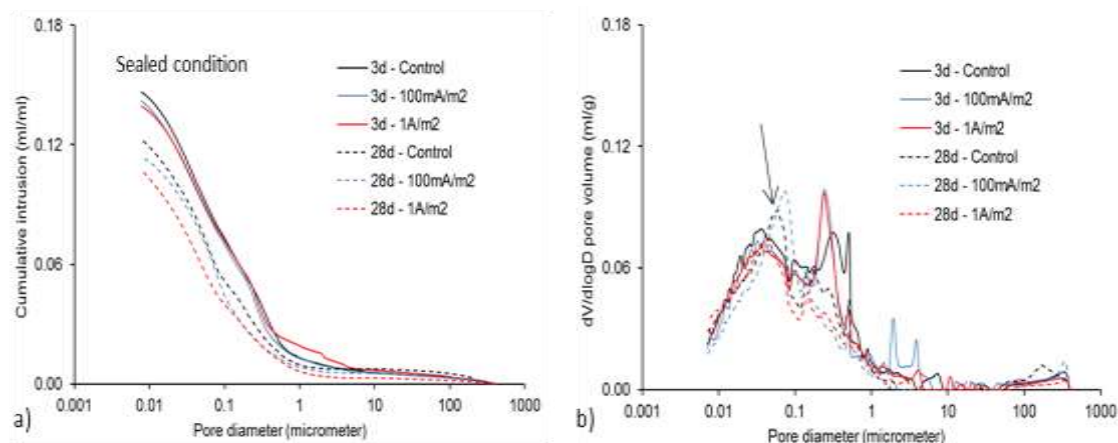


Fig. 4.7 MIP-derived porosity and pore size distribution for *sealed* mortar at 3 and 28 days of age - control and “under current” of 100 mA/m<sup>2</sup> & 1A/m<sup>2</sup>.

#### 4.3.3.2 The effect of stray current and varying medium

4

*Control specimens in all conditions:* Figs. 4.6a,b) show the water conditioned group, where the effect of hydration alone was minimal, with almost no change in porosity between 28 and 112 days. Figs. 4.6c,d) and Fig. 4.7a,b) depict the Ca(OH)<sub>2</sub> condition and sealed specimens, respectively, where the effect of cement hydration alone is well pronounced, with well visible reduction in porosity from earlier ages to 112 days. For the water conditioned control specimens, the effect of cement hydration would be counterbalanced by leaching-out and subsequent re-distribution of initially smaller pores towards larger size, evident from Fig. 4.6b (marked regions). For the control specimens in Ca(OH)<sub>2</sub> and sealed, concentration gradient is not present and leaching-out not relevant.

*“Under current” conditions:* For specimens in water, the concentration gradient (diffusion-controlled transport) adds-up to the migration-controlled transport. As can be seen in Fig. 4.6a), the higher the current density level, the higher the level of observed structural modification. For 28 days of age, higher porosity was recorded for specimens in the 100mA and 1A groups, compared to controls. Porosity increased for the “under current” regime at 28 days of age with ca. 31.8% and 26.78% for current density levels 1A/m<sup>2</sup> and at 100mA/m<sup>2</sup>, respectively, compared to control specimens. At 112 days of age the increase was with ca. 15.34% and 4.76% for the “under current” specimens. This was accompanied by an obvious re-distribution of pore size for these specimens from (potentially) smaller pore size to pore enlargement, evidenced by the significant distortion of the differential curves between 0.5μm and 1μm at both 28 days and 112 days of age (Fig. 4.6b, marked region). The effect is similar to the partly submerged in

water conditions (Fig. 4.5a)b), but more significant due to the higher current density levels (along with larger relative humidity, as in saturated condition). At the age of 112 days, the trend of increased porosity and pore size re-distribution for water treated specimens remained. At both 28 and 112 days, the most significant microstructural changes were observed for the highest current density level of  $1\text{A/m}^2$ .

For  $\text{Ca}(\text{OH})_2$ -treated specimens, the effect of stray current was positive at 28 days of age, if judged from the reduction in porosity for the “under current” specimens – Fig. 4.6c)d). For these specimens, leaching-out was not relevant (no concentration gradient present). Therefore, enhanced ion and water migration in “under current” conditions resulted in enhanced cement hydration (Fig. 4.10), followed by reduction in total porosity at earlier stages (28 days) and no significant difference in porosity at the later stage of 112 days. Critical pore size remained similar and not affected by the current flow at 28 days of age, while re-structuring of the pore network in terms of pore size distribution was observed for 112 days (Fig. 4.6d). This change is attributed to the effect of current flow and, similarly to the water-conditioned specimens, was more pronounced for the higher level of current density of  $1\text{A/m}^2$ .

*Sealed conditions* (Fig. 4.7), the MIP analysis was performed at a very early hydration age – 3 days, and at 28 days. As can be observed (and as expected due to the fresh matrix), porosity and pore size reduced from 3 days to 28 days for all sealed specimens. At the stage of 3 days, no significant change was observed between control and “under current” conditions (Fig.7a), slightly reduced porosity was recorded in the presence of current flow. After 28 days, a more pronounced effect of the current flow was already observed (Fig. 4.7a,b), with reduced porosity and pore size, more significant for the specimens at the higher current density level of  $1\text{A/m}^2$ .

If a comparison is made between *Ca(OH)<sub>2</sub>-treated specimens and sealed specimens* for the stage of 28 days of age, the following can be noted: the difference between control and “under current” regimes (Fig. 4.7a and Fig. 4.6c) was comparable for both conditions. Although limited migration-controlled ion and water transport for the sealed specimens would be relevant (transport processes limited to the pore water only), the absence of concentration gradient in both test series determined similar microstructural development. For both series, the effect of current flow appeared to be only positive for the time frame of the test, with reduced porosity and re-distribution towards smaller pore size over time (Figs. 4.6c,d; 4.7a,b). Similarly to all other tested conditions, the effect of the larger current density level of  $1\text{A/m}^2$  was more pronounced, compared to the lower level of  $100\text{mA/m}^2$ .

#### 4.3.4 Microstructural properties as derived by ESEM image analysis

4.3.4.1 *Partly submerged conditions*,  $\text{H}_2\text{O}$  and alkaline ( $\text{Ca}(\text{OH})_2$ ) external medium Figs. 4.8,4.9,4.11,4.12 present the bulk matrix for partly submerged (water and  $\text{Ca}(\text{OH})_2$ ) specimens and the relevant pore structure analysis after 28 days and 84 (112) days of conditioning. Figure 4.8 depicts the bulk cement paste of water conditioned specimens at 28 days and 84 days of age, Fig. 4.9 presents the pore structure analysis from 7 days of age, through 28, 56, 84 and 112 days of age. As can be clearly observed in Fig. 4.9 coarsening of the matrix between 28 days and 112 days of age was relevant for the specimens in water. The effect is more pronounced for the “under current”

regimes. An initially positive effect of the stray current was observed, Fig. 4.9a), reflected by matrix densification in “under current” conditions (compare 7 days result in Fig. 4.9a) for specimens R (control) and S (10mA/m<sup>2</sup>). At this early stage the critical pore size remained similar, which was as expected for a fresh mortar matrix (24h cured only).

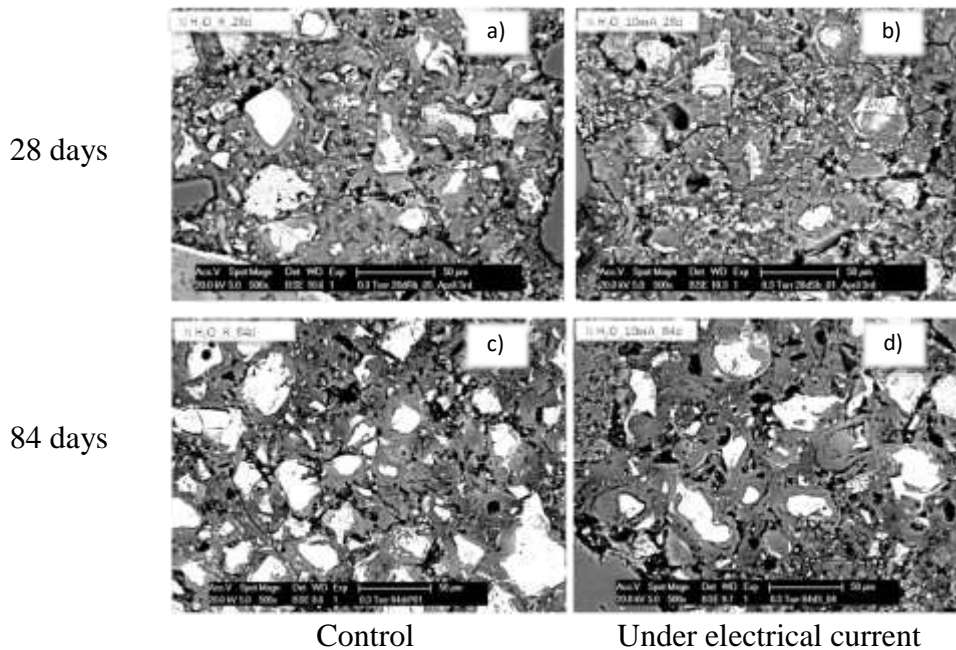


Fig. 4.8 ESEM micrographs, 500× of mortar bulk matrix at 28 days (top row) and 84 days of age (bottom row) in *partly submerged in water* conditions: control (a,c) and “under current” regime (10mA/m<sup>2</sup>) (b,d)

4

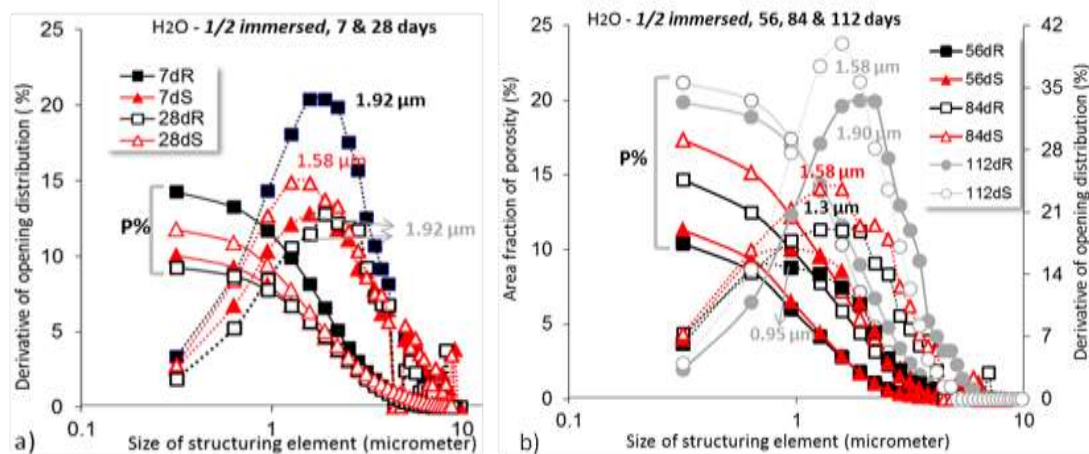


Fig. 4.9 Porosity and pore size distribution – mortar bulk matrix in *partly submerged in water* conditions in control and “under current” regime (10mA/m<sup>2</sup>)– a) overlay of results for 7 and 28 days of age; b) overlay of results for 56, 84 and 112 days of age.

At 28 and 56 days of age similar values were recorded for both S and R specimens, slightly higher for the former case (Fig. 4.9a,b). Critical pore size remained the same for

control conditions, R and decreased for “under current” conditions, S. After 84 days and at the end of the test, coarsening was observed with an already larger difference in pore structure parameters, with increase of porosity and pore size in both R and S conditions, (Fig. 4.9b). The pore structure alterations would be mainly attributed to leaching-out related coarsening in the sense of enlargement of initially smaller pores. Although a straightforward correlation between MIP and ESEM image analysis cannot be made for several reasons, e.g. the nature of parameters derivation and/or the fact that MIP tests refer to the full volume of material tested, while image analysis refers only to the bulk cement paste, the results from image analysis are in line with those from MIP as far as the effect of stray current is considered and especially with prolonged treatment. Additionally, image analysis is only relevant to pore space larger than  $0.317\ \mu\text{m}$  (marked region e.g. in Fig. 4.5a). To that end, the MIP and image analysis results for the control specimens between 28 days and 84 days of age are contradictory at a first glance, while in line between 84 days and 112 days. The MIP results (Fig. 4.5a) depict a reduction in overall porosity between 28 and 84 days and increase between 84 and 112 days, while image analysis presents reduction in porosity between 7 and 56 days of age, but increase between 56 and 112 days of age (Fig. 4.9). The changes in porosity derived by image analysis are accompanied with a larger critical pore size at 28 days ( $1.92\ \mu\text{m}$ , Fig. 4.9a), reducing to  $0.95\ \mu\text{m}$  at 56 days and increase to  $1.3\ \mu\text{m}$  and  $1.9\ \mu\text{m}$  at 84 days and 112 days, Fig. 4.9b). These alterations were not fully detected by MIP, although the differential curves show a large variation for pore sizes, larger than  $0.05\ \mu\text{m}$  (marked region in Fig. 4.5b) at later stages. This outcome is as expected due the fact that mortar was tested (rather than cement paste), resulting in a significant contribution of the matrix heterogeneity within the MIP tests, while the ESEM image analysis is based on direct observations of the bulk cement paste matrix.

Summarising, for partly submerged in water specimens, the alliance of counteracting enhanced ion and water transport (potentially enhanced cement hydration) and (enhanced) leaching-out in conditions of stray-current, resulted in a more pronounced matrix degradation at the end of the test, if compared to control conditions. In fact, the initially enhanced cement hydration due to current flow, was evidenced by the amount of hydrated (chemically bound) water, derived by chemical analysis - Fig. 4.10a) for water-conditioned specimens.

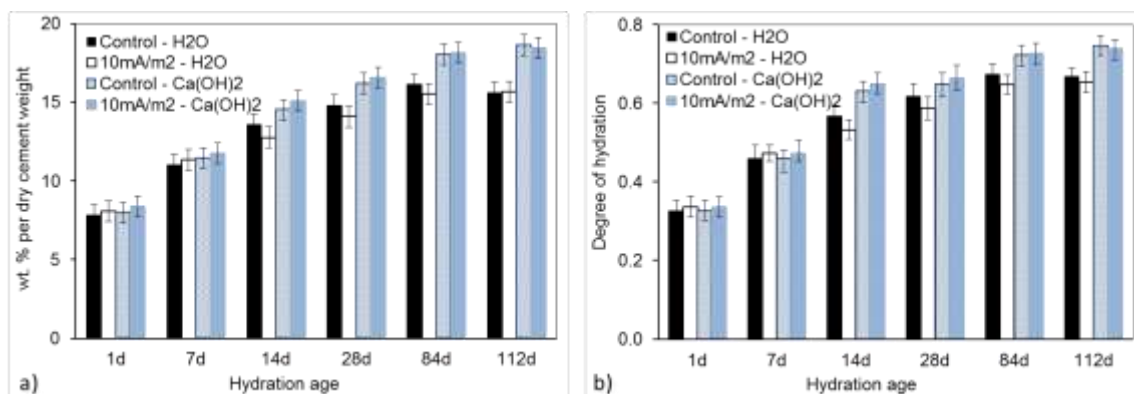


Fig. 4.10 (a) Weight percent of hydrated (chemically bound water) per dry cement weight for specimens partly-submerged in water and in  $\text{Ca}(\text{OH})_2$  at various hydration ages; (b) degree of hydration, calculated as specified in Section 2.3.5.

While the initial stages showed elevated hydrated water content in “under current” specimens, compared to control ones, this trend was reversed after 14 days of age, Fig. 4.10a). The difference is not significant, but clearly supports the fact that with on-going cement hydration, the hydration rate increased over time for all cases, however, was counteracted by leaching-out (Fig. 4.3) due to diffusion and/or migration-controlled ion and water transport. The effect of current flow was initially positive (Fig. 4.10a), but later on (>14 days), negative.

In contrast to the partly-submerged in water specimens (Figs.4.8, 4.9), the test series of partly-submerged in  $\text{Ca(OH)}_2$  mortar cubes (Figs. 4.11, 4.12) present a different trend of pore structure development. It is well visible that the microstructural variation between control and under current conditions at both 28 days and 112 days of age was not as significant (Fig. 4.12), as otherwise clearly observed for the partly-submerged in water specimens (Fig.9). At 28 days of age (Fig. 4.12a), porosity and critical pore size remained in the same range for all regimes, both significantly lower if compared to the partially-submerged in water specimens (Fig. 4.9a). Total porosity decreased from 28 days to 112 days (Fig. 4.12a,b), but maintained higher for the “under current” regime.

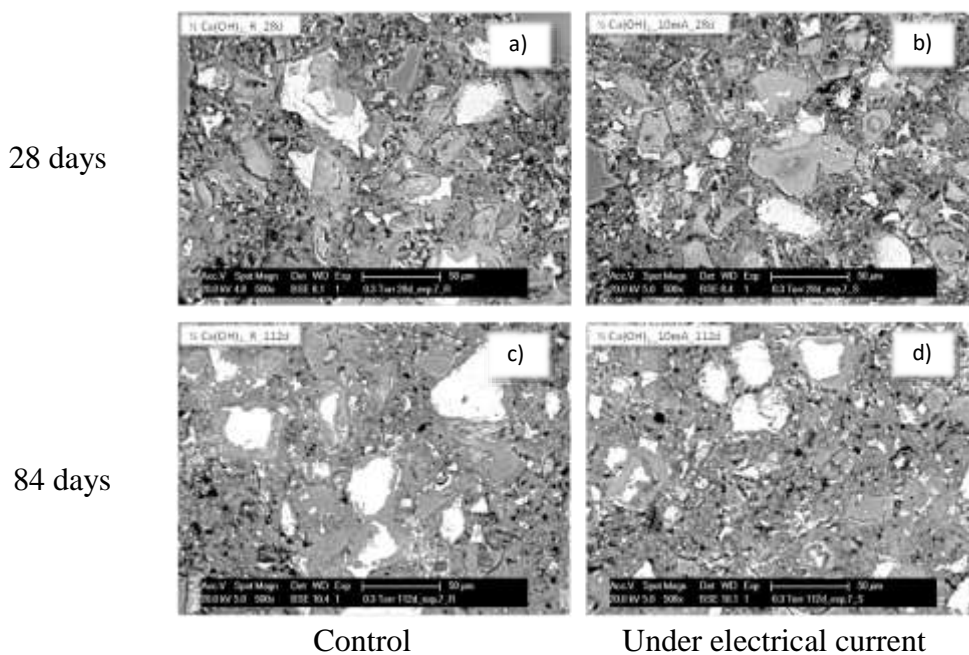


Fig. 4.11 ESEM micrographs, 500 $\times$  of mortar bulk matrix at 28 days (top row) and 112 days of age (bottom row) - partly submerged in  $\text{Ca(OH)}_2$  conditions for control (a,c) and “under current” regime (10mA/m<sup>2</sup>) (b,d).

As can be observed from the differential curves in Fig. 4.12b), although critical pore size remained similar, a slight re-distribution in pore size seemed to be relevant for both control and under current specimens between 28 days and 112 days, which was not as expected. This is in line with the MIP results for this series (Fig. 4.5c,d), showing restructuring in the family of capillary pores (> 0.1  $\mu\text{m}$ ). The result can be interpreted as follows: in partly submerged  $\text{Ca(OH)}_2$  conditions, on-going cement hydration would be

enhanced when stray current was involved. Therefore, densification of the bulk matrix at earlier stages (28 days) was expected for the “under current” conditions and was as observed (Fig. 4.12a), although not significant. No concentration gradient was relevant between the submerged portion of the mortar cubes and the external medium. However, concentration gradient was possible between the bottom (submerged) part of the cube and the top (on air) part. Therefore, a slight coarsening of the pore structure in “under current” conditions, compared to control conditions, is possible and was as observed, (Figs. 4.5d, 4.12b). This is attributed to uneven relative humidity in the total volume of the specimens.

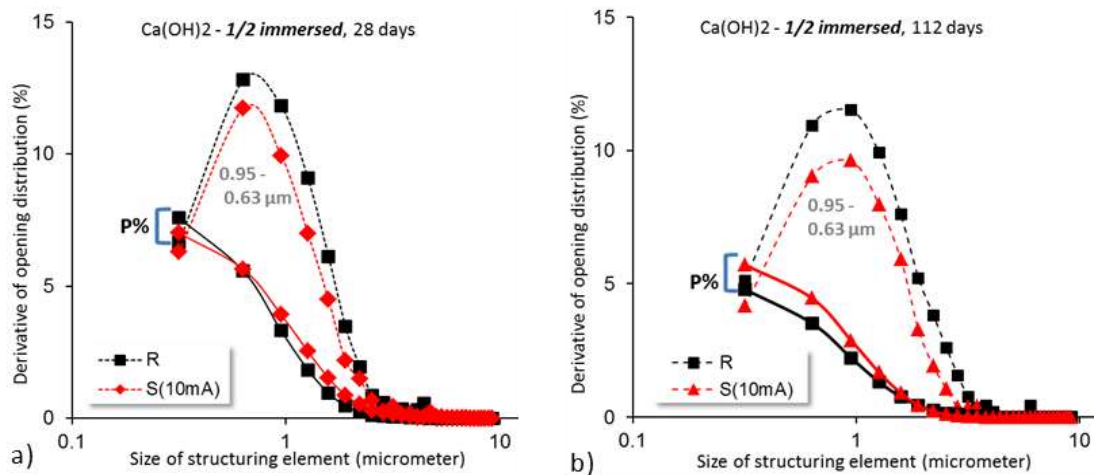


Fig. 4.12 Porosity and pore size distribution for mortar bulk matrix in control and “under current” regime ( $10\text{mA/m}^2$ ) - partly submerged in  $\text{Ca}(\text{OH})_2$  conditions – a) overlay of results for 28 days of age; b) overlay of results for 112 days of age.

The above results and discussion for partly-submerged in  $\text{Ca}(\text{OH})_2$  specimens were supported by the recorded hydrated water content and the derived degree of hydration, respectively, as depicted in Fig. 4.10a)b). Similarly to the partly-submerged in water conditions, slightly enhanced hydration rate was relevant for the “under current” regime in  $\text{Ca}(\text{OH})_2$  medium at earlier ages, with no further significant effects at later stages. Fig. 4.10 also clearly shows the effect of external medium on hydration rate and cement hydration in general. The difference in values between water-treated and  $\text{Ca}(\text{OH})_2$  treated specimens (Fig. 4.10a,b) is well evident and corresponding to the already discussed microstructural differences and pore network parameters for the two groups.

**4.3.4.2 Fully submerged conditions,  $\text{H}_2\text{O}$  and alkaline ( $\text{Ca}(\text{OH})_2$ ) external medium**  
 Figures 4.13 to 4.16 present micrographs and pore structure analysis for fully submerged conditions. In these tests, the employed current density levels were higher, i.e.  $100\text{mA/m}^2$  and  $1\text{A/m}^2$ . The conditions in these series of experiments can be viewed as mortar in saturated conditions in water and  $\text{Ca}(\text{OH})_2$ , where in the former case concentration gradient was present, while not relevant for the latter case.

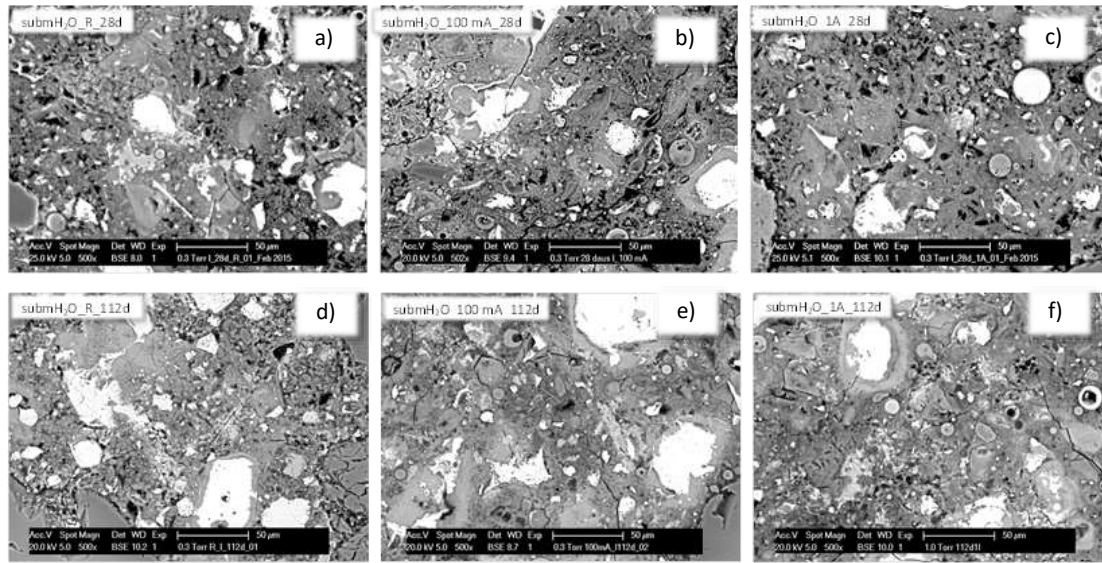


Fig. 4.13 ESEM micrographs 500 $\times$  of mortar bulk matrix at 28 days (top row) and 112 days of age (bottom row) - *fully- submerged in water* conditions for control (a,d), “under current” regime of 100mA/m<sup>2</sup> (b,e) and “under current” regime of 1A/m<sup>2</sup> (c,f).

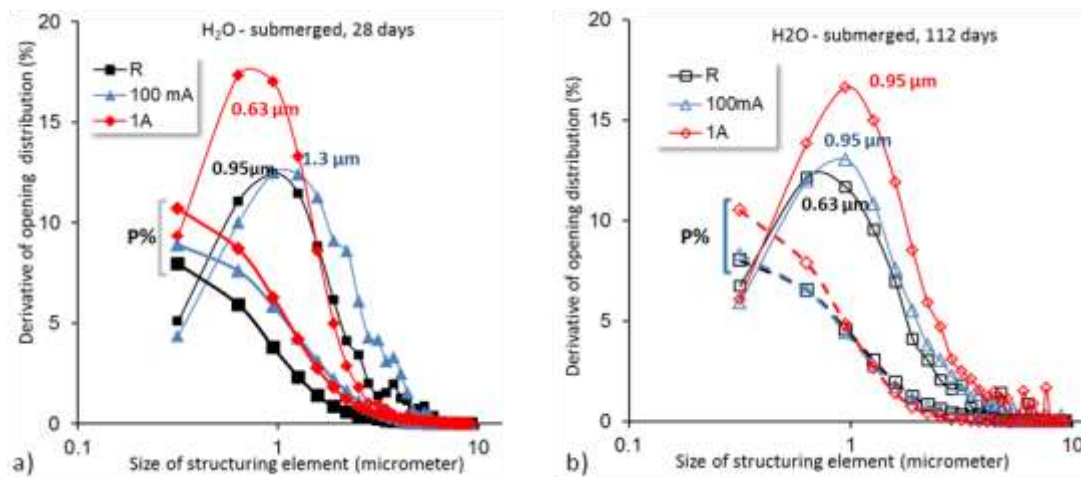


Fig. 4.14 Porosity and pore size distribution – mortar bulk matrix for control and “under current” regimes of 100mA/m<sup>2</sup> and 1A/m<sup>2</sup> in *fully submerged in water* conditions – a) overlay of results for 28 days of age; b) overlay of results for 112 days of age.

For fully-submerged in water conditions, increased porosity and pore size from 28 days to 112 days were recorded for both 100 mA/m<sup>2</sup> and 1A/m<sup>2</sup> regimes. A more distinct effect of the higher current density, 1A/m<sup>2</sup>, was recorded at both 28 days (Fig. 4.14a) and 112 days (Fig. 4.14b). For the control specimens, the parallel processes of on-going cement hydration and leaching-out resulted in slightly reduced critical pore size and/or re-distribution of the pore network i.e. initially smaller pores became coarser after 28 days due to leaching-out, but similar porosity values were recorded between 28 and 112 days of age, together with reduced critical pore size at 112 days (Fig. 4.14a,b). The control specimens remained with the lowest porosity throughout the test.

For the specimens, conditioned at the lower current density level regime – 100 mA/m<sup>2</sup>, porosity and critical pore size increased, compared to control conditions at 28

days of age (Fig. 4.14a) and maintained at similar levels for 112 days (Fig.4.14b). At both 28 days and 112 days of age, the specimens under  $1\text{A}/\text{m}^2$  current flow presented the highest level of microstructural changes, with increased porosity and critical pore size at the end of the test (Fig. 4.14a,b). The results from image analysis are well in line with the MIP results (Fig. 4.6a,b) where an obvious re-distribution of the pore space was relevant, especially for the “under current” conditions (marked region in Fig. 4.6b). The microstructural investigation (both image analysis and ESEM) are also well in line with the derived compressive strength values (Fig. 4.2b), where a clear trend towards reduction of mechanical properties was recorded with age for the “under current” specimens i.e. at the end of the test, ca. 60 MPa were recorded for control cases, 50 MPa for the  $100\text{ mA}/\text{m}^2$  and 46 MPa for the  $1\text{A}/\text{m}^2$  regime.

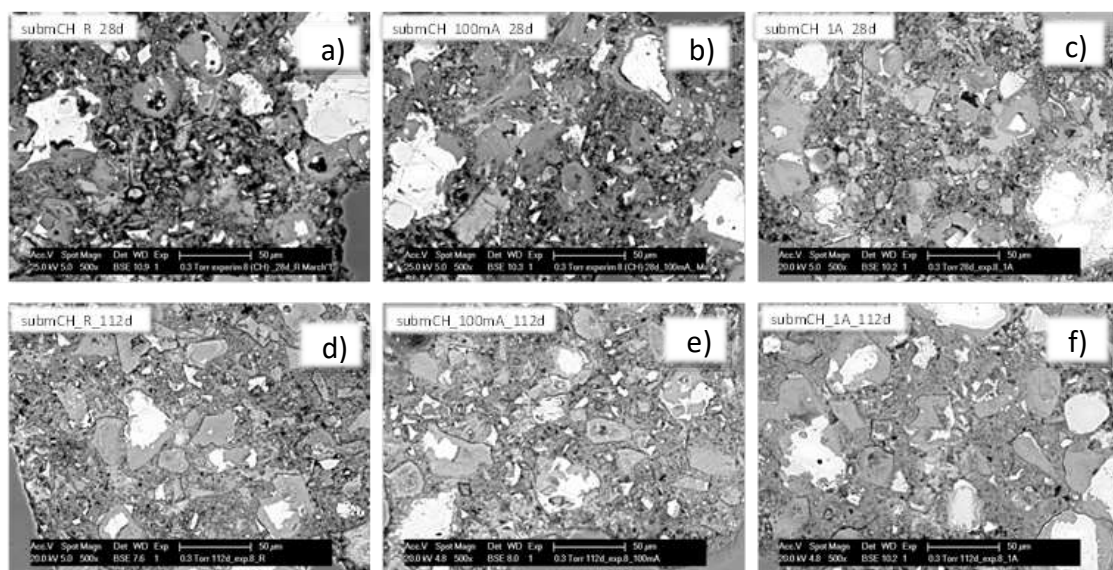


Fig. 4.15 ESEM micrographs  $500\times$  of mortar bulk matrix in *fully- submerged in  $\text{Ca}(\text{OH})_2$* : 28 days (top row) and 112 days of age (bottom row) for control (a,d), “under current” regime of  $100\text{mA}/\text{m}^2$  (b,e) and “under current” regime of  $1\text{A}/\text{m}^2$  (c,f).

For the *fully submerged in  $\text{Ca}(\text{OH})_2$  conditions*, Figs. 4.15 and 4.16, an entirely opposite trend to the water-conditioned specimens was recorded at 28 days of age (compare Fig. 4.15a and 4.16a). The highest porosity and critical pore size were recorded for control specimens, followed by the  $100\text{mA}/\text{m}^2$  and  $1\text{A}/\text{m}^2$  regimes (Fig. 4.16a). The trend towards matrix densification maintained at 112 days as well, with no significant difference between the groups of specimens at that age (Fig.4.16b). This is also visualised by the similar appearance of the bulk matrix in all three conditions at 112 days (Fig. 4.15d,e,f). Mortar specimens, saturated in alkaline medium, would not suffer leaching-out. Hence, the effect of current flow would result in enhanced cement hydration only, consequently in reduced porosity and critical pore size. While this was as observed (Fig. 4.16a,b), image analysis derived similar values for critical pore size at both 28 and 112 days of age for the “under current” regimes, especially the  $1\text{A}/\text{m}^2$  regime. Observation of the bulk matrix for  $1\text{A}/\text{m}^2$  conditions at 28 and 112 days also reveals almost no visual morphological changes or appearance (Fig. 4.15c,f).

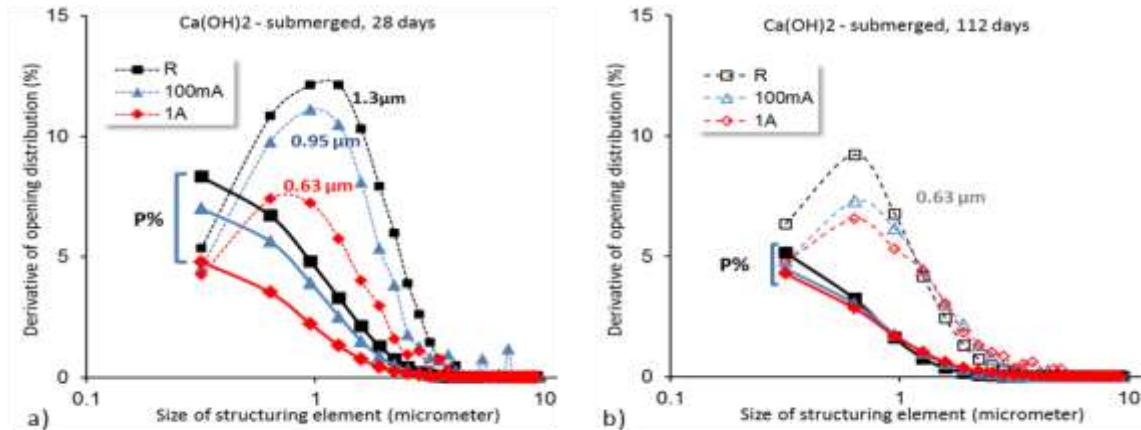


Fig. 4.16 Porosity and pore size distribution for mortar bulk matrix in control and “under current” regimes of  $100\text{mA/m}^2$  and  $1\text{A/m}^2$  in *fully submerged in  $\text{Ca}(\text{OH})_2$*  conditions – a) overlay of results for 28 days of age and b) 112 days of age.

The MIP results confirm re-structuring of the pore space and family of larger pores ( $> 0.1 \mu\text{m}$ , Fig. 4.6d), appearing at 112 days of age for “under current” conditions. These changes were, however, not significant and not responsible for a reduction in mechanical properties, as otherwise observed for the water conditioned test series (Fig. 4.2c). They are an indication, though, for the effect of the higher level of stray current on bulk matrix properties, even in saturated conditions, where leaching-out is avoided. Consequently, these results need to be taken into account in conditions where higher current densities are involved in practice e.g. above  $1$  to  $5 \text{ A/m}^2$  as within concrete desalination or re-alkalisation, stray currents, etc. With higher current density, enhanced migration-controlled transport could result in a pore-water dis-balance or internal concentration gradients, leading to undesired changes of the pore structure (e.g. internal leaching, effects similar to self-desiccation, etc.).

The results obtained for  $\text{Ca}(\text{OH})_2$  conditioned specimens are in a good agreement with reported experiments (Rafieipour et al. 2012), where lower porosity was obtained in lime saturated curing conditions. Additionally, other reports suggest that for specimens submerged in  $\text{Ca}(\text{OH})_2$  higher compressive strength is to be expected and recorded, compared to specimens cured in water (Bediako et al. 2015, Hayri et al. 2011). These dependencies were also observed in this work (Figs.4.5, 4.6, 4.14, 4.16).

#### 4.3.4.3 Sealed conditions

Figures 4.17 to 4.20 present the microstructural analysis for sealed conditions. These are in fact the most representative ones, as far as the effect of external environment and conditioning are to be split from the effects of stray current only. The employed current densities were at the levels of  $100 \text{ mA/m}^2$  and  $1\text{A/m}^2$ . The outcomes were compared to equally handled (equally sealed) control cases.

Fig. 4.17 and Fig. 4.18 depict results for sealed conditions for the *bulk matrix* (middle section in Fig. 4.1c). Visual observation revealed similar morphology at both 28 days and 112 days in all conditions (Fig. 4.17). A slightly coarser structure for the control specimens at 28 days (Fig. 4.17a, Fig. 4.18) was observed. At each time interval (7, 28 and 112 days), the difference in porosity and pore size between the three

investigated cases per hydration age (Fig. 4.18) was not as significant as was observed for all other, already discussed, test series. In sealed conditions, porosity and critical pore size gradually reduced over time, with both parameters maintaining highest values for the control specimens and lowest values for the 1A/m<sup>2</sup>-conditioned ones. The results from image analysis also correspond to the outcome from MIP analysis (Fig. 4.7) and are well in line with the previously discussed compressive strength results, (Fig. 4.2d). Consequently, the effect of stray current in sealed conditions can be only considered as a positive one, at least for the duration of this test.

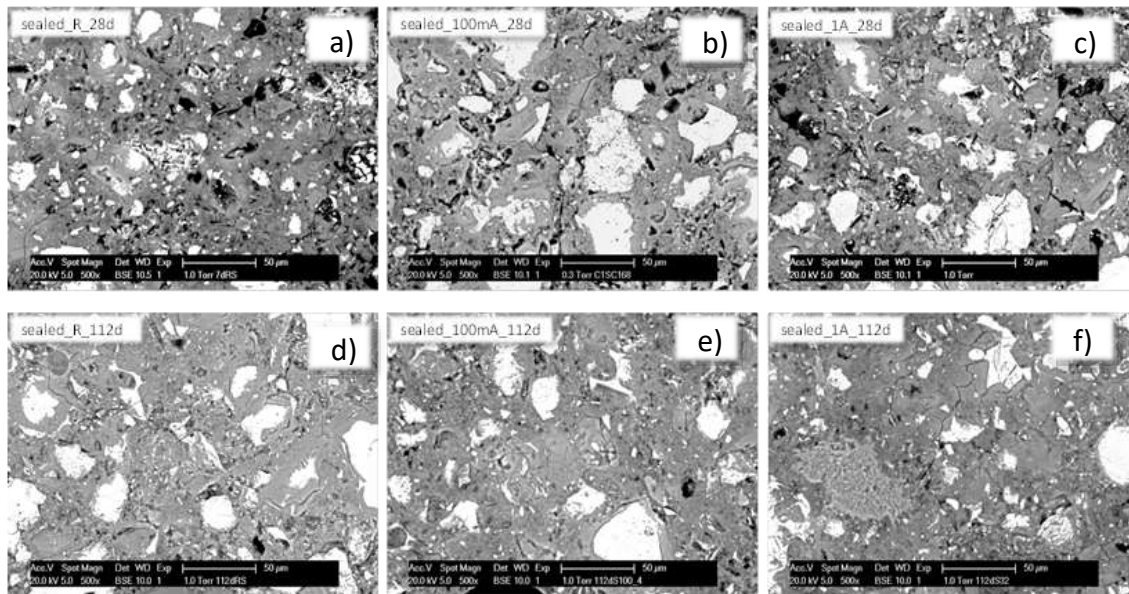


Fig. 4.17 ESEM micrographs 500× of mortar bulk matrix in *sealed conditions*: 28 days (top row) and 112 days of age (bottom row) for control (a,d), “under current” regime of 100mA/m<sup>2</sup> (b,e) and “under current” regime of 1A/m<sup>2</sup> (c,f).

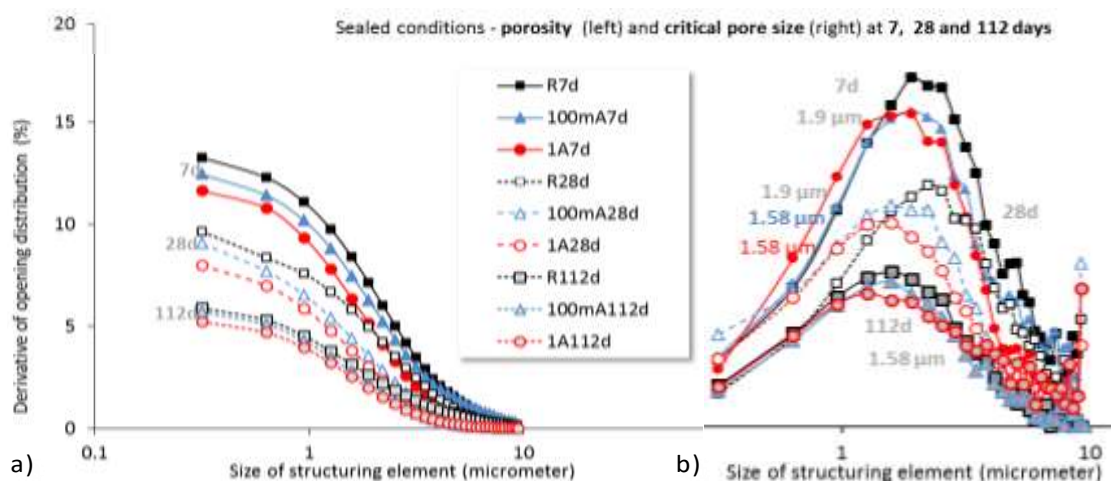


Fig. 4.18 Porosity (a) and pore size distribution (b) for the bulk matrix of mortar specimens in control and “under current” regimes of 100mA/m<sup>2</sup> and 1A/m<sup>2</sup> in *sealed conditions* as an overlay of results for 7 days, 28 days and 112 days.

### 4.3.5 Bulk matrix electrical resistivity

Enhanced ion and water flow (as within electrical current application) would result in altered cement hydration. Leaching-out effects due to diffusion-controlled transport (concentration gradients only) or when both diffusion and migration-controlled transport are present (as within concentration gradients and current flow) will result in mechanical and microstructural changes. All these were observed and discussed in the previous sections. These alterations will in turn affect the development of electrical resistivity in conditions of current flow, if compared to control conditions.

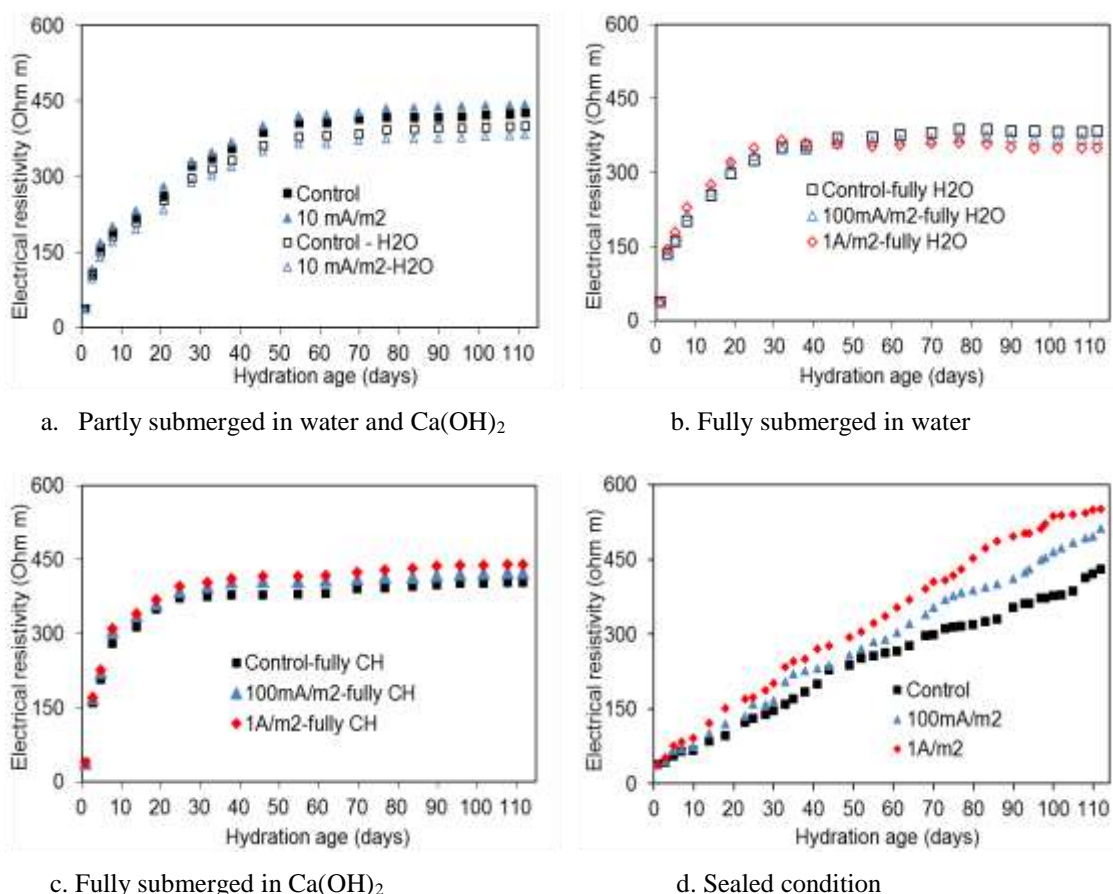


Fig. 4.19 Evolution of electrical resistivity as a function of hydration age for mortar specimens: (a) partly submerged in water and  $\text{Ca}(\text{OH})_2$  solution; (b) fully submerged in water; (c) fully submerged in  $\text{Ca}(\text{OH})_2$  and (d) sealed conditions with w/c ratio 0.5. The ambient temperature is about 25°C.

Fig. 4.19 depicts the automatically computed electrical resistivity for mortar specimens per group and per condition. Although more significant variation in electrical resistivity between specimens, conditioned in different regimes might have been expected, such were actually not really observed. The electrical resistivity development of the specimens can be elaborated at early and at later stages as follows:

#### a) At early stages

Since the electrical current is carried by the ions flowing through the pore solution in the concrete, higher moisture content (i.e. saturated condition and partially saturated

condition both in water and  $\text{Ca}(\text{OH})_2$  solution) results in “easier” electrical current flow. Hence, the electrical resistivity of the sample is lower. Furthermore, electrical resistivity of the specimens in saturated condition is lower than that of electrical resistivity of specimens in partially saturated condition. This is because the specimen in saturated condition has higher moisture content (or degree of saturation) than that of specimens in partially saturated condition. Woelfl and Lauer (1979) found that the electrical resistance of concrete decrease with increasing moisture content and vice versa for all the mixes used. At early stages, the electrical resistivity of specimens in sealed condition tends to have lower values than specimen in saturated condition and partially saturated condition. The most plausible explanation is that in sealed conditions the mortar matrix is insulated from the external environment. Hence water and temperature losses are minimised or none. As a consequence, the internal temperature of the specimen in sealed condition is higher compared to the specimen in saturated and partially saturated condition resulting in lower electrical resistivity. This is confirmed by Polder (2001), pointing out that a temperature increase causes a decrease of resistivity and vice versa. This is the result of temperature influences on ion mobility, ion-ion and ion-solid interactions.

#### b) At later stages

At later stage, the moisture content (or degree of saturation) of specimen in saturated and partially saturated condition remains constant/stable. In sealed condition, a reduced moisture content of the specimens may significantly increase the electrical resistivity as shown in Fig. 4.19d. At later stages, electrical resistivity of specimens in sealed condition was higher compared to specimens in saturated and partially saturated condition. In sealed/dry condition, denser capillary porosity of the specimen was noticed due to accelerated cement hydration by stray current compared to all other cases (Figs. 4.19a-c) resulting higher electrical resistivity.

More specifically, the results can be viewed as follows:

- For partly submerged in water and  $\text{Ca}(\text{OH})_2$  conditions (Fig. 4.19a), resistivity increased with hydration age until approx. 60 days of age and stabilised later-on. The highest values were recorded for the “10mA/m<sup>2</sup>” regime for  $\text{Ca}(\text{OH})_2$ -conditioned specimens, the lowest for the “10 mA/m<sup>2</sup>” regime of water-conditioned specimens i.e. in both test series the current flow exerted changes in electrical properties. While these were positive in the former case, a negative effect was observed in the latter case – result already commented in view of various aspects in the preceding sections. The results are in line with the recorded compressive strength values (Fig. 4.2a) and pore structure development (Figs. 4.7, 4.8): the lowest compressive strength and highest porosity for the water-conditioned “under current” specimens correspond to the lowest electrical resistivity values for these groups; in contrast, higher compressive strength, lower porosity and highest electrical resistivity correspond to the  $\text{Ca}(\text{OH})_2$ -conditioned, “under current” specimens (Fig. 4.19a).
- For the fully submerged in water and  $\text{Ca}(\text{OH})_2$  conditions (Fig. 4.19b,c), the increase in electrical resistivity was more pronounced between 1 day and 60 days of age, if compared to the partly submerged conditions and, in fact, stabilised earlier – around 35 days of age. This is related to the saturated conditions and altered cement hydration as already previously discussed. The effect of stray current is well seen, although the pattern of resistivity development seems to be similar. The lowest electrical resistivity values for water-conditioned specimens were recorded for the 1A/m<sup>2</sup> regime, corresponding to the highest derived porosity (Fig. 4.7a) and lowest compressive

strength (Fig. 4.2b) in these specimens. For the  $\text{Ca}(\text{OH})_2$ -conditioned specimens (Fig. 4.19c), the lowest electrical resistivity corresponds to the control mortar cubes, well in line with their highest bulk matrix porosity (Fig. 4.7b) and lowest compressive strength (Fig. 4.2c). The specimens conditioned in  $\text{Ca}(\text{OH})_2$  and in  $1\text{A}/\text{m}^2$  regime present the highest electrical resistivity of all saturated specimens (Fig. 4.9b,c), which is well supported by their highest compressive strength (Fig. 4.2c) and lowest porosity (Fig. 4.7b).

- For sealed conditions a significantly different pattern of electrical resistivity evolution with time was observed (Fig. 4.19d). Only increasing values were recorded throughout the test, with almost no signs for stabilisation towards the 110 days of age. The results can be interpreted as still on-going cement hydration with time and in sealed condition the water and temperature losses can be minimised or none, as mentioned before. This, together with the contribution of significantly lower (compared to other test series) relative humidity during measurements, as well as the contribution of the interfacial regions (cast-in terminals and cement paste) in relatively dry conditions, is reflected by a significantly higher values of electrical resistivity, compared to all other cases. Similar to all other groups, the effect of stray current is well seen: the highest resistivity values were recorded for the  $1\text{A}/\text{m}^2$  regime (Fig. 4.19d), corresponding to highest compressive strength (Fig. 4.2d) and lowest porosity (Fig. 4.7c); the lowest resistivity in sealed conditions was recorded for the control specimens (Fig. 4.19d), completely in line with the lowest compressive strength (Fig. 4.2d) and highest porosity (Fig. 4.7c).

Overall, it can be concluded that electrical resistivity is a property of cement-based materials, which indeed reflects well microstructural and transport properties. However, as seen from Fig. 4.19 it is determined by relative humidity at the most. Therefore, recording electrical properties only, would not be sufficient to derive specific information on pore network development, especially when diffusion- and migration-controlled ion and water transport are both relevant. When such a comprehensive and more specific information would be required, especially in the case of justifying the effect of one or another factor on cement-based material properties (as the hereby evaluated effect of stray current on bulk matrix properties), a combination of techniques, as the hereby employed approach, is necessary.

4

#### 4.4 Conclusions

This chapter discussed the effect of stray current flow on the development of material properties of mortar in water-submerged,  $\text{Ca}(\text{OH})_2$ -submerged and sealed conditions. The investigation referred to fresh (24h only cured) mortar, in order to address the practical issue of possible stray current interference within construction work of new buildings and structures. The following conclusions can be drawn:

- Stray current flowing through a cement-based material may cause positive or negative effects on the material properties and performance of the bulk matrix. In general, for fresh cement-based materials, the effect of stray current can be categorized as an effect on early age – e.g. between 1 day and 28 days at the maximum; and an effect on later ages (> 28 days).
- Positive and/or negative effects of stray current are determined by the external environmental conditions and the level of current density. The former are at hand

when concentration gradient with the external medium is avoided or not significant, e.g. for specimens conditioned in alkaline medium or for sealed specimens. Whereas the latter are to be observed in conditions where concentration gradients are present, e.g. water conditioned specimens.

- The contribution of migration-controlled ion and water transport, as within “under current” conditions, results in enhanced cement hydration at early stages (more significant < 28 days of age). The enhanced cement hydration at early stages results in improved compressive strength and reduced porosity of the matrix. These effects are, however, dependent on the external medium and are only predominant at early age.
- Although a general trend of electrical resistivity increase was recorded over time in all conditions (with on-going cement hydration), the evolution of electrical properties was found to be also dependent on the current density levels and the external medium. For water conditioned specimens, the stray current induced decrease in electrical resistivity if compared to control conditions. For specimens in alkaline medium or sealed conditions, the stray current induced increase in electrical resistivity. The most significant effects (both positive or negative) were observed at the highest current density levels.
- The negative effect of stray current flow on mortar specimens at stages after 28 days of age is mainly attributed to enhanced leaching-out as a consequence of increased ion and water migration when concentration gradients are present. The result was a more pronounced restructuring of the pore space towards coarsening of the pore network (enlargement of initially smaller pores), as otherwise generally known and observed in such circumstances. Water (or neutral to low pH medium) as external environment will be a prerequisite for negative effects, while alkaline medium (or sealed conditions) would minimise or prevent the leaching-out effects.



# 5

## **The effect of stray current on the hydration process and properties of cement-based materials**

---

**Abstract:** This chapter presents the effect of stray current flow on the hydration process and temperature development in hardening cement-based materials and evolution of materials properties like strength, porosity and diffusivity. Experiments were performed in isothermal condition at 20°C to investigate the effect of stray current on heat release and microstructural changes in hardening cement paste.

The stray current levels were subdivided in two levels: 1) current levels 10 mA/m<sup>2</sup>, 100 mA/m<sup>2</sup> and 1 A/m<sup>2</sup>, used in isothermal calorimetry tests and 2) current densities 10 A/m<sup>2</sup>, 40 A/m<sup>2</sup> and 60 A/m<sup>2</sup>, used in semi-adiabatic tests in hardening cement paste prisms with specimen size of 5.5×5.5×29.5 cm<sup>3</sup>. In parallel, numerical simulations were performed to quantify the hydration process and temperature development in these concrete specimens. Simulations of the hydration process in thicker concrete walls, viz. 20 cm, 40 cm, 60 cm, 70 cm, and 80 cm, were also performed in order to investigate possible size effects and consequences for real-size hardening structural elements. The stray current level applied in the simulations was in the range of 10 to 60A/m<sup>2</sup>.

In order to quantify possible effects of stray current on (internal) mechanical damage (i.e. cracking) in hardening concrete, temperature differentials and peak temperatures in stray current loaded specimen were numerically investigated. The evolution of the capillary porosity of cement paste as a function of the degree of hydration  $\alpha$  was calculated. Apparent diffusion coefficients were calculated from microstructure parameters, i.e. capillary porosity.

## 5.1 Introduction

Electrical current flow through cement paste causes an increase in temperature of the material due to resistive heating, or Joule heating. There are at least two effects of temperature on the hydration kinetics of cement-based materials. Firstly, the reaction rate increases with increasing temperature of the concrete (Kjellsen et al. 1990, 1991 and 1992; Escalante-Garcia 2003; Bentur et al. 1979). This so called resistive heating is the basis for electrical curing of concrete used to accelerate cement hydration (Uygunoğlu and Hocaoglu, 2018, Bredenkamp et al. 1993). Secondly, hydration at higher temperatures will result in a denser reaction product (lower gel porosity). This will decelerate permeation of free water through the hydration product surrounding hydrating cement particles, affecting the rate of hydration in the diffusion controlled stage. A lower gel porosity goes along with a higher capillary porosity. This makes the concrete more permeable and reduces the resistance against ingress of aggressive substances.

The main objective of this chapter is to quantify the effects of stray current flow on the hydration process and temperature development in cement-based materials. Temperature development and heat release in cement paste due to stray current flow were measured using isothermal calorimetry. Mercury intrusion porosimetry (MIP) tests were conducted to investigate possible microstructural changes (i.e. porosity and pore structure) of cement paste caused by stray current flow.

Numerical simulations were performed of the Joule heating effect caused by stray current flow through cement-based materials. The Joule heating promotes the temperature increase and influences the cement hydration and microstructural development of cement-based materials. Numerical simulations (3-dimensional) were carried out on small concrete specimen with size  $5.5 \times 5.5 \times 5.5 \text{ cm}^3$ . Simulations on bigger specimens were performed in order to investigate size effects and consequences of stray current-induced temperature effects for real size structural elements. The simulations were performed in concrete specimen cured under semi-adiabatic as well as adiabatic condition, the latter representing mass concrete.

### 5

Two groups of stray current levels are considered in this simulation as follow:

- a) Stray current levels (J) up to  $1 \text{ A/m}^2$  ( $0 < J \leq 1 \text{ A/m}^2$ )  
These stray current levels have been measured in real practice (Charalambous et al. 2014; Aylott et al. 2013; Galsgaard and Nielsen 2006) as mentioned in Section 4.1 (Chapter 4).
- b) Stray current levels between 1 and  $70 \text{ A/m}^2$  ( $1 < J < 70 \text{ A/m}^2$ )  
These current levels refer to the levels of electrical current used for electrical curing of cement-based materials (Heritage 2001). Heritage applied a power of 20W to the specimens ( $150 \times 150 \times 150 \text{ mm}^3$ ) with electrical resistivity 30 Ohm, 18 Ohm, 8 Ohm for w/c ratio 0.5, 0.57 and 0.75, respectively. The corresponding electrical current density was about 36, 47 and  $70 \text{ A/m}^2$ , respectively.

## 5.2 Experiments

Two series of experiments were performed to quantify the effect of stray current on temperature development in hardening cement paste:

- A. Isothermal calorimetry tests of hardening cement paste
- B. Semi-adiabatic tests of hardening cement paste.

### 5.2.1 Isothermal calorimetry tests of hardening cement paste

Isothermal calorimetry tests were performed on cement paste with two w/c ratios, 0.35 and 0.5. The tests were performed on four groups of specimens: a control group and the “10 mA/m<sup>2</sup>”, “100 mA/m<sup>2</sup>” and “1A/m<sup>2</sup>” groups. The experimental set up of calorimetry tests is presented in Fig. 5.1.

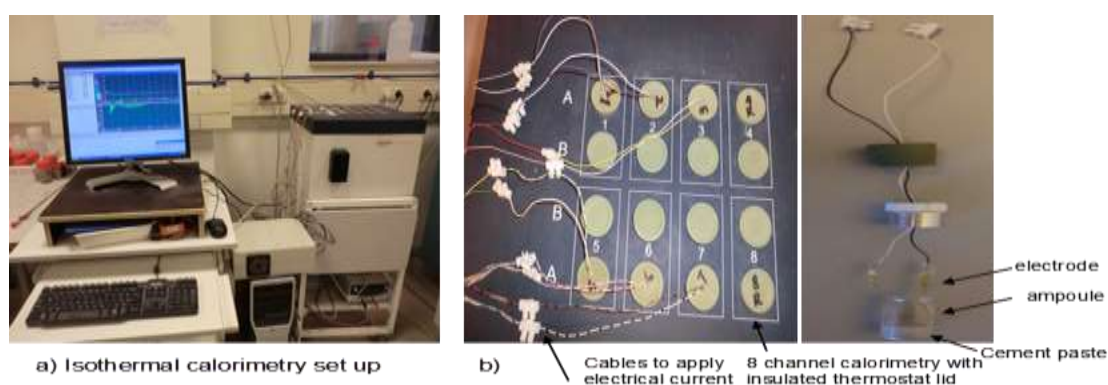


Fig. 5.1 (a) Isothermal calorimeter (TAM-Air-314) used to measure heat release of cement paste; (b) Schematic pictures of the holders for “under current” regime.

### 5.2.2 Semi-adiabatic tests: temperature development in hardening cement paste prism

Temperature development in hardening cement paste prisms was measured using thermocouples embedded in small prismatic specimens. Two main groups of specimens were investigated:

1. Control (reference) group - no DC current involved
2. Stray current group with subgroups, reflecting the level of DC current involved i.e. groups “1 A/m<sup>2</sup>”, “10 A/m<sup>2</sup>”, “40 A/m<sup>2</sup>”, and “60 A/m<sup>2</sup>”.

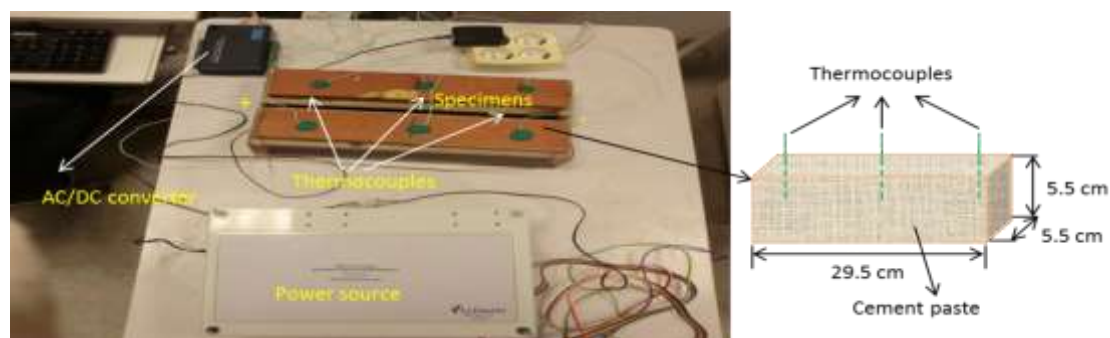


Fig. 5.2 Experimental set-up for measurements of temperature increase in cement paste specimens due to hydration and electrical current flow.

The set-up for DC current application is shown in Fig. 5.2. A negative and a positive terminal were connected to a 80 V source. The current density levels were adjusted by additional resistors. Thermocouples were placed in the middle and end part of the specimens immediately after casting to record automatically the temperature development of cement paste by connecting them to the AC/DC converter and the personal computer (PC).

### 5.3 Materials and methods for experimental studies

#### 5.3.1 Materials

*Isothermal calorimetry tests of hardening cement paste:* Cement paste samples with weight  $10 \pm 0.01$ g were cast for an isothermal calorimetry test. Portland cement CEM I 42.5 N was used with water-to-cement ratio 0.35 and 0.5. The details about the tests are given in section 5.3.2.1.

*Semi-adiabatic tests of hardening cement paste:* Cement paste prisms of  $5.5 \times 5.5 \times 29.5$  cm<sup>3</sup> (Fig. 5.2) with weight 1200 g were cast. Portland cement CEM I 42.5 N was used with water-to-cement ratio 0.35 and 0.5. The properties of cement CEM I 42.5 N are shown in Table 5.1. The specimens were maintained in sealed conditions for the total test duration of 4 days. Temperature development in specimens, with or without stray current involved, was recorded with embedded thermocouples.

Table 5.1 The properties of cement CEM I 42.5 N

| Properties   | Values                         |         |
|--|--------------------------------|---------|
|  | By weight (%)                  |         |
| Chemical composition   | CaO                            | 63.96   |
|  | SiO <sub>2</sub>               | 20.00   |
|  | Al <sub>2</sub> O <sub>3</sub> | 4.88    |
|  | Fe <sub>2</sub> O <sub>3</sub> | 3.36    |
|  | SO <sub>3</sub>                | 2.4     |
| Mineral composition  | By weight (%)                  |         |
|  | C <sub>3</sub> S               | 62      |
|  | C <sub>2</sub> S               | 10.5    |
|  | C <sub>3</sub> A               | 7.3     |
|  | C <sub>4</sub> AF              | 10.2    |
| Particle size distribution<br>(described by Rosin-Rammler function*) | n                              | 1.21267 |
|  | b                              | 0.0221  |
| Maximum particle size (mm)   |                                | 50      |
| Minimum particle size (mm)   |                                | 1       |
| Max heat (kJ/g)  |                                | 470     |
| Density (kg/m <sup>3</sup> )   |                                | 3150    |

\*The Rosin-Rammler function is an expressions used to describe the cumulative particle size distribution of cement, as given by the following equation (Rosin and Rammler 1933):

$$G(x) = 100 (1 - e^{-bx^n})$$

where G(x) is the percentage by mass passing the sieve with diameter x [%], x is characteristic particle size [ $\mu$ m], and b,n are constants.

### 5.3.2 Test methods

#### 5.3.2.1 Isothermal calorimetry tests

Heat evolution and rate of hydration of hardening cement paste were measured by isothermal conduction calorimetry (TAM-Air-314, an 8-channel heat flow calorimeter) with 60mW measuring range, using  $10 \pm 0.01$ g samples. Pastes with w/c ratio 0.35 and 0.5 were tested. Before mixing all the materials were tempered in the oven for at least 12 hours at the desired testing temperature of 20°C. The cement paste was cast into capped glass vials (ampoules) and afterwards placed in an isothermal calorimeter. The specimen preparation and experimental procedure followed standard procedures (Wadso 2003), except some modifications needed for applying the electrical current flow. For the “under current” samples, the same ampoules as for the control cases were used, but designed in a way to include two metal electrodes as electrical current conductors (schematic pictures in Fig. 5.1b). Electrical current was applied from an external source immediately after samples’ casting. The duration of the measurements was about 4 days. The temperature evolution in cement paste due to both cement hydration and electrical current flow were measured with thermocouples, embedded in the middle of the specimens.

#### 5.3.2.2 Semi-adiabatic tests of temperature development in hardening cement paste

To quantify the effect of stray current on hardening cement paste prisms, an electrical field was applied immediately after casting and until approximately 4 days of age. The temperature development due to both cement hydration and electrical current flow were measured in the specimens with thermocouples, embedded in the middle and end parts of the specimens (Fig. 5.2).

#### 5.3.2.3 Mercury intrusion porosimetry (MIP)

MIP measurements were performed for the specimens in isothermal calorimetry tests in order to characterize porosity changes in the matrix in case stray current is applied. For sample preparation of MIP tests a generally accepted and reported procedure was followed (Sumanasooriya et al. 2009; Hu 2004; Ye 2003). The samples were first submerged in liquid nitrogen for about 5 minutes at -195°C to stop cement hydration. After submersion in liquid nitrogen, the samples were placed in a freeze-dryer in which the temperature and vacuum were kept at -24°C and  $10^{-1}$  Pa, respectively. Water loss was monitored every 24 hours until a stable mass loss of 0.01%/day was reached for 10-20 days depending on the w/c ratio and curing age. The MIP tests were carried out by using Micromeritics Poresizer 9320 with a maximum pressure of 207 MPa to determine the porosity and the pore size distribution of the specimens.

## 5.4 Numerical simulation of temperature development and hydration process of concrete subjected to stray current flow

### 5.4.1 Effects of stray current on hardening concrete

In the introduction it was mentioned that stray current may affect the hydration process by resistive heating of the material. Due to resistive heating the temperature of the

hydrating material will increase. This temperature increase will cause an extra acceleration of the hydration process, resulting in an extra temperature increase. Stray current may accelerate the dissolution process of cement particles in water due to enhanced ion migration in or to the pore water. This will be observed as enhanced hydration of the cement. Higher temperatures in hardening concrete will increase the probability of temperature-induced (micro)cracking in hardening concrete. This may jeopardize the durability of the concrete.

Another effect of hydration at high temperature is that higher reaction temperatures will affect the density of the reaction products. The reaction product (gel) will become denser, while the capillary porosity, and hence the permeability, increases. As said, a higher permeability makes the concrete prone to ingress of aggressive substances and thus less durable. It is important, therefore, to know whether the stray-current induced temperature increase in hardening concrete is big enough to cause significant decrease of durability. Numerical simulations of stray current-induced temperature effects can be very helpful for judging the possible impact of stray current on the durability and service life of concrete structures.

## 5.4.2 Numerical simulation of temperature effects in hardening concrete

### 5.4.2.1 Numerical simulation of temperature due to cement hydration

Temperature development in hardening concrete structures is the result of heat evolution of the exothermic reaction of cement. The temperature field in hardening structures can be determined using the solution of the classic Fourier equation (Carlson 1937, Clover 1937, Newmark 1938):

$$\rho_c c_c \frac{\partial T}{\partial t} = \lambda_c \cdot \left( \frac{\partial^2 T}{\partial x^2} + \frac{\partial^2 T}{\partial y^2} + \frac{\partial^2 T}{\partial z^2} \right) + q_c(x, y, z, t, T) \quad (5.1)$$

where  $T$  is the temperature in the concrete [ $^{\circ}\text{C}$ ],  $\rho_c$  the specific mass of concrete [ $\text{kg}/\text{m}^3$ ],  $c_c$  the specific heat of concrete [ $\text{J}/\text{kg}\cdot\text{K}$ ],  $\lambda_c$  the heat conduction coefficient [ $\text{W}/\text{m}\cdot\text{K}$ ],  $q_c$  is the heat source [ $\text{W}/\text{m}^3$ ],  $t$  the time [ $\text{s}$ ],  $x, y, z$  the coordinates of a particular point in the concrete [ $\text{m}$ ]. In hardening concrete the heat source  $q_c$  represents the exothermal hydration process. The rate of hydration, i.e. of heat production, depends on the type of cement, composition of the mixture and the actual reaction temperature  $T$ . In a real concrete structure this temperature is not known in advance (unless a prescribed temperature regime is imposed). The fact that the heat source is generally not known in advance means that there is no closed solution for eq. (5.1). Hence, eq. (5.1) has to be solved in a step-wise procedure, whereby in each time step the heat production at the actual reaction temperature have to be determined.

In numerical programs for determination of the hydration process and temperature evolution in hardening concrete, the heat source  $q_c(x, y, z, t, T)$  can be determined by adjusting a known (reference) hydration curve for the actual reaction temperature. This known hydration curve, i.e. reference curve, can be an isothermal, adiabatic hydration or semi-adiabatic hydration curve (see Fig. 5.3). In the following adiabatic hydration curves of the mixtures will be used as input for numerical simulations of temperature effects in young concrete. Adiabatic hydration curves can be obtained from adiabatic

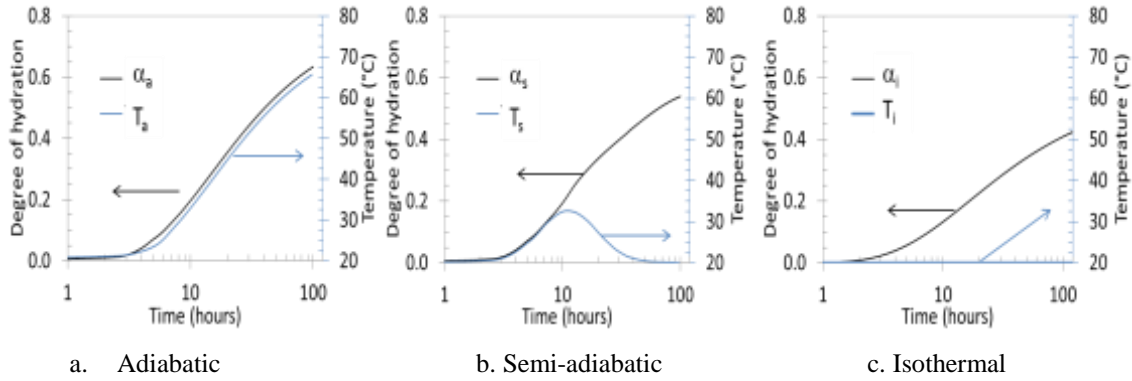


Fig. 5.3 Adiabatic (a), semi-adiabatic (b) and isothermal (c) hydration curves and temperature development of concrete (log scale). Initial mix temperature is 20°C.

tests or from a numerical simulation with an advanced simulation program, e.g. HYMOSTRUC3D (van Breugel 1991, Ye 2003, see also part 5.4.2.4).

An adiabatic hydration curve, obtained by either a numerical simulation or an adiabatic test, can be approximated by an analytical expression (Helland 1986):

$$Q_a(t) = Q_{max}^* e^{-\left(\frac{t}{\tau}\right)^\beta} \quad (5.2)$$

where  $Q_a(t)$  is the heat of hydration in hardening concrete under adiabatic condition [kJ/kg],  $Q_{max}^*$  is the maximum amount of heat produced by the hydration reaction in adiabatic condition of the mixture in view [kJ/kg],  $\tau$  is an empirical constant [h],  $\beta$  the hydration shape factor ( $0.7 < \beta < 0.9$ ), and  $t$  is the hydration time [h]. The hydration parameters (i.e.  $\tau$  and  $\beta$ ), that control the shape of the degree of hydration curve, can be determined from curve fitting of measured or simulated adiabatic hydration curves.

Note that the maximum amount of heat  $Q_{max}^*$  is generally lower than the amount of heat produced when all the cement in the mixture would have reacted, i.e.  $Q_{max}$ . (van Breugel 1991). In this respect we have to distinguish between the *rate of reaction*  $\alpha_r(t)$

$$\alpha_r(t) = \frac{Q(t)}{Q_{max}^*} \quad (5.3)$$

and the *degree of hydration*  $\alpha(t)$

$$\alpha(t) = \frac{Q(t)}{Q_{max}} \quad (5.4)$$

The value of  $Q_{max}^*$  can be obtained from an adiabatic test as the asymptotic value of the heat production. The value of  $Q_{max}$  can be obtained from the chemical composition of the cement. For Portland cement it holds (Verbeck 1960, van Breugel 1991):

$$Q_{max} = q_1 \cdot (C_3S) + q_2 \cdot (C_2S) + q_3 \cdot (C_3A) + q_4 \cdot (C_3AF) + q_5 \cdot (C) + q_6 \cdot (M_gO) \quad (5.5)$$

where  $q_1.. q_6$  represent the heat of hydration of the constituents of the cement in view.

When in a real structure the hydration process starts to deviate from an adiabatic process due to heat loss to the environment, the temperature of the concrete will drop and the hydration process will slow down. The effect of temperature on the rate of hydration, i.e. the rate of hydration liberation, can be described with an Arrhenius function. This function relates the reaction rate of the actual (non-adiabatic) hydration process at a certain degree of hydration to the known rate of reaction of the adiabatic input curve at that particular degree of hydration. In formula form (van Breugel 2001):

$$\frac{\Delta Q_p}{\Delta t} = \frac{\Delta Q_a}{\Delta t} \cdot e^{\frac{E_a}{R} \left( \frac{T_p(t) - T_a(t)}{(T_p + 273)(t) * (T_a + 273)(t)} \right)} \quad (5.6)$$

where  $\Delta Q_p/\Delta t$  is the reaction rate of the actual hydration process,  $\Delta Q_a/\Delta t$  is the reaction rate of the adiabatic hydration process at the same degree of hydration,  $E_a$  is the activation energy [20-77 kJ/mol (Kondo et al. 1968, Brunauer et al. 1973)],  $R$  is the universal gas constant [8.31 J/mol. K],  $T_p(t)$  and  $T_a(t)$  are the actual temperature [°C] of the concrete and of the adiabatic hydration process, respectively.

The amount of liberated heat  $Q_p(t)$  in hydrating concrete at time  $t$  can be calculated by summarizing all heat increments  $\Delta Q_{p,i}$  ( $i = 1, 2, \dots, n$ ):

$$Q_p(t) = Q_{p,n} = \sum_{i=1}^n \Delta Q_{p,i} \quad (5.7)$$

Note that in this calculation procedure the adiabatic temperature  $T_a(t)$  includes the initial temperature of the mixture  $T_{Ref}$  [°C] and the temperature increase caused by the hydration of the cement. Hence (van Breugel 2001, Koenders 2005):

$$T_a(t) = T_{Ref} + \frac{c Q(t)}{\rho_c c_c} = T_{Ref} + \frac{c Q_{max}}{\rho_c c_c} \alpha(t) \quad (5.8)$$

where  $C$  is the cement content in the mixture [kg/m<sup>3</sup>] and  $\alpha(t)$  the degree of hydration of the cement.

5

#### 5.4.2.2 Numerical simulation of thermal effects caused by hydration and stray current flow

Stray current flow acts as another heat source that will affect the rate of hydration and temperature fields generated in hardening concrete. Electrical current flow causes resistive heating, or Joule heating. The temperature field in concrete due to stray current flow can be simulated using eq. (5.1), but now with an extra heat source  $Q_{el}(J, E, t)$ , representing the resistive heating. In formula form:

$$\rho_c c_c \frac{\partial T}{\partial t} = \lambda_c \cdot \left( \frac{\partial^2 T}{\partial x^2} + \frac{\partial^2 T}{\partial y^2} + \frac{\partial^2 T}{\partial z^2} \right) + q_c(x, y, z, t, T) + Q_{el}(J, E, t) \quad (5.9)$$

For  $Q_{el}(J, E, t)$  it holds:

$$Q_{el}(J, E, t) = J(t) \cdot E(t) \quad (5.10)$$

in which  $E(t)$  is the electrical field:

$$E(t) = -\nabla V(t) \quad [\text{Volt/m}] \quad (5.11)$$

where  $Q_{ei}(J,E,t)$  is the heat generated per cubic meter due to the electrical current flow which is a function of the current density  $J$  and the electrical field  $E$  [ $\text{W/m}^3$ ],  $V(t)$  is the voltage [Volt].

Development of the current density  $J(t)$  through cement-based systems is governed by the following equations (Jianming 2002, Pryor 2011):

$$J(t) = \sigma(T, t).E(t) + \frac{\partial D(t)}{\partial t} \quad [\text{A/m}^2] \quad (5.12)$$

with:

$$D(t) = \varepsilon_0 \varepsilon_r E(t) \quad (5.13)$$

$$\nabla \cdot J(t) = \frac{\partial \rho_v}{\partial t} \quad (5.14)$$

$$\sigma(T, t) = \frac{\sigma_{eff}(t)}{1 + \alpha_T \cdot (T - T_{Ref})} \quad (5.15)$$

where  $D(t)$  is the electric flux density [ $\text{C/m}^2$ ],  $\varepsilon_r$  is the relative permittivity and  $\varepsilon_0$  the vacuum permittivity [ $8.85 \times 10^{-12} \text{ F/m}$ ],  $\rho_v$  the charge density [ $\text{C/m}^3$ ],  $\sigma(T,t)$  the electrical conductivity as a function of temperature and time  $t$  [ $\text{S/m}$ ],  $\sigma_{eff}(t)$  is the effective electrical conductivity as a function of time at temperature  $20^\circ\text{C}$  [ $\text{S/m}$ ],  $\alpha_T$  the temperature coefficient of resistivity [ $0.035/^\circ\text{C}$ ] (McCarter et. al. 2005),  $T_{ref}$  the reference temperature [ $^\circ\text{C}$ ].

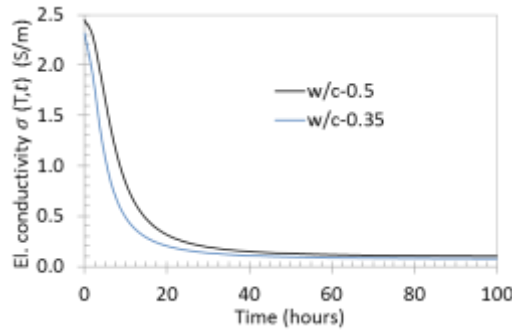


Fig.5.4 Typical evolution of electrical conductivity  $\sigma(T, t)$  of hardening cement paste as a function of time with w/c ratio 0.35 and 0.5 calculated with eq. (5.15), where  $\sigma_{eff}(t)$  (eq. 5.16) was calculated with input parameters  $\sigma_i=2.32$ ,  $\sigma_f=0.07$ ,  $t_s = 4.5$  (h),  $b=1.85$ .

In this simulation, the effective electrical conductivity of cement paste  $\sigma_{eff}(t)$  is determined with the equation proposed by Manchiryal et al. (2009):

$$\sigma_{eff}(t) = \sigma_f + \frac{\sigma_i - \sigma_f}{1 + (t/t_s)^b} \quad (5.16)$$

where  $\sigma_i$  is the initial conductivity of fresh paste [S/m],  $\sigma_f$  is the conductivity at the point where the conductivity–time curve starts to plateau, i.e. to reach a steady-state condition (typically beyond 24 h),  $t_s$  is a time parameter of the particular paste [h], which is weakly related to its final setting time, and  $b$  is a constant. The typical evolution of electrical conductivity of cement paste with w/c ratio 0.35 and 0.5 is given in Fig. 5.4.

#### 5.4.2.3 Boundary condition of the numerical simulation

In order to simulate the effect of stray current flow on the hydration process and temperature development in cement-based specimen, boundary conditions need to be specified (see Fig. 5.5). In the simulations used in this thesis the temperature at the surface of concrete specimens was 20°C. The heat conduction in concrete is governed by the following equation (Ozisik 1985):

$$\lambda_c \cdot \left( \frac{\partial T}{\partial x} + \frac{\partial T}{\partial y} + \frac{\partial T}{\partial z} \right) = h \cdot (T_{Ref} - T) \quad (5.17)$$

where  $h$  is the heat transfer coefficient [ $\text{W}/\text{m}^2 \cdot \text{K}$ ].

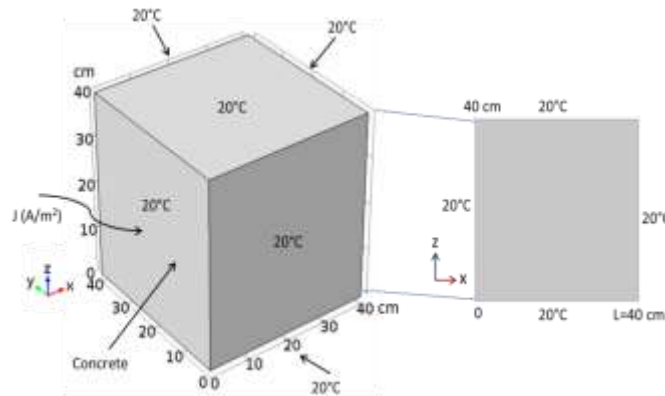
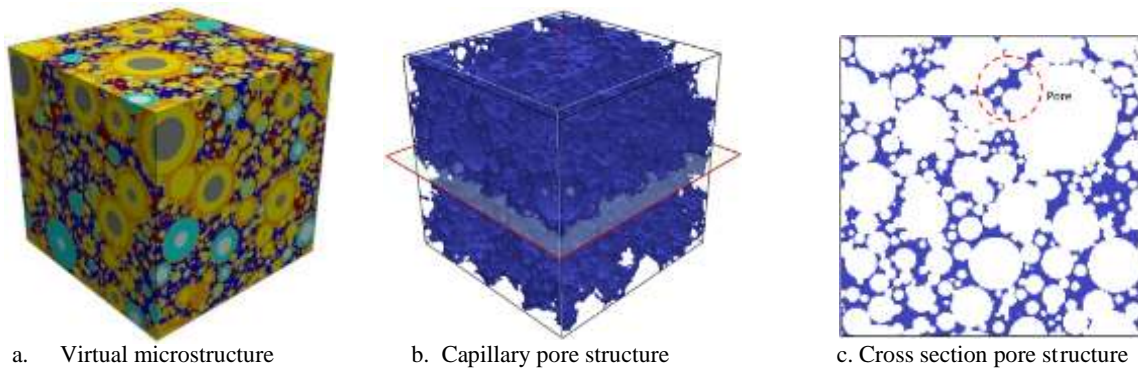


Fig. 5.5 Schematic of boundary conditions for numerical simulation of temperature development in hardening cement-based materials subjected to stray current with dimension  $40 \times 40 \times 40 \text{ cm}^3$ .

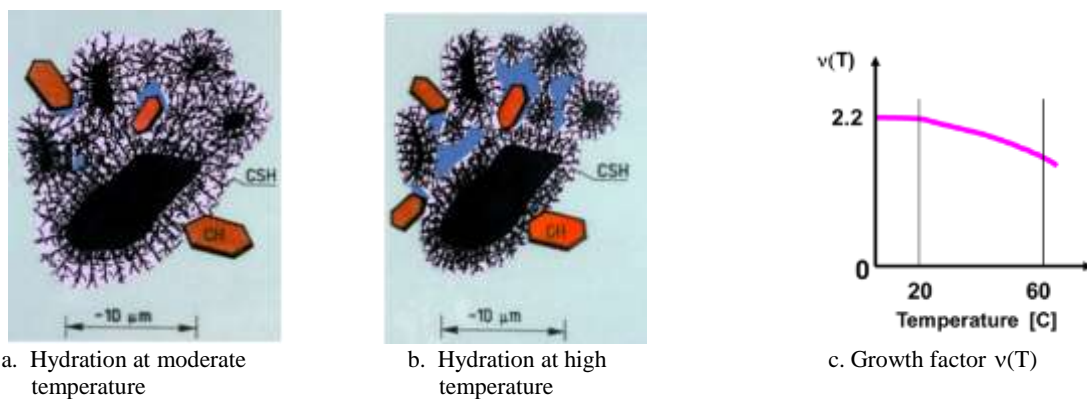
#### 5.4.2.4 Numerical simulation of temperature effects on the evolution of microstructure

The effect of the actual temperature on the capillary porosity can be simulated with the numerical program HYMOSTRUC3D (van Breugel 1991, Ye 2003). With this simulation program the 3D microstructure of hydrating cement paste is simulated as a function of the particle size distribution of the cement, the water/cement ratio, the chemical composition of cement and the reaction temperature. The output consists of the degree of hydration and the microstructure, the latter built up of unhydrated cores of reacting particles, Calcium Silicate Hydrates (CSH) and Calcium Hydroxide (CH). A typical simulated 3D microstructure is shown in Fig. 5.6, taken from Gao Peng (2018).



a. Virtual microstructure      b. Capillary pore structure      c. Cross section pore structure

Fig. 5.6 Typical examples simulated virtual microstructure obtained with HYMOSTRUC3D (Gao Peng, 2018).



a. Hydration at moderate temperature      b. Hydration at high temperature      c. Growth factor  $v(T)$

Fig. 5.7 Effect of reaction temperature on microstructure. Microstructures formed at moderate temperature (a) and high temperature (b). Fig. 5.7c gives the conversion (or growth) factor  $v(T)$  (van Breugel, 1991).

The microstructure can be considered as being built up of gradually growing particles, each of them representing a particular cement particle or another reactive or inert powder. The space left by the solid microstructure is the capillary pore space. If hydration takes place at relatively high temperatures the reaction product becomes denser, resulting in less outward growth of the reacting particles and hence a coarser capillary pore structure. This phenomenon is shown schematically in Fig. 5.7. In HYMOSTRUC3D the effect of temperature on the capillary porosity has been taken into account with a temperature dependent conversion factor  $v(T)$  (van Breugel, 1991). This factor defines the volume of the reaction product relative to the volume of the reacted binder. For reaction temperatures up to 20°C the conversion factor  $v(T)$  has a constant value of 2.2 (see Fig. 5.7c). For reaction temperatures beyond 20°C the conversion factor gradually decreases, resulting in less outward growth of the reaction products and hence a higher capillary porosity. For the temperature-dependent conversion factor  $v(T)$  it holds (van Breugel 1991):

$$v(T) = 2.2 * e^{-28.10^{-6} * T^2} \quad (5.18)$$

where T is the temperature [°C].

### 5.4.3 Capillary porosity and apparent diffusion coefficient

As stated in section 5.4.1, the temperature of hardening cement-based material will increase due to Joule heating and will affect the capillary porosity as well as the apparent diffusion coefficient (Care 2008). To investigate the effect of stray current on durability, the relationship between development of capillary porosity, as affected by stray current, and apparent diffusion coefficient is given in the following.

#### 5.4.3.1 Capillary porosity of cement paste

The capillary porosity of cement paste at a degree of hydration  $\alpha$  and hydrated at temperature  $T$  [°C] can be calculated using the following equation (van Breugel, 1991):

$$V_{por}^{cap}(\alpha) = \frac{\omega_0}{\rho_w} - \frac{\alpha}{\rho_s} * (v(T) - 1) \quad (5.19)$$

where  $V_{por}^{cap}(\alpha)$  is the capillary porosity of cement paste at a degree of hydration  $\alpha$ ,  $\omega_0$  is the water-to-cement ratio,  $\rho_w$  is the specific weight of water [1 g/cm<sup>3</sup>] and  $\rho_s$  is the specific weight of cement [3.15 g/cm<sup>3</sup>].

#### 5.4.3.2 Apparent diffusion coefficient

The capillary porosity affects the apparent diffusion coefficient used for calculating chloride transport in concrete. The apparent diffusion coefficient depends on several factors, such as microstructural parameters (e.g. porosity, pore size diameter) temperature, humidity, and degree of water saturation (Mingzhong 2013, Sun et al. 2011). Numata et al. (1990) proposed a relationship between the diffusion coefficient and porosity of cement-based materials as follows:

$$D_o = 3.55 \times 10^{-11} \phi^{0.947} \approx 3.55 \times 10^{-11} \phi^{0.95} \quad (5.20)$$

where  $D_o$  is the diffusion coefficient of concrete [m<sup>2</sup>/s] and  $\phi$  is the capillary porosity. For the porosity  $\phi$  the expression (5.19) for  $V_{por}^{cap}(\alpha_{28})$  can be used. For the apparent diffusion coefficient at 28 days it then holds:

$$D_{a,28}(\alpha_{28}) = 3.55 \times 10^{-11} \left( V_{por}^{cap}(\alpha_{28}) \right)^{0.95} \quad (5.21)$$

where  $D_{a,28}(\alpha_{28})$  is the apparent diffusion coefficient of concrete as a function of the degree of hydration at 28 days, viz.  $\alpha_{28}$ , [m<sup>2</sup>/s].

### 5.4.4 Input parameters of numerical simulations

To simulate the temperature development in concrete specimens due to hydration and stray current flow, Equations 5.2-5.15 were implemented in the finite element package COMSOL Multiphysics V 5.4\* software in the AC/DC module (Pryor et al. 2011). The numerical analyses were performed for concrete specimens with size 5.5×5.5×5.5 cm<sup>3</sup>,

\*In order to obtain simulation results with high resolution, the simulations were performed in the finite element analysis software COMSOL Multiphysics V 5.4 with a small element size, i.e. 0.2 cm.

$20 \times 20 \times 20 \text{ cm}^3$ ,  $40 \times 40 \times 40 \text{ cm}^3$ ,  $60 \times 60 \times 60 \text{ cm}^3$ ,  $70 \times 70 \times 70 \text{ cm}^3$ , and  $80 \times 80 \times 80 \text{ cm}^3$ , as well as for concrete walls. Adiabatic hydration curves of mixtures with w/c ratio 0.35 and 0.5 were simulated with HYMOSTRUC3D, using input from Table 5.1. The simulated adiabatic input curves are shown in Fig. 5.8. These curves are approximated by eq. (5.2). The hydration parameter  $\beta$  in eq. (5.2) was determined from curve fitting of simulated adiabatic hydration curves. To simulate the temperature development in concrete specimens, the following initial and boundary conditions were used as input:

a. Initial and thermal boundary conditions:

- Initial temperature of the concrete mixture:  $T_{Ref}(x,y,z,0) = 20^\circ\text{C}$
- Ambient (room) temperature:  $T_{Amb} = 20^\circ\text{C}$
- Thermal boundary conditions:

$$\lambda_c \cdot \left( \frac{\partial T}{\partial x} + \frac{\partial T}{\partial y} + \frac{\partial T}{\partial z} \right) \Big|_{x=0} = h \cdot (T_{Ref} - T(x=0, y, z, t))$$

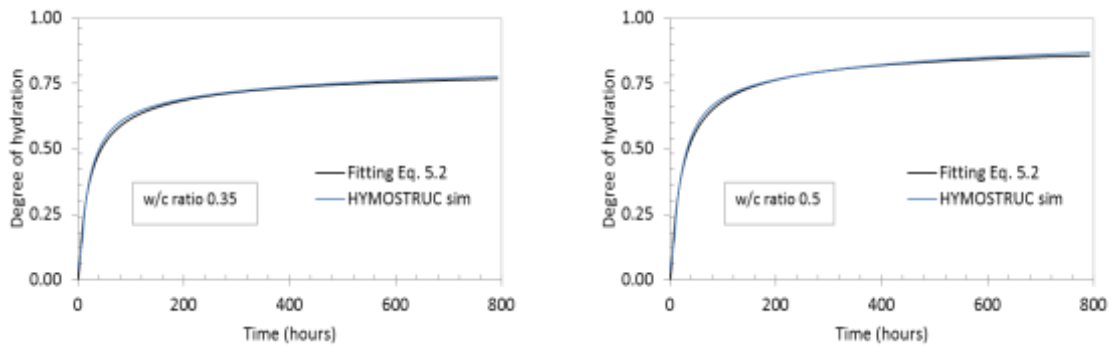
$$\lambda_c \cdot \left( \frac{\partial T}{\partial x} + \frac{\partial T}{\partial y} + \frac{\partial T}{\partial z} \right) \Big|_{x=L} = h \cdot (T_{Ref} - T(x=L, y, z, t))$$

where L is length of the specimen.

b. Initial and electrical boundary conditions:

- Initial electrical conductivity:
  - $\sigma_i(t=0) = 2.32 \text{ S/m}$  (w/c ratio 0.35)
  - $\sigma_i(t=0) = 2.45 \text{ S/m}$  (w/c ratio 0.5)
- Initial current density:  $J(t=0) = 0, 10, 40, 60 \text{ A/m}^2$

The other input parameters for simulating the temperature development in concrete specimens are given in Table 5.2.



a. Degree of hydration for w/c ratio 0.35

b. Degree of hydration for w/c ratio 0.5

Fig. 5.8 Adiabatic hydration curves simulated with HYMOSTRUC3D and fitting curves to determine hydration parameters ( $\tau$  and  $\beta$ ) for concrete with w/c 0.35 and 0.5. For obtained  $\tau$  and  $\beta$  values, see Table 5.2.

Table 5.2 Input parameters for simulating temperature development in concrete

| Input parameters  | Symbol           | Eq.        | Mixture 1<br>(w/b=0.35)        | Mixture 2<br>(w/b=0.5)         |
|---|------------------|------------|--------------------------------|--------------------------------|
| Maximum degree of hydration   | $\alpha_{h,max}$ | 5.4        | 0.78                           | 0.87                           |
| Maximum potential heat (kJ/kg)  | $Q_{max}$        | 5.5        | 367                            | 409                            |
| Cement content (kg/m <sup>3</sup> )   | C                | 5.8        | 400                            | 400                            |
| Cement content : sand ratio   | -                | -          | 1:3                            | 1:3                            |
| Aggregates content (%)  | -                | -          | 70                             | 70                             |
| Specific mass of concrete (kg/m <sup>3</sup> )                                      | $\rho_c$         | 5.8        | 2450                           | 2398                           |
| Specific heat of concrete (J/kg.K)  | $c_c$            | 5.8        | 1042                           | 1042                           |
| Initial temperature of the concrete mixture (°C)                                    | $T_{Ref}$        | 5.8, 5.15  | 20                             | 20                             |
| Heat conduction coefficient of concrete (W/m.K)                                     | $\lambda_c$      | 5.9        | 2.5                            | 2.5                            |
| Heat conduction coefficient of concrete insulation (W/m.K)                          | $\lambda_i$      | 5.26       | 0.125                          | 0.125                          |
| Thickness of insulation material (m)  | d                | 5.26       | 0.04                           | 0.04                           |
| Apparent activation energy (kJ/mol)   | $E_A$            | 5.6a, 5.6b | 33                             | 33                             |
| Universal gas constant (J/mol. K)   | R                | 5.6a, 5.6b | 8.31                           | 8.31                           |
| Empirical constant (hours)  | $\tau$           | 5.2        | 14.32                          | 14.32                          |
| Hydration shape factor  | $\beta$          | 5.2        | 0.81                           | 0.74                           |
| Temperature coefficient (°C <sup>-1</sup> )   | $\sigma_T$       | 5.15       | 0.035                          | 0.035                          |
| Heat transfer coefficient (W/m <sup>2</sup> .k)                                     | h                | 5.17       | 15                             | 15                             |
| Relative permittivity of concrete   | $\epsilon_r$     | 5.13       | 12                             | 12                             |
| Electrical current density (A/m <sup>2</sup> )                                      | J                | 5.12       | Low (<10) and high level (≥10) | Low (<10) and high level (≥10) |
| Initial conductivity (S/m)  | $\sigma_i$       | 5.16       | 2.32                           | 2.45                           |
| Conductivity at the point where the conductivity–time curve starts to plateau (S/m) | $\sigma_f$       | 5.16       | 0.07                           | 0.10                           |
| A time parameter of the particular paste (h)  | $t_s$            | 5.16       | 4.5                            | 6.1                            |
| A constant  | b                | 5.16       | 1.85                           | 2.1                            |

## 5.5 Results of experimental studies and discussion

In this section, experimental studies of the effect of stray current on the hydration process, temperature development and microstructural changes in cement paste are presented. As mentioned in section 5.2, two series of experiments will be conducted:

- Isothermal hydration tests on small cement paste samples with mass  $10 \pm 0.01$  g and low stray current levels (i.e. 10 mA/m<sup>2</sup>, 100 mA/m<sup>2</sup>, 1 A/m<sup>2</sup>). For safety reasons, current levels in these small samples were not higher than 1A/m<sup>2</sup>.
- Semi-adiabatic hydration tests on cement paste prisms (size: 5.5×5.5×29.5 cm<sup>3</sup>) with higher stray current levels (i.e. 10 A/m<sup>2</sup>, 40 A/m<sup>2</sup>, 60 A/m<sup>2</sup>).

It is not clear yet whether there is an extra effect of stray current on the rate of hydration, on top of the effect of higher temperature due to Joule heating. A possible additional effect of stray current on hydration will be investigated in section 5.5.1.3 and 5.5.2.2.

### 5.5.1 Isothermal calorimetry tests

#### 5.5.1.1 Heat generated in hardening cement paste under stray current

Fig. 5.9a shows the measured effect of electrical current flow on the rate of heat evolution  $dQ_d(t)/dt$  of cement paste with w/c ratio 0.35 measured by isothermal calorimetry at 20°C curing. The shape of the heat curve shows that the peak of the rate of discharge of heat increases with increasing level of stray current flow and occurs at about 13 to 14 hours after casting. The cumulative amount of discharged heat of cement paste is given in Fig. 5.9b.

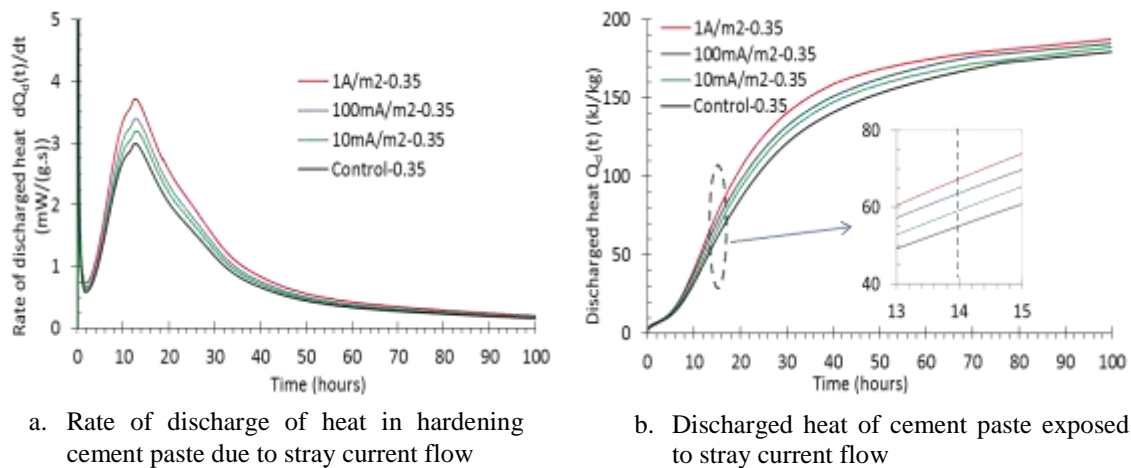


Fig. 5.9 Measured rate of discharge of heat  $dQ_d(t)/dt$  (a) and discharged heat  $Q_d(t)$  (b) in hardening cement paste (control) and with stray current level of 10mA/m<sup>2</sup>, 100mA/m<sup>2</sup> and 1A/m<sup>2</sup> for w/c 0.35 in isothermal condition.

#### 5.5.1.2 Temperature development in hardening cement paste during isothermal hydration

The temperature development in hardening cement paste samples in the isothermal calorimeter was measured with thermocouples, embedded in the middle of the specimens. Fig. 5.10 depicts the influence of stray current on temperature development in hardening cement paste. The figure shows that already without stray current a small increase of temperature of the cement paste sample cannot be avoided. With stray current, the temperature increase is higher.

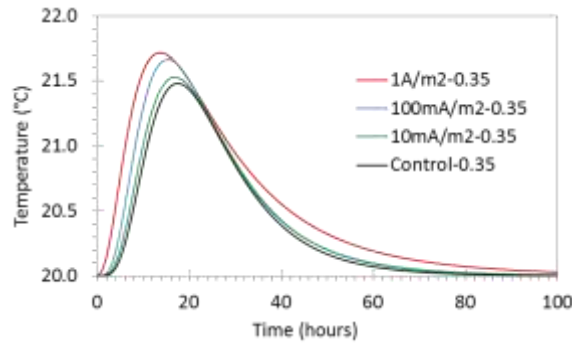


Fig. 5.10 Temperature development of hardening cement paste as a function of time. Samples with w/c ratio 0.35, measured in isothermal condition.

### 5.5.1.3 Analysis of stray current effect on hydration in isothermal calorimeter test

For a preliminary analysis of the effect of stray current on cement hydration in an isothermal calorimeter the hydration process during the first 14 hours of the test will be analysed. That's the period until the maximum temperatures were reached.

#### *Heat of hydration in the reference sample (no stray current)*

In the reference sample the hydration process is the only heat source. Most of the heat is discharged ( $Q_d(t)$ ), while a small amount of the produced heat, i.e.  $Q_s(t)$ , is used for heating of the sample. For the total amount of liberated heat  $Q_{tot}(t)$  it thus holds:

$$Q_{tot}(t) = Q_d(t) + Q_s(t) \quad (5.22)$$

Figure 5.11 shows a close up of Figure 5.9b of the measured amount of discharged heat  $Q_d(t)$  of the reference sample during the first 14 hours. After 14 hours the amount of discharged heat was:  $Q_{d,14h} = 55.47 \text{ kJ/kg}$ .

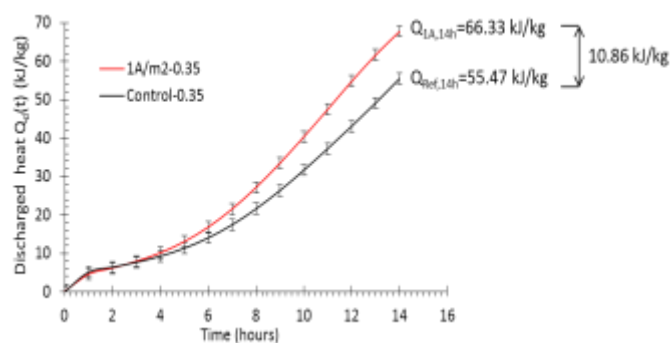


Fig. 5.11 Discharged heat  $Q_d(t)$  in hardening cement paste (control) and with stray current level  $1\text{A/m}^2$  for w/c 0.35 in isothermal condition.

The amount of heat  $Q_s(t)$  needed to heat up the sample to the measured maximum temperature increase, i.e.  $\Delta T_{\max}$ , depends on the mass and specific heat of the sample. In formula form:

$$Q_s(t) = \frac{\Delta T_{\max} \cdot \rho_{cp} \cdot c_{cp}}{C} \quad (5.23)$$

in which  $\rho_{cp}$  [kg/m<sup>3</sup>] is the specific mass of the cement paste,  $c_{cp}$  [J/kg.K] the specific heat of the paste,  $C$  [kg/m<sup>3</sup>] the amount of cement in the paste.  $\Delta T_{\max}$  stands for the measured maximum temperature (Fig. 5.10) minus the reference temperature  $T_{\text{ref}} = 20^\circ\text{C}$ . For the reference case it holds:  $\Delta T_{\max} = 21.36 - 20.0 = 1.36^\circ\text{C}$ . For the paste with  $w/c = 0.35$  and specific mass of the cement  $\rho_{ce} = 2950 \text{ kg/m}^3$ , the cement content in the paste is  $741 \text{ kg/m}^3$  and the resulting specific mass of the cement paste is  $\rho_{cp} = 1960 \text{ kg/m}^3$ . The specific heat of the cement paste is calculated at  $c_{cp} = 1418 \text{ J/kg.K}$  (according to US DIBR 1940-1949). With these values for  $\rho_{cp}$ ,  $c_{cp}$  and  $\Delta T_{\max}$ , the amount of heat  $Q_s(t)$  to realise a temperature increase of the sample of  $1.36^\circ\text{C}$  is calculated with eq. (5.24) at  $5.10 \text{ kJ/kg}$ . The total amount of heat produced by the hydrating cement in the first 14 hours is now found with eq. (5.22):

$$Q_{\text{tot}}(14\text{h}) = Q_{d,14\text{h}} + Q_{s,14\text{h}} = 55.47 + 5.10 = 60.57 \text{ kJ/kg}$$

#### *Heat of hydration in the sample with stray current of 1 A/m<sup>2</sup>*

In the sample with stray current both the hydration process and the current generate heat. Also in these tests most of the heat is discharged ( $Q_d(t)$ ), while a small amount the produced heat, i.e.  $Q_s(t)$ , is used for heating of the sample. The amount of heat of discharged in the first 14 hours is shown in Figure 5.11. It holds:  $Q_{d,14\text{h}} = 66.33 \text{ kJ/kg}$ .

The maximum temperature increase of the sample with a stray current of  $1 \text{ A/m}^2$  is  $\Delta T_{\max} = 1.72^\circ\text{C}$  (see Fig. 5.10). With values for  $\rho_{cp}$  and  $c_{cp}$  given in the foregoing, the amount of heat needed to realise this temperature increase is calculated with eq. (5.23) at  $6.45 \text{ kJ/kg}$ . The total of the discharged heat and the heat needed for the temperature increase of the sample is now (eq. (5.22)):

$$Q_{\text{tot}}(14\text{h}) = Q_{d,14\text{h}} + Q_{s,14\text{h}} = 66.33 + 6.45 = 72.78 \text{ kJ/kg}$$

The difference between this amount of heat and amount of heat determined in the reference test is  $72.78 - 60.57 = 12.21 \text{ kJ/kg}$ . This difference is caused by the stray current of  $1 \text{ A/m}^2$ .

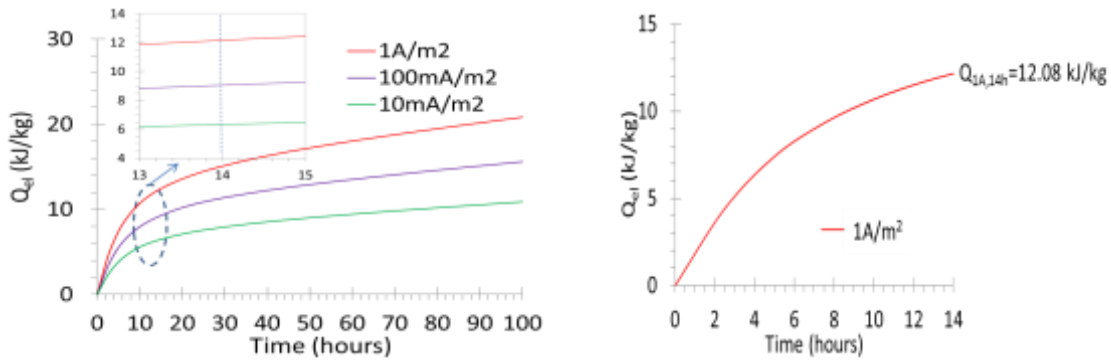
#### *Heat generated in the sample caused by stray current*

As discussed in section 5.4.2.2, cement paste subjected to a stray current will increase in temperature because of Joule heating. The cumulative heat input from stray current  $Q_{el}(J,E,t)$  (eq. (5.10)) at time  $t$  can be calculated by summarizing all heat increments  $\Delta Q_{el,i}$  ( $i = 1, 2, \dots, n$ ):

$$Q_{el}(J, E, t) = Q_{el,n} = \sum_{i=1}^n \Delta Q_{el,i} \quad (5.24)$$

Fig. 5.12a shows the cumulative heat generated by a stray current of  $10 \text{ mA/m}^2$ ,  $100 \text{ mA/m}^2$  and  $1 \text{ A/m}^2$ , while Fig. 5.12b shows a close-up of the cumulative heat generated by a current of  $1 \text{ A/m}^2$  in the first 14 hours of hydration. As shown in Fig. 5.12b, the cumulative heat input from the stray current of  $1 \text{ A/m}^2$  in the first 14 hours of hydration is  $12.08 \text{ kJ/kg}$ . This amount is in close agreement with the above mentioned difference in the total amount of heat of  $12.21 \text{ kJ/kg}$  between the reference test and the test with

stray current. It can be deduced from isothermal calorimetry tests that there is no additional effect of stray current on hydration beyond the effect of Joule heating.



a. Cumulative heat input from stray current  $Q_{el}$

b. Cumulative heat input by stray current 1 A/m<sup>2</sup>

Fig. 5.12 Cumulative heat input from stray current flow  $Q_{el}$  (calculated with eq. (5.25)). a) Cumulative heat curves for three current levels. b) Cumulative heat input from stray current (from 0 to 14 hours). Cement paste with w/c ratio 0.35.

## 5.5.2 Semi-adiabatic tests

### 5.5.2.1 Temperature development in small hardening cement paste prism under stray current

In section 5.5.1 the effect of stray current on hydration process has been analysed in case of isothermal condition. Those results will be used for predicting the temperature development in samples of  $5.5 \times 5.5 \times 29.5 \text{ cm}^3$  subjected to stray current with different current densities, i.e. 1, 10, 40 and 60 A/m<sup>2</sup> for non-isothermal hydration. Heat input from stray current, i.e. Joule heating, affects the temperature development in hardening cement paste. The heat input from stray current strongly depends on current density  $J(t)$ , while the current density depends on the electrical conductivity  $\sigma(T, t)$  of hardening cement paste.

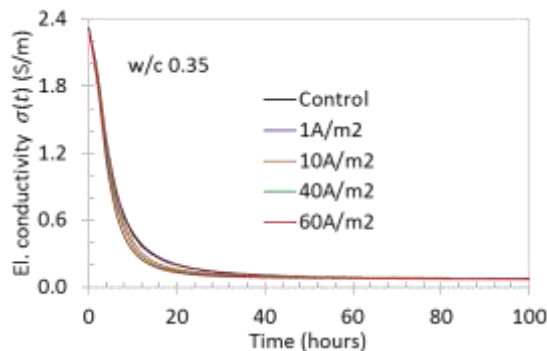


Fig. 5.13 Evolution of electrical conductivity  $\sigma(t)$  of hardening cement paste under stray current flow with current density 1, 10, 40, and 60A/m<sup>2</sup> calculated with eq. (5.15), where  $\sigma_{eff}(t)$  (eq. 5.16) was calculated with input parameters  $\sigma_i=2.32$ ,  $\sigma_f=0.07$ ,  $t_s = 4.5$  (h),  $b=1.85$ .

Fig. 5.13 shows the evolution of electrical conductivity  $\sigma(T, t)$  of hardening cement paste with and without stray current flow. As shown already in Fig. 5.4, the electrical conductivity decreases rapidly with progress of the hydration process. Furthermore, the electrical conductivity of hardening cement paste slightly decreases with increasing level of current density up to about 24 hours. Stabilization was achieved after 24 hours. From that time on the values of conductivity of control specimen and specimen under stray current are almost the same. The development of current density in hardening cement paste is given in Fig. 5.14. Following eq. (5.12), the current densities sharply decrease due to decreasing electrical conductivity of hardening cement paste.

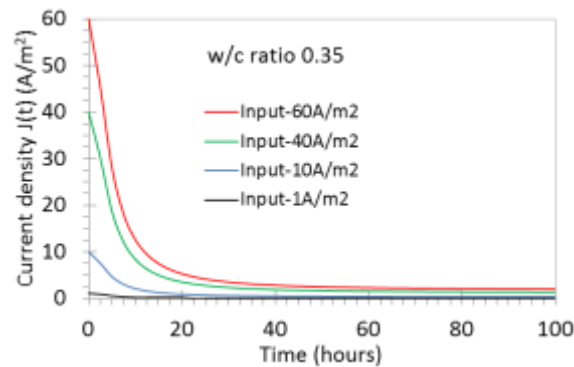
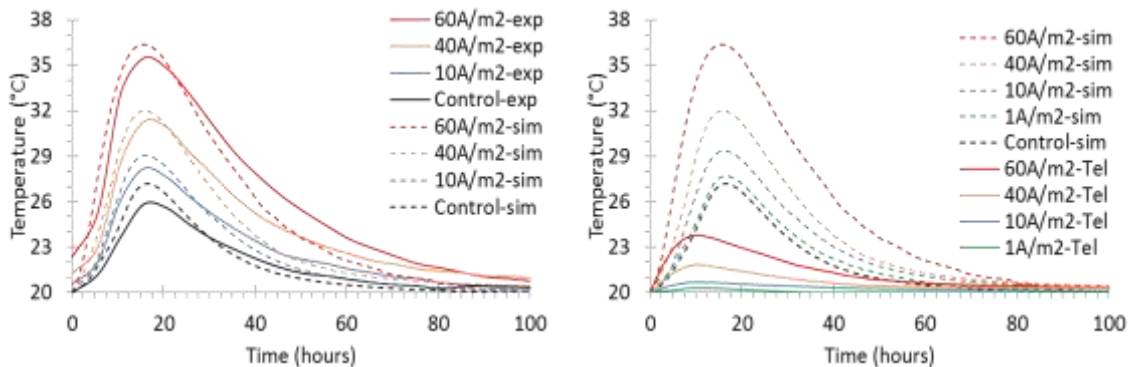


Fig. 5.14 Development of current density  $J(t)$  in hardening cement paste with applied current density 1, 10, 40, and 60A/m<sup>2</sup>, calculated with eq. (5.12).



a. Simulated and measured temperature development in hardening cement paste subjected to stray current

b. Simulated temperature development in hardening cement paste subjected to stray current (dashed line) and temperature development caused by stray current only  $T_{el}$  (solid line).

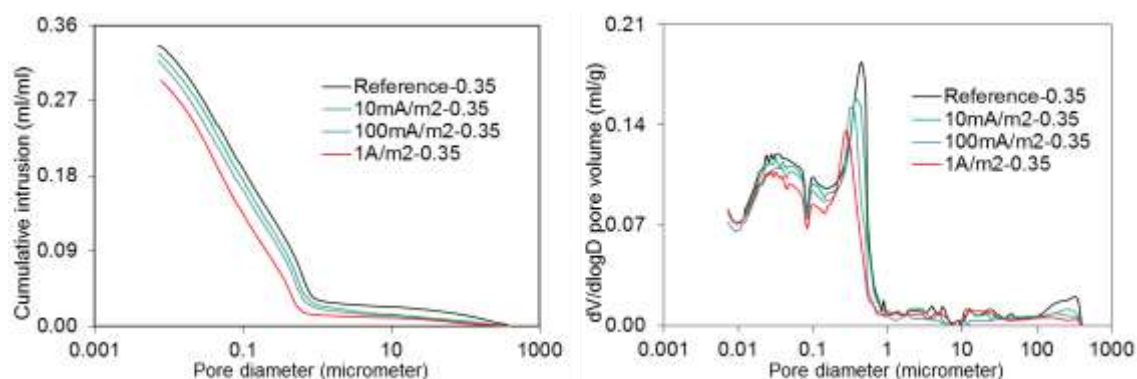
Fig. 5.15 (a) Simulated and measured temperature development in hardening cement paste subjected to stray current (b). Comparison between temperature development of hardening cement paste subjected to stray current and temperature development caused by stray current only  $T_{el}$ . Water-to-cement ratio used was 0.35. The sample size is 5.5×5.5×29.5 cm<sup>3</sup>.

Fig. 5.15 shows the simulated and measured temperature development in hardening cement paste prisms with and without stray current flow. Simulations were carried out with eq. (5.9). As shown in Fig. 5.15a, the simulated temperature development in hardening cement paste prisms is in good agreement with the experimental results. In

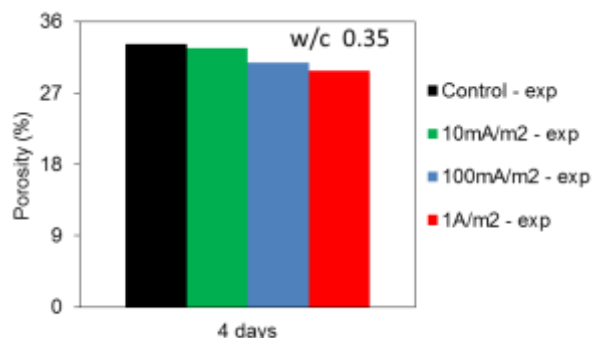
addition, comparison of simulated temperature evolution caused by hydration *and* stray current and caused by *only* stray current  $T_{el}$  is given in Fig. 5.15b. Fig. 5.15b shows that Joule heating substantially increases temperature evolution in hardening cement paste prisms. For example temperature increase due to stray current only with level  $60A/m^2$ , i.e. about  $4^{\circ}C$ , promotes significantly on temperature increase in hardening cement paste, i.e. about  $10^{\circ}C$ .

### 5.5.3 Measured effect of electrical current on pore structure of isothermally cured cement paste, w/c = 0.35

For mixtures with w/c ratio 0.35 Figs. 5.16a,b show the capillary porosity and the pore size distribution of hardening cement paste after 4 days of isothermal hydration, respectively. These figures show that the capillary porosity reached after 4 days decreases with increasing level of electrical current. A summary of the capillary porosity of hardening cement paste for w/c ratio 0.35 is given in Fig. 5.16c. The differential curves (Fig. 5.16b) reveal that the pore size distribution is slightly shifted towards small pores with an increase of the current density. The reason for this is a higher degree of hydration of hardening cement paste when subjected to stray current during hydration (see Fig. 5.17).

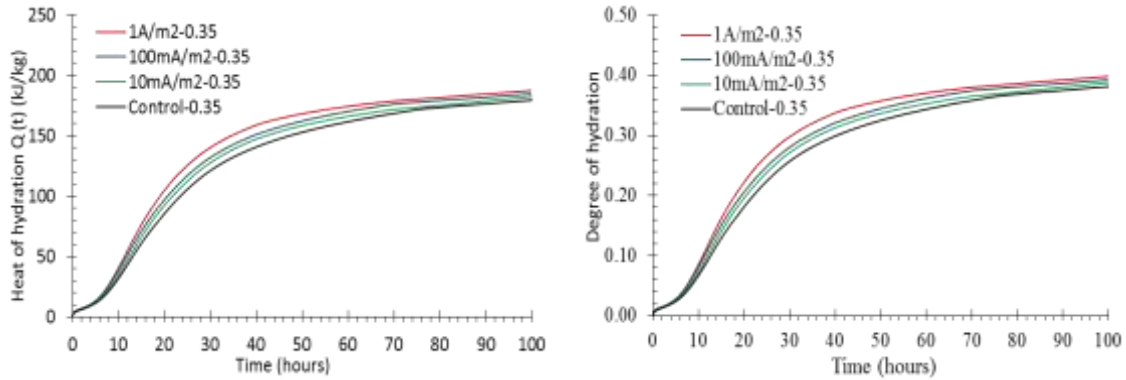


a. Capillary porosity of cement paste subjected to stray current with w/c 0.35 at 4 days. b. Pore size distribution of cement paste subjected to stray current with w/c 0.35 at 4 days.



c. Capillary porosity of cement paste subjected to stray current with w/c 0.35 at 4 days.

Fig. 5.16 Capillary porosity (a) and pore size distribution (b) of isothermally cured cement pastes at 4 days with w/c ratio 0.35 and summary porosity (c) of cement paste obtained from MIP tests with current density levels of  $10mA/m^2$ ,  $100mA/m^2$  and  $1A/m^2$ . Isothermal tests.



a. Heat of hydration of isothermally hardening cement paste subjected to stray current

b. Degree of hydration of isothermally hardening cement paste subjected to stray current

Fig. 5.17 Heat of hydration  $Q(t)$  (a) and degree of hydration  $\alpha(t)$  (b) of isothermally hardening cement paste subjected to stray current with different current density calculated with eq. (5.4), where  $Q_{\max}$  is 367 kJ/kg (see Table 5.2).

## 5.6 Numerical simulation of stray current effects on the hydration process

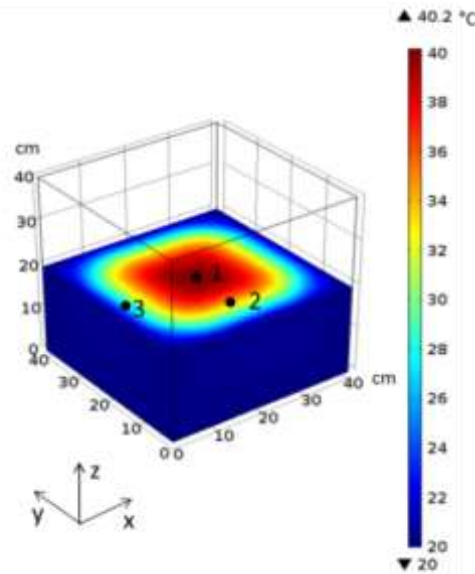
### 5.6.1 Effect of stray current on hydration and temperature distribution in hardening concrete cube, $40 \times 40 \times 40 \text{ cm}^3$

#### 5.6.1.1 Hydration and temperature development in a concrete cube, $40 \times 40 \times 40 \text{ cm}^3$ , without effect of stray current

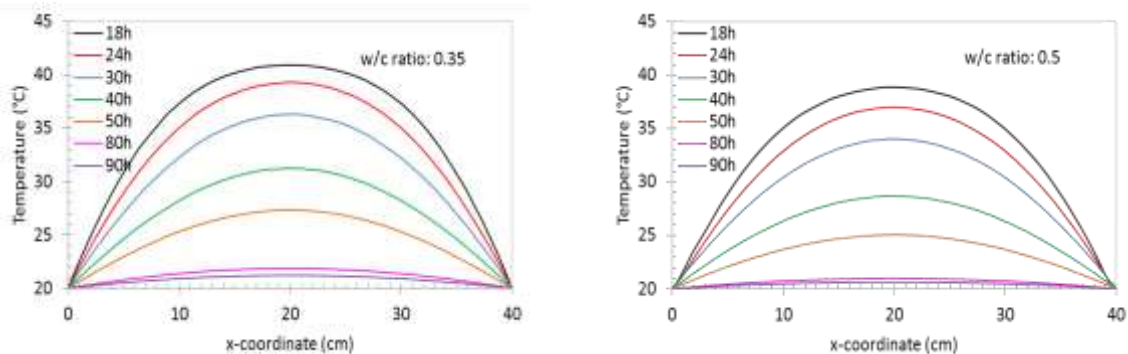
In Fig. 5.15a a good agreement was shown between experimental results and numerical simulations of temperature development in (relatively small) hardening cement paste prisms subjected to stray current. Considering that result, scaling up from hardening *paste* to hardening *concrete* seems justified and enables to simulate the effect of stray current on temperature development in larger hardening concrete elements. First the hydration and temperature evolution in a concrete cube,  $40 \times 40 \times 40 \text{ cm}^3$ , in case of *natural* hydration, i.e. *without* the effect of stray current, will be presented.

Figure 5.18 shows an example of simulated 3D temperature fields in a concrete cube,  $40 \times 40 \times 40 \text{ cm}^3$ . In this simulation, the imposed outside temperature is  $20^\circ\text{C}$ . Fig. 5.18a shows the temperature fields in the cross section of the concrete cube with w/c ratio 0.35 after 18 hours hydration. Temperature profiles in the concrete cube from 18 to 90 hours are shown in Fig. 5.18b for mixture with w/c ratio 0.35 and 0.5, respectively.

Fig. 5.19 shows an example of the temperature development, heat of hydration and degree of hydration at three different locations in the concrete cube, w/c ratio 0.35, as function of time. The highest temperature is reached in the centre of the specimen. The temperature gradually decreases from the centre (point 1) to the surface (point 2 and 3) of the concrete due to discharge of heat to the surroundings. Fig. 5.19c clearly shows that close to the surface, i.e. in point 3, the hydration process is delayed compared to the hydration in the centre of the cube. This is a well-known phenomenon, which implies that the microstructures in the outer zone are different from that in the centre. The presence of stray current will further enhance this effect. This will be investigated in the next section for concrete walls with different wall thickness.



- a. Example temperature field in hardening concrete cubes with specimen size  $40 \times 40 \times 40 \text{ cm}^3$  for w/c ratio 0.35 at cross section  $z=20 \text{ cm}$  from the bottom at three different locations (i.e. point 1 ( $xyz = 20, 20, 20$ ), point 2 ( $xyz = 20, 8, 20$ ), point 3 ( $xyz = 3, 20, 20$ )) after 18 hours of hydration.



- b. Simulated spatial distribution of temperature in hardening concrete in x direction for w/c ratio 0.35 (left) and 0.5 (right) after 18 hours.

Fig. 5.18 Simulated temperature field (a) and temperature profile in hardening concrete specimen in x direction, for  $y=20 \text{ cm}$  and  $z=20 \text{ cm}$  (b). Sample size:  $40 \times 40 \times 40 \text{ cm}^3$ . Imposed outside temperature is  $20^\circ\text{C}$ .

### 5.6.1.2 Effect of stray current on maximum temperature in hardening concrete walls

In section 5.4.2.4. it has been explained that curing at elevated temperatures will go along with coarsening of the capillary pore structure, which, on its turn, will affect the resistance against ingress of hazardous species. On top of that high temperatures may give rise to internal micro-cracking, mainly in the cooling phase. The analysis of hydration-induced stresses is outside the scope of this thesis. Here we refer to a thumb rule, which states that for producing a good quality concrete the maximum temperature of the concrete during hardening should not exceed  $60^\circ\text{C}$ . This maximum determines, to a certain extent, the risk of internal damage, i.e. temperature-induced microcracking (DANISH Ministry of Transport 1985).

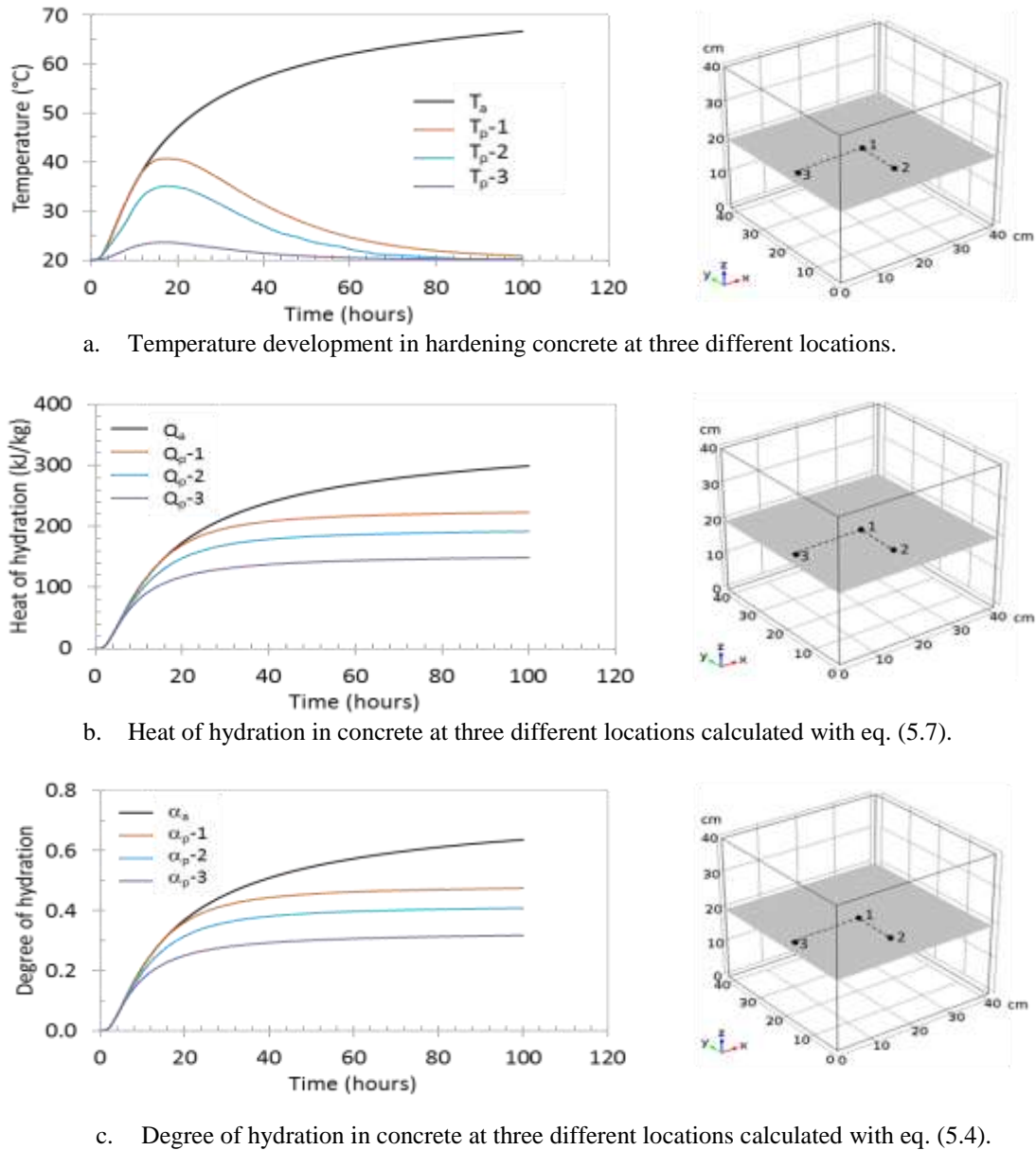
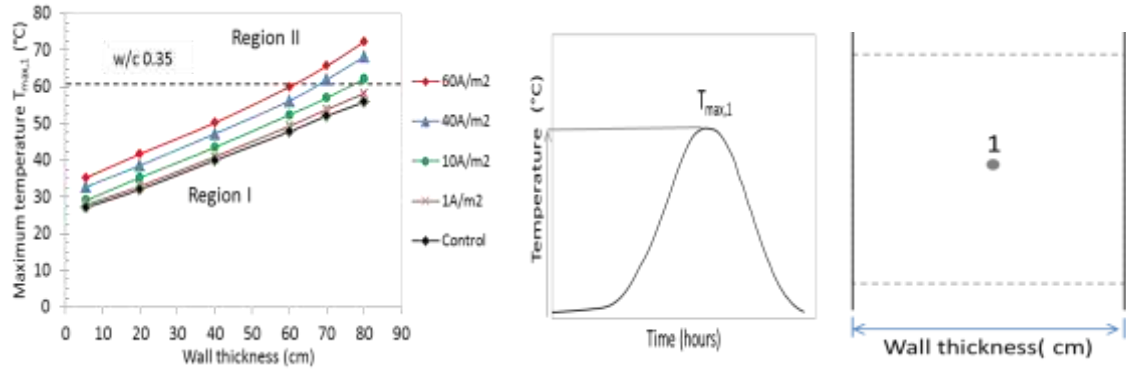


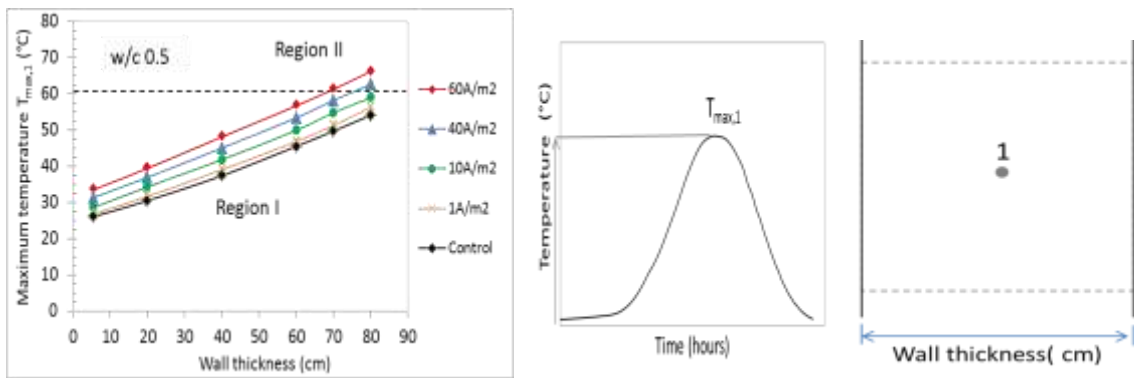
Fig. 5.19 Simulated temperature development, heat of hydration and degree of hydration of hardening concrete at three different locations (i.e. point 1 ( $xyz = 20,20,20$ ), point 2 ( $xyz = 20,8,20$ ), point 3 ( $xyz = 3,20,20$ )) with specimen size  $40 \times 40 \times 40 \text{ cm}^3$  for w/c ratio 0.35.

Fig. 5.20 and Fig. 5.21 show the maximum temperature in hardening concrete walls subjected to stray current as a function of the wall thickness and current density for concretes with w/c ratios 0.35 and 0.5, respectively. The imposed outside temperature is  $20^\circ\text{C}$ . The maximum temperature in the centre of the concrete walls reaches higher values with increasing wall thickness and increasing stray current levels.

For judging the effect of stray current on the properties of the concrete, the maximum temperatures were divided in two regions, i.e. region I and region II. Region I refers the scenarios where the maximum temperature in the core of the hydrating walls does not exceed  $60^\circ\text{C}$ . Region II refers to scenarios where the maximum temperature exceed the  $60^\circ\text{C}$  limit and the concrete may suffer from curing at elevated temperatures.



a. Maximum temperature in the centre of hardening concrete walls with w/c ratio 0.35



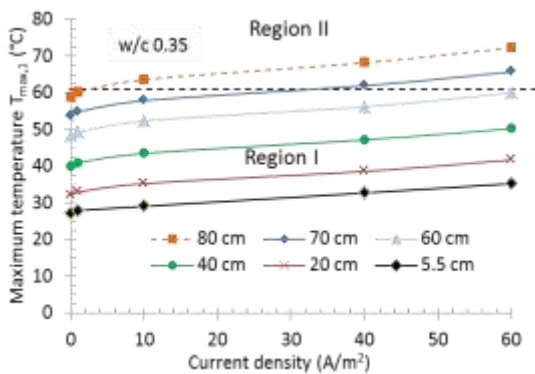
b. Maximum temperature in the centre of hardening concrete walls with w/c ratio 0.5.

Fig. 5.20 Maximum temperature ( $T_{max,1}$ ) in the centre of hardening concrete walls subjected to current level as a function of wall thickness for w/c ratio 0.35 (a) and 0.5 (b). Concrete mixture: cement content  $400 \text{ kg/m}^3$ , aggregate content 70%. Imposed ambient temperature:  $20^\circ\text{C}$ .

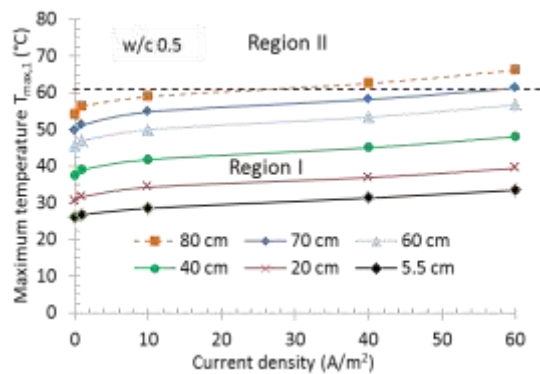
Region I: Peak temperatures are higher due to presence of stray current, but still  $< 60^\circ\text{C}$

Region II: Peak temperatures reach values  $> 60^\circ\text{C}$ , with enhanced risk of internal damage to the concrete.

5



a. Maximum temperature in hardening concrete walls with w/c ratio 0.35



b. Maximum temperature in hardening concrete walls with w/c ratio 0.5

Fig. 5.21 Maximum temperature ( $T_{max,1}$ ) in centre of hardening concrete walls with w/c ratio 0.35 (a) and 0.5 (b) as a function of current density. Concrete mixture: cement content  $400 \text{ kg/m}^3$ , aggregate content 70%. Imposed ambient temperature:  $20^\circ\text{C}$ .

### 5.6.1.3 Effect of stray current on degree of hydration, porosity and strength of a 40 cm thick concrete wall, with and without insulation.

As mentioned in Ch. 2, hydration at elevated temperatures results in a higher capillary porosity. A higher capillary porosity goes along with a lower compressive strength and higher diffusion coefficients. This may jeopardize the quality and service life of concrete structures, particularly in case a higher porosity and higher diffusion coefficients are reached in the outer zones of concrete walls. High concrete temperatures in the outer zones of concrete walls are conceivable in case insulated formwork is used. Simulations will be performed, therefore, of temperature distributions in 40 cm thick hardening concrete walls *with* and *without* insulated formwork (see below, subsection A). The relationship between capillary porosity, diffusion coefficient and compressive strength will be elucidated below under subsection B. Results of simulation are presented in subsection C.

#### A. Thermal boundary conditions

In order to allow for the effect of insulation of the hardening concrete walls, the numerical simulations will be performed with the following boundary conditions:

##### *a). Boundary condition of hardening concrete walls with insulation*

The schematic of the boundary conditions for numerical simulation of the hydration process and properties of hardening concrete walls with insulation subjected to stray current is given in Fig. 5.22. The boundary conditions can be specified from the expression of the continuity of heat conduction through the insulation material-concrete wall interface as follow:

$$\lambda_c \cdot \left. \frac{\partial T}{\partial x} \right|_{x=0} = \lambda_i \frac{T(x=0,t) - T_{Ref}}{d} \quad (5.25a)$$

$$\lambda_c \cdot \left. \frac{\partial T}{\partial x} \right|_{x=L} = \lambda_i \frac{T(x=L,t) - T_{Ref}}{d} \quad (5.25b)$$

$$\lambda_i \cdot \left. \frac{\partial T}{\partial x} \right|_{x=-d} = h \cdot (T_{Ref} - T(x = -d, t)) \quad (5.25c)$$

$$\lambda_i \cdot \left. \frac{\partial T}{\partial x} \right|_{x=L+d} = h \cdot (T_{Ref} - T(x = L + d, t)) \quad (5.25d)$$

where  $\lambda_c$  is the heat conduction coefficient of concrete [W/m.K],  $\lambda_i$  is the heat conduction coefficient of insulation material [W/m.K],  $d$  is the thickness of the insulation material [m],  $h$  is the heat transfer coefficient [W/m<sup>2</sup>.K] and  $L$  is the wall thickness.

The initial conditions are specified as follow:

- Initial temperature of the concrete mixture:  $T_{Ref}(x,t=0) = 20^\circ\text{C}$
- Ambient (room) temperature:  $T_{Amb} = 20^\circ\text{C}$
- Initial electrical conductivity of hardening concrete  $\sigma_i(t = 0) = 2.32 \text{ S/m}$
- Initial current density  $J(t = 0) = 0, 10, 40, 60 \text{ A/m}^2$

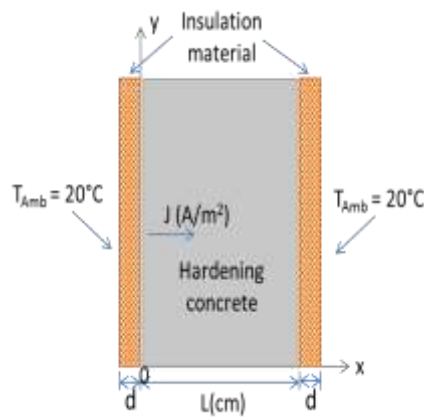


Fig. 5.22 Schematic of boundary conditions for numerical simulation of temperature development in hardening concrete walls with insulation subjected to stray current. The wall thickness is  $L$  (in cm). The thickness of the insulation material is  $d$  (in cm).

*b). Boundary condition of hardening concrete walls without insulation*

The schematic of the boundary conditions for numerical simulation of the hydration process and properties of hardening concrete walls *without* insulation subjected to stray current is given in Fig. 5.23. The boundary condition is given by:

$$\lambda_c \cdot \left. \frac{\partial T}{\partial x} \right|_{x=0} = h \cdot (T_{Ref} - T(x=0, t)) \quad (5.26a)$$

$$\lambda_c \cdot \left. \frac{\partial T}{\partial x} \right|_{x=L} = h \cdot (T_{Ref} - T(x=L, t)) \quad (5.26b)$$

where  $\lambda_c$  is the heat conduction coefficient of concrete [W/m.K],  $h$  is the heat transfer coefficient [W/m<sup>2</sup>.K], and  $L$  is the wall thickness.

All initial conditions used as input for numerical simulation of the hydration process and properties of hardening concrete walls with insulation are adopted. In this section, however, the numerical simulation is performed in hardening concrete walls without insulation.

5

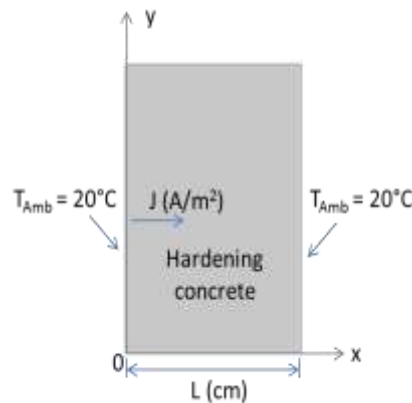


Fig. 5.23 Schematic of boundary conditions for numerical simulation of temperature development in hardening concrete walls without insulation subjected to stray current. The wall thickness is  $L$  (in cm).

### B. Capillary porosity, diffusion coefficient and compressive strength

For a certain mixture the capillary porosity is a function of the degree of hydration and can be calculated with eq. (5.19). From the capillary porosity of cement paste, the apparent diffusion coefficient in the centre of hardening concrete without insulation at reference time 28 days,  $D_{a,28}(J)$ , was calculated with eq. (5.21).

The compressive strength of the concrete will be calculated as a function of the capillary porosity of cement paste using the Balshin equation (Balshin 1949):

$$f_c = f_{co}(1 - p)^n \quad (5.27)$$

where  $f_c$  is the compressive strength of concrete,  $f_{co}$  is the intrinsic strength of concrete at zero porosity [here 98.79 MPa (Chakradhara Rao 2010)],  $p$  is the capillary porosity of cement paste,  $n$  is a coefficient (Grudemo 1975). Typical curves of compressive strength of concrete as a function of capillary porosity of cement paste are given in Fig. 5.24 (left). Schematic range values of compressive strength of hardened concrete as a function of capillary porosity of cement paste with w/c ratio 0.35-0.5 are presented in Fig. 5.24 (right). In this study, the amounts of cement paste are  $540 \text{ kg/m}^3$  and  $600 \text{ kg/m}^3$  for w/c ratio 0.35 and 0.5, respectively.

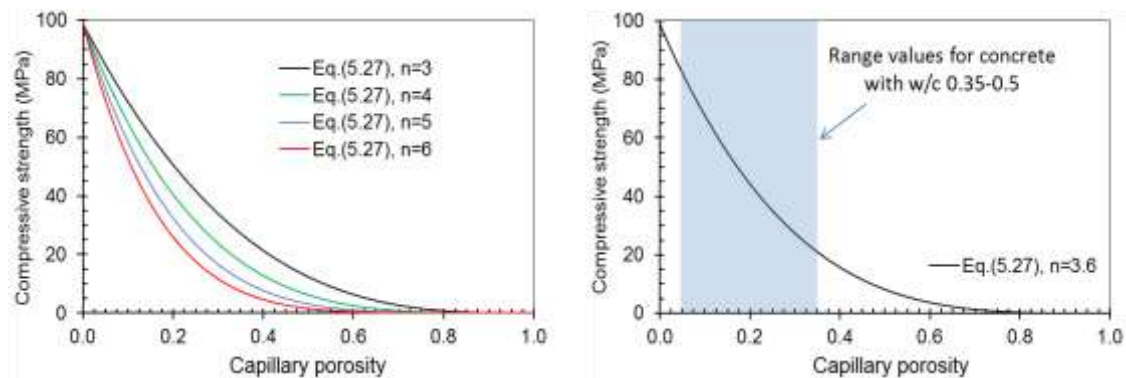
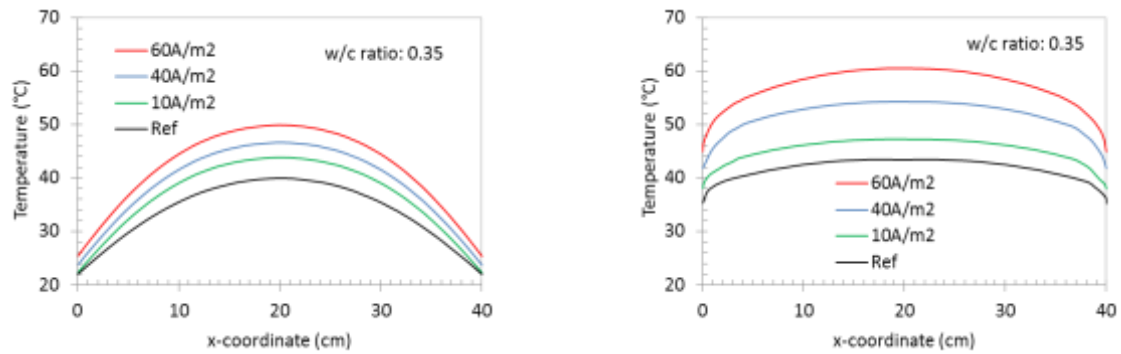


Fig. 5.24 Typical curves of compressive strength of concrete as a function of capillary porosity of cement paste calculated with eq. (5.27) with different  $n$  values (left) and schematic range values of compressive strength of concrete as a function of capillary porosity of cement paste with w/c ratio 0.35-0.5 (right). In this work, a coefficient  $n$  was chosen as 3.6 (Chakradhara Rao 2010).

### C. Numerical simulations of the effect of stray current on core and outer zone concrete

The numerical simulations presented in this subsection focus on the effect of the presence of insulation during hydration of a 40 cm thick concrete wall and how the presence of stray current further enhances this effect.

The effect of insulation on the temperature distribution in a 40 cm thick concrete wall is shown in Fig. 5.25. Fig. 5.25b shows that the temperatures in the outer zone of concrete walls with insulation significantly increase compared to concrete walls without insulation (Fig. 5.25a). The presence of stray current further enhances this effect. High temperatures in the outer zone will result in higher final values of the porosity, which might be a point of concern for the durability of the concrete.



- a. Temperature profile in the outer zone of concrete walls without insulation subjected to stray current
- b. Temperature profile in the outer zone of concrete walls with insulation subjected to stray current

Fig. 5.25 Example of temperature profiles after 18 hours of hydration in a 40 cm thick concrete wall with and without insulation and meanwhile subjected to stray current.

The effects of insulation on the temperature evolution, degree of hydration, capillary porosity and compressive strength in the centre and in the outer zone of a 40 cm thick concrete wall are presented in Fig. 5.26 and 5.27 as a function of time. In Fig. 5.26 the results of numerical simulations are presented which refer to the centre of the wall, whereas Fig. 5.27 refers to the outer zone of the wall.

#### *Temperature in centre of the 40 cm thick wall*

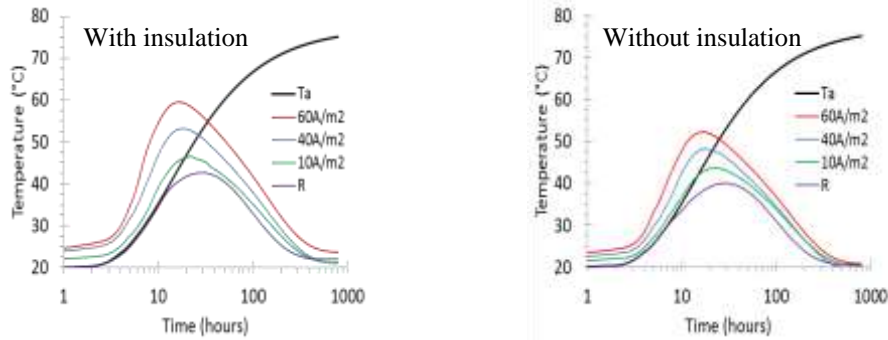
As shown in Fig. 5.26 the temperature in the centre of a 40 cm thick hardening concrete wall will increase with increasing stray current. For a 40 cm thick wall, the presence or not of insulation has only a minor effect. The presence of stray current will accelerate the hydration process at early age and hence increases the rate of strength development (Fig. 5.26d). Hydration at higher temperatures, however, will result in higher capillary porosity and a *lower final strength*. The higher capillary porosity in the centre of the concrete elements also results in a higher diffusion coefficient (to be discussed in more detail in section 5.6.2.2). A higher apparent diffusion coefficient will generally not be problematic for the service life as long as it concerns the centre of hardening concrete structures. Similar simulations as presented in the Fig. 5.26 for a 40 cm thick concrete wall are given for other wall thicknesses in Appendix Fig B.1 and Fig. C1.

#### *Temperature in surface zone of 40 cm thick wall*

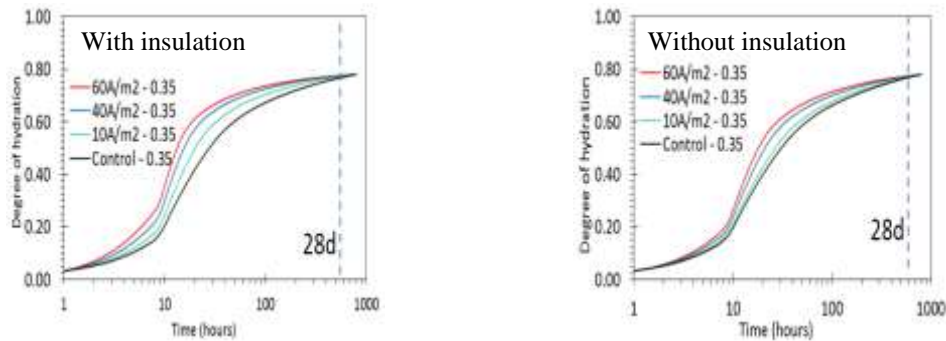
Fig. 5.27 shows the results of numerical simulations of the evolution of temperature, degree of hydration, capillary porosity and compressive strength in the outer zone of a 40 cm thick concrete wall with and without insulation. A significant effect of stray current on temperatures was noticed in the outer zone of hardening concrete with insulation (Fig. 5.27a, left). In the outer zone of concrete walls without insulation no significant change of temperature will occur, since in this case the generated heat is immediately discharged to the environment (Fig. 5.27a, right). Obviously, microstructural changes, as well as compressive strength, due to stray current seem particularly relevant for the outer zone of concrete walls with insulation. As seen in Fig. 5.27, initially the temperature increase in the outer zone of hardening concrete with insulation accelerates hydration process and subsequently reduces the capillary porosity

and increase the compressive strength. At later ages, however, a high capillary porosity remains because hydration had proceeded at relatively high temperatures, resulting in a lower compressive strength and a higher apparent diffusion coefficient, which will reduce durability and service life of concrete structures.

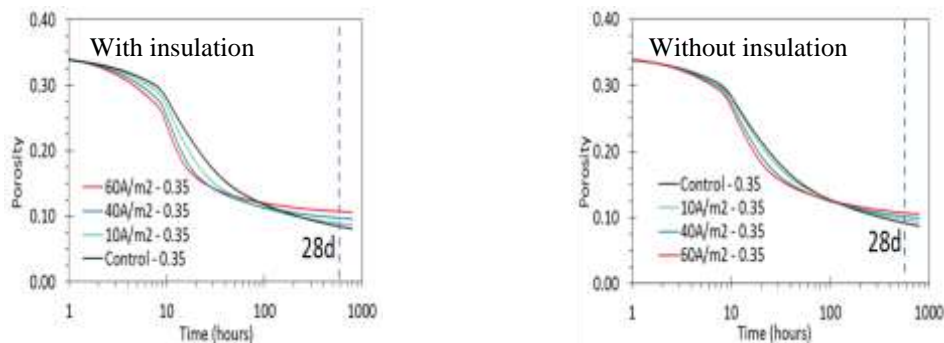
The effects of stray current on capillary porosity and apparent diffusion coefficient in the outer zone of hardening concrete after 28 days hydration will be further discussed in section 5.6.2. Numerical simulation results for different wall thickness are given in Appendix Fig. B.2 and Fig. C.2.



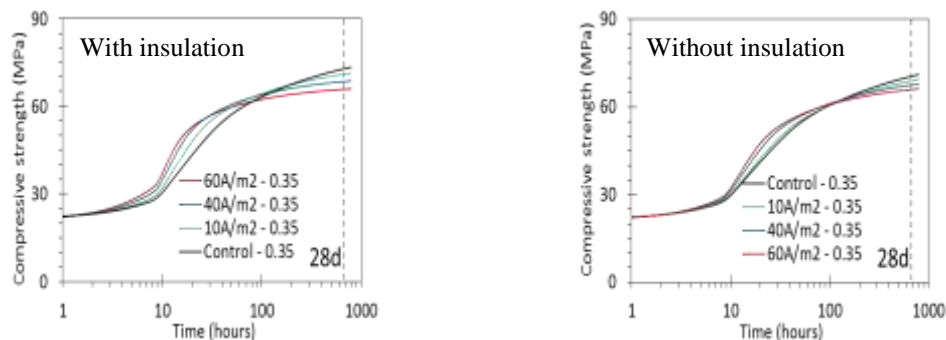
- a. Temperature development in the *centre* of hardening concrete *with* (left) and *without* (right) insulation for wall thickness 40 cm.



- b. Degree of hydration in the *centre* of hardening concrete *with* (left) and *without* (right) insulation for wall thickness 40 cm.

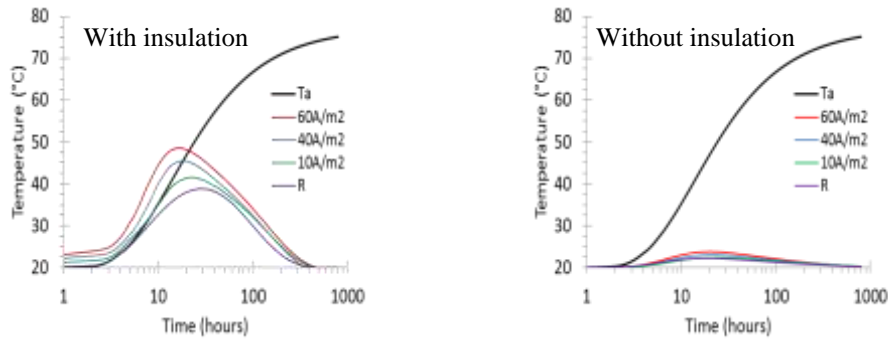


- c. Capillary porosity in the *centre* of hardening concrete *with* (left) and *without* (right) insulation for wall thickness 40 cm.

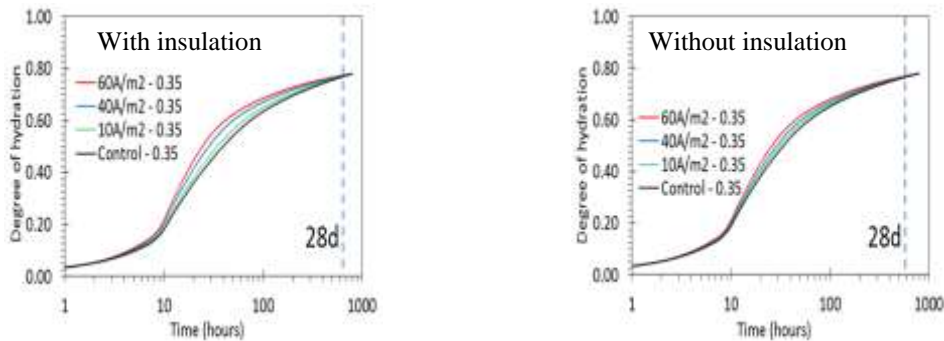


- d. Compressive strength in the *centre* of hardening concrete *with* (left) and *without* (right) insulation for wall thickness 40 cm.

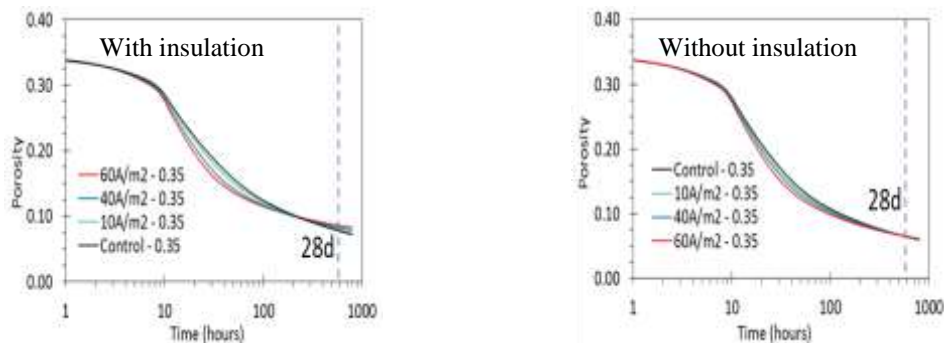
Fig. 5.26 Temperature development (a), degree of hydration (b), capillary porosity (c) and compressive strength (d) in the *centre* of hardening concrete *with and without insulation* for wall thickness 40cm and w/c ratio 0.35.



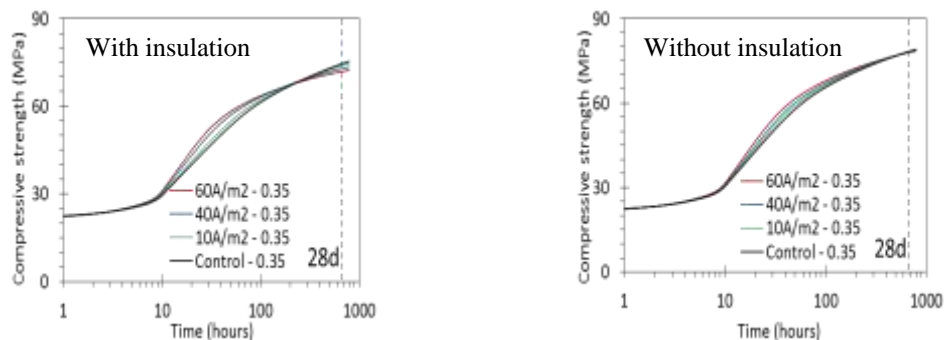
a. Temperature development in the *outer zone* of hardening concrete with (left) and *without* (right) insulation for wall thickness 40 cm.



b. Degree of hydration in the *outer zone* of hardening concrete with (left) and *without* (right) insulation for wall thickness 40 cm.



c. Capillary porosity in the *outer zone* of hardening concrete with (left) and *without* (right) insulation for wall thickness 40 cm.



d. Compressive strength in the *outer zone* of hardening concrete with (left) and *without* (right) insulation for wall thickness 40 cm.

Fig. 5.27 Temperature development (a), degree of hydration (b), capillary porosity (c) and compressive strength (d) in the *outer zone* of hardening concrete *with and without insulation* for wall thickness 40cm and w/c ratio 0.35.

## 5.6.2 Simulated effect of stray current on concrete outer zone

### 5.6.2.1 Effect of stray current on capillary porosity in the outer zone of concrete walls with and without insulation after 28 days hydration (outside temperature 20°C)

The effect of the insulation on the temperatures in the outer zone of a 40 cm thick concrete wall has been shown already in Fig. 5.25b. In this section the focus is on the concrete in the *outer* zone of concrete wall with different thicknesses. The outer zone is the most critical zone in view of durability.

The maximum temperature in the outer zone of hardening concrete walls with and without insulation is shown in Fig. 5.28. In case insulation is present, the temperature in the surface zones will increase with increasing wall thickness and increasing stray current. Note that in Fig. 5.28 only the maximum temperatures are presented. From this figure, it cannot be inferred how the degree of hydration and associated porosity develop with time.

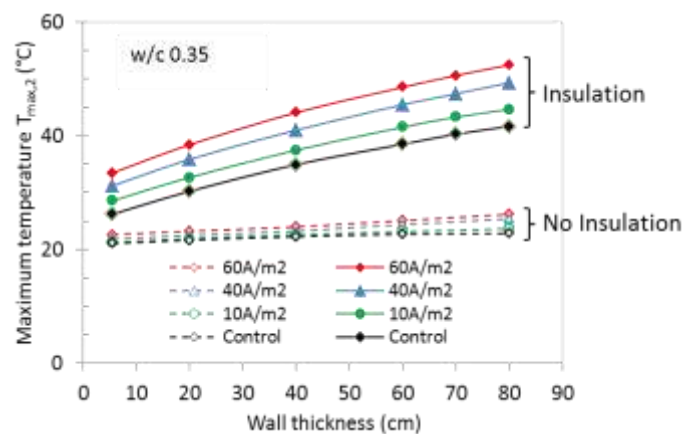


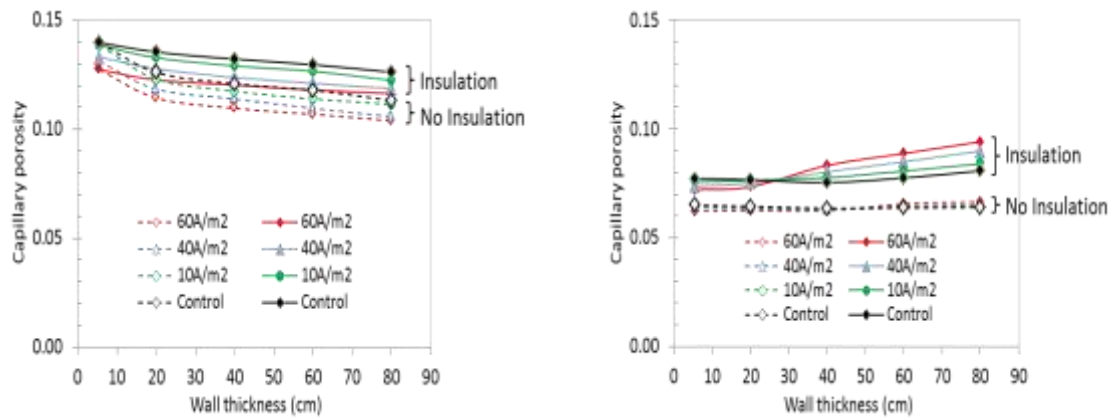
Fig. 5.28 Maximum temperature ( $T_{max,2}$ ) in outer zone of hardening concrete walls with and without insulation as a function of wall thickness for different magnitude of the stray current.

5

Since the hydration processes proceed at different temperatures and at different rates and since the porosity is affected by the reaction temperatures, the evolution of the porosity is not a linear function of time. This is further illustrated with Fig. 5.29a,b, where the evolution of the capillary porosity in the outer zone of the wall is presented after 3 days and 28 days, respectively, as function of the wall thickness. No significant change of capillary porosity in the outer zone of concrete walls without insulation was noticed, irrespective of the presence of stray current. In general, the capillary porosity in the outer zone of concrete walls without insulation was lower compared to that in the outer zone of concrete walls with insulation (see Fig. 5.29).

Fig. 5.29a clearly shows the effect of stray current on the evolution of the capillary porosity. Up to three days, hydration at higher temperatures results in faster hydration and hence a lower capillary porosity. After 28 days hydration at elevated temperatures the situation is different, as can be seen in Fig. 5.29b. Now the effect of coarsening of the capillary porosity due to hydration at higher temperatures is dominant. The thicker the walls, the higher the reaction temperatures and the coarser the capillary pore

structure. In thin walls the temperature had not reached high values and coarsening of the pore structure was hardly noticeable.



- Calculated capillary porosity of cement paste (eq. (5.19)) after 3 days of hydration in outer zone of hardening concrete walls with and without insulation as a function of wall thickness.
- Calculated capillary porosity of cement paste (eq. (5.19)) after 28 days of hydration in outer zone of hardening concrete walls with and without insulation as a function of wall thickness.

Fig. 5.29 Calculated capillary porosity of cement paste (eq. (5.19)) in outer zone of concrete walls *with* and *without insulation* subjected to stray current for different wall thickness after 3 days (a) and 28 days (b) hydration. Concrete mixture: cement content  $400 \text{ kg/m}^3$ , aggregate content 70%, w/c ratio 0.35.

### 5.6.2.2 The effect of stray current on apparent diffusion coefficients in outer zones of concrete walls with and without insulation, after saturation with water

In this section the apparent diffusion coefficient in outer zones of concrete with and without insulation and subjected to stray current is presented. The background of the calculations is an exposure scenario real concrete structures might experience in the practice. At first the concrete is supposed to harden in more or less *sealed* condition. This is the situation that is also considered in the numerical simulations executed so far. The chloride diffusion coefficients, however, are normally determined in a chloride migration tests performed on *saturated* concretes. It is now assumed that structures, being curing under sealed condition for 28 days, will be exposed to water and become saturated after 28 days. Then, the apparent diffusion coefficient of the concrete in saturated condition can be calculated with eq. (5.21).

Fig. 5.30 shows an example of calculated apparent diffusion coefficient  $D_a$  ( $\text{m}^2/\text{s}$ ) in the outer zone of a 40 cm thick hardening concrete wall as a function of time. The figure shows that the apparent diffusion coefficient in the outer zone of the concrete wall *with* insulation is higher compared to the apparent diffusion coefficient in outer zone of a wall *without* insulation. In case insulation is present, stray current accelerates the hydration process at early ages. This will result in a lower capillary porosity and a corresponding lower apparent diffusion coefficient.

In the Fig. 5.31a,b the apparent diffusion coefficient of concrete with w/c ratio 0.35 is presented after 3 and 28 days hydration, respectively, as a function of the wall thickness. The curves showing the diffusion coefficients show similar trends as those

for the capillary porosity shown in Fig. 5.29a,b (which is evident from eq. (5.21)).

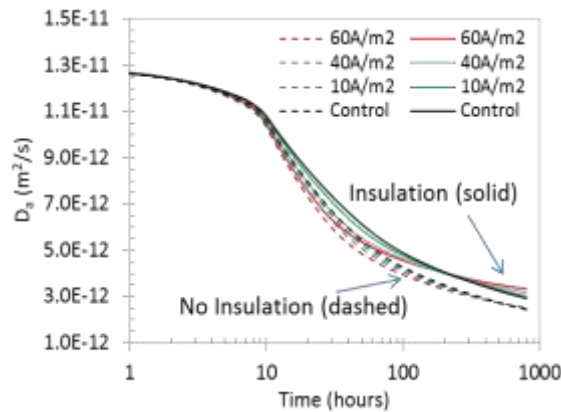
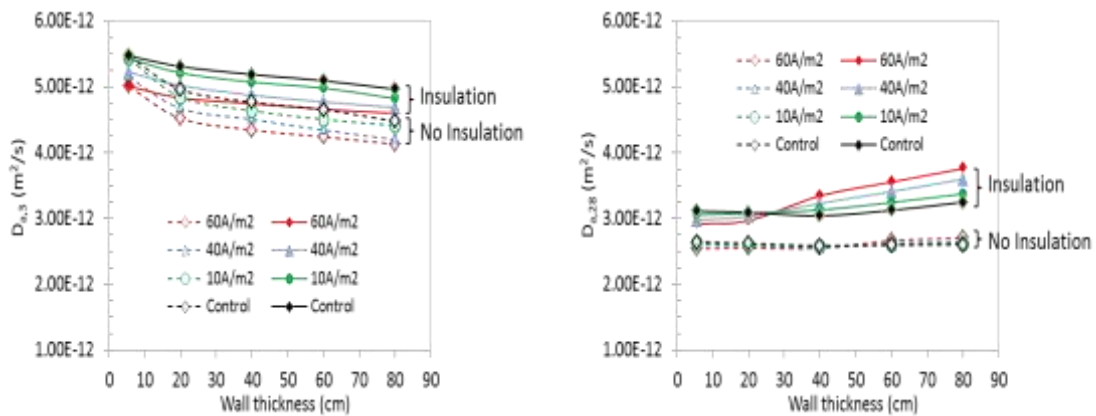


Fig. 5.30 Apparent diffusion coefficient in outer zone of a 40 cm thick hardening concrete wall with and without insulation for different values of the stray current as a function of time.



- a. Apparent diffusion coefficient in outer zone of hardening concrete with and without insulation for different wall thickness after 3 days of hydration.
- b. Apparent diffusion coefficient in outer zone of hardening concrete with and without insulation for different wall thickness after 28 days of hydration.

Fig. 5.31 Apparent diffusion coefficients in outer zones of concrete walls *with* and *without* insulation for different wall thickness after 3 days (a) and 28 days (b) of hydration calculated with eq. (5.21). After 28 days hydration the concrete specimen is saturated with water. Concrete mixture: cement content 400 kg/m<sup>3</sup>, aggregate content 70%, w/c ratio 0.35.

Fig. 5.31b shows hardly any effect of stray current on the 28-days diffusion coefficients outer zone of hardening concrete *without* insulation. In case insulation is present hydration will proceed faster. For wall thicknesses up to 20 cm faster hydration caused by stray current results in lower apparent diffusion coefficients (Fig. 5.31b). In walls thicker than 20 cm the presence of stray current results in higher reaction temperatures and coarsening of the capillary pore structure, resulting in higher diffusion coefficients in concrete walls with insulation (see Fig. 5.31b), which will affect the service life of concrete structures.

## 5.7 Conclusions

This chapter dealt with the influence of stray current flow on the hydration process and the resulting temperature and porosity development in cement-based materials and concrete structures. The experimental results were accompanied by numerical simulations in order to analyse possible positive and/or negative effects of stray current. The following conclusions can be drawn:

1. Experimental results show that due to stray current induced Joule heating the hydration process was accelerated. The effects of stray current on temperature fields and porosity in hardening concrete structures can be simulated quite accurately with the finite element analysis software COMSOL Multiphysics V 5.4.
2. The most significant effect of stray current on capillary porosity and apparent diffusion coefficient occurs in the interior of concrete elements, where the highest temperatures are reached. Coarsening of the capillary pore structure in the centre of concrete elements with and without insulation due to Joule heating can affect material properties: a) lower mechanical properties (e.g. compressive strength) and b) increased apparent diffusion coefficient. More pronounced effects of stray current on capillary porosity, compressive strength and diffusion coefficient in the centre of concrete with insulation was noticed compared to concrete without insulation. A higher porosity in the centre of concrete structures, however, will generally not affect the service life of concrete structures.
3. Hardly any effect of stray current on capillary porosity and associated diffusion coefficient was noticed in the outer zone of hardening concrete without insulation. In case *insulation* is present, capillary porosity in *the outer zone of concrete elements* increases due to hydration at higher temperature, resulting in a higher diffusion coefficient (which is negative for the durability).
4. The temperature in the outer zones of insulated concrete increases with increasing wall thickness and stray current levels (Fig. 5.28). Higher temperatures at early ages (e.g. 3 days) in the outer zones of insulated concrete results in faster hydration and hence a lower capillary porosity (Fig. 5.29a) and diffusion coefficient (Fig. 5.30 and Fig. 5.31a). At later ages (>28 days), coarsening of the capillary porosity due to hydration at higher temperature will result in a higher diffusion coefficient (Fig. 5.31b). The thicker the walls, the higher the reaction temperatures and the coarser the capillary pore structure. In thin walls ( $\leq 30$  cm), stray current up to  $60\text{A/m}^2$  hardly induced coarsening of the pore structure, since temperature rise in the outer zones of insulated concrete had not reached high values.



# 6

## **The effect of stray current flow on material properties of hardened mortar specimens\***

This chapter presents the effect of stray current flow on materials properties of mortar specimens after 28-days hardening in a fog-room with 98% RH. The combined effects of water-to-cement ratio, curing age, different external environment and stray current on the microstructural (porosity and pore size), electrical (resistivity) and mechanical (compressive strength) properties of hardened cement-based materials were investigated. The evolution of the porosity and pore size distribution of mortar specimens subjected to stray current was assessed by correlating the performance of 28-days cured mortar in a fog-room of 98% RH with that of young (24h-cured only) mortar specimens in the same environmental condition. Three different levels of electrical current density (i.e. 10mA/m<sup>2</sup>, 100mA/m<sup>2</sup> and 1A/m<sup>2</sup>) were applied to simulate stray current flow through hardened mortar specimens with water-to-cement ratio of 0.5 and 0.35. Different environmental conditions were employed, i.e. sealed conditions, partly submerged and fully submerged in water and calcium hydroxide medium. Microstructural, mechanical and electrical properties were monitored in the course of 140 days.

---

\*) This chapter is based on:

1. Susanto, A., Koleva, D. & van Breugel, K. (2017). The Effect of Water-to-Cement Ratio and Curing on Material Properties of Mortar Specimens in Stray Current Conditions, *Journal of Advanced Concrete Technology*. 15, 10, p. 627-643.

## 6.1 Introduction

From the cement chemistry point of view, hydration is the reaction of cement with water, resulting in setting and hardening of the hydrated cement paste. The term ‘setting’ means a rather sudden loss of plasticity of the original paste and its conversion into a solid material with a barely measurable strength. The term ‘hardening’ refers to the development of hardness and strength that follows the setting phase (Hewlett 2003). For complete hydration, cement must be mixed with a sufficient amount of water, commonly represented by the water-to-cement ratio, i.e. 0.4 (Powers et al. 1947, Young et al. 1986).

In this chapter, fresh and hardened concrete will be dealt with. Fresh concrete is the stage when setting and hardening did not start yet. The properties of fresh and hardened concrete mainly depend on the curing conditions after casting and during hydration. Curing is the process of controlling the external temperature and moisture after casting and during hydration. Proper curing plays an important role to obtain the designed strength and maximum concrete durability (James et al. 2002). In addition, improper curing results in undesired effects, such as lower strength, cracking, low resistance to weathering, high permeability, dusting (Neville 1995, ACI 1981, ACI 1982, Samir et al. 1988). The influence of the type of curing is significant at early ages. Since strength development of concrete occurs most rapidly at early age, the greatest benefit from curing is achieved during this period (Troxell et al. 1968). The required duration of curing depends on several factors, such as mixture proportions, specified strength, size and shape of the concrete element, environmental and exposure conditions (IS 2000). Traditionally, 28 days curing is required for cement-based materials, resulting in properties (both mechanical and microstructural), sufficiently developed for the required performance.

While measures can be taken for optimum curing on site, the hydration process and concrete hardening, respectively, can be affected by a variety of external factors. Although some of these, as the above mentioned optimum humidity of concrete, can be controlled, others are unpredictable and cannot be easily controlled. Such an effect of external environment, that is hard to control in practical applications, is stray current in the vicinity of newly built structures (or freshly poured concrete mixtures on site). The intensity of stray current strongly depends on the resistivity of the medium, where stray current would flow. Of equal significance is the speed of stray current “discharge” or “dissipation” from a conductive path (e.g. steel reinforcement).

One of the main consequences of stray current, especially for a fresh cement-based material, concern the effect on water (Probstein 2003, Lyklema 1995) and ion transport in the matrix. In an electrical field, ion and water migration will add-up to the internal diffusion-controlled mechanisms of cement hydration, which will change the hydration process. While migration can be positive at very early stages of the bulk matrix development, e.g. resulting in the so-called “electrical curing” (Bredenkamp *et al.* 1993), it can also be detrimental. The negative effect of stray current will be pronounced when concentration gradients are present. The result will be enhanced alkali ions leaching-out and pore network coarsening, both during and after hardening of the still young concrete matrix, but also later on (Susanto *et al.* 2017). In case the concrete structures are located close to the stray current sources, the possible effect of stray currents should be considered. Additionally, the age of cement-based materials at which

stray currents affect and/or induce ion and water migration will determine the level of these positive or negative effects.

The aim of this chapter was to investigate the joint effect of water-to-cement ratio, curing conditions, different external environment on the properties of already hardened mortar specimens, initially cured for 28 days while subjected to stray current. The results were correlated and compared with those for young (24h-cured) mortar specimens. With regard to the long-term behaviour of cement-based materials in conditions of stray current, the ageing factors and apparent diffusion coefficients were derived, based on experimentally recorded electrical resistivity development. The outcomes were compared to the relevant control cases and serve the purpose of evaluating the overall performance of cement-based materials, when ion and water migration contribute to diffusion-controlled transport mechanisms.

## 6.2 Materials and experimental methods

### 6.2.1 Materials

Mortar cubes of  $40 \times 40 \times 40$  mm<sup>3</sup> were cast, using OPC CEM I 42.5N with w/c ratio of 0.5 and 0.35. The cement-to-sand ratio used was 1:3. The chemical composition (in wt. %) of CEM I 42.5N (ENCI, NL) is as follows: 63.9% CaO; 20.6% SiO<sub>2</sub>; 5.01% Al<sub>2</sub>O<sub>3</sub>; 3.25% Fe<sub>2</sub>O<sub>3</sub>; 2.68% SO<sub>3</sub>; 0.65% K<sub>2</sub>O; 0.3% Na<sub>2</sub>O. After casting and prior to conditioning, the specimens were cured in a fog-room with 98% RH, at  $20 \pm 2^\circ\text{C}$  for 28 days.

### 6.2.2 Sample designation, current regimes and conditioning

The 28-day cured mortar specimens were cast in two main groups, i.e. specimen with w/c ratio 0.35 and 0.5. These two groups were divided into four sub-groups:

- 1) control group - no current involved
- 2) group "10 mA/m<sup>2</sup>"
- 3) group "100 mA/m<sup>2</sup>"
- 4) group "1 A/m<sup>2</sup>"

where DC current was applied at the indicated current levels. The samples designation (and relevant external medium) is given in Table 6.1.

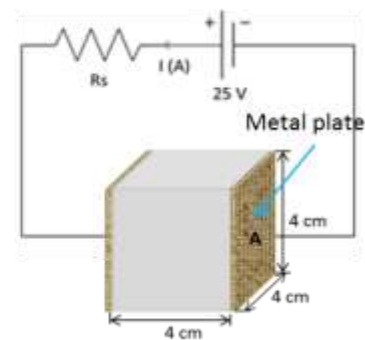
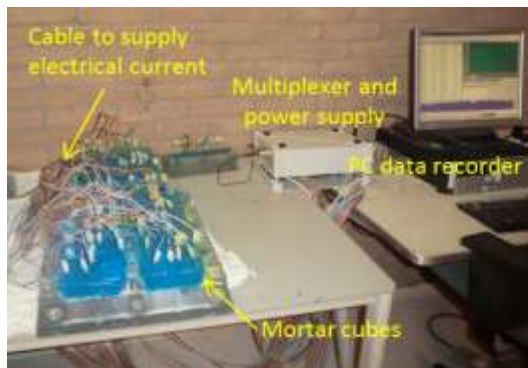
Concrete structures exposed to the atmosphere are scarcely saturated. Even for concrete submerged in water (underwater concrete), only the outer part of concrete will become saturated, while the interior part is unsaturated. Although the properties of unsaturated cement-based materials differ from those of sealed and fully saturated materials, these properties are not well-documented (because of experimental constraints). Considering these aspects, the experiments in this study were conducted in two extreme conditions, i.e. submerged/saturated and sealed conditions. In addition, experiments were also conducted in partly (half) submerged condition. This partly submerged condition was meant to mimic the real practice in which the concrete is neither completely saturated nor sealed (Zhang 2018).

Besides different exposure conditions, specimens were exposed to water and Ca(OH)<sub>2</sub> solution. The Ca(OH)<sub>2</sub> solution was used to minimize or avoid concentration gradient (i.e. alkali ions leaching-out is avoided) between mortar specimen and the

external environment. Sample designation 28d refers to mortar of w/c ratio 0.5, cured for 28 days and conditioned for 140 days.

Table 6.1 Sample designation and experimental conditions

| Specimens groups     | Sample designation   | Experimental conditions |                     |                  |                     |        |
|----------------------|--|-------------------------|---------------------|------------------|---------------------|--------|
|                      |  | Half submerged          |                     | Fully submerged  |                     | Sealed |
|                      |  | H <sub>2</sub> O        | Ca(OH) <sub>2</sub> | H <sub>2</sub> O | Ca(OH) <sub>2</sub> |        |
| Control              | R1/2,H <sub>2</sub> O, 28d<br>(Control-1/2 H <sub>2</sub> O,28d)           | ×                       |                     |                  |                     |        |
|                      | R1/2,H <sub>2</sub> O, 28d<br>(Control-1/2 CH,28d)                         |                         | ×                   |                  |                     |        |
|                      | R full, H <sub>2</sub> O, 28d  |                         |                     | ×                |                     |        |
|                      | R full, CH, 28d  |                         |                     |                  | ×                   |        |
|                      | R sealed, 28d  |                         |                     |                  |                     | ×      |
| 10mA/m <sup>2</sup>  | 10mA,H <sub>2</sub> O, 28d<br>(10mA/m <sup>2</sup> -H <sub>2</sub> O,28d)  | ×                       |                     |                  |                     |        |
|                      | 10mA,CH, 28d<br>(10mA/m <sup>2</sup> -CH,28d)                              |                         | ×                   |                  |                     |        |
| 100mA/m <sup>2</sup> | 100mA,H <sub>2</sub> O,28d<br>(100mA/m <sup>2</sup> -H <sub>2</sub> O,28d) |                         |                     | ×                |                     |        |
|                      | 100mA,CH, 28d<br>(100mA/m <sup>2</sup> -CH,28d)                            |                         |                     |                  | ×                   |        |
|                      | 100mA sealed, 28d  |                         |                     |                  |                     | ×      |
| 1A/m <sup>2</sup>    | 1A,H <sub>2</sub> O, 28d<br>(1A/m <sup>2</sup> -H <sub>2</sub> O,28d)      |                         |                     | ×                |                     |        |
|                      | 1A,CH, 28d<br>(1A/m <sup>2</sup> -CH,28d)                                  |                         |                     |                  | ×                   |        |
|                      | 1A sealed, 28d   |                         |                     |                  |                     | ×      |



a. Experimental set up of mortar specimens in sealed condition subjected to stray current

b. Schematic of stray current flow through mortar specimen in sealed condition.

Fig. 6.1 a) Experimental set-up for mortar specimens subjected to stray current in sealed condition with multiplexer and PC data recorder to record electrical resistance; b) Schematic of electrical circuit, where  $R_s$  is the resistor to adjust electrical current flow through the mortar specimen.

After demoulding, the current regimes were applied through external (DC) current sources. The experimental set-up for the 28 days cured specimens is presented in Fig. 6.1a. Schematic of stray current flow through mortar specimen in sealed condition is

given in Fig. 6.1b. For partly submerged (refers to splash zone in real practice) and fully submerged conditions the specimens were positioned in water or  $\text{Ca}(\text{OH})_2$  solution and the current was applied via external conductors (metal plates), following previously reported set-up (Susanto *et al.* 2013, Susanto *et al.* 2017). For sealed condition (Fig. 6.1a), electrical connections were made to apply electrical current through initially cast-in electrodes (brass mesh plates) on the two opposite sides of each cube. The electrodes also served the purpose of measuring electrical resistivity.

### 6.2.3 Experimental methods

#### 6.2.3.1 Standard compressive strength

Standard compressive strength tests were performed on the  $40 \times 40 \times 40$  mm<sup>3</sup> three replicates mortar specimens at the hydration age of 28 days and later on after 31, 42, 84, 112 and 140 days of age. The compressive strength tests were performed within a 5 minutes time interval.

#### 6.2.3.2 Mercury intrusion porosimetry (MIP)

MIP tests were performed to determine the porosity and pore size distribution of the bulk matrix according to standard sample preparation and measurement procedures, as reported in detail in Appendix A.

#### 6.2.3.3 Electrical resistivity measurements

The electrical resistivity measurement of mortar specimens is done in the same manner as previously reported in Section 3.3.3.2, Chapter 3.

## 6.3 Results and discussion

### 6.3.1 Compressive strength of hardened (28 day-cured) mortar specimens

Mechanical properties are often used as key indicator for the performance of cement-based materials, reflecting concrete quality. A high compressive strength is generally associated with a low capillary porosity. Low capillary porosity reduces/prevents chloride ingress into concrete. There are several factors that affect the strength of cement-based materials, such as: water/cement ratio, cement type, admixtures and curing conditions, including humidity, temperature and time (Mehta *et al.* 2001, Nehdi *et al.* 2011). Compressive strength tests were performed to quantify the influence of stray current flow on the mechanical properties of 28-day cured mortar specimens with different w/c ratio (i.e. 0.5 and 0.35), subsequently conditioned in different external media and conditions (i.e.  $\text{H}_2\text{O}$  submerged,  $\text{Ca}(\text{OH})_2$  submerged and sealed).

As can be observed in Fig. 6.2(a) to Fig. 6.2(d), irrespective of external medium, as well as irrespective of w/c ratio, the compressive strength for all specimens increased with time. This was as expected and consistent with the ongoing cement hydration. The increase in compressive strength for the water-submerged control specimens (designation control  $\text{H}_2\text{O}$  in Fig. 6.2), was in the range of 11.5% to 13.8% higher for the group of lower w/c ratio 0.35, compared to those of w/c ratio 0.5. Higher compressive

strength was recorded for the control specimens conditioned in calcium hydroxide (specimens with designation *Control – 1/2 CH* in Fig. 6.2(a,c) and *Control – CH* in Fig. 6.2(b,d), compared to all analogical cases in water. This result was also expected, since in the absence of a concentration gradient between pore solution in mortar specimen and water, leaching-out is largely prevented. Hence mechanical and microstructural properties are expected to improve due to densification of bulk matrix.

The largest effect of stray current on compressive strength was noticed in specimen with the highest current density level (i.e.  $1 \text{ A/m}^2$ ) for specimens with both w/c 0.35 and 0.5. At a current density of  $1 \text{ A/m}^2$ , the lowest compressive strength was recorded for specimens submerged in water Fig. 6.2(b,d), while the highest strength was recorded for specimens submerged in calcium hydroxide solution Fig. 6.2(b,d). For specimens partly submerged in calcium hydroxide solution (Fig. 6.2), only a positive effect (increased compressive strength) was recorded for specimens “under current”. For the water-conditioned groups, a reverse trend was observed.

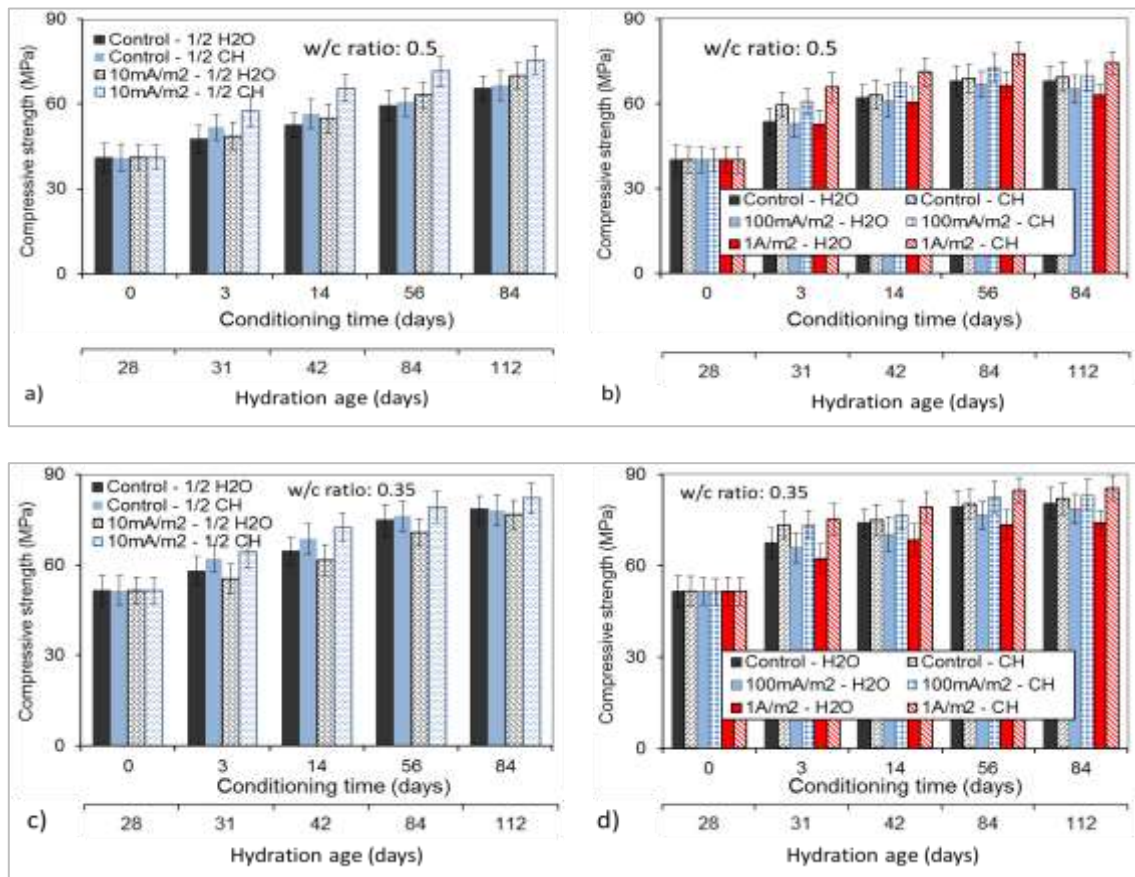


Fig. 6.2 Compressive strength of mortar specimens  $40 \times 40 \times 40 \text{ mm}^3$  cured for 28 days with conditioning time from 0 to 84 days (hydration age of 28 to 112 days) in partly (a, c) and fully (b, d) submerged in  $\text{H}_2\text{O}$  and  $\text{Ca}(\text{OH})_2$  conditions. The w/c ratios used were 0.5 and 0.35. The electrical current was applied from 28 days of hydration onwards i.e. immediately after de-moulding of the specimens.

Figure 6.3 depicts a comparison of compressive strength of 28 days-cured mortar specimens with w/c ratio 0.35 and 0.5, partly (a) and fully (b) submerged in  $\text{H}_2\text{O}$  with

conditioning from 0 to 84 days (Fig. 6.3a,b). At hydration age of 28 days (or conditioning time “0” days), the compressive strength for all cases was almost identical. For the specimens *partly submerged in water*, with the lowest stray current of 10 mA/m<sup>2</sup>, the specimens with w/c ratio 0.35 (Fig. 6.3a) presented a more pronounced reduction in compressive strength than the mortar with w/c ratio 0.5 (Fig. 6.3a). At 112 days, however, there was no significant difference between these groups of specimens. Both showed a compressive strength decrease of about 4 MPa, compared to the relevant control cases.

For mortar specimens fully submerged in water with w/c ratio 0.5 and current density of 100mA/m<sup>2</sup> and 1A/m<sup>2</sup>, improvement of properties at initial stages 0-3 days was noticed (Fig. 6.3b). With age, a reduction in strength was observed. This reduction was more pronounced for the specimens with w/c ratio 0.35 (Fig. 6.3b, middle section of the plot). At 112 days of hydration, a small reduction of the compressive strength at current density 1A/m<sup>2</sup> by 5 and 6 MPa for w/c ratios 0.5 and 0.35 respectively compared to control specimen was observed (Fig. 6.3b).

The most significant effect of stray current was observed in specimens subjected to the highest current density level of 1A/m<sup>2</sup> and w/c ratio of 0.35. Obviously a lower w/c ratio accelerated the negative effect of stray current in aged specimens, 112 days of hydration. Although the difference as such (in absolute values) is not significant on a global scale, the trend clearly shows that stray current affects a mature matrix with lower pore water volume, to a larger extent than mixture with w/c ratio of 0.5.

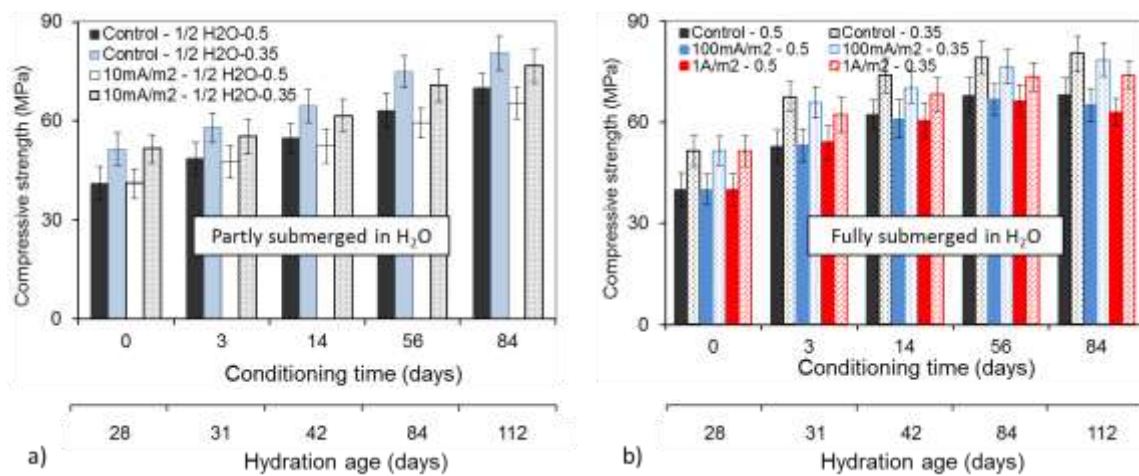


Fig. 6.3 Evolution of compressive strength of mortar specimens with w/c ratios 0.5 and 0.35 partly (a) and fully (b) submerged in H<sub>2</sub>O after 28 days.

The effect of leaching-out due to enhanced migration in conditions of stray current and concentration gradients with the surrounding medium can be visualized better if the results for compressive strength of water-conditioned specimens are compared to results for sealed specimens. The evolution of compressive strength for sealed and submerged mortar specimens of w/c ratios 0.5 and 0.35, at identical hydration ages in control and under current regimes of 1 A/m<sup>2</sup>, is depicted in Fig. 6.4. As expected, the effect of ion/water migration on mechanical properties is observed in mortar specimens fully submerged in water (Fig. 6.3b, specimens "Control and 1A/m<sup>2</sup>" at both w/c 0.35 and

0.5), reflected in lower compressive strength with time due to stray current. The negative effect (reduction in compressive strength) after 56 days exposures (conditioning time) is more evident for the lower w/c ratio in fully submerged conditions (Fig. 6.4b). In contrast, the compressive strength in sealed conditions was higher compared to mortar specimens fully submerged in water. The positive effect in sealed conditions is more evident at higher w/c ratio (Fig. 6.4a). The results on mechanical performance for all specimens and conditions are fully supported by microstructural investigation and results on development of the bulk matrix in time, which will be discussed in the next sections.

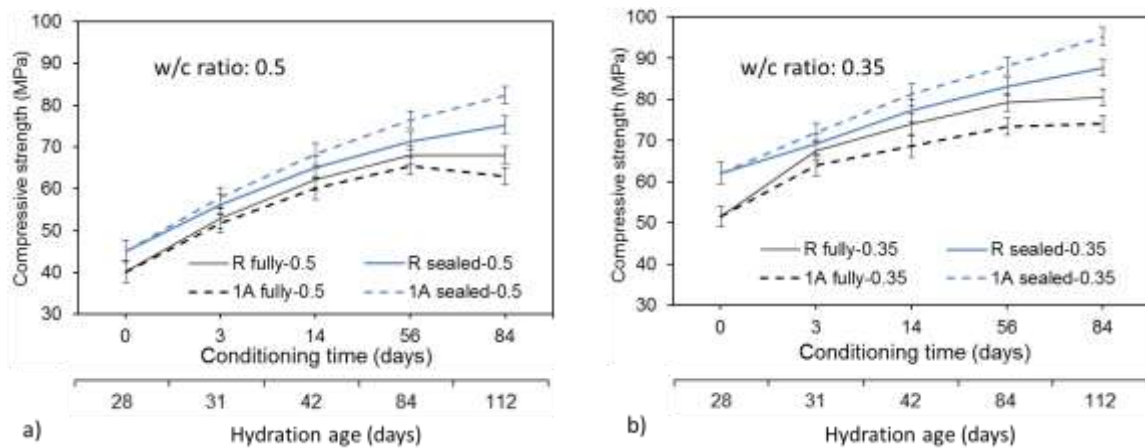


Fig. 6.4 Comparison of compressive strength development of 28-days cured mortar specimens fully submerged in water and in sealed conditions with w/c ratio 0.5 (a) and w/c 0.35 (b).

### 6.3.2 The effect of curing and stray current on pore structure (identical w/c ratio 0.5, different curing time i.e. 24h and 28 days)

MIP tests were performed to quantify the simultaneous effect of curing age, w/c ratio and stray current flow on the microstructural changes of mortar specimens. The complete study on 24h cured specimens of w/c ratio 0.5 for all conditions and stray current regimes have already been reported (Susanto *et al.* 2017). The results at the first and final tested time intervals for the 24h cured specimens are only partly discussed here in comparison to 28 days cured mortar, for comparative purposes and to elucidate the effect of curing on pore network development.

The actual MIP results for all specimens subject to discussion in the following sections 6.3.2.1, 6.3.2.2 and 6.3.3 are presented for the hydration age of 112 days (Figs. 6.5, 6.8, 6.11, 6.13). For an easy comparison (in view of the large amount of recorded MIP data), the full range of MIP results for all discussed specimens are summarized and discussed with relevance to Figs. 6.6, 6.7, 6.9, 6.12, 6.14.

#### 6.3.2.1. Mortar specimens partly and fully submerged in water

The MIP results for partly and fully submerged water-conditioned specimens at hydration age of 112 days are shown in Fig. 6.5(a-d) as a comparison of: control and 10 mA/m<sup>2</sup> current regime of the 24h and 28 days old specimens (Fig. 6.5a,b) and control, 100 mA/m<sup>2</sup> and 1A/m<sup>2</sup> of 24h and 28 days old specimens (Fig. 6.5c,d).

Porosity and pore size (including critical pore size) were derived from MIP. Porosity was based on the cumulative intrusion vs pore size curves (Fig. 6.5a,c). The pore size distribution and critical pore size were based on the differential curves (Figs. 6.5b,d). As aforementioned, for the sake of simplicity and clear comparison the MIP results for the rest of the discussed hydration ages, together with the 112 days results, are summarized in Figures 6.6 and 6.7.

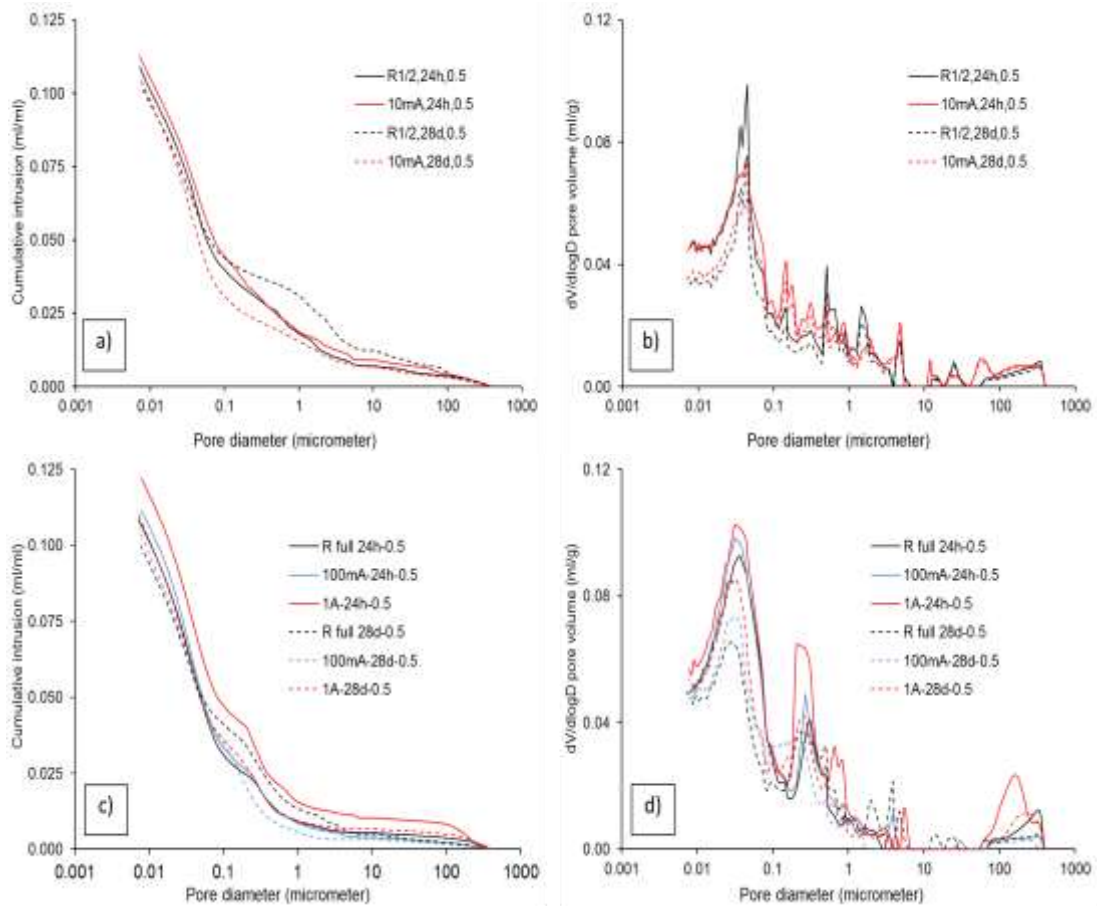


Fig. 6.5 MIP-derived porosity and pore size distribution at 112 days old specimens with w/c ratio 0.5 but different curing time intervals, i.e. cured for 24h and cured for 28 days: (a, b) partly submerged in water and 10 mA/m<sup>2</sup> regime (c, d) fully submerged in water, 100 mA/m<sup>2</sup> and 1A/m<sup>2</sup> regimes.

As previously commented, the microstructural properties of mortar are strongly affected by calcium ions leaching. This will occur when a concentration gradient with the surrounding medium is present, e.g. as for the mortar specimens in conditions of partly and fully submerged in water. The leaching-out process would be enhanced in conditions of stray current, which results from ion and water migration, together with diffusion-controlled ion and water transport. As can be seen from the results in Figs. 6.5 to 6.7, porosity increased with increasing stray current for both half (Fig. 6.5a,b and Fig. 6.6) and fully (Fig. 6.5c,d and Fig. 6.7) submerged in water specimens. This was relevant for both groups of mortar cured for 24h and cured for 28 days.

For specimens partly submerged in water after for 24h moist curing, *at hydration age of both 28 and 112 days* (Fig. 6.6), porosity increased with 0.64% at 28 days and ca. 1.35% at 112 days due to current flow at the level of 10 mA/m<sup>2</sup> (specimens 10mA, 24h), compared to control conditions (specimens R ½, 24h). For the 28 days-cured specimens, the difference in porosity due to stray current of 10 mA/m<sup>2</sup> in half-submerged in water conditions was not as significant at 112 days of age (Fig. 6.6). Increased critical pore size for the 10mA regime, compared to the control case was observed (Fig. 6.6, specimen 10 mA, 28d), hence coarsening of the matrix due to stray current was relevant. At the age of 140 days both porosity and pore size for the 28 days cured specimens maintained similar to those derived for 112 days (Fig. 6.6).

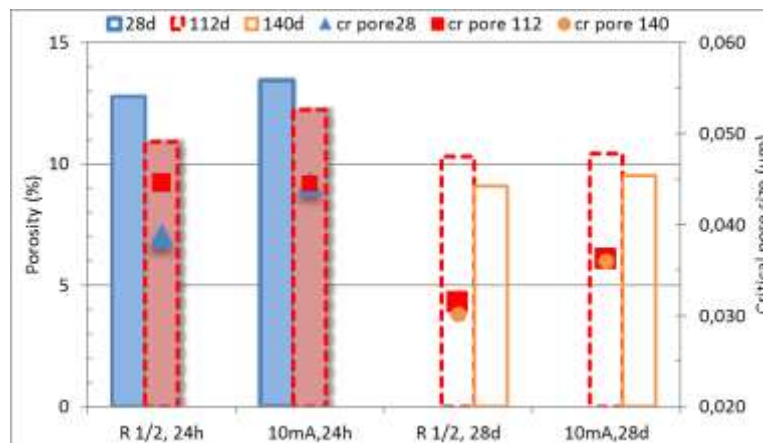


Fig. 6.6 Porosity (column; solid column for 24h cured) and critical pore size (symbol, “cr.pore” in legend) at hydration ages of 28 days, 112 days and 140 days for 24h and 28 days moist mortar with w/c ratio 0.5, half submerged in H<sub>2</sub>O. The plot presents a comparison of control cases (designation R for both 24h and 28d cured) and those, subjected to 10 mA stray current (designation 10 mA for both 24h and 28d cured).

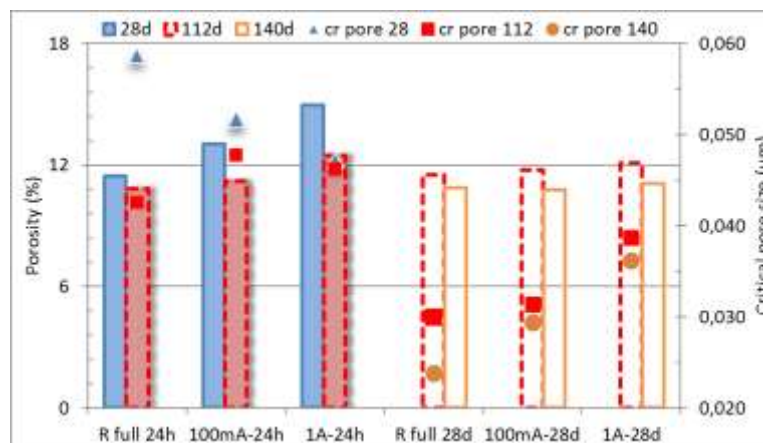


Fig. 6.7 Porosity (column; solid column for 24h cured) and critical pore size (symbol, “cr.pore” in legend) at hydration ages of 28 days, 112 days and 140 days for 24h and 28 days moist mortar of identical w/c ratio 0.5, fully submerged in H<sub>2</sub>O. The plot presents a comparison of control cases (designation R for both 24h and 28d cured) and those, subjected to 100 mA/m<sup>2</sup> and 1 A/m<sup>2</sup> stray current (designation 100mA and 1A for both 24h and 28d cured).

For fully submerged in water conditions and larger current densities (Fig. 6.7), the difference in recorded porosity and pore size values for the 28days-cured specimens at

84 days of conditioning (112 days of age) and 112 days of conditioning (140 days of age) was more obvious. The results showed a 1.4% increase for the 100 mA and 1.79 % increase for the 1A regime, compared to control conditions at 112 days of age and almost equal values at 140 days of age. A difference in critical pore size was also observed, similar to half-submerged conditions, where the highest critical pore size was relevant for the highest current density level of 1 A/m<sup>2</sup> (Fig. 6.7, specimen 1A-28d), corresponding to the higher porosity in this condition. If these results are compared to the derived values for 24h-cured specimens subjected to the same levels of stray current and considering identical hydration age of 112 days (Fig. 6.5c,d), a significantly different pore network development was observed for the 24h-cured groups (Fig. 6.5c,d and Fig. 6.7), where porosity increased significantly at 28 days, with variation of > 3% due to stray current. At the age of 112 days, the effect was less obvious, but still more pronounced compared to the 28 days-cured specimens i.e. 0.35% increase for the 100 mA and 1.65% increase for the 1A regime, compared to the control conditions in the 24h-cured series (Fig. 6.5c,d, Fig. 6.7). Critical pore size remained larger as well, if compared to that of the 28days-cured specimens at equal hydration age (e.g. 112 days, Fig. 6.7).

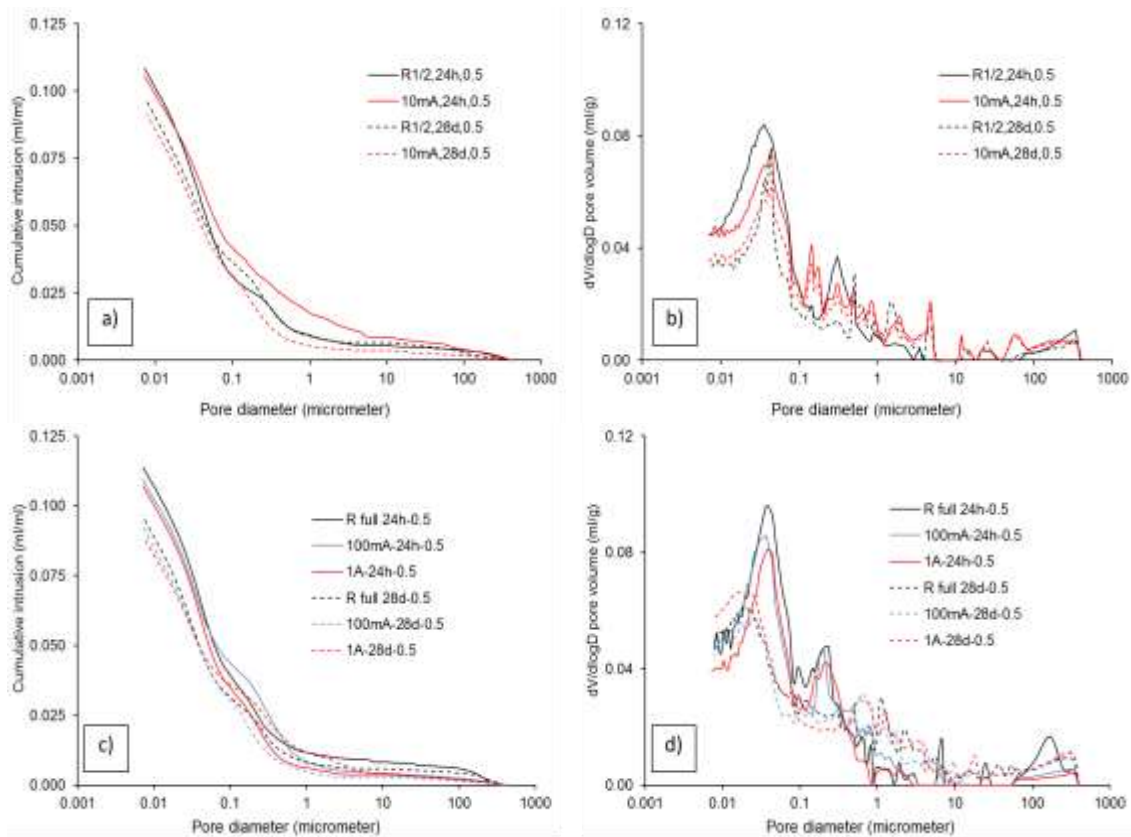
What can be stated is that *for equal w/c ratio* (0.5 in this case) the effect of stray current on bulk matrix microstructural properties is affected by the curing of the cement-based material i.e. 28 days curing results in less pronounced negative effect on porosity and pore size. In contrast, 24h curing only, equivalent to a fresh/young matrix on site in practical conditions, will be affected more significantly by stray current flow. This is linked to enhanced ion and water migration in the bulk matrix in fresh state, leading to leaching-out of alkali ions and matrix degradation (Susanto *et al.* 2013, Susanto *et al.* 2017), especially pronounced at early ages. In contrast, although negatively influenced as well, a more mature and adequately cured matrix of identical w/c ratio, would be less affected. This is at least to the level of stray current flow in the range of 10 mA to 1 A/m<sup>2</sup>, as applied in this chapter. This dependence, however, is not straightforward, as will be demonstrated in the following sections.

#### 6.3.2.2. Calcium hydroxide submerged conditions

The MIP results for 112 days hydration age for specimens conditioned in Ca(OH)<sub>2</sub> are presented in Fig. 6.8. The summarized results for all reported hydration ages, including 112 days of age, are depicted in Figs. 6.9 and 6.10. For half submerged in calcium hydroxide conditions, for the 28 days-cured groups at 112 days of conditioning (Fig. 6.8a)b), Fig. 6.9), 0.9% decrease in porosity was recorded due to current density of 10mA/m<sup>2</sup>, compared to the control specimens in this group. For fully submerged conditions in the same group (Fig. 6.8c,d, Fig. 6.10), the porosity decreased with 0.4 % and 0.6% for the current levels of 100mA/m<sup>2</sup> and 1A/m<sup>2</sup>, respectively. In contrast, for the 24 hours-cured specimens, at conditioning age of 28 days porosity decreased with ca. 1% for the 10mA regime, compared to control cases (Fig. 6.9). In the same 24h-cured group, for fully submerged in calcium hydroxide condition (Fig. 6.8c,d), porosity decreased with ca.1.5% and ca. 2% for 100mA/m<sup>2</sup> and 1A/m<sup>2</sup>, respectively (Fig. 6.10), compared to control conditions. In other words, for Ca(OH)<sub>2</sub>-conditioned specimens, irrespective of curing time and regime of conditioning, densification only of the bulk matrix was observed for all cases.

The effect of all current levels was in fact only positive, enhanced ion and water transport exerting raised cement hydration, which was more pronounced for the 24h-

cured group, because of the young mortar state. If the 28days-cured specimens are considered, elevated ion and water transport would be also at hand, judged by the lower porosity of the specimens as derived in all conditions, mostly pronounced for the highest current density level of  $1 \text{ A/m}^2$  (Figs. 6.8, 6.10). The as recorded porosity changes for 28 days-cured specimens at w/c ratio 0.5 and for all conditions (Figs. 6.5-10) are well in line with the recorded compressive strength development (Figs. 6.2 to 6.4). The strength of the mortar specimens increased with a decrease in porosity and vice versa, as also stated by other authors (Mehta *et al.* 2001, Roy *et al.* 1993, Lian *et al.* 2011).



6 Fig. 6.8 MIP-derived porosity and pore size distribution at 112 days of age for specimens of identical 0.5 w/c ratio but different curing time intervals i.e. 24h cured and 28 days cured specimens: (a, b) half-submerged in  $\text{Ca(OH)}_2$  control (R1/2) and  $10 \text{ mA/m}^2$  regime (10mA) (c, d) fully submerged in  $\text{Ca(OH)}_2$  control (Rfull),  $100 \text{ mA/m}^2$  (100 mA) and  $1 \text{ A/m}^2$  (1A) regimes (designation 24h and 28d refers to the respective curing time).

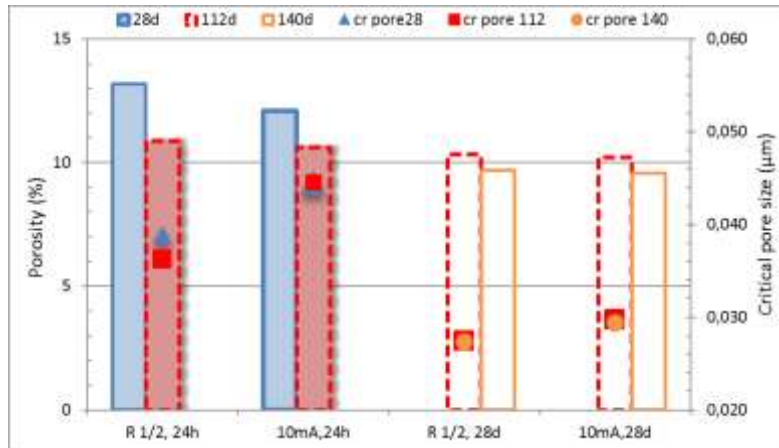


Fig. 6.9 Porosity (column; solid column for 24h cured) and critical pore size (symbol, “*cr.pore*” in legend) at hydration ages of 28 days, 112 days and 140 days for 24h and 28 days cured mortar of identical w/c ratio 0.5, half submerged in  $Ca(OH)_2$ . The plot presents a comparison of control cases (designation R for both 24h and 28d cured) and those, subjected to 10 mA stray current (designation 10 mA for both 24h and 28d cured).

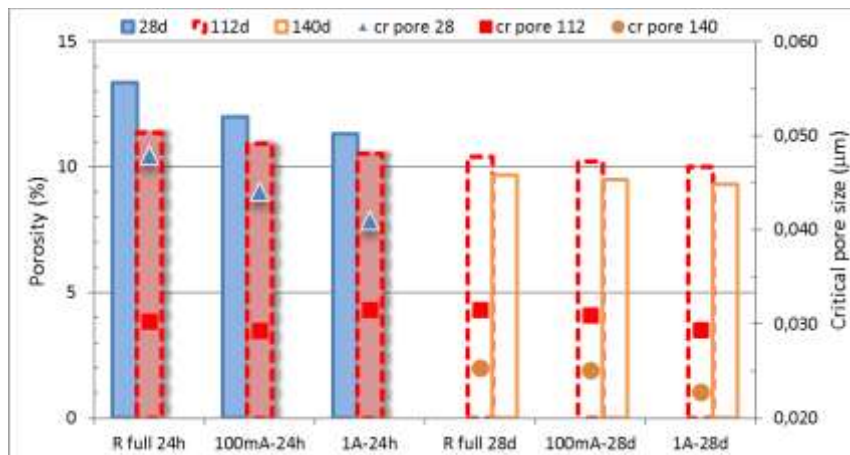


Fig. 6.10 Porosity (column; solid column for 24h cured) and critical pore size (symbol, “*cr.pore*” in legend) at hydration ages of 28 days, 112 days and 140 days for 24h and 28 days cured mortar of identical w/c ratio 0.5, fully submerged in  $Ca(OH)_2$ . The plot presents a comparison of control cases (designation R for both 24h and 28d cured) and those, subjected to 100 mA/m<sup>2</sup> and 1 A/m<sup>2</sup> stray current (designation 100mA and 1A for both 24h and 28d cured).

What can be concluded is that when curing conditions and stray current are judged in parallel for identical in w/c ratio specimens (identical mortar mixtures and identical external medium), the factor determining performance is the level of stray current. The curing conditions (24h or 28 days as in this case) are only important at early age and when concentration gradient with the surrounding medium is present (as in water conditions). With increased maturity of the cement matrix, the initially different curing conditions are not a decisive factor for the potentially negative effect of stray current, but rather the external medium and level of current will be decisive parameters. This is reflected by pore network coarsening of both 24h-cured and 28 days-cured water-conditioned specimens at hydration age of > 100 days and subjected to higher current density (> 100 mA/m<sup>2</sup> in this test).

### 6.3.3 The effect of w/c ratio (0.5 and 0.35) in stray current conditions on pore structure development of equally cured (hardened) bulk matrix (28 days-cured mortar)

Water-to-cement ratio has an important role for strength and durability of concrete. In general, higher w/c ratio results in an increase of capillary porosity (Sahu *et al.* 2004, Powers *et al.* 1958), subsequently reduced strength. Figures 6.11 and 6.13 show the MIP results for 28 days-cured mortar at the hydration age of 112 days for the specimens discussed in this section i.e. w/c ratio 0.35 and 0.5, water and Ca(OH)<sub>2</sub> submerged. Figures 6.12 and 6.14 depict the summarized information from MIP results for all discussed time intervals, including the 112 days of age.

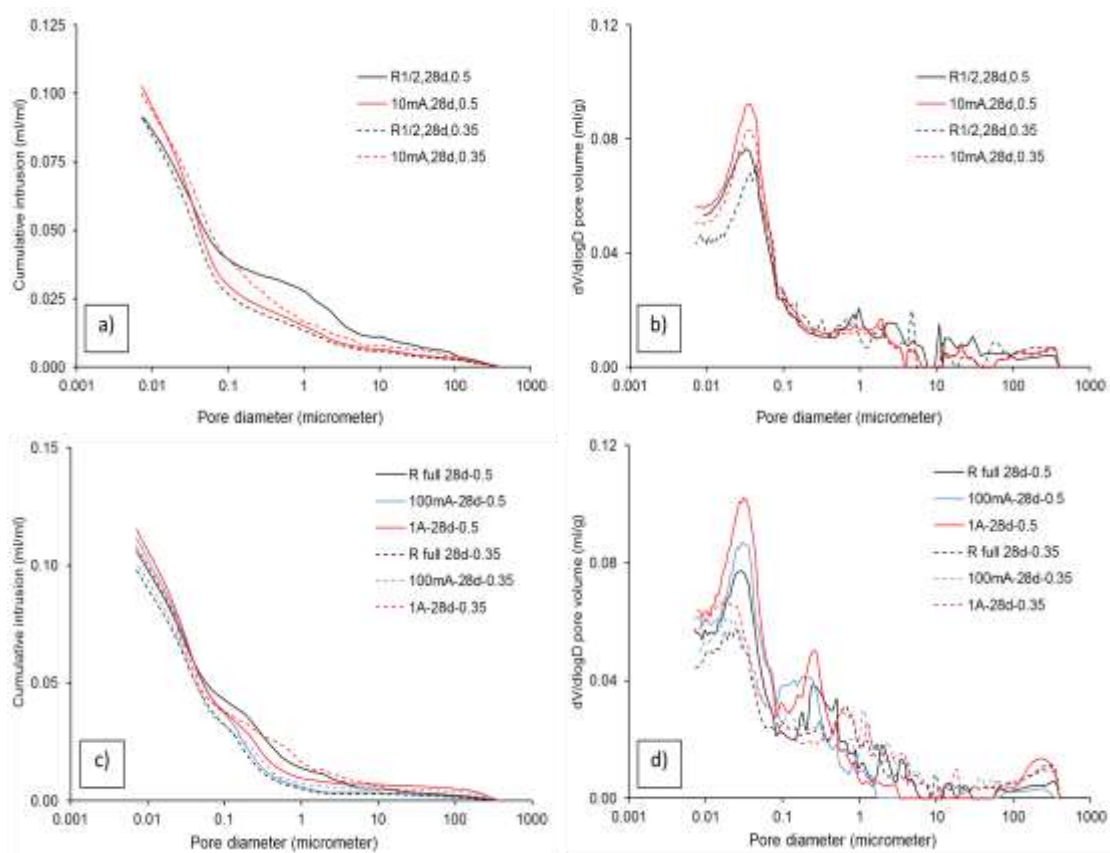


Fig. 6.11 MIP-derived porosity and pore size distribution at 112 days of age for 28 day-cured mortar specimens: (a, b) *half-submerged in water* specimens as a comparison of w/c ratio 0.5 and 0.35 in control (R1/2) and 10 mA/m<sup>2</sup> current regime (10mA); (c, d) *fully submerged in water*, 28-day cured specimens of w/c ratio 0.35 and 0.5 in control (R full), 100 mA/m<sup>2</sup> (100 mA) and 1 A/m<sup>2</sup> (1A) current regime.

For partly submerged in water conditions and level of current density 10 mA/m<sup>2</sup>, the effect of w/c ratio together with the stray current effect, was not significant (Fig. 6.11a,b; Fig. 6.12). As can be observed in Fig. 6.12(a), similar porosity was recorded for the control cases (R ½ specimens 0.5 and 0.35) at 112 days and only a slight densification of the matrix was relevant for the w/c 0.35 group at 140 days. Critical pore size was also similar for the control groups, irrespective of w/c ratio (Fig. 6.11(a,b); Fig.

6.12a). For the “under current” specimens (10 mA) of w/c ratios at both 0.5 and 0.35, coarsening was observed, compared to the relevant control case, slightly more pronounced for the 0.5 group at the stage of 112 days. Critical pore size remained similar, as for the control groups.

For fully submerged in water specimens (Fig. 6.11(c,d), Fig. 6.12b), a larger effect of the w/c ratio was observed, also in combination with the already larger current density levels of 100 mA/m<sup>2</sup> and 1 A/m<sup>2</sup>. Similarly to half submerged in water conditions, the control cases presented a slight difference due to w/c ratio, reduced critical pore size and 0.3 % lower porosity at 140 days for the mortar of w/c 0.35, compared to that of w/c 0.5 at the same age. The effect of stray current was not significant at later hydration ages, except the slightly lower porosity and pore size for the 0.35 w/c ratio specimens (Fig. 6.12b). Coarsening of the pore network was evident in both 0.5 and 0.35 cases, more pronounced for the specimens of w/c ratio 0.5 (Fig. 6.12b), although a family of pores around 1 micrometer appeared to be pronounced for the 0.35 w/c ratio group in fully submerged conditions and in 100 mA and 1A current regimes (Fig. 11d). The critical pore size, however, for both groups of w/c ratio 0.5 and 0.35 remained similar per case/condition, reduced for the 0.35 w/c ratio group (Fig. 6.11d).

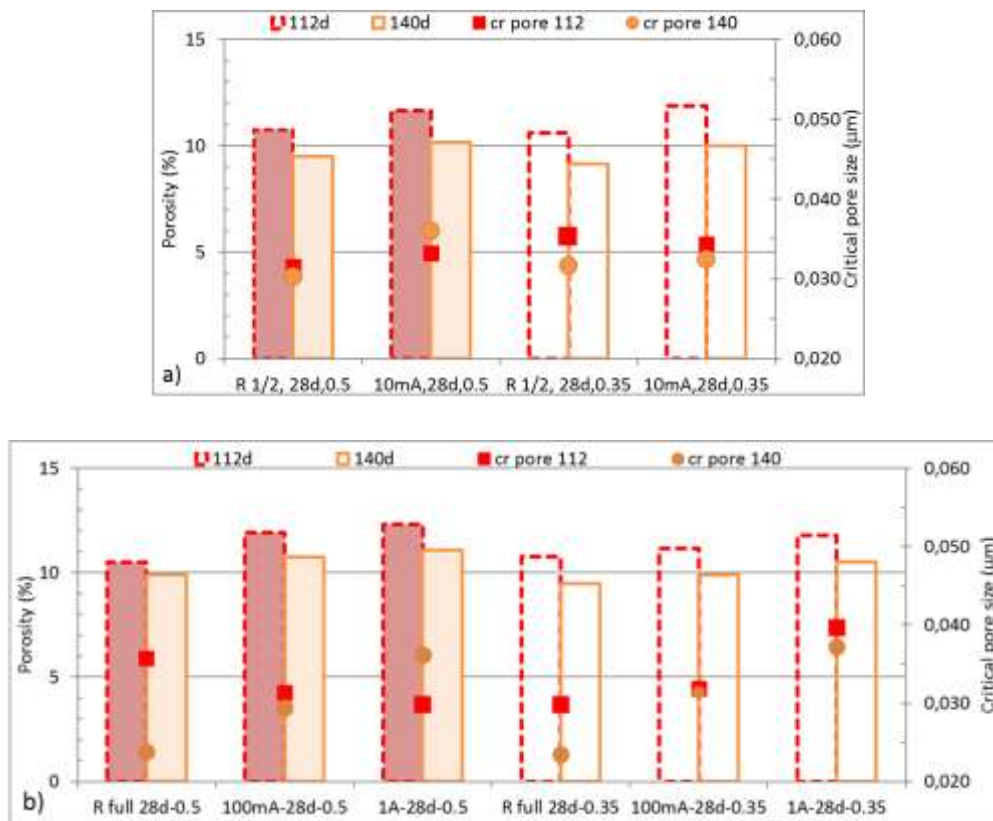


Fig. 6.12 Porosity (column; solid column for w/c 0.5) and critical pore size (symbol, “cr.pore” in legend) at hydration ages of 112 days and 140 days for 28 days cured mortar of different w/c ratio (0.5 and 0.35), halfsubmerged in H<sub>2</sub>O (a) and fully submerged in water (b). The plot a) presents a comparison of control cases (designation R1/2) and those, subjected to 10 mA/m<sup>2</sup> (designation 10 mA); b) compares control cases (designation Rfull) with 100 mA/m<sup>2</sup> (designation 100 mA) and 1 A/m<sup>2</sup> (designation 1A).

The most pronounced (negative) effect of stray current in these (fully submerged in water) conditions was recorded for the highest current density level of  $1 \text{ A/m}^2$  and the higher w/c ratio of 0.5 (Fig. 6.11(d), Fig. 6.12b). However, the almost equal values for the  $1 \text{ A/m}^2$  case in both series of w/c 0.35 and w/c 0.5 at identical hydration age, suggests that the negative effect of stray current does not depend significantly on w/c ratio and/or curing conditions. The above statements are well in line with the recorded compressive strength values (Fig. 6.2). Moreover, this correlation of results even suggests that stray current can result in enhanced reduction of global mechanical properties in specimens of lower w/c ratio, because of restricted cement hydration in a lower pore water volume, which would otherwise positively counterbalance ion and water migration. In fact, a more significant reduction in compressive strength was observed for the lower w/c ratio of 0.35, as already commented in Section 6.3.1 (Fig. 6.3). Consequently, optimum curing and improved concrete mixture would only delay, but not prevent the influence of stray currents in practical situations.

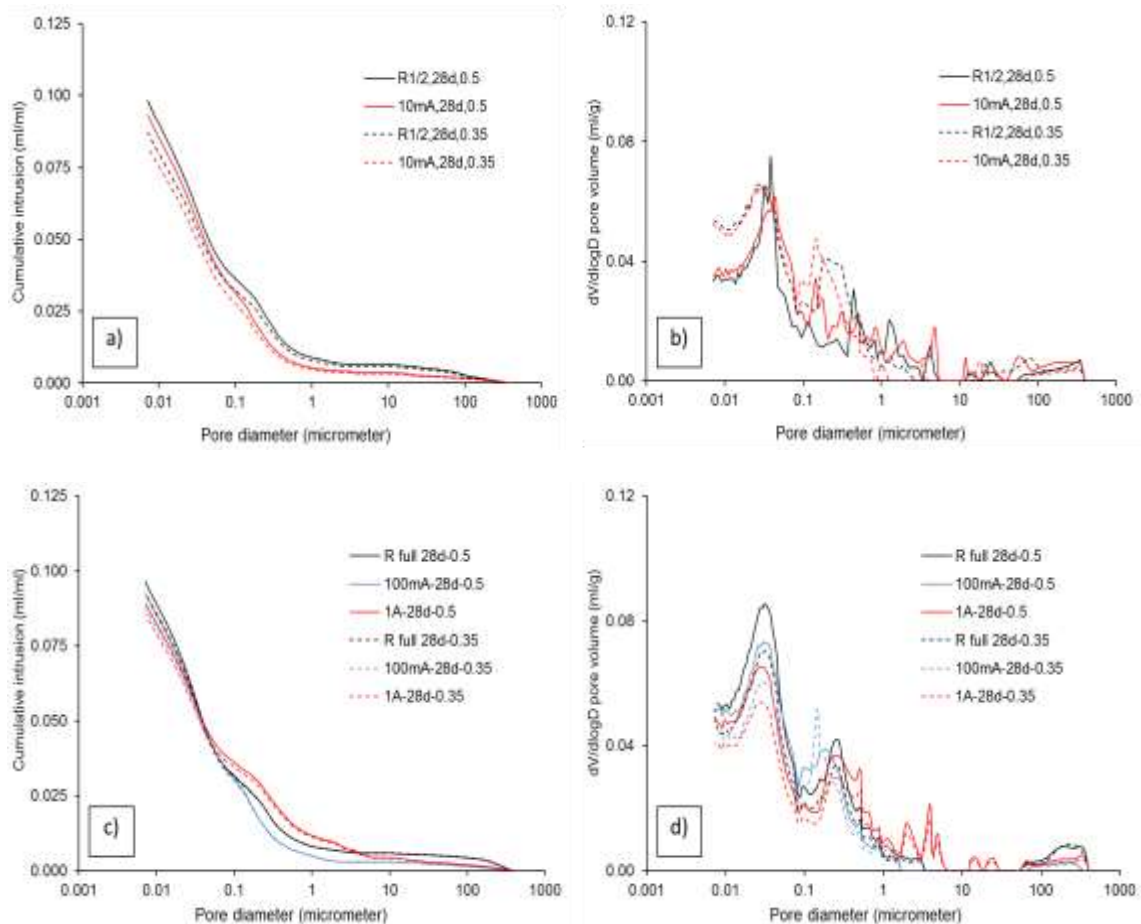


Fig. 6.13 MIP-derived porosity and pore size distribution at 112 days of age for 28 day-cured mortar specimens: (a, b) *half-submerged in  $\text{Ca}(\text{OH})_2$*  specimens as a comparison of w/c ratio 0.5 and 0.35 in control (R1/2) and  $10 \text{ mA/m}^2$  current regime (10mA); (c, d) *fully submerged in  $\text{Ca}(\text{OH})_2$* , 28-day cured specimens of w/c ratio 0.35 and 0.5 in control (R full),  $100 \text{ mA/m}^2$  (100 mA) and  $1 \text{ A/m}^2$  (1A) regime.

In contrast to partly or fully submerged in water conditions, the results for all specimens conditioned in calcium hydroxide, present only densification of the pore network i.e. positive effect of the stray current, irrespective of w/c ratio and/or current density levels. Porosity and critical pore size for all specimens reduced with time and with the application of stray current in both partly and fully submerged conditions (Figs. 6.13, 6.14). Slightly lower values were observed for the series of w/c ratio 0.35, compared to those for the series of w/c ratio 0.5. The largest effect of stray current was observed for the highest current density level of 1 A/m<sup>2</sup>. These results are in line with the mechanical performance of these series of specimens, where a gradual increase of compressive strength values was observed at all time intervals and for all specimens in calcium hydroxide environment (Fig. 6.2). As previously discussed, in conditions where concentration gradient between the pore water and surrounding medium is avoided, the stray current effect, up to the level of the hereby tested current densities, is only positive.

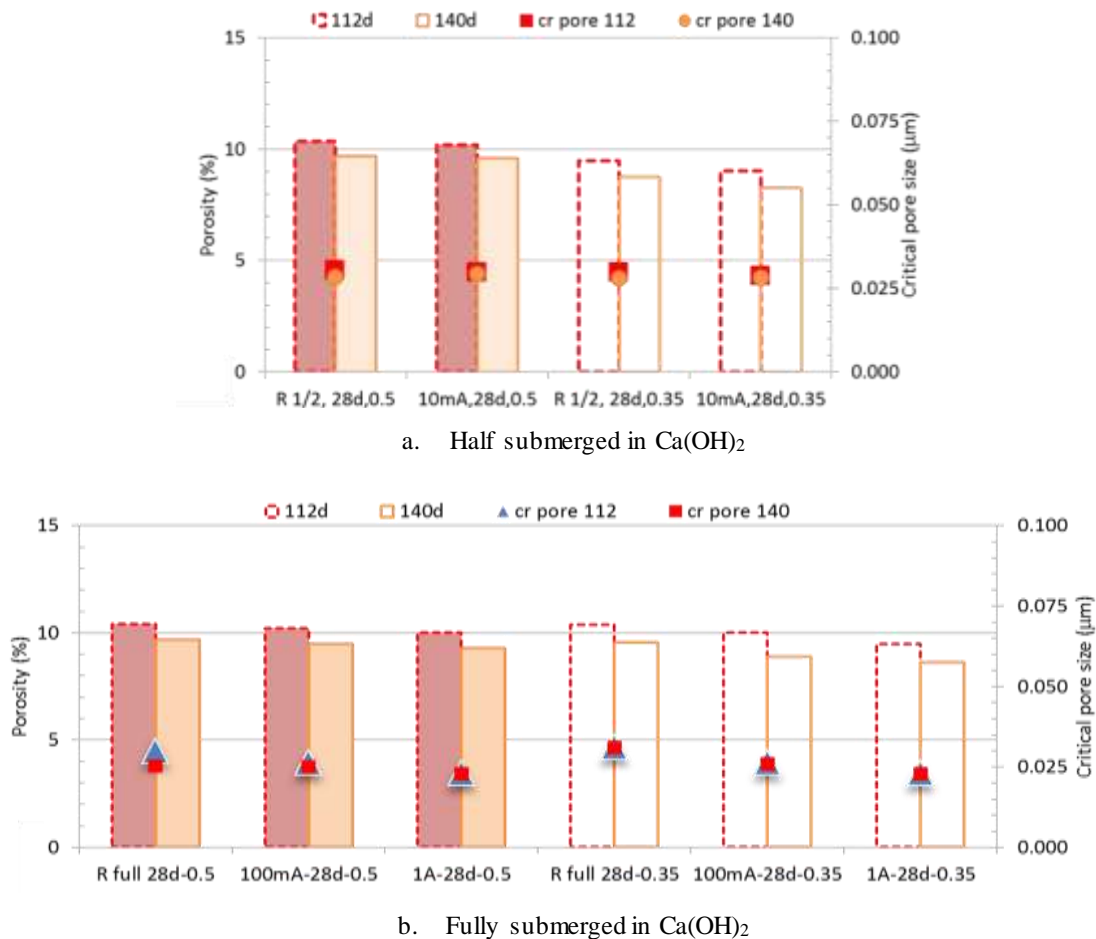


Fig. 6.14 Porosity (column; solid column for w/c 0.5) and critical pore size (symbol, "cr.pore" in legend) at hydration ages of 112 days and 140 days for 28 days cured mortar of different w/c ratio (0.5 and 0.35), halfsubmerged in Ca(OH)<sub>2</sub> (a) and fully submerged in Ca(OH)<sub>2</sub> (b).

### 6.3.4 Evaluation of the effect of stray current on porosity and compressive strength of mortar specimens

From the experimental results the relationship between porosity and compressive strength of mortar specimen can be plotted. The results were compared with those according to the expression that relates compressive strength porosity (Balshin 1949). Since the compressive strength-porosity relationship of cement-based materials (e.g. is predominantly governed by the capillary porosity of the cement paste (Granju 1974, Young et al. 1973), the Balshin equation (eq. 5.27, which has been applied for concrete) can also be applied for mortar. For the compressive strength of the mortar as a function of the porosity of cement paste it then holds:

$$f_m = f_{mo}(1 - p)^n \quad (6.1)$$

where  $f_m$  is the compressive strength of mortar,  $f_{mo}$  is the intrinsic strength of the mortar at zero porosity [i.e. in the range from 90 to 130MPa (Powers 1962), here is chosen 130 MPa],  $p$  is the capillary porosity of cement paste,  $n$  is an empirical constant with values in the range from 3 to 14.47 (Balshin 1949, Powers 1958, Rößler and Odler 1985). It was reported that an empirical constant  $n$  for ordinary *concrete* is in the range from 3 (Powers 1958) to 8.15 (Balshin 1949).

Fig. 6.15 shows the measured and calculated compressive strength of mortar specimens subjected to stray current as a function of porosity. Fig. 6.15a gives results for mortars in fully submerged condition and Fig. 6.15b in partly submerged condition. An empirical constant  $n$  can be determined from the measured compressive strength of mortar specimens subjected to stray current as a function of porosity (Fig. 6.15a) by curve fitting with eq. (6.1). The  $n$  values obtained from curve fitting with eq. (6.1) are 3.7, 4.1, and 4.7 for control specimen in fully submerged condition and specimen under stray current levels 100mA/m<sup>2</sup> and 1 A/m<sup>2</sup>, respectively. For mortar specimen partly submerged in water (Fig. 6.15b), the  $n$  values are 4.1 and 4.5 for control specimen and specimens under current of 10mA/m<sup>2</sup>. In general, the  $n$  values of control specimens are in the range from 3 to 5, which is in line with the  $n$  values reported in the literature (Balshin 1949, Powers 1958, Rößler and Odler 1985), both for mortar specimens partly and fully submerged in water. In case of current, hardly any change of the  $n$  values compared to specimen without current is observed. There is tendency, however, that  $n$  values increase in case a current is applied.

From Fig. 6.15 it can be deduced that mortar specimens partly submerged in water and under current (Fig. 6.15b) show almost the same trend as mortar specimens fully submerged in water (Fig. 6.15a). During the hydration process capillary suction takes place in mortar specimens partly submerged in water, resulting in an increase in degree of saturation of the mortar specimens. Consequently, the degree of saturation in mortar specimens partly submerged in water is getting close to the mortar specimens fully submerged in water.

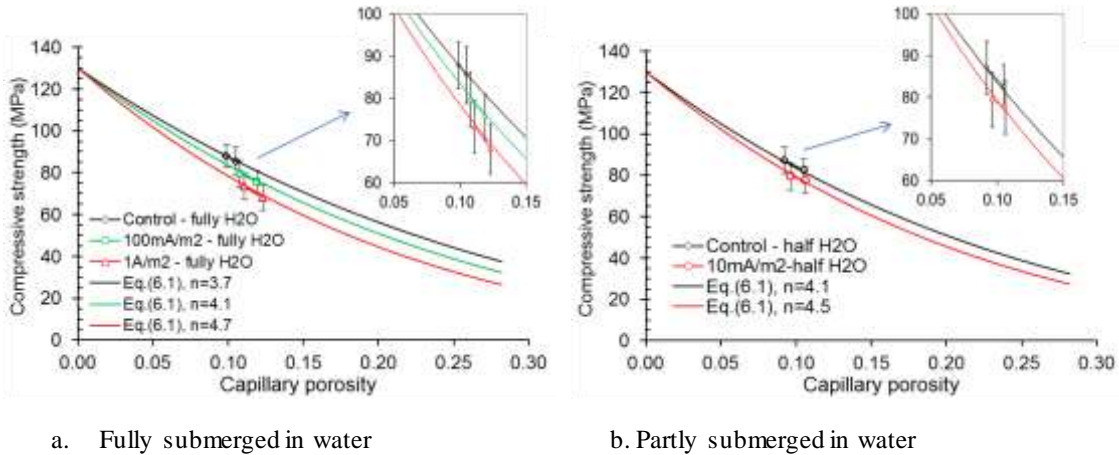


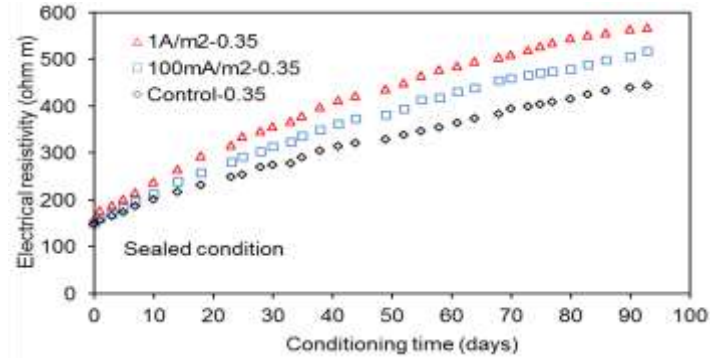
Fig. 6.15 Measured and calculated compressive strength of mortar specimens fully submerged (a) and partly submerged in water (b) subjected to stray current as a function of porosity. Water-to-cement ratio 0.5.

### 6.3.5 Electrical resistivity of 28-day cured mortar in condition of stray current flow

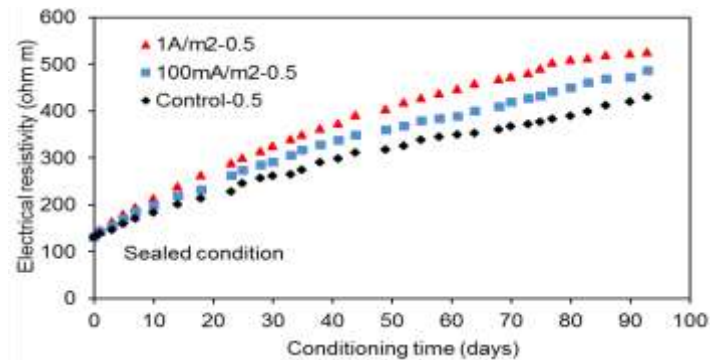
As discussed above, the stray current flow through mortar specimens stored under different environmental conditions led to a change in porosity and pore size distribution of the bulk matrix. This will also change the electrical properties of the specimens. According to Archie's law (Archie 1942), the electrical resistivity is mainly influenced by porosity and moisture. Electrical resistivity is reported to be an indicator of the interconnectivity and tortuosity of the pore network (Andrade *et al.* 2000). As reported by Lakshminarayanan *et al.* (1992), the electrical resistivity of the concrete depends on the pore volume and pore size distribution. Interconnected pores influence the electrical resistivity, since these pores are the pathways determining transport properties (i.e. diffusion and permeability). In general, the electrical properties of concrete, i.e. electrical resistivity increase with decreasing in porosity.

#### 6.3.5.1 Electrical resistivity development of mortar specimens in sealed condition

Fig. 6.16 shows electrical resistivity development of mortar specimens in sealed condition. As expected, the electrical resistivity values gradually increase with time due to the progress of cement hydration. Since the electrical current is carried by ions in the pore solution of the mortar specimens, a higher water/cement ratio (0.5) results in an "easier" electrical current flow (i.e. low electrical resistance/resistivity). In contrast, a lower w/c ratio (0.35) impedes electrical current flow (i.e. high electrical resistance/resistivity). For specimens exposed to current, i.e. 100 mA/m<sup>2</sup> and 1A/m<sup>2</sup>, cement hydration was enhanced, resulting in higher electrical resistivity over time – in the range of 480 to 530 Ohm.m, compared to control conditions – approximately 350 Ohm.m towards the end of the test. Slightly higher values were recorded for the lower w/c ratio group (0.35) compared to the 0.5 w/c ratio group in both control and under current conditions.



a. Mortar specimens in sealed condition with w/c ratio 0.35



b. Mortar specimens in sealed condition with w/c ratio 0.5

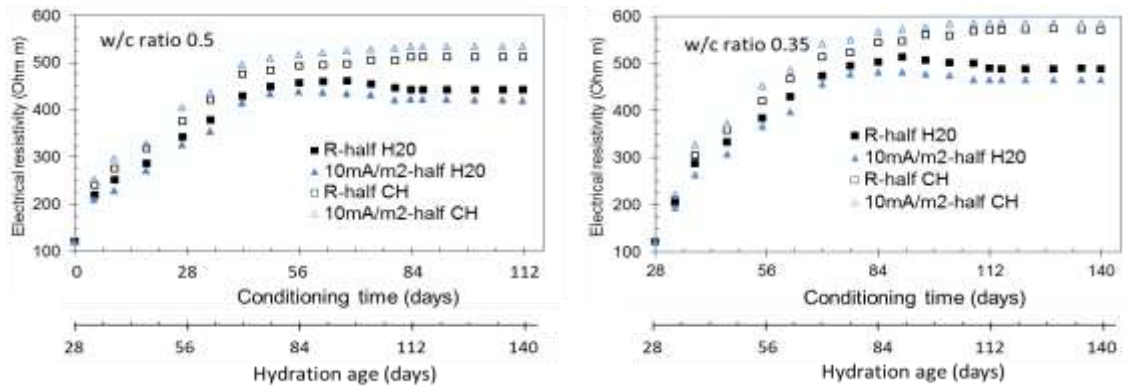
Fig. 6.16 Electrical resistivity development of mortar specimens in sealed condition for w/c ratio 0.35 (a) and w/c ratio 0.5 (b). Conditioning time of  $t=0$  is equal to 28 days of hydration age.

### 6.3.5.2 Electrical resistivity development of mortar specimens partly and fully submerged in water or calcium hydroxide solution

Figures 6.17 and 6.18 present the evolution of electrical resistivity of 28 days old mortar specimens with w/c ratios 0.5 and 0.35, partly and fully submerged in either water or a calcium hydroxide solution. The figures show that, from 28 days until ca. 40 days, the electrical resistivity for all specimens increased with time (following the sealed condition trend), irrespective of w/c ratio and exposure conditions. This is logic and as expected, reflecting ongoing cement hydration. In addition, stray current and ambient temperature of about 25°C (higher compared to the temperature in the fog room of 20°C) will accelerate the hydration process, resulting in an increase in electrical resistivity at early ages. Electrical resistivity of mortar specimens submerged in  $\text{Ca}(\text{OH})_2$  remains constant after 40 to 55 days of conditioning (Figs. 6.17, 6.18, open symbols, designation CH), whereas a decrease in electrical resistivity was observed for specimens submerged in water (Fig. 6.17, 6.18, solid symbols, designation  $\text{H}_2\text{O}$ ).

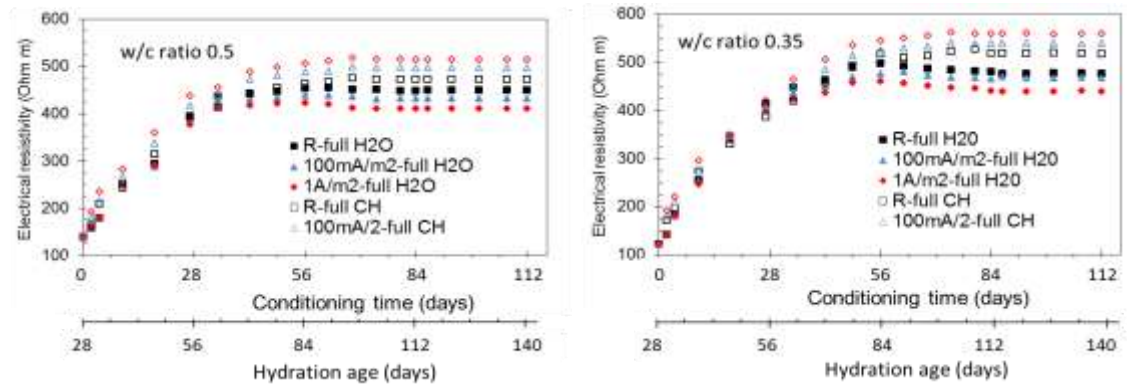
The “turning point” of resistivity development - decrease of electrical resistivity for the water-conditioned specimens after longer treatment ( $> 50$  days), for both partly submerged (Fig. 6.17) and fully submerged (Fig. 6.18) specimens, was obviously related to the leaching-caused coarser pore structure and degree of saturation. In those cases, the negative effect of stray current takes place, reflected by the lowest electrical resistivity for specimen, subjected to the highest current density levels (Fig. 6.18). As

can also be observed in both Fig. 6.17 and Fig. 6.18, the negative effect of stray current was independent of the w/c (phenomenon observed for w/c ratio 0.35 and 0.5).



- a. Partly submerged in water and calcium hydroxide with w/c ratio 0.5
- b. Partly submerged in water and calcium hydroxide with w/c ratio 0.35

Fig. 6.17 Electrical resistivity of mortar specimens cured in fog room for 28 days, *partly submerged* in water and calcium hydroxide, conditioned from 28 to 112 days: a) specimens of w/c ratio 0.5; b) specimens of w/c ratio of 0.35. Ambient temperature is about 25°C.



- a. Fully submerged in water and calcium hydroxide with w/c ratio 0.5
- b. Fully submerged in water and calcium hydroxide with w/c ratio 0.35

Fig. 6.18 Electrical resistivity of mortar specimens cured in fog room for 28 days, *fully submerged* in water and calcium hydroxide, conditioned from 28 to 112 days: a) specimens of w/c ratio 0.5; b) specimens of w/c ratio of 0.35. Ambient temperature is about 25°C.

The electrical resistivity of mortar specimens in calcium hydroxide solution increased with time and with the intensity of stray current. For the specimens with w/c=0.5 (Fig. 6.17a and Fig. 6.18a) an increase of electrical resistivity was observed for the specimens in 10 mA/m<sup>2</sup>, 100 mA/m<sup>2</sup> and 1 A/m<sup>2</sup> regimes, compared to control conditions. A similar trend was recorded for the mortar with w/c=0.35, (Fig. 6.17b and Fig. 6.18b). For all specimens stabilization of the resistivity after 60 days of conditioning is observed, specifically for fully submerged conditions (Fig. 6.18). This is irrespective of w/c ratio and current density. From Fig. 6.17 and Fig. 6.18 can be inferred that stray current is not harmful for cement-based materials located in the

surrounding environment with high PH (e.g. in calcium hydroxide solution). In contrast, stray current have potential to accelerate degradation processes in cement-based materials submerged in water due to leaching of the microstructure.

## 6.4 Conclusions

This chapter reports on the effect of stray current flow on materials properties of mortar specimens subjected to stray current for about 112 days, after 28-days hardening in a fog-room with 98% RH without current. The w/c ratios used were 0.35 and 0.5. The following conclusions can be drawn:

1. The compressive strength of mortar specimens subjected to stray current, after 28-days hardening in a fog-room with 98% RH (without current), is affected by stray current flow. The effect strongly depends on the exposure conditions and the current density.
  - a. In case there is no ion concentration gradient between the pore water of the mortar specimens (i.e. mortar specimens submerged in calcium hydroxide) and the surrounding medium (i.e. alkali ions leaching-out is avoided), compressive strength generally increases due to enhanced cement hydration.
  - b. In conditions where ion concentration gradients exist (i.e. mortar specimens submerged in water), the stray current promotes ions migration towards the surrounding medium. A coarser microstructure (Figs. 6.6, 6.7 and 6.12) caused by alkali ions leaching was observed at current densities larger than  $100\text{mA/m}^2$ , resulting in a lower compressive strength of mortar specimens (Fig. 6.3).
2. Negative effects of leaching in mortar specimens submerged in water due to stray current (i.e. coarser pore structures) occur at current density larger than  $100\text{mA/m}^2$ , both for w/c ratios 0.35 and 0.5.
3. In sealed condition, stray current with current density up to  $1\text{A/m}^2$  has a positive effect on the development of electrical resistivity of mortar specimens (i.e. higher electrical resistivity over time compared to control conditions) due to accelerated cement hydration.
4. Electrical resistivity of mortar specimens partly and fully submerged in water subjected to stray current increases at early age of hydration and decreases at later ages ( $> 50$  days). It was noticed that the drop of electrical resistivity (Figs. 6.17 and 6.18) is caused by alkali ions leaching and degree of saturation of the coarser pore structure.

# 7

## **Retrospection, Conclusions and Recommendations for Future Research**

---

This chapter summarises the results of experiments and numerical simulations presented in this thesis. Next, general conclusions are presented. Finally, recommendations for future research are given.

## 7.1 Retrospection

As mentioned in the previous chapters, stray current causes an increase of temperature of hardening concrete due to Joule heating, which will accelerate cement hydration. The accelerated cement hydration has been used as a basis for electrical curing to improve/increase compressive strength development of concrete. When concrete is exposed to water, however, leaching of alkali ions will decrease the compressive strength and increase the diffusion coefficient of concrete. Under stray current, leaching of alkali ions is accelerated, which will increase the level of structural degradation. It was reported in literature that stray current does not only affect steel reinforcement embedded in concrete and underground infrastructures, but can also induce degradation of the cement-based matrix. Concrete damage due to stray current flow is a process that involves many mechanisms. The main factors include ions transport, electrical conduction, heat transfer and corresponding occurrence of mechanical stresses. However, the study on the effect of stray current on material properties (e.g. microstructural, mechanical, electrical properties) and long-term performance/durability of cement based materials is still not completely understood and rarely reported.

The aim of this project was to investigate the effects of stray current on long-term performance of cement-based materials. This project focuses on the effect of stray current on hardening cement-based materials in different environmental conditions (e.g. sealed and partly and fully submerged in saturated calcium hydroxide and in water). Simulations and experimental studies were carried out to quantify the effect of stray current flow on the hydration process and properties of cement-based materials like porosity, strength and diffusivity of specimens with and without exposure to stray current. In addition, the effect of stray current on hardened cement-based materials was investigated.

In Chapter 3, the effect of low level stray current flow (i.e.  $10 \text{ mA/m}^2$ ) on material properties of cement-based materials, partly submerged in water, was investigated. Numerical simulation of the stray current distribution in the specimens was performed, meant to serve as a basis for modelling of the level of current density that could exert significant microstructural alterations in a bulk cement-based matrix.

In Chapter 4, experiments were carried out under the joint action of stray current and different environmental conditions (i.e. sealed, submerged in water and in saturated calcium hydroxide) to distinguish between a diffusion-controlled process (including ions leaching due to concentration gradient between the pore solution in cement-based materials and the external medium) and a migration-controlled process (ion/water transport in stray current conditions) with 24 hours curing. Stray current levels applied to the cement-based materials were  $10 \text{ mA/m}^2$ ,  $100 \text{ mA/m}^2$  and  $1 \text{ A/m}^2$ , values also measured in real practice. Material properties (i.e. mechanical, electrical and microstructural properties) of the cement-based material subject to stray current were evaluated to quantify negative effects of stray current due to alkali ion leaching and/or possible positive effects of stray current on cement hydration.

In Chapter 5, the effects of stray current flow on the hydration process and temperature development and evolution of materials properties in hardening cement-

based materials were quantified. Experiments were performed in isothermal condition at 20°C to investigate the rate of heat release and microstructural changes in cement paste caused by stray current flow with current density 10 mA/m<sup>2</sup>, 100 mA/m<sup>2</sup> and 1 A/m<sup>2</sup>. In addition, semi-adiabatic tests were performed in hardening cement paste prisms with specimen size of 5.5×5.5×29.5 cm<sup>3</sup> and current densities 10 A/m<sup>2</sup>, 40 A/m<sup>2</sup> and 60 A/m<sup>2</sup>. In parallel, numerical simulations were performed to quantify the hydration process and temperature development in hardening cement-based materials. The effect of stray current on hardening cement-based materials with different element sizes was simulated to investigate possible size effects and consequences for hardening in real-size structural elements. In order to quantify possible mechanical internal damage (i.e. cracking) in hardening concrete, maximum temperatures induced by stray current were numerically investigated. The evolution of capillary porosity of cement paste as function of the degree of hydration  $\alpha$  and the temperature during the reaction was calculated. Apparent diffusion coefficients of concrete subjected to stray current were calculated from microstructure parameters (i.e. capillary porosity).

In Chapter 6, the effect of stray current flow on material properties of different mixtures of hardened mortar specimens, 28-days cured in a fog-room with 98% RH, was studied. The joint effect of water-to-cement ratio, curing age, different external environment and stray current on the microstructural (porosity and pore size), electrical (resistivity) and mechanical (compressive strength) properties of 28 days-cured cement-based materials were investigated.

## 7.2 Conclusions

In this research, experiments on 24 hours-cured and 28 days-cured mortar specimens in a fog-room with 98% RH with w/c ratio of 0.35 and 0.5 subjected to stray current were performed and summarized in Table 7.1. In addition, experiments on hardening cement paste subjected to stray current were carried out and listed in Table 7.2.

Table 7.1 Summary of the experiments of the effect of stray current on material properties (i.e. microstructural, mechanical and electrical properties) of mortar specimens.

| No | Current density<br>Group | Environmental conditions |                  |                     |                  |                     |
|----|--------------------------|--------------------------|------------------|---------------------|------------------|---------------------|
|    |                          | Sealed                   | Fully submerged  |                     | Partly submerged |                     |
|    |                          |                          | H <sub>2</sub> O | Ca(OH) <sub>2</sub> | H <sub>2</sub> O | Ca(OH) <sub>2</sub> |
| 1  | Control                  | ×                        | ×                | ×                   | ×                | ×                   |
| 2  | 10mA/m <sup>2</sup>      | ×                        |                  |                     | ×                | ×                   |
|    | 100mA/m <sup>2</sup>     | ×                        | ×                | ×                   |                  |                     |
|    | 1A/m <sup>2</sup>        | ×                        | ×                | ×                   |                  |                     |

Table 7.2 Summary of the experiments of the effect of stray current on heat of hydration and temperature development in cement paste.

| No | Experiments                  | Current density      | Environmental condition |
|----|------------------------------|----------------------|-------------------------|
|    |                              | Group                | Sealed                  |
| 1  | Isothermal calorimetry tests | Control              | ×                       |
|    |                              | 10mA/m <sup>2</sup>  | ×                       |
|    |                              | 100mA/m <sup>2</sup> | ×                       |
|    |                              | 1A/m <sup>2</sup>    | ×                       |
| 2  | Non-isothermal tests         | Control              | ×                       |
|    |                              | 10A/m <sup>2</sup>   | ×                       |
|    |                              | 40A/m <sup>2</sup>   | ×                       |
|    |                              | 60A/m <sup>2</sup>   | ×                       |

The conclusions of this research are as follows:

### 7.2.1 General conclusions

- Stray current flow through hardening cement based-materials will cause an increase of the temperature of the material due to Joule heating. The temperature increases with increasing current densities. This temperature increase will accelerate cement hydration, resulting in faster evolution of materials properties (e.g. stiffness and strength) and also a faster decrease of the capillary porosity. Hydration at higher temperatures, however, will also result in - for the same degree of hydration - a higher capillary porosity, a lower final compressive strength and a higher diffusion coefficient at later ages. This may reduce the durability and service life of concrete structures.
- As said in the foregoing paragraph, stray current results in a higher hydration rate and a higher peak temperature. In case of peak temperatures beyond about 60°C (DANISH Ministry of Transport 1985), internal microcracking in hardening concrete may occur once the central part cools down.
- When hardened cement paste, mortar or concrete is exposed to *water*, leaching of alkali ions occurs due to concentration gradients between the pore solution in the specimen and the surrounding medium. Under stray current, leaching of alkali ions is accelerated. Leaching of alkali ions will increase the capillary porosity and decrease the compressive strength of cement-based materials. In case specimens are exposed to an *alkaline* medium, leaching of alkali ions is prevented/avoided.

### 7.2.2 Effects of stray current on material properties in the centre of hardening concrete

- The maximum temperature in the *centre* of hardening concrete elements reaches higher values with increasing specimen size and increasing stray current levels (see also section 7.2.1). Hydration at higher temperature results in coarsening of the capillary pore structure in the centre of concrete specimens, a lower final compressive strength and a higher diffusion coefficient. A lower final compressive

strength and higher capillary porosity in the centre of concrete elements, however, is generally not considered problematic as it will not affect the service life of concrete structures.

### **7.2.3 Effects of stray current on material properties in outer zone of hardening concrete**

#### *Without insulation*

- To what extent Joule heating caused by stray current may affect the hydration process in the outer zone of concrete structures strongly depends on the presence and type of insulation during the hydration process and the ambient temperature. There is no significant effect of stray current on the properties of the outer zone of hardening concrete as long as the heat discharge to the environment is fast enough to keep the concrete temperature in the outer zone of the concrete low. This is generally the case if no formwork insulation is used. However, the outer zone of hardening concrete *without thermal insulation* may reach high temperatures if the ambient temperature is high. In that case stray current will further increase the temperature in the outer zone of the concrete. In this case the capillary porosity of the concrete in the outer zone may become coarser, which may impair the concrete's durability.

#### *With insulation*

- The capillary porosity and the associated apparent diffusion coefficient in the outer zone of hardening concrete decrease with ongoing cement hydration. This decrease is faster with increasing current density. In case thermal insulation is present, the temperature of the concrete in the outer zone will reach higher values and hydration will be faster compared to the case without insulation. Faster hydration will result in faster evolution of materials properties (e.g. strength, stiffness etc.). A higher temperature during hydration, however, may also result in higher capillary porosity compared to hydration at lower temperature, given the same degree of hydration. At early ages the concrete may benefit from the faster evolution of mechanical properties (e.g. earlier demoulding is possible). At later ages, however, a higher capillary porosity caused by hydration at high temperatures, may result in a higher apparent diffusion coefficient and hence lower durability.

### **7.2.4 Cement-based materials submerged in water or alkaline medium subjected to stray current**

- Stray current flow through *hardening* mortar specimen submerged in water accelerates cement hydration, which can be considered as a positive effect. At the same time, stray current promotes ion migration towards the surrounding medium, i.e. leaching of alkali ions. Leaching results in coarsening of the concrete, which eliminates the positive effect of stray current. This will result in a lower compressive strength and a lower electrical resistivity of the concrete compared to control specimens. A similar effect takes place in *hardened* mortar specimens subjected to stray current. In this case, however, when submerged in water the leaching process is much slower than in *hardening* mortar specimens. In case mortar specimens are submerged in an alkaline medium, leaching of alkali ions is prevented/avoided and the material will not suffer from leaching effects.

### 7.3 Recommendations for future research

Although several aspects of the influence of stray current flow on cement-based materials have been considered in this thesis, the following aspects are recommended for future research.

- *Experimental validation of the effect of stray current on apparent diffusion coefficient of cement-based materials*

As mentioned in this thesis, stray current affects the properties of cement-based materials. Temperature increase in hardening concrete due to stray current will accelerate cement hydration resulting in a faster evolution of material properties and a faster decrease of the capillary porosity. Hydration at higher temperature, however, results in coarsening of the capillary pore structure, a lower final compressive strength and a higher diffusion coefficient of concrete at later ages. However, experimental studies of the long-term performance of cement-based material subjected to stray current are still lacking. To investigate the effect of stray current on long-term performance of cement-based materials, the apparent diffusion coefficient has been determined in this thesis by numerical simulation. In order to accurately predict the time-dependent chloride diffusivity, experimental tests (e.g. the rapid chloride migration (RCM) test or the diffusion cell test following NT BUILD 443) are needed for validating the apparent diffusion coefficient values obtained from numerical simulation.

- *Experimental validation of the effect of high stray current levels on materials properties of cement-based materials.*

In this thesis, the effect of high stray current levels (i.e. up to  $60\text{A/m}^2$ ) on the hydration process and temperature development in hardening cement-based materials and evolution of materials properties has been numerically investigated. Capillary porosity and apparent diffusion coefficients were calculated. However, experimental validation of the effect of high stray current levels on material properties of hardening concrete (e.g. microstructural, mechanical and transport properties) is still needed.

- *Analysis and experimental validation of stray current induced damage in cement-based materials.*

Stray current increases the maximum temperature in hardening concrete. This higher temperature may induce (micro)cracking in hardening concrete. Simulation and experimental validations are important to get better understanding about the effect of stray current and associated Joule heating on thermal stresses which promote deterioration and/or internal damage in hardening concrete.

- *Alternative stray current scenarios*

In this thesis the stray current has been assumed constantly present, both in the experiments and in the numerical simulations. In practice stray current is normally present in a non-steady mode. In view of practical application realistic stray current scenarios need to be investigated in more detail.

## **Appendix A**

Determination of pore structure parameters and image analysis

### A.1 Determination of pore structure parameters

Porosity and pore size distribution of all specimens in all tested conditions were evaluated by Mercury Intrusion Porosimetry (MIP) and through Environmental scanning electron microscopy (ESEM). The experimental procedures for both MIP and ESEM followed already reported sequence of sample preparation, where cement hydration was ceased by submersion in liquid nitrogen, followed by freeze-drying until reaching a constant weight (Ye 2003; Sumanasooriya et al. 2009; Struble et al. 1989; Kjellsen et al. 2003; Ye et al. 2002). The samples for both MIP and ESEM analysis were taken from identical geometrical location in the cubes for each test series (Fig.1c). The MIP tests were carried out by using Micromeritics Poresizer 9320 (with a maximum pressure of 207 MPa). The drawbacks of MIP, e.g. “ink-bottle effect”, surface tension and contact angle within Hg intrusion/extrusion, etc. are well known and reported in numerous works (e.g. Diamond et al. 1995; Winslow et al. 1970; Willis et al. 1998). However, MIP is largely employed to study the bulk matrix of cement-based materials, including mortar and concrete (Ye 2003; Laskar et al. 1997; Kumara et al. 2004). Therefore, by “bulk matrix” in this study, the total volume of the mortar matrix refers to MIP, while the bulk cement paste only was evaluated by ESEM image analysis. More importantly, absolute values are not claimed, but rather a comparative analysis between equally handled specimens from identical geometrical location in the same test series is considered, in view of the effect of stray current and relevant environmental conditions. ESEM imaging and image analysis have been successfully used in studying the pore structure of cement-based materials (Lange et al. 1994; Diamond et al. 1995; Olson et al. 1997). The image analysis in this work was performed on an average of 35 locations per sample of 20×20 mm<sup>2</sup> size. The image analysis complies with previously reported methodology for pore structure and phase distribution analysis of cement based materials, implementing mathematical morphology and stereology approaches (Serra 1982; Hu et al. 2003). Main details and considerations with regard to image analysis are as follows.

### A.2 Image analysis

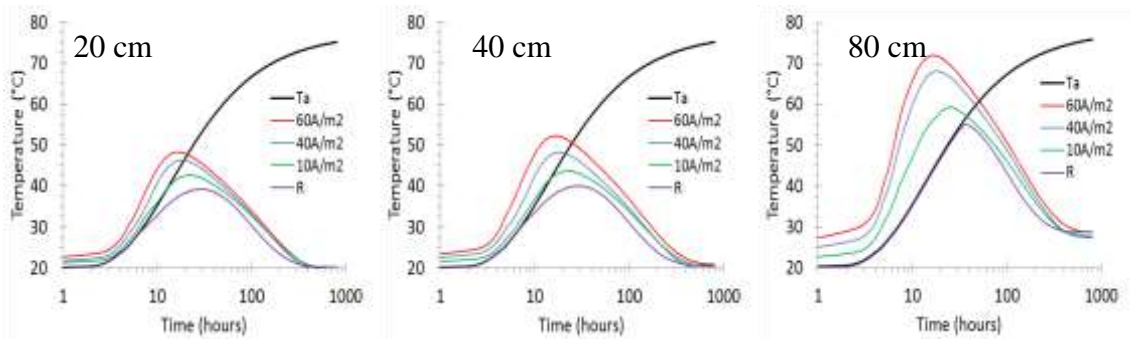
The image analysis complied with the generally used methodology for pore structure analysis of cement based materials (Ye 2003; Hu 2004). The image analysis performed in this study is as reported in (Koleva 2007), main considerations of which are as follows: Scanning electron microscopy (using ESEM Philips XL30) was employed for visualization and microstructure investigations. Section images of the specimens were obtained with backscattered electron (BSE) mode (a set of ESEM images were made at random locations throughout the full size of polished sections). The physical size of the reference region of each image is 226 μm in length and 154 μm in width, with the resolution of 0.317 μm/pixel (corresponding to a magnification of 500x). Small capillary pores play an important role in the transport properties of cement based specimens (Hu 2003). Hence, it is necessary to strike a balance between a representative area element revealing sufficiently large pore section, and a satisfactory resolution for detection of these small capillary pores. Higher magnification could be expected to reveal more details in the pore structure, however, as reported in (Hu 2003), resolutions of 0.293 μm/pixel (1000x) and 0.146 μm/pixel (2000x) gave similar values. The image analysis was performed using OPTIMAS software package.

The combination of ESEM images and quantitative image analysis allows deriving structural information of the pore space, such as the porosity and critical pore size. On the basis of mathematical morphology transformations, a pore size distribution can be obtained by using a sequence of similarly shaped structuring elements of increasing size (Serra 1982). In this study, the so called ‘opening distribution’ was used, where the binary image is opened by a series of squares of increasing size (Hu 2003; Koleva 2007). The original BSE image (or a selected area, excluding any aggregate particles, if any) is segmented by applying a grey-level threshold to create a binary image, reflecting the pore phase. The threshold grey level between porosity and solid phases is selected based on the shape of the histogram of the BSE image. The anhydrous material and calcium hydroxide (CH) have fairly uniform grey levels, resulting in certain peaks in the histograms. Due to variation in composition, the grey levels of the other hydration products (calcium silica- hydrate (C-S-H)) form a shallower but still identifiable peak in the histograms. For properly choosing a threshold value of the grey level for segmentation of the pore space, it has been found that consistent results can be obtained by selecting an arbitrary point on the lower slope of the peak produced by the other hydration products (Scrivener 2004). The binary image is then subjected to quantitative image analysis for derivation of structural parameters (pore size distribution, critical pore size, etc.). The cumulative pore size distribution curve is obtained by plotting the pore area fraction after an opening operation versus linear dimension of the structuring element. This gives a type of “size” classification in the case of an interconnected structure, like pore space in mortar. The critical pore size can be conceived as the diameter of the pore that completes the first interconnected pore pathway in a network, developed by a procedure of sequentially adding pores of diminishing size to this network.

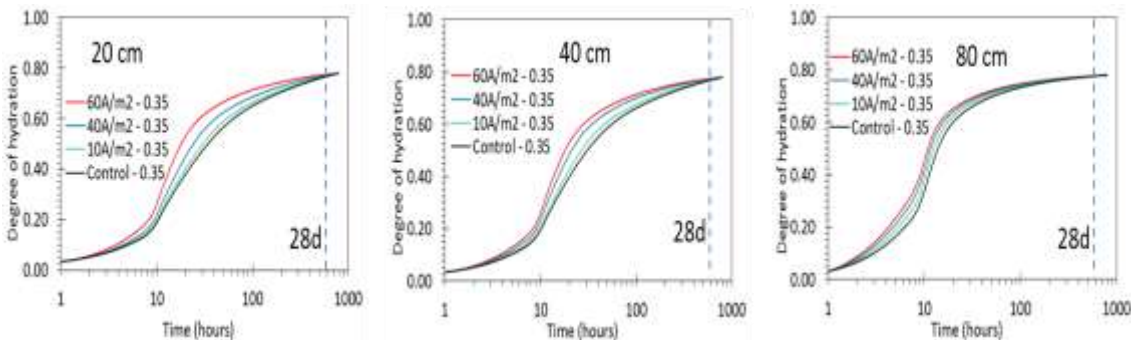


## **Appendix B**

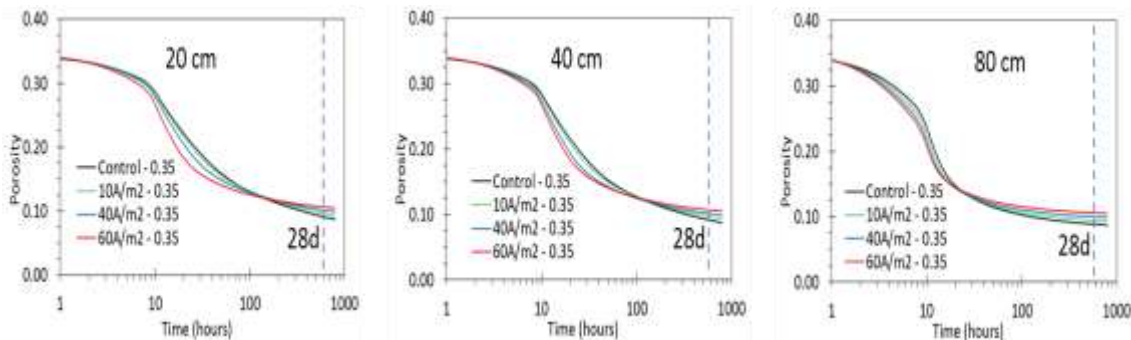
Numerical simulations results for the evolution of temperature, degree of hydration, capillary porosity and compressive strength in the centre and outer zone of concrete elements without insulation subjected to stray current for different wall thickness



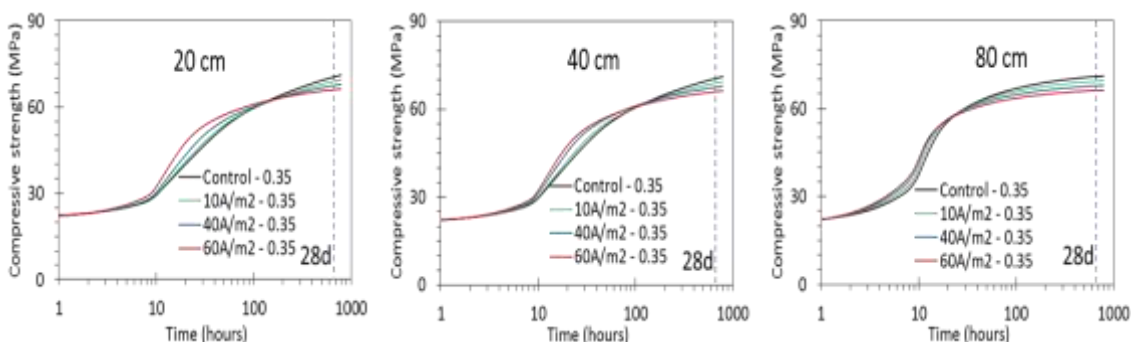
a. Temperature development in the *centre* of hardening concrete *without insulation* for wall thickness 20cm (left), 40 cm (middle) and 80 cm (right).



b. Degree of hydration in the *centre* of hardening concrete *without insulation* for wall thickness 20cm (left), 40 cm (middle) and 80 cm (right).



c. Capillary porosity in the *centre* of hardening concrete *without insulation* for wall thickness 20cm (left), 40 cm (middle) and 80 cm (right).



d. Compressive strength in the *centre* of hardening concrete *without insulation* for wall thickness 20cm (left), 40 cm (middle) and 80 cm (right).

Fig. B.1 Temperature development (a), degree of hydration (b), capillary porosity (c) and compressive strength (d) in the *centre* of hardening concrete *without insulation* for different wall thickness (i.e. 20cm, 40 cm and 80 cm) and w/c ratio 0.35.

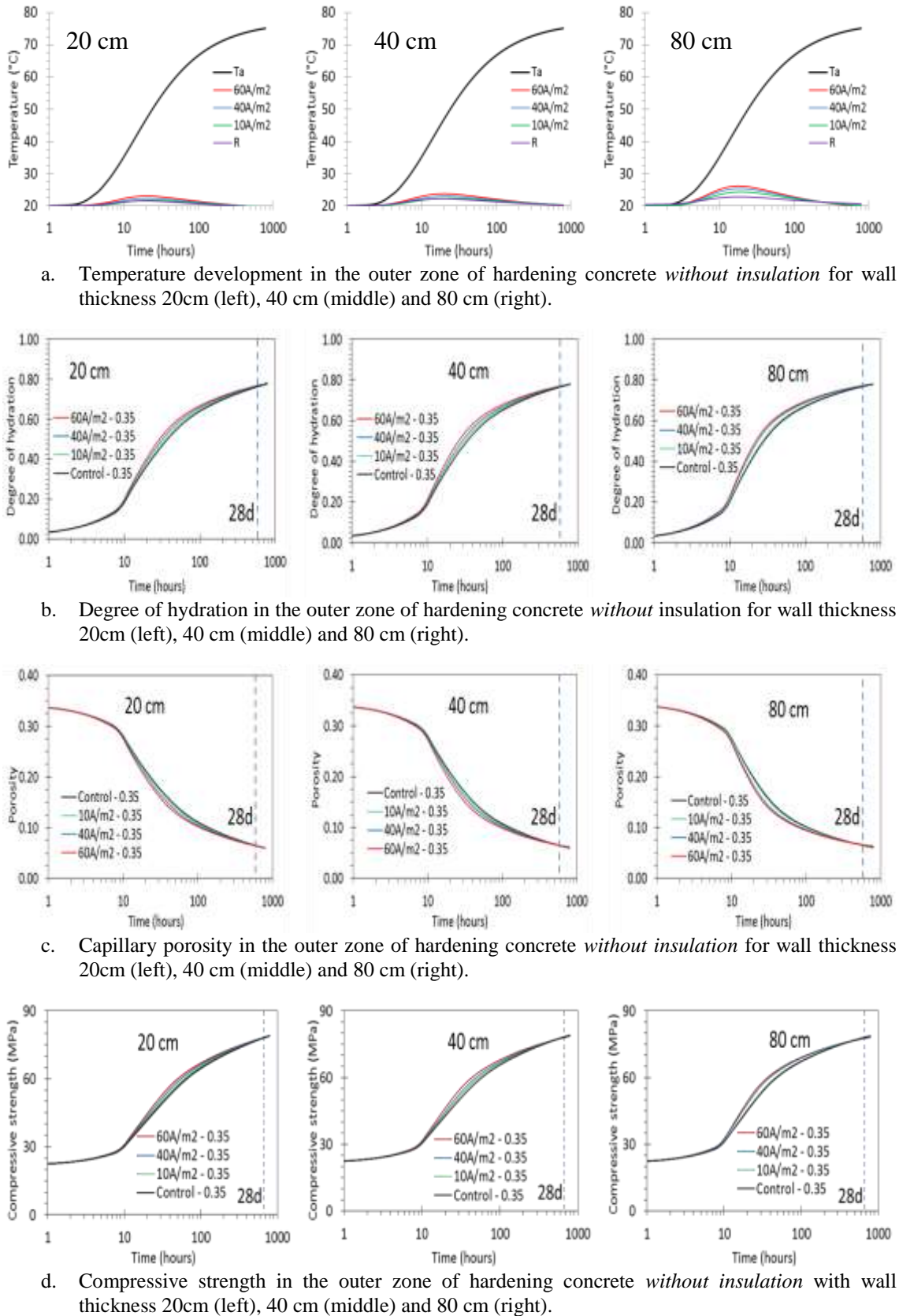


Fig. B.2 Temperature development (a), degree of hydration (b), capillary porosity (c) and compressive strength (d) in the *outer* zone of hardening concrete *without insulation* for different wall thickness (i.e. 20cm, 40 cm and 80 cm) and w/c ratio 0.35.



## **Appendix C**

Numerical simulations results for the evolution of temperature, degree of hydration, capillary porosity and compressive strength in the centre and outer zone of concrete elements with insulation subjected to stray current for different wall thickness

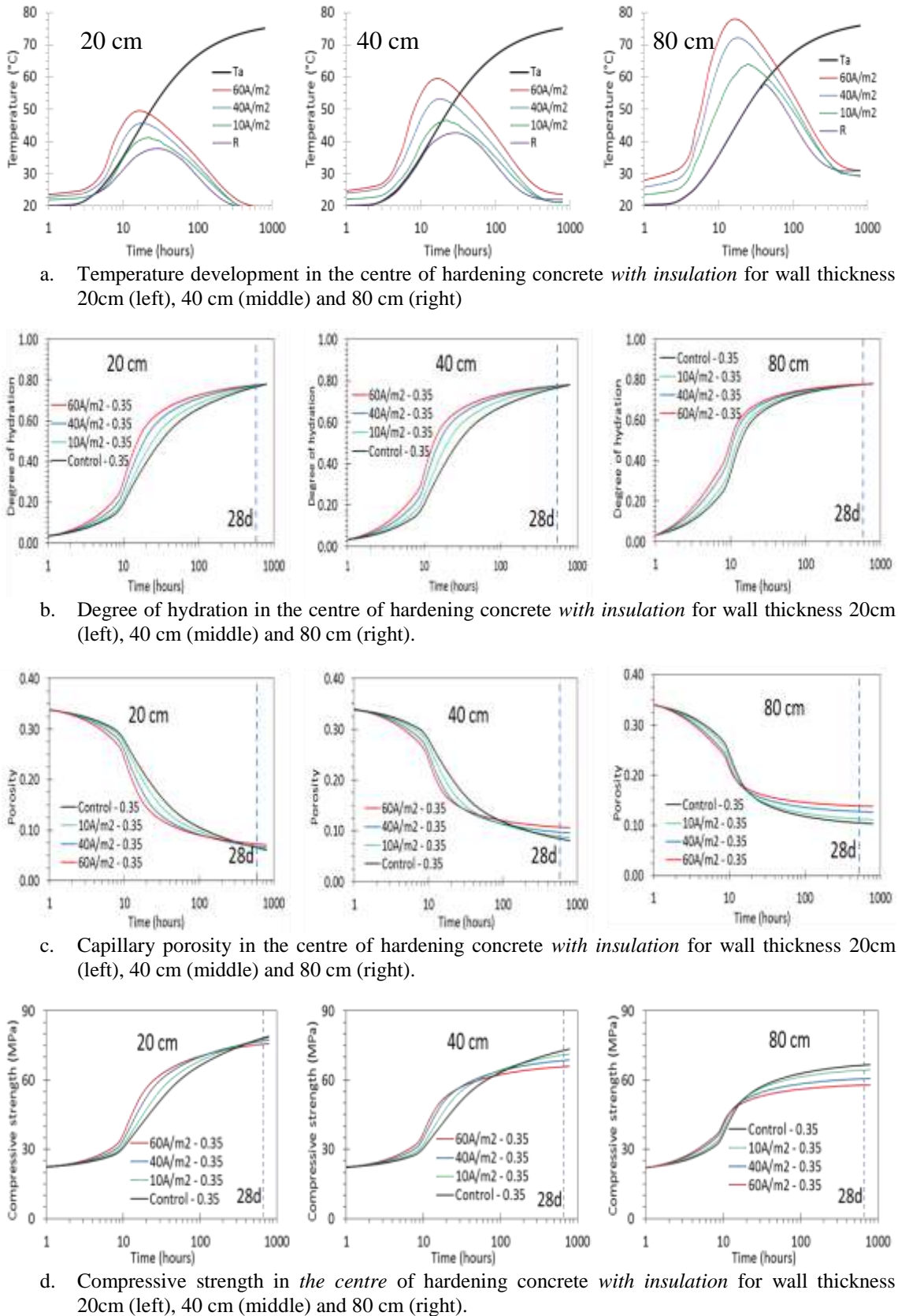
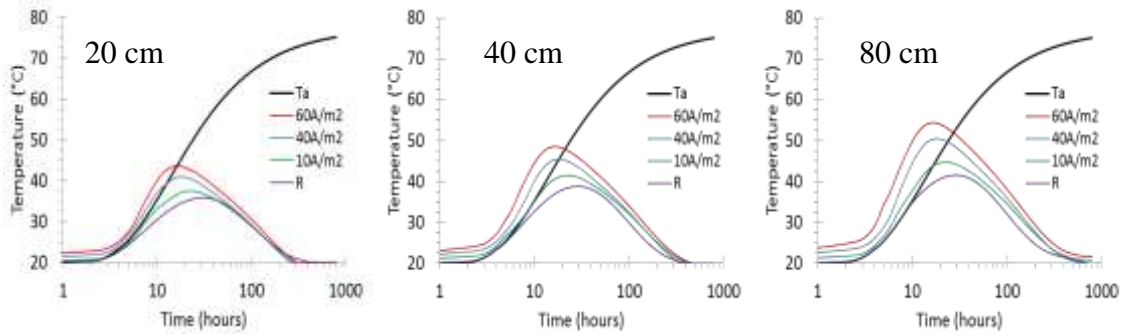
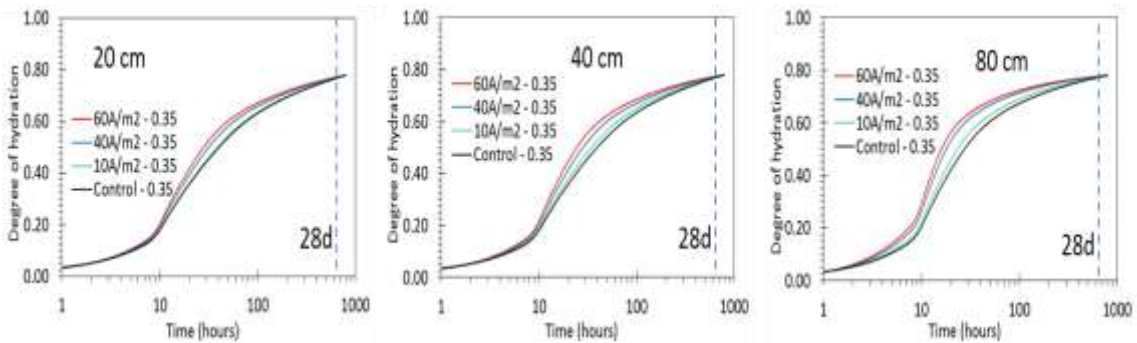


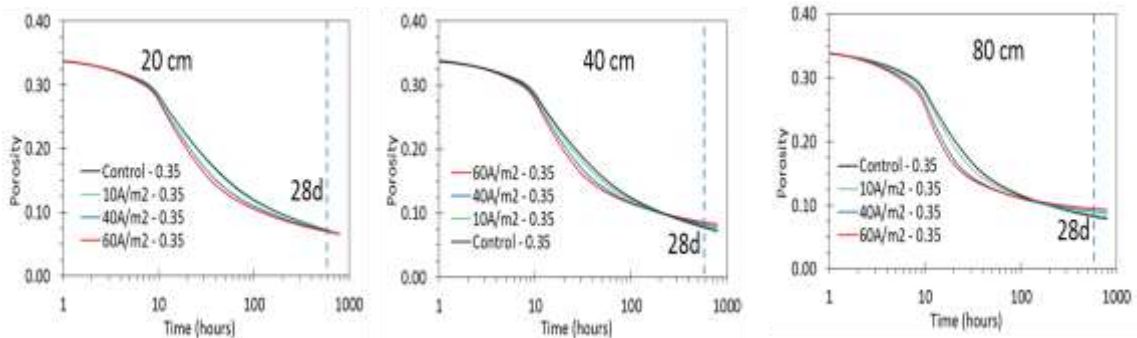
Fig. C.1 Temperature development (a), degree of hydration (b), capillary porosity (c) and compressive strength (d) in the *centre* of hardening concrete *with insulation* for different wall thickness (i.e. 20cm, 40 cm and 80 cm) and w/c ratio 0.35.



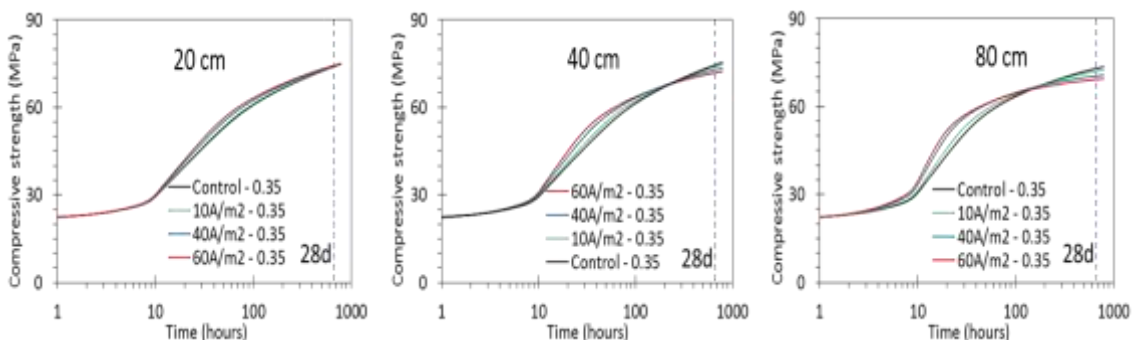
a. Temperature development in the outer zone of hardening concrete *with insulation* for wall thickness 20cm (left), 40 cm (middle) and 80 cm (right).



b. Degree of hydration in the outer zone of hardening concrete *with insulation* for wall thickness 20cm (left), 40 cm (middle) and 80 cm (right).



c. Capillary porosity in the outer zone of hardening concrete *with insulation* for wall thickness 20cm (left), 40 cm (middle) and 80 cm (right).



d. Compressive strength in the outer zone of hardening concrete with insulation with wall thickness 20cm (left), 40 cm (middle) and 80 cm (right).

Fig. C.2 Temperature development (a), degree of hydration (b), capillary porosity (c) and compressive strength (d) in the *outer* zone of hardening concrete *with insulation* for different wall thickness (i.e. 20cm, 40 cm and 80 cm) and w/c ratio 0.35.



## References

---

- Accelerated Curing of Concrete at Atmospheric Pressure —State of the Art, ACI 517.2R-87 (Revised 1992), American Concrete Institute, 1980.
- ACI 207.2R, Report on thermal and volume change effects on cracking of mass concrete, American Concrete Institute.
- ACI Committee 305 Report, “Hot Weather Concreting”, ACI 305R-77 (ACI, Detroit, Mich. 1982).
- ACI Committee 308 Report, “Standard Practice for Curing Concrete”, ACI 308-81 (ACI, Detroit, Mich. 1981).
- Aghajani, A., Saatchi, A., Golozar, M. A., Raeissi, K., & Shabani, S. (2015). Effects of DC Stray Current on Concrete Structures, *AJSR - Civil and Environmental Engineering*, Vol 47, No. 3, Winter 2015, pp. 9-12.
- Aghajani, A., Urgen, M. and Bertolini, L. (2016). “Effects of DC Stray Current on Concrete Permeability.” *J. Mater. Civ. Eng.*, 28 (4).
- Ahmed, D. A., & Ragai, S. M. (2013). Retardation effect and corrosion detection of blended cement pastes. *HBRC Journal*, 9(1), 22-26.
- Al-Ani, S. H., Mokdad, A., and Al Zaiwary, K., (1988). “The effect of curing delay on concrete in hot weather”. *Materials and Structures*, Vol. 21 Number 3, pp. 205-212.
- Alexandra von Meier, *Electric power systems: a conceptual introduction*, p67, 2006, John Wiley & Sons, USA.
- Aligizaki, K. K., (2005). “Pore Structure of Cement-based Materials: Testing, Interpretation and Requirements.” September 27, 2005.
- Aligizaki, K. K., (2006). *Pore structure of cement-based materials*, Taylor & Francis.
- Alonso, C., Andrade, C. and González, J.A., (1988). “Relation Between Resistivity and Corrosion Rate of Reinforcements in Carbonated Mortar made with Several Cement Types,” *Cement and Concrete Research*, Vol. 18 (5), 687-698.
- Al-Zahrani, M. M., Al-Dulaijan, S. U., Ibrahim, M., Saricimen, H., Sharif, F. M., 'Effect of waterproofing coatings on steel reinforcement corrosion and physical properties of concrete', *Cem Concr Compos*, 24 (2002) 127-137.
- Andrade, C., (2010). “Types of models of service life of reinforcement: The case of the resistivity.” *Concrete Research Letters*, Vol. 1 [2] - June 2010.
- Andrade, C., Alonso, C., Arteaga, A., Tanner, P., (2000). “Methodology based on the electrical resistivity for calculation of reinforcement service life.” *Fifth CANMET/ACI International Conference*, 899–915.
- Archie, G.E., (1942) “The electrical resistivity log as an aid in determining some reservoir characteristics.” *Transactions of the American Institute of Mining and Metallurgical Engineers*, 146, 54–62.
- Atkins, P.W., (1990). “Physical chemistry” Oxford: Oxford University Press.
- Audenaert, K., Yuan, Q., de Schutter, G., (2010). On the time dependency of the chloride migration coefficient in concrete. *Constr Build Mater*, 24(3), 396-402.
- Aylott, P. J., Cotton, I. and Charalambous, C. A., (2013). “Impact and management of stray current on DC rail systems.” *CHAPCIS Intertek*, United Kingdom.
- Backe, K. R., Lile, O. B., and Lyomov, S. K. (1998). *Characterising Curing Cement Slurries by Electrical Conductivity*. In *SPE Western Regional Meeting*. Society of Petroleum Engineers.
- Balshin, M. Y. (1949, May). Relation of mechanical properties of powder metals and their porosity and the ultimate properties of porous metal-ceramic materials. In *Dokl Akad Nauk SSSR* (Vol. 67, No. 5, pp. 831-834).
- Bamforth, P.B. (1999), The derivation of input data for modelling chloride ingress from eight year UK coastal exposure trials, *Magazine of Concr. Research*, v. 51, no. 2, pp. 87-96.
- Basheer, P. A. M., (2001). “Concrete Science”, Ch.16, Norwich, Noyes/William Andrew.
- Bentur, A., Berger, R.L., Kung, J.H., Milestone, N.B., Young, J.F. (1979). Structural properties of calcium silicate pastes: II, effect of the curing temperature, *Journal of the American Ceramic Society* 62 (7–8), 362–366.
- Bentz, D. P. (1997). Three Dimensional Computer Simulation of Portland Cement Hydration and Microstructure Development. *Journal of the American Ceramic Society*, 80(1), 3-21.
- Bentz, D. P. (2010). Blending different fineness cements to engineer the properties of cement-based materials. *Magazine of Concrete Research*, 62(5), 327-338.

- Bentz, D. P., Garboczi E. J., (1999). "Effects of cement particle size distribution on performance properties of Portland cement-based materials." *Cement and Concrete Research*, 29 (10): 1663-1671.
- Bentz, D.P. (2006). Influence of water-to-cement ratio on hydration kinetics: simple models based on spatial considerations. *Cement and Concrete Research* 36, 238–244.
- Bertolini, L., Carsana, M., and Pedferri, P., (2007). "Corrosion behaviour of steel in concrete in the presence of stray current." *Corrosion Science*, 49 (3), 1056-1068.
- Bertolini, L., Elsener, B., Pedferri, P. and Polder, R., (2004). "Corrosion of Steel in Concrete – Prevention Diagnosis." *Repair*, Wiley-VCH, Weinheim.
- Boylestad, R. L. (2016). *Introductory circuit analysis*. Pearson Education.
- Bourdi, T., Rhazi, J. E., Boone, F., & Ballivy, G. (2012). Modelling dielectric-constant values of concrete: An aid to shielding effectiveness prediction and ground-penetrating radar wave technique interpretation. *Journal of Physics D: Applied Physics*, 45(40), 405401.
- Bourdi, T., Rhazi, J. E., Boone, F., and Ballivy, G. (2008). Application of Jonscher model for the characterization of the dielectric permittivity of concrete. *Journal of Physics D: Applied Physics*, 41(20), 205410.
- Brandt, A. M. (2009). *Cement-based composites: materials, mechanical properties and performance*. CRC Press.
- Bredenkamp, S., Kruger, D. and Bredenkamp, G.L., (1993). "Direct electric curing of concrete." *Magazine of Concrete Research*, Vol. 45, No. 162, March 1993, pp. 71-74.
- Brichau, F., Deconinck, J. and Driesens, T., (1996). "Modeling of underground cathodic protection stray currents." *Corrosion Engineering*, June, 1996.
- Broomfield, J. B., (1997). "Corrosion of Steel in Concrete." FN Spon, an Imprint of Chapman & Hall, London, UK, 238 pages.
- Broomfield, J. P., Rodriguez, J., Ortega, L.M. and Garcia, A. M., (1993). "Corrosion Rate Measurement and Life Prediction for Reinforced Concrete Structures," *Proceedings of Structural Faults and Repair*, 93 (2), 155-164, Engineering Technical Press, University of Edinburgh, U.K.
- Brouard, M., Parker, D. H., & van de Meerakker, S. Y., (2014). Taming molecular collisions using electric and magnetic fields. *Chemical Society Reviews*, 43(21), 7279-7294.
- Brown, P., Barret, P., Double, D. D., Frohnsdorff, G., Johansen, V., Parrot, L. J. & Young, J. F. (1986). Hydration of tricalcium aluminate and tetracalcium aluminoferrite in the presence of calcium sulfate, 19, pp. 137-147.
- Brown, P.W., Dex, S., Skalny, J.P., (1993) Porosity/permeability relationships. Parts of 'Concrete microstructure porosity and permeability'. Roy DM, Brown PW, Shi D, Scheetz BE, May W. Strategic Highway Research Program, National Research Council, Washington, DC 1993. SHRP-C-628
- Brown, R. D., (1980). "Mechanisms of Corrosion of Steel in Concrete in Relation to Design, Inspection and Repair of Offshore and Coastal Structures." ACI SP-65, Performance of Concrete in Marine Environments, 169-204, American Concrete Institute, Farmington Hills, MI.
- Brown, T. D., and Javaid, M. Y., (1970). The thermal conductivity of fresh concrete. *Matériaux et Construction*, 3(6), 411-416.
- Brue, F., Davy, C.A., Skoczylas, F., Burlion, N., (2012). Effect of temperature on the water retention properties of two high-performance concretes, *Cem. Concr. Res.* 42, 384–396.
- Brunauer, S., Yudenfreund, M., Odler, I., & Skalny, J. (1973). Hardened portland cement pastes of low porosity VI. Mechanism of the hydration process. *Cement and Concrete Research*, 3(2), 129-147.
- Bürchler, D., Elsner, B., and Böhni, H., *Electrical Resistivity and Dielectric Properties of Hardened Cement and Mortar*, Institute of Materials Chemistry and Corrosion, Swiss Federal Institute of Technology, ETH Hönggerber, CH-8093 Zurich, Switzerland, 1996.
- Caballero, J., Polder, R. B., Leegwater, G. A., Fraaij, A. L. A. (2012) Chloride penetration into cementitious mortar at early age. *Heron* 57(3):185–196
- Cady, P. D. and Weyers, R. E., (1984). "Deterioration rate of concrete bridge decks." *J. Transp. Eng.*, 110 (1), 34-44.
- Cao, X. (1997). Modeling electrokinetically enhanced transport of multispecies in porous media under transient electrical field, Master thesis, Lehigh University.
- Care, S. (2008). Effect of temperature on porosity and on chloride diffusion in cement pastes. *Construction and Building Materials*, 22(7), 1560-1573.
- Carlson, R.W., 1937, ACI-J, Vol. 34, Nov.-Dec., pp. 89-102.

- Castellote, M., Andrade, C., d'Andréa, R., (2009). "The use of resistivity for measuring aging of chloride diffusion coefficient." Proceedings RILEM TC 211-PAE International Conference - Concrete in Aggressive Aqueous Environments, Toulouse.
- Chakradhara Rao, M. (2010). Characterisation and behaviour of recycled aggregate concrete (Doctoral dissertation, Ph. D. Thesis, Indian Institute of Technology Kharagpur, West Bengal, India).
- Chang, J. J., (2003). "Bond degradation due to the desalination process." *Construction and Building Materials*, 17, 281–287.
- Charalambous, C. A. and Aylott, P., (2014). "Dynamic stray current evaluations on cut-and-cover sections of DC metro systems." *IEEE Transactions on Vehicular Technology*, 63(8), 3530-3538.
- Che, F., Gray, J. T., Ha, S., Kruse, N., Scott, S. L., & McEwen, J. S. (2018). Elucidating the Roles of Electric Fields in Catalysis: A Perspective. *ACS Catalysis*, 8(6), 5153-5174.
- Chen, M., Wang, K., Wu, Q., and Qin, Z. (2012). "An experimental corrosion investigation of coupling chloride ions with stray current for reinforced concrete." *Applied Mechanics and Materials*, Vol. 166, pp. 1987-1993.
- Chen, Z. G., Qin, C. K., Zhang, Y. J. and Tang, J. X., (2011). "Research of impact of stray current from urban rail transit system on buried gas pipeline." *Advanced Material Research*, Vols. 239-242, 1219-1222.
- Chen, Z., Koleva, D. A., & van Breugel, K. (2017). Electrochemical Tests in Reinforced Mortar Undergoing Stray Current-Induced Corrosion. In *Concrete Durability* (pp. 83-108). Springer, Cham.
- Claisse, P. A. (2014). Transport properties of concrete: Measurements and applications. Elsevier.
- Clover, R.E., 1937, *ACI-J*, Vol. 34, pp. 105-116
- Cook, R.A. and Hover, K.C. (1993) 'Mercury porosimetry of cement-based materials and associated correction factors,' *American Concrete Institute Materials Journal*, vol. 90 (2) pp. 152-161.
- Cook, R.A., Hover, K.C. (1999) 'Mercury porosimetry of hardened cement pastes', *Cement and Concrete Research*, vol.29 (6) pp. 933-943.
- CUR-Bouw&Infra 2009. Duurzaamheid van constructief beton met betrekking tot chloride-geïnitieerde wapeningscorrosie - Leidraad voor het formuleren van prestatie-eisen- Achtergrondrapport (in Dutch), Tu Delft, 19 Mei 2009.
- DANISH Ministry of Transport, 'The road directorate: the concrete of the Faroe bridges', 1985, pp.156.
- Deshmukh, S. D., & Tsori, Y. (2016). Communication: Control of chemical reactions using electric field gradients, *The Journal of Chemical Physics*, 144, 191102 (2016).
- Diamond, S. (1971) 'A critical comparison of mercury porosimetry and capillary condensation pore size distributions of Portland cement pastes', *Cement and Concrete Research*, vol. 1 (5) pp. 531-545.
- Diamond, S. (2000) 'Mercury porosimetry: an inappropriate method for the measurement of pore size distributions in cement-based materials', *Cement and Concrete Research*, vol. 30 (10) pp. 1517-1525.
- Ding, Q., Geng, J. and Hu, S., (2008). "The effect of stray current on the process and threshold concentration of chloride ion causing steel bar corrosion." 1st International Conference on Microstructure Related Durability of Cementitious Composites, 13-15 October 2008, Nanjing, China.
- Duranceau, S. J., Johnson, W.J. and Pfeiffer-Wilder, R. J., (2011). "A study examining the effect of stray current on the integrity of continuous and discontinuous reinforcing bars." *Experimental Techniques*, September/October 2011.
- Elkey, W., & Sellevold, E. J. (1995). Electrical resistivity of concrete.
- Elkhadiri, I., Palacios, M., Puertas, F. Effect of curing temperature on cement hydration, *Ceramics – Silikáty* 53 (2) 65-75 (2009) 65.
- Elsener, B., & Angst, U. (2007). Mechanism of electrochemical chloride removal. *Corrosion Science*, 49(12), 4504-4522.
- EN 50122-2: 1999, "Railway applications-Fixed installations, Part 2: Protective provisions against the effect of stray currents caused by d.c. traction systems".
- EN-50122-1:1997, "Railway applications-Fixed installations, Part 1: Protective Provisions relating to electrical safety and earthing".
- EN50122-3:2010, "Railway applications – Fixed installations – Electrical safety, earthing and the return circuit Part 3. Mutual Interaction of a.c. and d.c. traction systems".
- Erdem, T. (2003). "Setting time: an important criterion to determine the length of the delay period before steam curing of concrete". *Cement and Concrete Research*. 33: 741–050.
- Ernati, Tjaronge, M. W., & Irfan, U. R. (2015). Porosity, pore size and compressive strength of self compacting concrete using sea water. *Procedia Engineering*, 125, 832-837.

- Escalante-Garcia, J. I., & Sharp, J. H. (2000). The effect of temperature on the early hydration of Portland cement and blended cements. *Adv Cem Res*, 12(3), 121-130.
- Escalante-Garcia, J.I. (2003). Non-evaporable water from neat OPC and replacement materials in composite cements hydrated at different temperatures, *Cement and Concrete Research* 33 (11), 1883–1888.
- Federation Internationale de la Precontrainte (FIP), (1982). Acceleration of concrete hardening by thermal curing: guide to good practice, pp. 1–16.
- Feliu, S., Andrade, C., Gonzalez, J.A., Alonso, C. (1996) A new method for in situ measurement of electrical resistivity of reinforced concrete. *Mater Struct* 29:362–365.
- Galsgaard, F. and Nielsen L. V., (2006). “AC/DC interference corrosion in pipelines.” Summary report by MetriCorr., The Danish Gas Technological Center.
- Garboczi, E. J. (1990). Permeability, diffusivity, and microstructural parameters: a critical review. *Cement and concrete research*, 20(4), 591-601.
- Garboczi, E.J. and Bentz, D.P. (1992). Computer simulation of the diffusivity of cement-based materials, *Journal of Materials Science*, 27(8), 2083-2092.
- Gehlen, C. (2000) Probabilistische Lebensdauerbemessung von Stahlbetonbauwerken, Dafst 510. Beuth Verlag, Berlin
- Geng, J., Ding, Q. and Hu, S., (2008). “Influence of stray current and chloride ion on the compressive strength of reinforce concrete.” 1st International Conference on Microstructure Related Durability of Cementitious Composites, 13-15 October 2008, Nanjing, China.
- Gjørøv OE, Vennesland Ø, El-Busaidy, AHS. Electrical resistivity of concrete in the oceans. 9th Annual Offshore Technology Conference. 1977, paper 2803. Houston.
- Granju, J.L., 1974, M&C, Vol. 7, No. 37, pp. 25-35.
- Griffiths, David (1999). Introduction to Electrodynamics (3 ed.). Upper Saddle River, NJ: Prentice-Hall. p. 289.
- Grudemo, A. (1975). Development of strength properties of hydrating cement pastes and their relation to structural features, *Proc. Symp. on Some Recent Research on Cement Hydration*, 8 pp. (Cembureau, 1975).
- Gulikens J, 2006. Pitfalls and practical limitation in probabilistic service life modeling of reinforced concrete structures, in Proceedings of the Eurocorr 2006, Maastricht 25-28 September 2006.
- Guyer, J. P. (Ed.). (2018). An introduction to cathodic protection. Guyer Partners.
- Hale, W.M., Bush, T.D., Russell, B.W., Freyne, S.F., Effect of curing temperature on hardened concrete properties, *Transportation Research Record: Journal of the Transportation Research Board* 1914 (2005) 97–104.
- Halliday, D., Resnick, R., & Walker, J. (2013). *Fundamentals of Physics*. John Wiley & Sons.
- Hamlin, A. W., (1986). “Alternating current corrosion.” *Materials Performance*, 25 (1), 55–58.
- Hammond, E. and Robson, T. D., Comparison of electrical properties of various cement and concretes, *the Engineer*, Jan. 21, 1995, pp. 78-80.
- Helland, S. (1986), *Nordisk Betong*, 1-2-1986, pp. 63-70
- Heritage, I. (2001). Direct electric curing of mortar and concrete, Napier University, Edinburgh, UK.
- Hewlett P. C. (2004). *Lea’s chemistry of cement and concrete*, 4th ed. Oxford: Butterworth-Heinemann.
- Hewlett, P. C., (2003). “Lea’s chemistry of cement and concrete.” New York: John Wiley & Sons, Inc.
- Hu, J. (2004). Porosity of concrete, morphological study of model concrete, PhD thesis, Delft University of Technology, Delft.
- Hu, J. and Stroeven, P. (2006). “Proper characterisation of pore size distribution in cementitious materials, International Symposium on Environmental Ecology and Technology of Concrete (EETC 2005), JUN 06-08, 2005 Urumqi, China, Environmental Ecology and Technology of Concrete, Key Engineering Materials 302-303, 479-485.
- Hu, J. and Stroeven, P., (2003). “Application of image analysis to assessing critical pore size for permeability prediction of cement paste.” *Image Analysis & Stereology*, 22, 97-103.
- Hu, J., (2004). “Porosity of concrete, morphological study of model concrete.” PhD thesis, Delft University of Technology, Delft.
- Huang, Q., Wang, C., Zeng, Q., Yang, C., Luo, C., & Yang, K. (2016). Deterioration of mortars exposed to sulfate attack under electrical field. *Construction and Building Materials*, 117, 121-128.
- Hughes, B.P., Soleit, A.K.O., and Brierly, R.W. (1985), “New Technique for Determining the Electrical Resistivity of Concrete,” *Magazine of Concrete Research*, Vol. 37, No. 133, pages 243-248.
- Hughes, D.C. (1985) ‘Pore structure and permeability of hardened cement paste, *Magazine of concrete research*’, vol. 37 (133) pp. 227-233.

- Hunkeler, F., "The Resistivity of Pore Water Solution - A Decisive Parameter of Rebar Corrosion and Repair Methods," *Construction and Building Materials*, Vol. 10, No. 5, pages 381 to 389, 1996.
- IEC 61439 (Italian standard), Part 1 and Part 2, "Low voltage assemblies and relevant applicability".
- IS 456:2000, Indian Standard-"Plain and Reinforced concrete-Code of Practice", 4th revision, page 27.
- James K. Cable, Kejin Wang and Zhi Ge, (2002). "Investigation into improved pavement curing materials and Techniques, part 1 (phase I and II)." Iowa DOT TR-451. Iowa Highway Research Board 800 Lincoln way.
- Jianming, J. (2002). *The Finite Element Method in Electromagnetics*, 2<sup>nd</sup> ed., Wiley-IEEE Press, May 2002.
- John, G.W. and Narendra, K.G., (2004). "Equipment for the investigation of the accelerated curing of concrete using direct electrical conduction." *Measurement* 35, 243–250.
- Jones, D. A., (1978). "Effect of alternating current on corrosion of low alloy and carbon steels." *Corrosion*, 34 (12), 428–433.
- Kafry, I. D., (1980). 'Direct electrical curing of precast products', *Precast Concrete*, Vol. II, no. 7.
- Kai, W., Quan-shui, W., Chen, M. and Li, X., (2011). "Corrosion fatigue of reinforced concrete in the presence of stray current." *IEEE*, 1133-1136.
- Kale, E.D. and Sanders, M. Prevention of stray current by the maintenance-of-way, Dallas, Texas.
- Katz, A.J. and Thompson, A.H. (1986) 'Quantitative prediction of permeability in porous rock', *Physical Review. B*, vol. 34 pp. 8179–8181.
- Kerimov, A. M., Spirin, P. A. and Kerimov, R. A., (2006). "Relationship between the parameters of stray current circuits and the traction load." *Protection of Metals*, 42 (4), 409–411.
- Kim, Y. S., Jeong, G. J. and Sohn, H. J., (1999). "Mathematical modeling on the corrosion of unprotected structure due to stray current resulting from cathodic protection." *System, Metals and Materials*, 5 (1), 93-99.
- Kish, G. D., (1981). "Control of Stray Currents in Underground DC Railway Systems." *Materials Performance*, Vol. 20 (9), 27-31.
- Kjellsen, K.O. and Detwiler, R.J. (1992). Reaction kinetics of Portland cement mortars hydrated at different temperatures, *Cement and Concrete Research* 22 (1), 112–120.
- Kjellsen, K.O., Detwiler, R.J., Gjorv, O.E. (1990). Backscattered electron imaging of cement pastes hydrated at different temperatures, *Cem. Concr. Res.* 20, 308–311.
- Kjellsen, K.O., Detwiler, R.J., Gjorv, O.E. (1991). Development of microstructures in plain cement pastes hydrated at different temperatures, *Cem. Concr. Res.* 21, 179–189.
- Koenders E.A.B. (2005). Mix design for venice barriers, Report Nr. 15.5-05-08, Confidential Communication.
- Kolář, V., & Hrbáč, R. (2014, May). Measurement of ground currents leaking from DC electric traction. In *Proceedings of the 2014 15th International Scientific Conference on Electric Power Engineering (EPE)* (pp. 613-617). IEEE.
- Koleva, D. A., van Breugel, K. and de Wit, J. H.W., (2008). "The effect of electrical current flow, as a simulation of cathodic prevention, on early hydration rate and microstructure of cement-based materials", paper No: 1486 pp. 1-7, EUROCORR 2008, Edinburgh, UK, 7th – 11th September 2008, Publ. European Federation of Corrosion, No:299.
- Koleva, D. A., de Wit, J. H. W., van Breugel, K., Veleva, L., van Westing, E. P. M., Copuroglu, O. and Fraaij, A. L. A., (2008). "Correlation of microstructure, electrical properties and electrochemical phenomena in reinforced mortar. Breakdown to multi-phase interface structures. Part II: pore network, electrical properties and electrochemical response." *Materials Characterization*, 59, 801-815.
- Koleva, D. A., Van Breugel, K., De, W., Delft, T. U., Civil, E., & Geosciences, T. D. D. (2007). *Corrosion and protection in reinforced concrete: Pulse cathodic protection: an improved cost-effective alternative*. TU Delft.
- Koleva, D.A., Copuroglu, O., van Breugel, K., Ye, G. and de Wit, J. H. W., (2008). "Electrical resistivity and microstructural properties of concrete materials in conditions of current flow." *Cem.Concr.Compos.*, 30, 731-744.
- Kondo, R. and Ueda, S. (1968). Kinetics and Mechanisms of the Hydration of Cements, *Proceedings of the Fifth International Symposium on the Chemistry of Cement*, Tokyo, pp. 203–248.
- Kurumisawa and Nawa, (2016). "Electrical conductivity and chloride ingress in hardened cement paste, *Journal of Advanced Concrete Technology*, 14(3), 87-94.
- Kwan, A.K.H. and Ma, F.J. Two-dimensional early thermal crack analysis of concrete structures by finite element method, *Engineering Structures* 143 (2017) 1–10.

- Lakshminarayanan, V., Ramesh, P.S., Rajagopalan, S.R., (1992). "A new technique for the measurement of the electrical resistivity of concrete." *Magazine of Concrete Research*, 44(158), 47–52.
- Lange, D.A., Jennings, H.M., Shah, S.P. (1994). Image analysis techniques for characterization of pore structure of cement-based materials, *Cement and Concrete Research* 24 (5):841-53.
- Lawrence, A. M. (2009), A finite element model for the prediction of thermal stresses in mass concrete, Doctoral thesis, University of Florida.
- Layssi, H., Ghods, P, Alizadeh, A.R., and Salehi, M., Electrical Resistivity of concrete- Concepts, applications, and measurement techniques, *Concrete International*, May 2015.
- Lemeshko, M., Kreams, R. V., Doyle, J. M., & Kais, S. (2013). Manipulation of molecules with electromagnetic fields. *Molecular Physics*, 111(12-13), 1648-1682.
- Lian, C., Zhuge, Y., & Beecham, S. (2011). The relationship between porosity and strength for porous concrete. *Construction and Building Materials*, 25(11), 4294-4298.
- Liang, M. T., Lin, L. H. and Liang, C. H., (2002). "Service life prediction of existing RC bridges exposed to chloride environment." *Journal of Infrastructure System*, 76-85.
- Liang, M.T., Wang, K. L., and Liang, C. H., (1999). "Service life prediction of reinforced concrete structures." *Cem. Concr. Res.*, 29, 1411-1418.
- Lin, Y., and Chen, H. L. (2015). Thermal analysis and adiabatic calorimetry for early-age concrete members. *Journal of Thermal Analysis and Calorimetry*, 122(2), 937-945.
- Lingvay, C., Cojocar, A., Visan, T. and Lingvay, I., (2011). "Degradation of reinforced concrete structures due to DC and AC stray currents." *U.P.B. Sci. Bull., Series B*, Vol. 73, Iss. 4.
- Liu, P., and Chen, G. F. (2014). *Porous materials: processing and applications*. Elsevier.
- Liu, Q., Li, L., Easterbrook, D., Yang, J. (2012). Multi-phase modelling of ionic transport in concrete when subjected to an externally applied electric field, *Engineering Structures* 42, 201-213.
- Liu, Y.Q., Liang, Z. S., Chen, H. Y. and Luo, P., (2011). "Use FFT method for the detection and characterization of pipeline's AC stray current interference." *NACE international Corrosion and conference and expo*, 2011.
- Liu, Y., and Shi, X. (2012). Ionic transport in cementitious materials under an externally applied electric field: Finite element modeling. *Construction and Building Materials*, 27(1), 450-460.
- Livingston, R.A., Schweitzer, J.S., Rolfs, C., Becker, H-W. and Kubsky, S. (2001). Characterization of the induction period in tricalcium silicate hydration by nuclear resonance reaction analysis, *J. Mater. Res.*, Vol. 16, No. 3, Mar 2001.
- Lothenbach, B., Matschei, T., Möschner, G., & Glasser, F. P. (2008). Thermodynamic modelling of the effect of temperature on the hydration and porosity of Portland cement. *Cement and Concrete Research*, 38(1), 1-18.
- Lyklema, J. (1995) *Fundamentals of Interface and Colloid Science*, Vol. 2, p. 3.208.
- Maage, M., Helland, S., Poulsen, E., Vennesland, O., and Carl, J. E. (1996). Service life prediction of existing concrete structures exposed to marine environment, *ACI Materials Journal*, 93(6), 602-608.
- MacDonald, K. A., and Northwood, D.O., (1999). Rapid estimation of water-cementitious ratio and chloride ion diffusivity in hardened and plastic concrete by resistivity measurement, S-P-191, M. S. Khan, American Concrete Institute, Farmington Hills, pp 57–68.
- MacDonald, K.A. and Northwood, D.O. (1995). Experimental measurements of chloride ion diffusion rates using a two-compartment diffusion cell: effects of material and test variables. *Cem Concr Res* 25(7):1407–1416
- Maes, M., Caspeele, R., Van den Heede, P., De Belie, N. (2013) Influence of sulphates on chloride diffusion and the effect of this on service life prediction of concrete in a submerged marine environment. In: Strauss A, et al *Life-cycle and sustainability of civil infrastructure systems proceedings of the third international symposium on life-cycle civil engineering (IALCCE'12)*, Vienna, 3–6 Oct, 2012. pp 899–906.
- Mangat, P., Molloy, B. (1994). Prediction of long term chloride concentration in concrete. *Mater Struct*, 27(6), 338-346.
- Marcotte, T.D., Hansson, C.M. and Hope, B.B., (1999). "The effect of the electrochemical chloride extraction treatment on steel-reinforced mortar Part I: Electrochemical measurements." *Cement and Concrete Research*, 29, 1555–1560.
- McCarter, W. J., Butler, A., Chrisp, T.M., Emerson, M., Starrs, G. and Blewett, J., (2001). "Field trials on concrete monitoring sensors," *Proceedings of the Institution of Civil Engineers - Structures and Buildings*, 146(3), 295-305.
- McCarter, W. J., Chrisp, T. M., Starrs, G., Basheer, P. A. M., & Blewett, J. (2005). Field monitoring of electrical conductivity of cover-zone concrete. *Cement and Concrete Composites*, 27(7-8), 809-817.

- McInerney, M. K., Cooper, S. G., Hock, V. F., & Morefield, S. W. (2004, January). Measurements of Water and Ion Transport in Concrete Via Electro-osmosis. In *CORROSION 2004*. NACE International.
- McInerney, M. K. et al (2002). *Electro-Osmotic Pulse (EOP) Technology for Control of Water Seepage in Concrete Structures* (No. ERDC/CERL-TR-02-21). Engineer Research and Development Center Champaign II Construction Engineering Research Lab.
- Mehta, P. K. and Monteiro, P.J.M., (2001). "Concrete: Microstructure, Properties and Materials", McGraw-Hill, October 20, 2001.
- Mehta, P.K. and Manmohan, C. (1980) 'Pore size distribution and permeability of hardened cement paste', 7th International congress on the chemistry of cement, Paris, France, vol. 3 (7) pp. 1-5.
- Merrick, M. F., (1994). "Stray Current Control Metropolitan Atlanta Rapid Transit System," Stray Current Corrosion: The Past, Present, and Future of Rail Transit Systems." Michael J. Szeliga, ed., 125-136, NACE International, Houston, TX.
- Millard, S.G. and Gowers K.R. (1992). Resistivity assessment of in-situ concrete: the influence of conductive and resistive surface layers, Proc. Inst. Civil. Eng. Struct. Build., 94(4):389-96.
- Mindess, S., Young, J.F., Darwin, D. (2003). Concrete: Prentice-Hall, Upper Saddle River, New Jersey, USA.
- Mithra, R., Selvaraj, R., & Suganya, O. (2017). Electro-kinetic technique for enhancing durability of concrete. *International Journal of Civil Engineering and Technology (IJCIET)*, 8(4), 801-808.
- Monfore, G.E. "The Electrical Resistivity of Concrete," *Journal of the PCA Research and Development Laboratories*, Vol. 10, No. 2, pages 35 to 48, May 1968.
- Mosavat, N., Oh, E., & Chai, G. (2012). A review of electrokinetic treatment technique for improving the engineering characteristics of low permeable problematic soils. *International journal of GEOMATE*, 2(2), 266-272.
- Nehdi and Soliman, (2011). "Early-age properties of concrete: overview of fundamental concepts and state-of-the-art research." *Construction Materials*, 164: 57-77.
- Neville, A. M., (1995). "Properties of concrete." 4th and final Ed., Longman's, London.
- Newmark, N.M., (1938). ACI-J, Vol. 34, March-April, pp. 104-115.
- Ngala, V. T., Page, C. L., Parrott, L., & Yu, S. W. (1995). Diffusion in cementitious materials: II, further investigations of chloride and oxygen diffusion in well-cured OPC and OPC/30% PFA pastes. *Cement and Concrete Research*, 25(4), 819-826.
- NT BUILD 443, Approved 1995-11, Concrete, Hardened: Accelerated Chloride Penetration
- Numata, S., Amano, H., and Minami, K. (1990). Diffusion of tritiated water in cement materials. *Journal of Nuclear Materials*, 171(2-3), 373-380.
- Odler, I., et al., 1986, SMDDHC, MRS, Boston, Proc. Vol. 85, pp. 33-38.
- Odler, I., et al., 1979, CCR, 9, pp. 239-248; 9, pp. 277-284; Disc. 9, pp. 799.
- Page, C.L., Short, N.R., Holden, W.R., "The influence of different cements on chloride-induced corrosion of reinforced steel", *Cem. Concr. Res.*, 16, 79-86 (1986).
- Pan, C., Geng, J., & Ding, Q. (2018). Stray Current Affects the Release of Bound Chloride Ions in Hydrated Cement Paste. *Int. J. Electrochem. Sci*, 13, 6098-6111.
- Peelen, W., Polder, R.B., Siemes, A.J.M. (2002). "State-of-the-art stray current induced corrosion." Report DARTS, p. 21.
- Peelen, W.H.A. and Courage, W.M.G., "An advanced finite element reliability tool for stray current corrosion assessments." TNO, Delft, Netherlands.
- Phung, Q. T., et al. (2016). Modelling the evolution of microstructure and transport properties of cement pastes under conditions of accelerated leaching, *Construction and Building Materials* 115, 179-192
- Pichler, C., Schmid, M., Traxl, R., & Lackner, R. (2017). Influence of curing temperature dependent microstructure on early-age concrete strength development. *Cement and Concrete Research*, 102, 48-59.
- Pimenta Teixeira, K., Perdigão Rocha, I., De Sá Carneiro, L., Flores, J., Dauer, E. A., and Ghahremaninezhad, A. (2016). The effect of curing temperature on the properties of cement pastes modified with TiO<sub>2</sub> nanoparticles. *Materials*, 9(11), 952.
- Polder R., Andrade C., Elsener B., Vennesland O., Gulikers J., Weidert R. and Raupach M., Rilem TC 154-EMC: electrochemical techniques for measuring metallic corrosion - Test methods for on site measurement of resistivity of concrete, *Materials and Structures/Materiaux et Constructions*, Vol. 33, December 2000, pp 603-611.

- Powers, T. C., Proceedings, Fourth International Symposium on the Chemistry of Cement, Monograph 43, National Bureau of Standards, U.S. Department of Commerce, Washington, DC, Vol. II, 1962, pp. 577–608.
- Powers, T. C., (1958). “The physical structure and engineering properties of concrete.” PCA Res Dept Bull: 90.
- Powers, T.C., et al., 1946/1947, ACI-J, Part 1-9.
- Presuel-Moreno, F., Wu, Y. Y., and Liu, Y. (2013). Effect of curing regime on concrete resistivity and aging factor over time. *Construction and Building Materials*, 48, 874-882.
- Pritula, E.V.A. and Pritula, V.V. (1960). “Protection of underground installations from corrosion by stray current.” *Metallov*, Aug. 1960, #8, pp. 39-47.
- Probststein, R.F. (2003). “Physicochemical hydrodynamics – An Introduction”, John Wiley and Sons, Inc.
- Pryor, R. W., (2011). “Multiphysics Modeling using COMSOL: a First Principles Approach.” Jones and Bartlett Publisher, Sudbury, Massachusetts, USA.
- Revie, R. W. (2008). Corrosion and corrosion control: an introduction to corrosion science and engineering. John Wiley & Sons.
- Riskin, J. (2008). “Electrocorrosion and Protection of Metal: general approach with particular consideration to electrochemical.” 1<sup>st</sup> Ed, Oxford, UK.
- Rößler, M., & Odler, I. (1985). Investigations on the relationship between porosity, structure and strength of hydrated portland cement pastes I. Effect of porosity. *Cement and Concrete Research*, 15(2), 320-330.
- Rosin, P. and Rammler, E., 1933. Laws governing the fineness of powdered coal, *J. Inst.Fuel*, I: 29.
- Roy, D. M. and Idorn, G. M., (1993). “Concrete Microstructure.” Strategic Highway Research Program, National Research Council, Washington, DC.
- Safiuddin, M., Soudki, K., 'Sealer and coating systems for the protection of concrete bridge structures', *International Journal of the Physical Sciences*, 6 (2011) 8188 8199.
- Sahu, S., Badger, S., Thaulow, N., Lee, R.J., (2004). “Determination of water–cement ratio of hardened concrete by scanning electron microscopy.” *Cement & Concrete Composites* 26 (2004) 987–992.
- Saito, H. and Nakane, S., (1999). "Comparison between diffusion test and electrochemical acceleration test for leaching degradation of cement hydration products." *ACI Mater. J.*, 96 (2), 208-213.
- Saito, H., and Deguchi, A. (2000). Leaching tests on different mortars using accelerated electrochemical method. *Cement and Concrete Research*, 30(11), 1815-1825.
- Saito, H., Nakane, S., Ikari, S. and Fujiwara, A., (1992). “Preliminary study on the deterioration of cementitious materials by an acceleration method.” *Nuclear Engineering and Design*, 138, 151-155.
- Saridemir, M., Severcan, M. H., Ciflikli, M., Celikten, S., Ozcan, F., & Atis, C. D. (2016). The influence of elevated temperature on strength and microstructure of high strength concrete containing ground pumice and metakaolin. *Construction and Building Materials*, 124, 244-257.
- Šavija, B., Luković, M., and Schlangen, E. (2014). Lattice modeling of rapid chloride migration in concrete. *Cement and Concrete Research*, 61, 49-63.
- Scrivener, K.L. (1989). The use of backscattered electron microscopy and image analysis to study the porosity of cement paste. In: Roberts LR and Skalny JP, eds. *Proc.of Material Research Society Symposium* 137, Boston, 129-40.
- Sengul, O. (2013). Factors affecting the electrical resistivity of concrete, *Nondestructive Testing of Materials and Structures*, RILEM Bookseries 6, doi 10.1007/978-94-007-0723-8-38, © RILEM 2013.
- Sengul, O., and Gjørsv, O. E. (2008). Electrical resistivity measurements for quality control during concrete construction. *ACI Materials Journal*, 105(6), 541.
- Serra, J. (1982). *Image Analysis and Mathematical Morphology*, Academic Press, London.
- Shiple, R. W., Darwin, D., Carl E. Locke, C.E. (1997). “Stray current corrosion due to utility cathodic protection.” University of Kansar Center for Research, Inc. Lawrence, Kansas, December 1997.
- Shreir, L. L., Jarman, R. A. and Burstein, G. T. (1994), *Corrosion*, Third ed., Butterworth Heinemann, London.
- Singh, Y. (2013). Electrical Resistivity Measurements: A Review, *International Journal of Modern Physics: Conference Series* Vol. 22, 745–756.
- Skibsted, G. (2013). Matrix changes and side effects induced by electrokinetic treatment of porous and particulate materials, PhD thesis, Technical University of Denmark.
- Smulders, H.M.W. and Jansenn, M.F.P., “Modelling d.c. stray currents using a multi-layer model.” *Movares*, Utrecht, The Netherlands.

- Stanish K. and Thomas M. (2003). The use of bulk diffusion tests to establish time-dependent concrete chloride diffusion coefficients. *Cem Concr Res* 33:55–62
- Steve Kosmatka et al, *Design and Control of Concrete Mixtures*, 15th Edition, EB001, PCA Engineering Bulletin EB 001, Portland Cement Association, Skokie, IL 2002.
- Steyn, B.M., Cronje, W.A., Wyk, H. V. and Jansen, B., “Stray current performance and design of tubular track.” Spoornet, Railway Engineering, Johannesburg.
- Sumanasooriya, M.S. and Neithalath, N., (2009). “Stereology- and morphology-based pore structure descriptors of enhanced porosity (previous) concrete.” *ACI Materials Journal*, 106 (5), 429-438.
- Sun, G., Zhang, Y., Sun, W., Liu, Z., & Wang, C. (2011). Multi-scale prediction of the effective chloride diffusion coefficient of concrete. *Construction and Building Materials*, 25(10), 3820-3831.
- Susanto, A, Koleva, DA, Copuroglu, O, Beek, C van & Breugel, K van (2013). Mechanical, electrical and microstructural properties of cement-based materials in conditions of stray current flow, *Journal of Advanced Concrete Technology*, 11(3), 119-134.
- Susanto, A., Koleva, D. A., & van Breugel, K. (2017). *The Influence of Stray Current on the Maturity Level of Cement-Based Materials*. In *Concrete Durability* (pp. 57-82). Springer International Publishing.
- Susanto, A., Koleva, D. A., Copuroglu, O., van Beek, K. and van Breugel, K., (2013). “Mechanical, electrical, and microstructural properties of cement-based materials in condition of stray current flow.” *Journal of Advanced Concrete Technology*, 11, 119-134.
- Susanto, A., Koleva, D. A., van Breugel, K., (2017). “The Influence of Stray Current on the Maturity Level of Cement-Based Materials”, Book Chapter, Springer International Publishing.
- Susanto, A., Koleva, D. A., van Breugel, K., van Beek, C., (2017). “Stray current-induced development of cement-based microstructure in water-submerged, Ca(OH)<sub>2</sub>-submerged and sealed conditions.” *Journal of Advanced Concrete Technology*, Vol. 15, pp. 244-268.
- Susanto, A., Koleva, D.A., Koenders, E.A.B, and van Breugel, K. (2015). The effect of temperature rise on microstructural properties of cement-based materials: HYMOSTRUCT3D modeling incorporating an “electrical enhancement” factor, *European Corrosion Congress (EUROCORR) 2015*, 6-10 September 2015, Graz, Austria.
- Susanto, A., Koleva, D.A. and van Breugel, K. (2014). “DC current-induced curing and ageing phenomena in cement-based materials.” In K van Breugel & EAB Koenders (Eds.), *Proceedings of the 1st international conference on ageing of materials and structures, AMS'14* (pp. 562-568). Delft: Ageing Center TU Delft.
- Susanto, A., Koleva, D.A., Copuroglu, O., van Beek, C. and van Breugel, K., (2013). “Mechanical, electrical and microstructural properties of cement-based materials in conditions of stray current flow.” *Journal of Advanced Concrete Technology*, Vol. 11, pp. 119-134.
- Tang, L. (1996). Chloride transport in concrete - measurement and prediction, Ph.D. thesis, Chalmers University of Technology, Gothenburg, Sweden.
- Tang, L. and Nilsson, L.O. (1992). Chloride diffusivity in high strength concrete at different ages, *Nordic Concrete Research*, 11(1), 162-171.
- Tang, Y. and Wei, K., (2010). “Stray current experiment and analysis for metro tunnel.” 2nd International Symposium on Service Life Design for Infrastructure, 4-6 October 2010, Delft, The Netherlands.
- Thaker, K. K. (2012). *Electrokinetic Remediation of Contaminated Soils*, PhD thesis, Institute of Technology, Nirma University, India.
- Toumi, B and Resheidat, M. (2010). Influence of High Temperatures on Surface Cracking of Concrete Studied by Image Scanning Technique, *Jordan Journal of Civil Engineering*, Volume 4, No. 2.
- Tremper, B., Benton, J. L. and Stratfull, R. F., (1958). “Fundamental Factors Causing Corrosion,” HRB Bulletin 182, *Corrosion of Reinforcing Steel and Repair of Concrete in a Marine Environment*, 18-41, Highway Research Board, Washington, D.C.
- Troxell, Davis and Kelly, (1968). “*Composition and Properties of Concrete.*”, 2nd Ed., McGraw-Hill, New York.
- Truc, O., Ollivier, J.P., Nilsson, L.O. (2000). Numerical simulation of multi-species transport through saturated concrete during a migration test—MsDiff code, *Cement and Concrete Research* 30, 1581–1592.
- Tuutti K. *Corrosion of steel in concrete*. Stockholm: CBI, 1982:468.
- U.S. Dep. Int. Bureau of Reclamation "Boulder Canyon Project Final Reports" ". VII Bull. 1, 3, 4, Denver, Colorado, 1940-1949.
- Udaya B. Halabe, Kenneth Maser, Eduardo Kausel, *Propagation Characteristics Of Electromagnetic Waves In Concrete*, U.S. ARMY RESEARCH OFFICE, 1988.

- Uygunoğlu, T., and Hocaoğlu, İ. (2018). Effect of electrical curing application on setting time of concrete with different stress intensity. *Construction and Building Materials*, 162, 298-305.
- Van Breugel, K. (1991), Simulation of hydration and formation of structure in hardening cement-based materials, PhD thesis, Delft University of Technology, the Netherlands.
- Van Breugel, K. (2001). Hydration of cement-based systems, Report BE96-3843/2001:17-6.
- van Dalen, S. M. (2005) Experimenteel onderzoek naar de RCM-methode (In Dutch). Master thesis, Delft University of Technology
- van der Wegen G.J.L., Boutz M.M.R., Sarabèr A.J., van Eijk R.J., 2014. Ageing coefficient of fly ash concrete and its impact on durability. AMS '14 - Proceedings of the 1st International Conference on Ageing of Materials & Structures, edited by K. van Breugel, E.A.B. Koenders, ISBN: 978-94-6186-314-0, p. 171-178, 26-28 May 2014, Delft, The Netherlands.
- Vassie, P. R., (1980). "A Survey of Site Tests for the Assessment of Corrosion in Reinforced Concrete." TRRL Laboratory Report 953, Transportation and Road Research Laboratory, Crowthorne, U.K.
- Velivasakis, E. E., Henriksen, S. K. and Whitmore, D., (1998). "Chloride extraction and realkalization of reinforced concrete stop steel corrosion." *Journal of Performance of Constructed Facilities*, 77-84.
- Verbeck, G.J., 1960, 4th ISCC, Washington, Paper IV-3, pp. 453-465.
- Wadhwa S.S., Srivastava L.K., Gautam D.K., Chandra D., Direct electric curing of in situ concrete, *Batiment International, Building Research and Practice*, 1987, 15:1-6, 97-101.
- Wadso, L. (2003). An experimental comparison between isothermal calorimetry, semi-adiabatic calorimetry and solution calorimetry for the study of cement hydration, *NORDTEST Report 522*.
- Wang, K. W., Cable, J. K., and Zhi, G. (2002). *Investigation into improved pavement curing materials and techniques: Part I (Phases I and II)* (No. Iowa DOT Project TR-451.).
- Washburn, E.W., (1921). "The dynamics of capillary flow, *Physical Review*. 17(3), 273-283.
- Weyers, R. E., Pyc, W. and Spirnkel, M. M., (1998). "Estimating the service life of epoxy-coated reinforcing steel." *ACI Mater. J.*, 95 (5), 546-557.
- Whiting, David, A., Nagi and Mohamad A., (2003). "Electrical Resistivity of Concrete - A Literature Review." R&D Serial No. 2457, Portland Cement Association, Skokie, Illinois, USA.
- Wilson, J.G. and Gupta, N.K. (1992). An overview of the methods of accelerated curing of concrete by elevated temperatures with emphasis on electroheat techniques, in: *Universities Power Engineering Conference Proceedings*, University of Bath, UK, September 1992, pp. 107-110.
- Wilson, J.G. and Gupta, N.K. (1996). Analysis of power distribution in reinforced concrete during accelerated curing using electroheat, *IEE Proceedings-Electric Power Applications* 143 (2), 172-176.
- Wittmann, F. H., (1997). "Corrosion of cement-based materials under the influence of electric field." *Materials Science Forum* Vol. 247, 107-126.
- Wong, H.S., Head, M.K. and Buenfeld, N.R., (2006). "Characterising the pore structure of cement based materials using backscattered electron and confocal microscopy." *Measuring, Monitoring and Modeling Concrete Properties*, Part 6, 495-502.
- Wu, Y. et al., (2011). "Analysis of stray current induced by cathodic protection on steel-framed masonry structures." *The Open Corrosion Journal*, 4, 34-39.
- Xia, J and Li, L. (2013). Numerical simulation of ionic transport in cement paste under the action of externally applied electric field. *Construction and Building Materials* 39:51-59.
- Xu, Y., Xu, Q., Chen, S., Li, X. (2017). Self-restraint thermal stress in early-age concrete samples and its evaluation, *Construction and Building Materials* 134, 104-115.
- Xu, S., Li, W., Xing, F., Wang, Y., Wang, R., & Wang, X. (2017). An Elimination Method of Temperature-Induced Linear Birefringence in a Stray Current Sensor. *Sensors*, 17(3), 551.
- Xu, S. Y., Xing, F. F., Li, W., Wang, Y. Q., Wang, X. H., & Wang, R. L. (2016). A stray current sensor based on an all-side cylindrical spiral fiber. *IEEE Photonics Journal*, 9(1), 1-14.
- Yang, S. and Yang, X., (2008) "Evaluation of stray current corrosion resistance of concrete in metro construction." *Front. Archit. Civil Eng. in China*, Vol. 2, No. 3, pp. 246-252.
- Ye, G., (2003). "Experimental study and numerical simulation of the development of the microstructure and permeability of cementitious materials." Ph.D. thesis. Delft: Delft University of Technology.
- Ye, G., Hu, J., van Breugel, K. and Stroeven, P., (2002). "Characterization of the development of microstructure and porosity of cement-based materials by numerical simulation and ESEM image analysis." *Materials and Structures*, 35, 603-613.
- Ye, H., Basaran, C., Hopkins, D., (2003). Thermomigration in Pb-Sn solder joints under Joule heating during electric current stressing, *Appl. Phys. Lett.* 82 (8).
- Young, J.F., et al., 1986, SMDDHC, Boston, MRS, Proc. Vol. 85, pp. 313-322.

- Young, J.F., et al., 1973, CCR, Vol. 3, No. 6, pp. 689-700.
- Yu, H.T., Khazanovich, L., Darter, M.I., Ardani, A. (1998). Analysis of concrete pavement responses to temperature and wheel loads measured from instrumented slabs, *Transportation Research Record* 1639, 94–101.
- Yu, Z. (2015) Microstructure development and transport properties of Portland cement-fly ash binary systems – in view of service life predictions. PhD thesis, Delft University of Technology, Delft
- Yun-Yong Kim et al., (2014). “Effect of W/C Ratio on Durability and Porosity in Cement Mortar with Constant Cement Amount”, *Advances in Materials Science and Engineering*, Volume 2014.
- Yu-qiao, W., Wei, L., Xue-feng, Y., Guo, Y., Qi-gao, F., and Li-ping, Z., (2010) “Modeling and simulation the distribution of metro stray current.” *International Conference on Computer Application and System Modeling (ICCASM 2010)*.
- Zhang, E. Q., Abbas, Z., and Tang, L. (2018). Predicting degradation of the anode–concrete interface for impressed current cathodic protection in concrete. *Construction and Building Materials*, 185, 57-68.
- Zhang, M., (2013). Multiscale lattice Boltzman-finite element modelling of transport properties in cement-based materials, PhD thesis, TU Delft.
- Zhang, Y. (2018). Non-saturated Chloride Diffusion in Sustainable Cementitious Materials, PhD Thesis TU Delft, the Netherlands.
- Zhiguang et al., (2011). “Research of impact of stray current from urban rail transit system on buried gas pipeline.” *Advanced Material Research*, Vols. 239-242, 1219-1222.
- Zhu Bofang, *Thermal Stresses and Temperature Control of Mass Concrete*, Tsinghua University Press, Published by Elsevier Inc, 2014.
- Zhu, Q., Jiang, L. H., & Chen, Y. (2012). Effect of Stray Current on Chloride Binding Mechanism in Concrete. In *Applied Mechanics and Materials* (Vol. 204, pp. 3720-3723). Trans Tech Publications.



## Summary

Stray current has become a main concern for many years due to its effect on (reinforced) concrete structures and underground infrastructures. It has been reported that stray current affects not only steel reinforcement embedded in concrete, but can also induce degradation of the cement-based matrix. Stray current causes an increase of temperature in hardening concrete due to Joule heating which will accelerate cement hydration. The accelerated cement hydration results in faster evolution of materials properties (e.g. stiffness and strength) and a faster decrease of the capillary porosity. The microstructural change due to stray current flow will affect transport properties, as well as the service life performance of cement-based materials. In case the concrete is exposed to water, leaching of alkali ions will decrease compressive strength and increase permeability and diffusion coefficient of concrete. Under stray current, leaching of alkali ions in concrete is accelerated which will increase level of structural degradation. Deterioration of concrete due to stray current involves many mechanisms including ion and mass transport, electrical conduction, heat transfer and corresponding occurrence of mechanical stresses. However, the study on the effect of stray current on material properties (e.g. microstructural, mechanical, electrical properties) and long-term performance/durability of cement based materials is still lacking. The aim of this thesis is to investigate the effects of stray current on long-term performance of cement-based materials. The results of this project will contribute to a better understanding on beneficial (positive) and/or detrimental (negative) effects of stray current on cement-based materials, which is a point of significant importance for real practice.

Firstly, the effect of low level current density (i.e.  $10 \text{ mA/m}^2$ ) on microstructural, mechanical and electrical properties of hardening mortar in arbitrary environmental condition (i.e. the hardening mortar specimens were partly submerged in water) was investigated. Numerical simulation of the stray current distribution is performed, meant to serve as a basis for further elaborated modelling of the level of current density that could exert significant microstructural alterations in a bulk cement-based matrix.

Secondly, experiments under synergetic action of stray current and different environmental conditions (i.e. submerged in water and saturated calcium hydroxide) on cement-based materials with 24 hours curing were performed. These experiments were used to distinguish between diffusion-controlled process (ions leaching due to concentration gradients) and migration-controlled process (ion/water transport in stray current conditions). Stray current levels applied to the cement-based materials were  $10 \text{ mA/m}^2$ ,  $100 \text{ mA/m}^2$  and  $1 \text{ A/m}^2$ , as measured in real practices, to quantify negative/detrimental effect of stray current due to alkali ion leaching and possible positive/beneficial effect of stray current on material properties (i.e. mechanical, electrical and microstructural properties) of cement-based materials.

Thirdly, the effects of stray current flow on the hydration process and temperature development in cement-based materials and evolution of materials properties were experimentally and numerically investigated. Experiments were performed in isothermal condition at  $20^\circ\text{C}$  to investigate heat release and microstructural changes in cement paste subjected to stray current with current density  $10 \text{ mA/m}^2$ ,  $100 \text{ mA/m}^2$  and  $1 \text{ A/m}^2$ . In addition, semi-adiabatic test were carried out in hardening cement paste

prism with specimen size of  $5.5 \times 5.5 \times 29.5 \text{ cm}^3$  and current densities  $10 \text{ A/m}^2$ ,  $40 \text{ A/m}^2$  and  $60 \text{ A/m}^2$ . Numerical simulations were performed to quantify the hydration process and temperature development in hardening cement-based materials and evolution of materials properties. The effect of stray current on hardening cement-based materials with different element sizes was simulated to investigate possible size effects and consequences for real-size hardening structural elements. To analyse negative or possibly positive effects of stray current on hardening concrete subjected to stray current, degree of hydration, capillary porosity and compressive strength in the centre of hardening concrete with and without insulation with different wall thickness have been determined from the temperature development. Apparent diffusion coefficients of concrete subjected to stray current were calculated from microstructure parameters (i.e. capillary porosity).

Finally, the effect of stray current flow on materials properties of hardened mortar specimens, 28-days cured in a fog-room with 98% RH, was studied. Synergetic effect of water-to-cement ratio, curing age and various external environment on the microstructural (porosity and pore size), electrical (resistivity) and mechanical (compressive strength) properties of hardened mortar specimens subjected to stray current were investigated.

## Samenvatting

Lekstromen zijn al jaren een belangrijk aandachtspunt vanwege het effect die ze hebben op (gewapend) betonconstructies en ondergrondse infrastructuren. In de vakliteratuur is gemeld dat lekstromen niet alleen staalwapening ingebed in beton aantast, maar ook degradatie van de cementgebaseerde matrix kan veroorzaken. Lekstromen veroorzaken een temperatuurverhoging in verhard beton door Joule-verwarming, wat de hydratatie van cement versnelt. De versnelde hydratatie van cement resulteert in een snellere evolutie van de materiaaleigenschappen (bijv. stijfheid en sterkte) en een snellere afname van de capillaire porositeit. De microstructurele verandering als gevolg van lekstromen zal de transporteigenschappen beïnvloeden, evenals de levensduurprestaties van materialen op basis van cement. Als het beton wordt blootgesteld aan water, zal de uitloging van alkali-ionen de druksterkte verminderen en de permeabiliteit en diffusiecoëfficiënt van beton verhogen. Onder lekstromen wordt de uitloging van alkali-ionen in beton versneld, wat de mate van structurele afbraak zal verhogen. Verslechtering van beton als gevolg van lekstromen omvat vele mechanismen, waaronder ion- en massatransport, elektrische geleiding, warmteoverdracht en overeenkomstig optreden van mechanische spanningen. Echter, onderzoek naar het effect van lekstromen op materiaaleigenschappen (bijv. microstructurele, mechanische, elektrische eigenschappen) en prestaties/duurzaamheid op lange termijn van materialen op basis van cement ontbreekt nog steeds. Het doel van dit proefschrift is het onderzoeken van de effecten van lekstromen op lange termijn prestaties van materialen op basis van cement. De resultaten van dit project zullen bijdragen tot een beter begrip van de gunstige (positieve) en / of nadelige (negatieve) effecten van lekstromen op materialen op basis van cement, wat van groot belang is voor de praktijk.

Ten eerste werd het effect van een lage stroomdichtheid (d.w.z.  $10 \text{ mA/m}^2$ ) op de microstructurele, mechanische en elektrische eigenschappen van verhardingsmortel in willekeurige omgevingsomstandigheden onderzocht (d.w.z. de hardende mortelspecimen waren gedeeltelijk ondergedompeld in water). Numerieke simulatie van de lekstroomverdeling is uitgevoerd, bedoeld als basis voor verder uitgewerkte modellering van het niveau van stroomdichtheid dat significante microstructurele veranderingen zou kunnen veroorzaken in een bulkcement-gebaseerde matrix.

Ten tweede werden experimenten uitgevoerd onder synergetische werking van lekstromen en verschillende omgevingsomstandigheden (d.w.z. ondergedompeld in water en verzadigd calciumhydroxide) op materialen op basis van cement met 24 uur uitharding. Deze experimenten waren gebruikt om onderscheid te maken tussen een diffusie-gecontroleerd proces (uitloggen van ionen als gevolg van concentratiegradiënten) en migratie-gecontroleerd proces (ionen/watertransport in lekstroom omstandigheden). De toegepaste lekstromenniveaus op de cement gebaseerde materialen waren  $10 \text{ mA/m}^2$ ,  $100 \text{ mA/m}^2$  en  $1 \text{ A/m}^2$ , zoals gemeten in de praktijk, om negatieve/nadelige effecten van lekstromen als gevolg van uitloging van alkali-ionen en mogelijk positief/gunstige effecten van lekstromen op materiaaleigenschappen (d.w.z. mechanische, elektrische en microstructurele eigenschappen) van materialen op basis van cement.

Ten derde werden de effecten van lekstromen op het hydratatieproces en de temperatuurontwikkeling in materialen gebaseerd op cement en evolutie van

materiaaleigenschappen experimenteel en numeriek onderzocht. Experimenten werden uitgevoerd in isotherme toestand bij 20 °C om de warmtevrijgave en microstructurele veranderingen in cementpasta te onderzoeken die werd blootgesteld aan lekstromen met een stroomdichtheid van 10 mA/m<sup>2</sup>, 100 mA/m<sup>2</sup> en 1 A/m<sup>2</sup>. Daarnaast werd een semi-adiabatische test uitgevoerd in een prisma van verhardende cementpasta met een monsterafmeting van 5.5-5.5-29.5 cm<sup>3</sup> en een stroomdichtheid van 10 A/m<sup>2</sup>, 40 A/m<sup>2</sup> en 60 A/m<sup>2</sup>. Numerieke simulaties werden uitgevoerd om het hydratatieproces en de temperatuurontwikkeling bij het harden van cementgebaseerde materialen en evolutie van materiaaleigenschappen te kwantificeren. Het effect van lekstromen op het harden van materialen op basis van cement met verschillende elementgroottes werd gesimuleerd om mogelijke omvangeffecten en gevolgen voor verhardende structurele elementen op ware grootte te onderzoeken. Om de negatieve of mogelijk positieve effecten van lekstromen op verhard beton dat onderhevig is aan lekstromen te analyseren, zijn hydratatiegraad, capillaire porositeit en druksterkte in het centrum van hard beton met en zonder isolatie met verschillende wanddikte bepaald uit de temperatuurontwikkeling. Schijnbare diffusiecoëfficiënten van beton die aan lekstromen zijn blootgesteld werden berekend op basis van microstructuurparameters (d.w.z. capillaire porositeit).

Ten slotte werd het effect van lekstromen op materiaaleigenschappen van geharde mortelspecimens, 28 dagen uitgehard in een mistruimte met 98% RH, bestudeerd. Er werd onderzoek gedaan naar het synergetische effect van de verhouding water/cement, uithardingsleeftijd en verschillende externe omgevingen op de microstructurele (porositeit en poriegrootte), elektrische (weerstand) en mechanische (druksterkte) eigenschappen van geharde mortelspecimen onderworpen aan lekstromen.

## Acknowledgement

All praise and thanks are due to Allah. Without His help and guidance, this thesis would never be completed. The financial support from the Directorate General of Higher Education Ministry of Education Republic of Indonesia (DIKTI) with grant number 1375.32/D4.4/2010 is gratefully acknowledged. I would like to thank Rector, Dean of MIPA, lecturers, and staffs of UNM for all their help and supports. This project would never have been possible without the support and guidance of various people.

Firstly, I would like to express all my deep and sincere gratitude to my promotor Prof.dr.ir. Klaas van Breugel, who offered me the opportunity to work on this project in Microlab, the Section of Materials and Environment TU Delft. Thank you for all the advice, ideas, moral support and patience in guiding me through this project.

I would like to express my sincere gratitude to my co-promotor Dr. ir. Dessi Koleva for supervision, guidance, motivation and support during my PhD study. Without her guidance and persistent help this PhD thesis would not have been possible. Dessi, thank you for all your helps and time for me.

The committee members, Prof.dr. Han Ay Lie, Prof. dr. ir. E.A.B. Koenders, Prof.dr.ir. R.P.B.J. Dollevoet, Prof.dr.ir. H.E.J.G. Schlangen and Dr. G. Ye, are very appreciated for spending their time and effort to review my thesis and attending my PhD defence.

I would like to thank the head of Microlab Prof. Erik Schlangen for permitting me to use laboratory facilities and all the support during my research. My sincere gratitude goes to secretaries (Claire, Claudia, Nynke, Melanie, Jacqueline) for their help with administration affairs. I also want to thank technicians of Section of Materials and Environment (Gerrit, Arjan, John, and Maiko) and Mr. Kees van Beek (Senior electronics design engineer, The Electronic and Mechanical Support Division (DEMO) TU Delft) for their help with my experimental works. Special thanks go to Mottaqiallah Taouil for translating summary of my thesis into the Dutch language.

I would like also to thank all the colleagues in the Section of Materials and Environment for a wonderful experience working with all of you. Special thanks go to Farhad Pargar, Zhipei Chen, Amir Zommorodian, Hitham Amin, Ennery, Enrico, Maria Farini, Philips, for their friendship, support, discussion and spending the great moments together. I am grateful to all Indonesian friends (Pak Senot, Bu Pungky, Pak Jun, Bu Ida, Pak Yazdi, Pak Adhi, Pak Wied, Pak Agung, Pak Dieky, Pak Zul, Bu Lasmini, Bu Ochie, Bu Reni, Pak Andri, Pak Budi, Pak Dudi, Pak Andi, Pak Isnaini and Indonesian Families in Leiden) for the friendship and kindness during my stay in the Netherlands. This makes I and my family feel like at home.

Last but not least, my deepest gratitude goes to my wife Rahma and my daughter Annisaa for their understanding and love during the past few years. Their unconditional support and encouragement were in the end what made this PhD thesis possible. Most importantly, I would like to thank my parents for their endless love, prayers and encouragement, and without which I would not have come this far.



## Curriculum Vitae



**Agus Susanto** received Bachelor of Sciences from Department of Physics in 2001 at Institute of Technology Bandung (ITB), Indonesia. He continued his study at Instrumentation and Control Engineering, Department of Engineering Physics, ITB. During master study, he visited Kasai Laboratory, Division of Precision Science & Technology and Applied Physics, Osaka University, Osaka, Japan for a year (2003-2004), as an exchange student and finished his master thesis. For supporting his PhD project in Microlab, Material and Environment, Faculty of Civil Engineering and Geosciences, Delft University of Technology (TU Delft), The Netherlands, he got scholarship from Directorate General of Higher Education Ministry of Education Republic of Indonesia from 2011-2015.

## List of Publications

1. **Susanto, A.**, Koleva, D.A., Copuroglu, O., van Beek, K. and van Breugel, K (2012). Mechanical, electrical and microstructural properties of cement-based materials in conditions of current flow, European corrosion congress (EUROCORR) (pp. 1-16), 9 - 13 September 2012, Istanbul, Turkey.
2. **Susanto, A.**, Koleva, D. A., Copuroglu, O., van Beek, K., and van Breugel, K. (2013). Mechanical, electrical and microstructural properties of cement-based materials in conditions of stray current flow. *Journal of Advanced Concrete Technology*, 11(3), 119-134.
3. **Susanto, A.**, Koleva, D.A., van Beek, K. And van Breugel, K. (2013). The effect of electrical stray current on material properties of mortar specimens, proceeding of the 6th Civil Engineering Conference in Asia Region (CECAR 6): Embracing the future through sustainability (pp. 1-8), 20-22 August 2013, Jakarta, Indonesia.
4. **Susanto, A.**, Koleva, D.A., Koenders, E.A.B., van Breugel, K. (2014). Modelling the effect of electrical current flow on the hydration process of cement-based materials, Extended abstract: Young researchers' Forum II: Construction materials (pp. 41-48), 19<sup>th</sup> February 2014, University College London, London.
5. **Susanto, A.**, Koleva, D.A. and van Breugel, K. (2014). DC current-induced curing and ageing phenomena in cement-based materials. In K van Breugel & EAB Koenders (Eds.), Proceedings of the 1st international conference on ageing of materials and structures, AMS'14 (pp. 562-568), 26-28 May 2014, Delft, Netherlands.
6. **Susanto, A.**, Koleva, D.A. and van Breugel, K. (2014). Altered cement hydration and subsequently modified porosity, permeability and compressive strength of mortar specimens due to the influence of electrical current, proceedings of the European corrosion congress (EUROCORR 2014), pp. 1-10, 8-12 September 2014, Pisa, Italy.

7. **Susanto, A.**, Koleva, D.A., Koenders, E.A.B. and van Breugel, K. (2015). A conceptual model for ionic transport in cement-based materials in conditions of externally applied electric field, proceedings of the 23th international materials research congress 2014 Vol. 1768. MRS Online Proceedings Library (pp. 1-6), Cambridge: Cambridge University Press.
8. **Susanto, A.**, Koleva, D.A., Koenders, E.A.B, and van Breugel, K. (2015). The effect of temperature rise on microstructural properties of cement-based materials: HYMOSTRUCT3D modeling incorporating an “electrical enhancement” factor, European Corrosion Congress (EUROCORR) 2015, 6-10 September 2015, Graz, Austria.
9. **Susanto, A.**, Koleva, DA, Koenders, EAB & van Breugel, K. (2015). The influence of stray current flow on the level of maturity of cement-based materials, XXIV International Material Research Congress (IMRC) 2015, 16-20 August 2015, Cancun, Mexico.
10. Hu, J., **Susanto, A.**, and Koleva, D.A. (2015). Digital image processing of cement-based materials for quali- and quantification of microstructural development, XXIV International Material Research Congress (IMRC) 2015, 16-20 August 2015, Cancun, Mexico.
11. Hu, J., **Susanto, A.**, and Koleva, D. A. (2016). Image processing of cement-based materials in conditions of current flow for microstructural analysis. *International Conference on Audio, Language and Image Processing (ICALIP)*, July 2016, pp. 246-250, IEEE, Shanghai, China.
12. **Susanto, A.**, Peng, G., Koleva, D.A., and van Breugel, K. (2016). Electrical Current Flow and Cement Hydration: Implications on Cement-Based Microstructure, 2nd International Conference on Architecture, Materials and Construction 2016 (ICAMC 2016), Dubai, UAE, 3-5 December, 2016.
13. **Susanto, A.**, Koleva, D.A. and van Breugel, K. (2017). The Influence of Stray Current on the Maturity Level of Cement-Based Materials, Springer International Publishing.
14. **Susanto, A.**, Koleva, D. A., van Breugel, K., and van Beek, K. (2017). Stray current-induced development of cement-based microstructure in water-submerged, Ca(OH)<sub>2</sub>-submerged and sealed conditions. *Journal of Advanced Concrete Technology*, 15(6), 244-268.
15. **Susanto, A.**, Koleva, D. A., and van Breugel, K. (2017). The effect of water-to-cement ratio and curing on material properties of mortar specimens in stray current conditions. *Journal of Advanced Concrete Technology*, 15(10), 627-643.